ANTI-MITOTIC ACTIVITY OF SIX ASTERACEAE PLANT EXTRACTS AND IDENTIFICATION OF THE SESQUITERPENE LACTONE HYMENORATIN FROM THE CANADIAN PLANT *HYMENOXYS RICHARDSONII*

LAYLA MOLINA
B. Sc. Pharmacy, University of Los Andes (Venezuela), 2014

A Thesis
Submitted to the School of Graduate Studies
of the University of Lethbridge
in Partial Fulfilment of the
Requirements for the Degree

MASTER OF SCIENCE

Department of Biological Sciences
University of Lethbridge
LETHBRIDGE, ALBERTA, CANADA

ANTI-MITOTIC ACTIVITY OF SIX ASTERACEAE PLANT EXTRACTS AND IDENTIFICATION OF THE SESQUITERPENE LACTONE HYMENORATIN FROM THE CANADIAN PLANT *HYMENOXYS RICHARDSONII*

LAYLA MOLINA

Date of defense: October 26, 2018

Dr. R. Golsteyn Thesis Supervisor	Associate professor	Ph.D.
Dr. E. Schultz Thesis Examination Committee Member	Associate professor	Ph.D.
Dr. S. Acharya Thesis Examination Committee Member	Research Scientist	Ph.D.
Dr. R. Andersen External Examiner University of British Columbia Vancouver, British Columbia	Professor	Ph.D.
Dr. S. Wiseman Chair, Thesis Examination Committee	Associate Professor	Ph.D.

ABSTRACT

In this thesis we investigate the anti-mitotic activity of six Canadian Asteraceae species. Three plant extracts arrested cancer cells in mitosis with different characteristics. *Hymenoxys richardsonii* extract induced a mitotic arrest measured by rounded cell morphology, phosphorylated histone H3, active Cdk1/Cyclin B, high levels of Plk1, and G2/M arrest by flow cytometry. Mitotic-arrested cells were characterized by chromosome congression failure, distorted mitotic spindles, and damaged DNA. Biology-guided fractionation led to the purification of the active compound hymenoratin, a sesquiterpene lactone closely related to pulchelloid A, which was isolated from the anti-mitotic plant *Gaillardia aristata*. This is the first time that *H. richardsonii* or hymenoratin is reported to elicit a biological activity on cancer cells. Investigation of the structure-activity relationship between sesquiterpene lactones and anti-mitotic activity is potentially useful to understand unknown biological mechanisms or to develop anticancer drug candidates.

ACKNOWLEDGEMENTS

Firstly, I would like to express my sincere gratitude to my supervisor Dr. Roy Golsteyn for the opportunity I was given and for the continuous support during my MSc program. His knowledge and his approachable, optimistic, and passionate character were an invaluable guidance that taught me essential research values and motivated me during my project.

This achievement has been possible thanks to my supervisory committee members, Dr. Elizabeth Shultz and Dr. Surya Acharya, who gave me useful feedback in our meetings and dedicated their time to help me improve my project. My special gratitude to Dr. Raymond Andersen for accepting to be an external examiner of this thesis and for collaborating, together with Dr. David Williams, on the chemical fractionation of our plants.

I am also grateful to members of the Biological Sciences Department: Dr. Robert Laird, Dr. Nehalkumar Thakor and his laboratory members, Sheila Matson, Nicola Spencer, and Dr. Andy Hudson and Diana Wilches in Biostores for the intellectual and technical assistance provided.

I would like to thank laboratory members who were always friendly and supportive when I needed: Alessandra Bosco, Jan Tuescher, and Danî Kalsbeek. I am thankful for the knowledge and all the valuable discussions shared. I must also express my gratitude to Michelle Tadey for participating on my project during her independent studies.

I would have not been able to accomplish this goal without the moral support, patience, encouragement, and kindness of friends and family. I am profoundly thankful to my parents Laudin Molina and Lady Troconis, and my brothers Alessandro, Leonardo, and Leonel for their unconditional love and support that have always been the root of my achievements. Special thanks

to the Lonseth family: Grant, Lana, Erika, and Matt. Their welcoming home, kind friendship, and love helped me feel home in Canada, supporting me and making this a priceless experience.

Finally, I gratefully acknowledge the funding received for the development of this project from the University of Lethbridge, the Canada Foundation for Innovation, and the Natural Sciences and Engineering Research Council.

TABLE OF CONTENTS

LIST OF TABLES

LIST OF FIGURES

LIST OF ABBREVIATIONS

γ-H2AX	Gamma histone H2AX
6-OAP	6-O-Angeloylplenolin
AP	Alkaline phosphatase
APC/C	Anaphase promoting complex/cyclosome
ATCC	American Type Culture Collection
ATM	Ataxia telangiectasia mutated
ATP	Adenosine triphosphate
ATPase	Adenosine triphosphatase
ATR	ATM and Rad3-related
BC	Before Christ
Bub	Budding uninhibited by benzimidazole proteins
BSA	Bovine serum albumin
CAP-Gly	Glycine-rich cytoskeleton-associated proteins
Cdc	Cell-division cycle protein
Cdk	Cyclin-dependent kinase
CENP-E	Centromere-associated protein E
CENP-F	Centromere-associated protein F
Chk	Checkpoint kinase
CO_2	Carbon dioxide
CPT	Camptothecin
DAPI	4′, 6-diamidino-2-phenylindole
DCM	Dichloromethane
DDR	DNA damage response
DMSO	Dimethyl sulfoxide
DNA	Deoxyribonucleic acid
DTT	Dithiothreitol
EDTA	Ethylenediaminetetraacetic acid
EGTA	Ethylene glycol tetraacetic acid
EtoAc	Ethyl acetate
EtOH	Ethanol

FBS	Fetal bovine serum
FTase	Farnesyl transferase
FTI	Farnesyl transferase inhibitor
GST	Glutathione S-transferase
G0	Resting phase
G1 phase	Gap 1 phase
G2 phase	Gap 2 phase
G2/M phase	Gap 2 or M phase
GPS	Global positioning system
GTP	Guanosine triphosphate
HEPES	4-(2-hydroxyethyl)-1-piperazineethanesulfonic acid
HPLC	High performance liquid chromatography
HT29	Human colorectal adenocarcinoma cell line
IκB	Inhibitor of NF-κB
IPEGAL	Octylphenoxypolyethoxyethanol
LRESIMS	Low-resolution electrospray ionization mass spectrometry
Mad	Mitotic-arrest-deficient proteins
M phase	Mitotic phase
M059K	Human glioblastoma cell line
ME	Mercaptoethanol
MeOH	Methanol
MeCN	Acetonitrile
MTT	3-((4,5)-dimethylthiazol-2-yl)-2,5-diphenyl-tetrazolium bromide
NF-κB	Nuclear factor kappa-light-chain-enhancer of activated B cells
NEB	Nuclear envelope breakdown
NMR	Nuclear magnetic resonance
PAGE	Poly-acrylamide gel electrophoresis
PBS	Phosphate buffered saline
PH3	Phospho-histone H3
PI	Propidium iodide
Plk-1	Polo-like kinase-1
PP1	Protein phosphatase 1

PP1Cα	Protein phosphatase 1 catalytic subunit alpha
RPMI	Roswell Park Memorial Institute medium
S phase	DNA synthesis phase
SAC	Spindle assembly checkpoint
SDS	Sodium dodecyl sulphate
Sgo1	Shugoshin protein
Skp1	S-phase kinase-associated protein 1
Skp2	S-phase kinase-associated protein 2
SL	Sesquiterpene lactone
STAT3	Signal transducer and activator 3
TBS	Tris-buffered saline
TCP	Tubulin carboxypeptidase enzyme
Ub	Ubiquitin
UPP	Ubiquitin-proteasome pathway
VASCAN	Database of vascular plants of Canada
WI-38	Human non-cancerous lung fibroblastic cell line

CHAPTER 1

Introduction

This thesis is about the investigation of the anti-mitotic activity of plants from the Asteraceae family. Under the Prairie to Pharmacy Program, our laboratory recently found that an extract prepared from a member of this family, *Gaillardia aristata,* exerts an anti-mitotic activity on cancer cells. The extract contained a secondary metabolite called pulchelloid A, which is a sesquiterpene lactone. In the present project, we analyzed six Asteraceae species and found that three of them induced mitotic arrest in cancer cells. We hypothesize that a subset of sesquiterpene lactones, known to be synthesized by species of the Asteraceae family, is the source of this anti-mitotic activity. To gain insight into this, *Hymenoxys richardsonii*, one of the three active species, was characterized for its anti-mitotic activity and was fractionated to isolate the active compound. The biology-guided fractionation led to the purification of the sesquiterpene lactone hymenoratin. The main characteristics that describe the mitotic arrest induced by *H. richardsonii* extract and hymenoratin are distorted mitotic spindles, a failure in chromosome congression, and foci of damaged DNA. This is the first time that the plant species *Hymenoxys richardsonii*, *Liatris punctata*, and *Arnica cordifolia*, together with the sesquiterpene lactone hymenoratin, are reported to induce an anti-mitotic activity. To understand better how natural products have become a source of scientific tools and medicines, and to discuss the possible mode of action of the natural compound hymenoratin, we will introduce how cells normally undergo mitosis and how diverse anti-mitotic agents, including sesquiterpene lactones, can inhibit this process.

1.1 Natural products as a source of bioactive molecules

Natural products represent an exceptional source of bioactive compounds. They are synthesized by organisms that have evolved to survive in an ecosystem where they compete with other organisms. There are many examples of the use of natural products for their medicinal properties or as science tools. However, only a small portion of natural products have been biologically investigated.

Medicinal use of natural products from plants, animals, or microorganism dates from prehistoric times. Pollen deposits in a grave from Shanidar (Iraqi Kurdistan) suggested that around 60,000 years ago Neanderthals were aware of medicinal properties of different plants (Solecki, 1975). Our ancestors made use of natural products to treat diverse afflictions. They would relieve pain by chewing on certain herbs or heal wounds by wrapping leaves around them (Ji et al., 2009). Different ancient medical texts describing usage of natural products have been found in the oldest civilizations, including clay tablets in Mesopotamia around 2600 BC; the Egyptian *Ebers Papyrus*, the Greek *Corpus Hippocraticum* from Hippocrates and *De Materia Medica* from Dioscorides, the Indian Ayurveda *Charaka Samhita*, or the traditional Chinese medicine with the *Wu Shi Er Bing Fang* (which translates to Prescriptions for Fifty-Two Diseases) (Ji et al., 2009). It was not until the 18th and 19th centuries that the identity of the active compounds in medicinal plants started to be investigated. Thanks to modern chemistry, active principles such as strychnine, morphine, atropine, and colchicine were purified (Newman et al., 2000). Importantly, with the advent of molecular biology and combinatorial chemistry, natural products took also a role in drug research and development making possible a more rational design of chemical compounds to target specific molecules (Ji et al., 2009).

It is especially in the areas of anti-infectives and anti-cancer drugs that natural products have had an impact. An extensive study compiling drugs that were approved from the beginnings of antitumor therapy from the late 1930s to 2014 revealed the leading role of natural products for drug development (Newman & Cragg, 2016). If the high-molecular-weight drugs (biologicals and vaccines) are removed from the 246 agents approved for anticancer therapy, 77% of the agents are natural small molecules, derivatives of them, or synthetic products that were developed to mimic natural products. Even if the synthetic mimics of natural products are not counted, 55% of the approved anticancer small molecules are natural products or their derivatives (Newman & Cragg, 2016). Examples from this list include the anticancer agents camptothecin, isolated from the Chinese tree *Camptotheca acuminate*; the *Vinca* alkaloids, vinblastine and vincristine, from the periwinkle *Catharanthus roseus*; paclitaxel, isolated from the bark of the Pacific Yew tree *Taxus brevifolia;* or the microbially-derived 7-hydroxy-staurosporin (UCN-01) isolated from a *Streptomyces* species (Newman et al., 2000). In the antibacterial field, 73% of the 112 small molecules approved from 1981 to 2014 account for natural products or derivatives (Newman & Cragg, 2016). Prominent examples in the anti-infective field are the antimalarial agent artemisinin from *Artemisia annua*, the β-lactam antibiotic penicillin from *Penicillium* fungi, or the macrolide erythromycin from *Streptomyces* bacteria (Newman et al., 2000).

Plants represent a source of bioactive compounds. Products of plant metabolism are categorized as primary and secondary metabolites. Primary metabolites are essential for plant growth and development and include carbohydrates, lipids, proteins, chlorophyll, and nucleic acids. Secondary metabolites, such as flavonoids, alkaloids, terpenoids, or saponins are defined as not having vital roles for plant development but more as defensive mechanisms that evolved from ecological

pressures (Hartmann, 1996). These secondary metabolites are critical for defensive strategies against herbivores or pathogens, plant-plant competitions, or beneficial interactions for the plant such as the attraction of pollinators or symbionts (Briskin, 2000). They also have protective roles against abiotic stressors such as changes in temperature, light intensity, UV exposure, among others (Pavarini et al., 2012). To promote survival, secondary metabolism in plants has evolved to interact with molecular targets that affect physiological functions in competing organisms (e.g. microorganisms, plants, animals) (Wink, 2003). These organisms, in turn, have developed adaptive responses, constituting what was termed animal-plant competition. This coevolutionary adaptation process resulted in the multitude of bioactive compounds that can be found in plants (Wöll et al., 2013). Hence, natural products have an inherent advantage over synthetic products in that they have been optimized throughout a process of natural evolution. Natural products may exert their action by synthesizing metabolites structurally similar to animal metabolites such as ligands, hormones, signal transduction molecules, or neurotransmitters, and may affect human physiology due to the resemblance in potential target sites (Briskin, 2000).

Natural products, thus, can potentially modulate cellular responses that are of interest in biological research or drug development. In one example, Lewis et al in 2017 screened a library of 657 actinomycetes bacterial strains to identify those that were bioactive and capable to alter the cell cycle and cell shape of fission yeast. Afterwards, they selected those that elicited specific phenotypes in fission yeast and studied the possible modes of action by analysis of diverse proteins involved (Lewis et al., 2017). With this study, the authors identified the pathways controlling yeast cell shapes, exemplifying how natural products can increase the number of experimental methodologies available to investigate biological mechanisms. The rationale for this approach was

the natural competition between bacteria (prokaryotic) and fungi (eukaryotic), two organisms with different mechanisms that determine their cell morphology and cell cycle. Eukaryotic-specific processes could be targets for bacterially synthesized secondary metabolites (Ho & Nodwell, 2016). Therefore, looking at natural products would likely provide a better source of bioactive compounds than a library of compounds randomly synthesized because evolution would have naturally selected, in this case, for prokaryotes able to produce antifungal agents (Lewis et al., 2017). Synthetic and medicinal chemists have largely benefited from natural products by understanding how organisms use enzymatic processes to synthesize active compounds. They try to mimic them synthetically to make ligands for cellular targets in drug development (Clardy & Walsh, 2004). Several examples of research assets using natural products can be found in Carlson 2010, and Chang and Kwon 2016. They presented the contributions of screening natural products to find new drug targets and their functions, as well as their diverse uses as molecular probes in biological research beyond drug development. For instance, studies with the natural product trapoxin, isolated from the fungus *Helicoma ambiens,* informed of the relationship between histone deacetylases and transcriptional regulation and cell cycle progression (Taunton et al., 1996; Carlson, 2010). Terpestacin, from the fungus *Embellisia chlamydospora*, was found to bind to a protein called ubiquinol cytochrome c reductase, which for the first time was reported to play a critical role in angiogenesis (i.e. new blood vessel growth by endothelial cells) via reactive oxygen species-mediated signaling (Jung et al., 2010) (Chang & Kwon, 2016). Thanks to the use of natural products as scientific tools more is known about biological processes that used to be obscure. The discovery of new small molecules of natural origin or new biological properties from already

described natural products is important to deconvolute biochemical mechanisms of scientific interest.

These is clear evidence of the importance of research of natural products; nonetheless, only a small percentage of natural products and plants have been investigated for their bioactive properties. Miller in 2011 estimated that between 540 to 23,490 new drugs remain to be found from plants, considering that discovery of 135 natural drugs resulted from the only 2,000 plant species that were chemically described or from about 60,000 species that had been screened in a total estimated of 300,000 to 350,000 plant species existing in the world (Miller, 2011). A great uncertainty on these estimates is whether all species have additive potential to synthesize new compounds or whether they are somewhat chemically redundant. However, most plant screenings are conducted for a specific bioactivity and other uses are not investigated (Miller, 2011). Moreover, this estimation is only taking into account natural products derived from plants and approved for medicinal purposes. The potential would be higher if we consider other natural sources, such as microorganisms, and not only the use of their metabolites directly as drugs but as guides for chemists to synthesize new drug candidates or as molecular probes for biomedical research. It is difficult to know the magnitude of the possibilities in investigating natural products, but it is likely that a large number of active compounds remain to be discovered and studied for their potential ability to influence human physiology.

These facts led us to believe that nature is an excellent source of active compounds where we could find agents that affect biological processes such as cell division. Plants represent an accessible and still largely uninvestigated supply with a long history of applications.

1.1.1 Canadian prairie plants

The prairie ecozone is one of the fifteen ecozones of Canada. It extends from the western edge of Alberta to the eastern edge of Manitoba and has its base in the Canada-United States border, comprising the northern extension of the Great Plains of North America (ESWG, 1996). It is characterized by relatively little topographic relief, grasslands, limited forests, and a sub-humid to semiarid climate (ESWG, 1996). Despite a strong presence of agricultural activity, very little research has been done regarding the potential biological activities of its native flora.

Sessile plants have developed specialized secondary metabolism throughout their existence and coevolution with other species to defend against herbivory and other biotic and abiotic stresses and promote ecological survival (Wink, 2003) (Wöll et al., 2013). Therefore, it is likely that an abundant diversity of bioactive compounds can be found in prairie plants. In agreement with this hypothesis, many plant species of western Canada, including the prairies, are known to cause livestock poisoning (Majak et al., 2008). An example of this comes from the genus *Thermopsis*, producing several alkaloids and flavonoids that were found to be toxic to cattle and to cause human poisoning (Keeler & Baker, 1990; McGrathHill & Vicas, 1997). Posterior analysis of the commonly known Buffalo bean, *Thermopsis rhombifolia*, resulted in the discovery of certain bioactivities with potential anticancer properties of this plant (Kernéis et al., 2015). Moreover, North American Aboriginal communities have been using prairie plants to treat many diseases (Kindscher, 1992). In 2012, Uprety et al. made an extensive analysis of 49 publications related with the medicinal uses of North American Aboriginal people, including Canada's First Nations, Metis, and Inuit, and reported 546 medicinal plant taxa used by Aboriginal people of the Canadian boreal forest (Uprety et al., 2012). For instance, the locally known Goat's rue plant, *Tephrosia virginiana,*

has been used by different North American Aboriginal communities to treat cough, lassitude, or worms (Kindscher, 1992). Recently, it was discovered that this plant contains the flavonoid deguelin, a compound that induces apoptosis and regulation of signaling pathways that was suggested to be useful for breast cancer therapy (Suh et al., 2013).

The medicinal use of prairie plants by Canadian Aboriginal people, the reported livestock poisoning attributed to prairie plant feeding, and the coevolution of these plants with mammal herbivores supports the hypothesis that there are plant species in Canada that produce bioactive compounds. Its study could lead to the discovery of a new compound or a known compound with a novel bioactivity that can be of interest for biological or medicinal research.

1.1.2 Asteraceae family

The Asteraceae, also known as Compositae or Daisy family, is the largest family of flowering plants containing 32,913 species in 1,911 genera distributed around the world except for Antarctica (The plant list, 2013). It was taxonomically divided into 11 subfamilies and 35 tribes by Panero and Funk in 2002 after analysis of DNA sequence data of chloroplasts genes (Panero & Funk, 2002). It is a monophyletic family characterized by a special type of inflorescence called pseudanthium, flower head, or capitulum, where disc and ray florets are arranged on a receptacle in centripetally and are surrounded by bracts that form the involucre. This family presents anthers fused in a ring with the pollen pushed out by the style, and achenes (cypselas) usually with a pappus (Funk, 2009) (**Figure 1**). There is a large variation among members, existing annual and perennial herbs, shrubs, vines, or trees, and although they are more common in open areas, they can be found in almost every type of habitat from forests to high elevation grasslands (Funk, 2009).

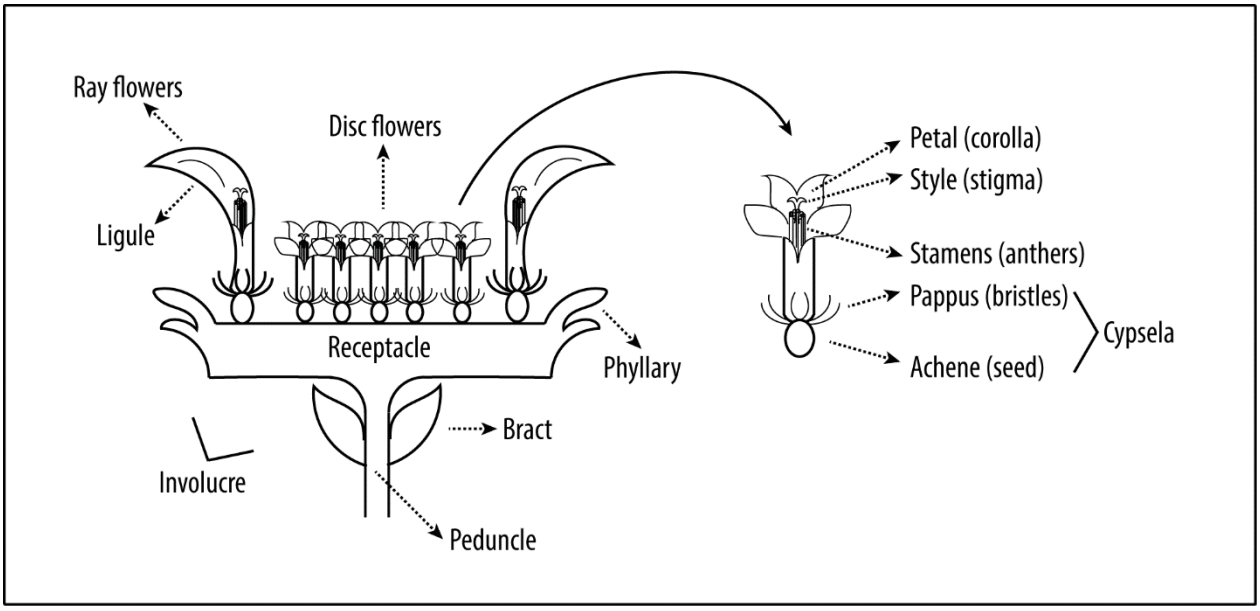

Figure 1. Botanical description of Asteraceae flower heads . Key morphological features that characterize the flower heads of members of this family are shown.

The best-known species of this family are the Sunflower (*Helianthus annuus*), Lettuce (*Lactuca sativa*), Chicory (*Cichorium intybus*), Artichoke (*Cynara scolymus*), and many ornamental flowers such as Chrysanthemums or Dahlias. In the medicinal area one of the most important example is *Artemisia annua,* which has been used in the Chinese traditional medicine as a remedy for fevers, headaches, and gastrointestinal problems. It is the source of artemisinin and its derivatives artesunate and dihydroartemisinin, which are major antimalarial drugs (Funk, 2009). The discovery that this plant was able to inhibit the parasite growth and the following isolation of the sesquiterpene lactone artemisinin from it is attributed to Tu Youyou (Miller & Su, 2011). For this discovery, Tu was awarded the Nobel Prize in 2015 since it represented an important medical advance for the treatment of malaria disease (Tu, 2016).

Documents of the Flora of North America have recorded 2413 Asteraceae species and 418 genera for the United States and Canada (FNA, 1993 +). In Canada, the Database of Vascular Plants of Canada (VASCAN) currently reports 691 species of the Asteraceae family from 163 genera and 19 tribes of the 4 subfamilies Asteroideae, Cichorioideae, Carduoideae, and Mutisioideae distributed across the country. It includes plants having one or more of five statuses. The status of *native* is given when a taxon is present in a region as a result of natural processes and not human intervention. Taxa are considered *introduced* if they established after European colonization for accidental or deliberate human activity. The status of *ephemeral* refers to taxa that recur in the wild in a near-annual basis, usually from cultivation, but is not permanent. The VASCAN database catalogues a taxon as *excluded* when it has been reported from a region but it is not established, or it was erroneously determined, and as *extirpated* if it was native to the region but it is now considered eradicated (Brouillet et al., 2010). From these 691 species, 332 are present in the prairie region (provinces of Alberta, Saskatchewan, and Manitoba) from 106 genera and 18 tribes. 245 species are considered native of this region, 58 introduced, 27 excluded, and 2 ephemerals. In Alberta, there are 270 species from 91 genera and 16 tribes from the Asteraceae family: 207 natives, 51 introduced, 11 excluded, and 1 ephemeral. **Table 1** presents all the species of the Asteraceae family present in Canada collected from the VASCAN database. It is indicated in brackets if the species are present in the prairies as well as their status in this region. Presence in the prairies can refer to either Alberta, Saskatchewan, Manitoba, or combinations of them.

Members of the Asteraceae family produce a wide range of secondary metabolites including: monoterpenes, diterpenes, triterpenes, sesquiterpenes and sesquiterpene lactones, polyacetylenes, flavonoids, phenolic acids, benzofurans, and coumarins (Zdero & Bohlmann, 1990). They do not

produce major classes of alkaloids, only pyrrolizidine alkaloids are found in Senecioneae and Eupatorieae tribes. The accumulation of lactonized sesquiterpenes and polyacetylenes, as well as the presence of many highly oxidized compounds, have been recognized as unique characters and a chemical signature for most of the members of this family (Zdero & Bohlmann, 1990). Therefore, these compounds are likely to be responsible for the medicinal uses that have been attributed to this family.

Table 1. Asteraceae family members in Canada according to the database of vascular plants (VASCAN). The presence and status within the Prairie region is indicated in parenthesis as follows: present (P), native (N), introduced (I), ephemeral (EP), or excluded (EX).

Subfamily	Tribe	Genus	Species
Asteroideae	Anthemideae	*Achillea*	*A. alpine (P-N), A. borealis (P-N), A. distans, A. filipendulina, A. millefolium, A. ptarmica, A. setacea.*
		Anthemis	*A. arvensis (P-I), A. cotula (P-I).*
		Arctanthemum	*A. arcticum (P-N).*
		Artemisia	*A. absinthium (P-I), A. frigida (P-N), A. woodii, A. abronatum (P-I), A. alaskana, A. annua, A. biennis (P-I), A. douglasiana, A. globularia, A. glomerata, A. hyperborea (P-N), A. laciniata, A. lactiflora, A. longifolia (P-N), A. ludoviciana (P-N), A. michauxiana (P-N), A. norvegica (P-N), A. pontica (P-I), A. stelleriana, A. suksdorfii, A. tilesii (P-N), A. vulgaris (P-I), A. borealis (P-N), A. campestris (P-N), A. dracunculus (P-N), A. cana (P-N), A. tridentata (P-N), A. tripartita.*
		Chrysanthemum	*C. coccineum.*
		Cladanthus	*C. mixtus.*
		Cota	*C. tinctoria (P-I).*
		Cotula	*C. australis, C. coronopifolia.*
		Glebionis	*G. coronaria, G. segetum.*
		Hulteniella	*H. integrifolia.*
		Leucanthemella	*L. serotine.*
		Leucanthemum	*L. lacustre, L. vulgare (P-I).*
		Matricaria	*M. chamomilla (P-I), M. discoidea (P-I).*
		Soliva	*S. sessilis.*
		Tanacetum	*T. balsamita (P-I), T. bipinnatum (P-N), T. parthenium (P-I), T. vulgare (P-I).*
		Tripleurospermum	*T. inodorum (P-I), T. maritimum.*
	Astereae	*Almutaster*	*A. pauciflorus (P-N).*
		Aster	*A. alpinus (P-N).*
		Baccharis	*B. halimifolia.*
		Bellis	*B. perennis.*
		Boltonia	*B. asteroides (P-N).*
		Canadanthus	*C. modestus (P-N)*
		Chrysothamnus	*C. viscidiflorus.*
		Dieteria	*D. canescens (P-N).*
		Doellingeria	*D. umbellate (P-N).*
		Ericameria	*E. bloomeri, E. nauseosa (P-N).*
		Erigeron	*E. acris (P-N), E. alpiniformis, E. annuus (P-N), E. aureus (P-N), E. borealis, E. caespitosus (P-N), E. canadensis (P-I), E. compositus (P-N), E. corymbosus, E. denalii, E. divaricatus, E. divergens (P-N), E. elatus (P-N), E. evermannii (P-EX), E. filifolius, E. flagellaris (P-N), E. formosissimus (P-EX), E. glabellus (P-N), E. glacialis (P-N), E. grandiflorus (P-N), E. humilis (P-N), E. hyperboreus, E. hyssopifolius (P-N), E. lackschewitzii (P-N), E. lanatus (P-N), E.*

			leibergii, E. linearis, E. lonchophyllus (P-N), E. muirii, E. nivalis (P-N), E. ochroleucus (P-N), E. pacalis, E. pallens (P-N), E. peregrinus (P-N), E. philadelphicus (P-N), E. poliospermus, E. porsildii, E. pulchellus, E. pumilus (P-N), E. purpuratus, E. radicatus (P-N), E. salishii, E. speciosus (P-N), E. strigosus (P-N), E. trifidus (P-N), E. uniflorus, E. yukonensis, E. arthurii (P-N).
		Eucephalus	*E. engelmannii (P-N), E. paucicapitatus.*
		Eurybia	*E. compacta, E. conspicua (P-N), E. divaricata, E. macrophylla, E. merita, E. radula, E. radulina, E. schreberi, E. sibirica (P-N).*
		Euthamia	*E. caroliniana, E. graminifolia (P-N), E. gymnospermoides, E. occidentalis.*
		Grindelia	*G. hirsutula (P-N), G. squarrosa (P-N).*
		Gutierrezia	*G. sarothrae (P-N).*
		Heterotheca	*H. villosa (P-N).*
		Ionactis	*I. linariifolia, I. stenomeres.*
		Machaeranthera	*M. tanacetifolia (P-N).*
		Nestotus	*N. macleanii.*
		Oclemena	*O. acuminata, O. nemoralis, O. blakei.*
		Pityopsis	*P. falcata.*
		Pyrrocoma	*P. carthamoides, P. lanceolate (P-N), P. uniflora (P-N).*
		Sericocarpus	*S. rigidus.*
		Solidago	*S. houghtonii, S. ohioensis, S. ptarmicoides (P-N), S. riddellii (P-N), S. rigida (P-N), S. bernardii (P-N), S. krotkovii, S. lutescens (P-N), S. bicolor (P-EX), S. asperula, S. bartramiana, S. beaudryi, S. calcicola, S. erskinei, S. arguta, S. patula, S. caesia, S. flexicaulis, S. macrophylla, S. bellidifolia (P-EX), S. chlorolepsis, S. gillmanii, S. glutinosa (P-N), S. ontarioensis, S. racemosa, S. randii, S. simplex (P-EX), S. juncea (P-N), S. missouriensis (P-N), S. sempervirens, S. uliginosa (P-N), S. mollis (P-N), S. nemorallis (P-N), S. radula, S. leiocarpa, S. multiradiata (P-N), S. hispida (P-N), S. jejunifolia (P-N), S. pallida, S. puberula, S. rigidiuscula, S. speciosa, S. squarrosa, S. petiolaris, S. altissima (P-N), S. brendae, S. canadensis (P-N), S. elongata, S. fallax, S. gigantean (P-N), S. lepida (P-N), S. latissimifolia, S. odora, S. rugosa, S. ulmifolia.*
		Stenotus	*S. armerioides (P-N).*
		Symphyotrichum	*S. ascendens (P-N), S. subulatum, S. ciliatum (P-N), S. frondosum, S. laurentianum, S. chilense (P-EX), S. cusickii (P-N), S. eatonii (P-N), S. foliaceum (P-N), S. hallii, S. spathulatum (P-N), S. subspicatum (P-N), S. anticostense, S. boreale (P-N), S. ciliolatum (P-N), S. cordifolium (P-N), S. dumosum, S. firmum (P-N), S. laeve (P-N), S. lanceolatum (P-N), S. lateriflorum (P-N), S. novi-belgii (P-EX), S. ontarionis, S. oolentangiense, S. parviceps, S. pilosum, S. praealtum (P-EX), S. prenanthoides, S. puniceum (P-N), S. racemosum, S. robynsianum (P-N), S. shortii, S. tradescantii, S. undulatum, S. urophyllum, S. subgeminatum, S. tardiflorum, S. campestre (P-N), S. ericoides (P-N), S. falcatum (P-N), S. nahanniense, S. novae-angliae (P-N), S. patens, S. pygmaeum, S. sericeum (P-N), S. yukonense, S. amethystinum.*
		Tonestus	*T. lyallii (P-N).*
		Townsendia	*T. condensate (P-N), T. exscapa (P-N), T. hookeri (P-N), T. parryi (P-N).*
		Xanthisma	*X. grindelioides, X. spinulosum, X. texanum (EXC.NP)*

	Bahieae	*Hymenopappus*	*H. filifolius (P-N).*
		Picradeniosis	*P. oppositifolia (P-I).*
	Calendulae	*Calendula*	*C. arvensis (P-EX), C. officinalis.*
		Dimorphotheca	*D. sinuata.*
	Chaenactideae	*Chaenactis*	*C. douglasii (P-N).*
	Coreopsideae	*Bidens*	*B. amplissima (P-I), B. aristosa, B. beckii (P-N), B. bipinnata, B. cernua (P-N), B. connata, B. discoidea, B. eatonii, B. frondosa (P-N), B. heterodoxa, B. hyperborea, B. pilosa, B. polylepsis, B. trichosperma, B. tripartite (P-N), B. vulgate (P-N).*
		Coreopsis	*C. tinctorial (P-N), C. grandiflora, C. lanceolata, C. rosea, C. tripteris, C. verticillata.*
		Cosmos	*C. bipinnatus.*
		Thelesperma	*T. subnudum (P-N).*
	Eupatorieae	*Ageratina*	*A. altissima (P-EX).*
		Brickellia	*B. grandifolia (P-N), B. oblongifolia.*
		Conoclinium	*C. coelestinum (P-EP).*
		Eupatorium	*E. altissimum, E. cannabinum, E. perfoliatum (P-N), E. serotinum.*
		Eutrochium	*E. dubium, E. fistulosum, E. maculatum (P-N), E. purpureum (P-EX).*
		Liatris	*L. aspera (P-EX), L. cylindracea, L. ligulistylis (P-N), L. pilosa, **L. punctata** (P-N), L. pycnostachya, L. spicata, L. gladewitzii, L. spheroidea.*
		Mikania	*M. scandens.*
	Gnaphalieae	*Anaphalis*	*A. margaritaceae (P-N).*
		Antennaria	*A. alpine (P-N), A. anaphaloides (P-N), A. aromatica (P-N), A. corymbose (P-N), A. densifolia, A. dimorpha (P-N), A. flagellaris, A. friesiana (P-EX), A. howellii (P-N), A. lanata (P-N), A. luzuloides (P-N), A. media (P-N), A. microphylla (P-N), A. monocephala (P-N), A. neglecta (P-N), A. parlinii (P-N), A. parvifolia (P-N), A. plantaginifolia (P-EX), A. pulchella (P-EX), A. pulcherrima (P-N), A. racemose (P-N), A. rosea (P-N), A. stenophylla, A. umbrinella (P-N), A. erigeroides.*
		Filago	*F. pyramidata, F. vulgaris.*
		Gamochaeta	*G. purpurea (P-N). G. ustulata.*
		Gnaphalium	*G. palustre (P-N), G. uliginosum (P-I).*
		Logfia	*L. arvensis (P-I), L. minima.*
		Omalotheca	*O. norvegica, O. supina, O. sylvatica.*
		Pseudognaphalium	*P. macounii (P-N), P. obtusifolium, P. stramineum, P. thermale (P-N).*
		Psilocarphus	*P. brevissimus (P-N), P. elatior (P-EX), P. tenellus.*
	Helenieae	*Gaillardia*	***G. aristata** (P-N), G. pulchella (P-I).*
		Helenium	*H. autumnale (P-N), H. flexuosum.*
		Hymenoxys	***H. richardsonii** (P-N).*
		Tetraneuris	***T. acaulis** (P-N), T. herbacea.*
	Heliantheae	*Acanthospermum*	*A. hispidum.*
		Ambrosia	*A. acanthicarpa (P-N), A. artemisifolia (P-N), A. chamissonis, A. psilostachya (P-I), A. trifida (P-N), A. helenae.*
		Balsamorhiza	*B. careyana, B. deltoidea, **B. sagittata** (P-N), B. hookeri.*

		Cyclachaena	*C. xantiifolia (P-N).*
		Echinacea	*E. angustifolia (P-N), E. pallida, E. purpurea.*
		Eclipta	*E. prostrata.*
		Galinsoga	*G. parviflora (P-I), G. quadriradiata (P-I).*
		Guizotia	*G. abyssinica.*
		Helianthella	*H. uniflora.*
		Helianthus	***H. annuus*** *(P-N), H. cusickii, H. decapetalus, H. divaricatus, H. giganteus (P-EX), H. grosseserratus, H. hirsutus, H. maximiliani (P-N), H. mollis, H. nuttallii (P-N), H. pauciflorus (P-N), H. petiolaris (P-N), H. strumosus, H. tuberosus (P-N), H. laetiflorus (P-EX).*
		Heliosis	*H. helianthoides (P-N).*
		Iva	*I. axillaris (P-N), I. frutescens.*
		Jaumea	*J. carnosa.*
		Ratibida	*R. columnifera (P-N), R. pinnata.*
		Rudbeckia	*R. laciniata (P-N), R. fulgida, R. grandiflora, R. hirta (P-N), R. trilobal.*
		Silphium	*S. integrifolium, S. laciniatum, S. perfoliatum, S. terebinthinaceum.*
		Verbesina	*V. alternifolia.*
		Wyethia	*W. amplexicaulis.*
		Xanthium	*X. spinosum (P-EP), X. strumarium (P-N).*
	Inuleae	*Dittrichia*	*D. graveolens.*
		Inula	*I. britannica, I. helenium (P-I), I. racemosa.*
		Pluchea	*P. odorata.*
	Madieae	*Anisocarpus*	*A. madioides.*
		Arnica	*A. angustifolia (P-N), A. chamissonis (P-N),* ***A. cordifolia*** *(P-N), A. fulgens (P-N), A. gracilis (P-N), A griscomii, A. lanceolate (P-N), A. latifolia (P-N), A. lessingii, A. lonchophylla (P-N), A. longifolia (P-N), A. louiseana (P-N), A. mollis (P-N), A. nevadensis, A. ovata (P-N), A. parryi (P-N), A. rydbergii (P-N), A. sororia (P-N).*
		Blepharipappus	*B. scaber.*
		Eriophyllum	*E. lanatum.*
		Hemizonella	*H. minima.*
		Lasthenia	*L. glaberrima, L. maritima.*
		Layia	*L. glandulosa.*
		Madia	*M. elegans, M. exigua, M. glomerata (P-I), M. gracilis, M. sativa.*
	Polymnieae	*Polymnia*	*P. canadensis.*
	Senecioneae	*Arnoglossum*	*A. plantagineum.*
		Cacaliopsis	*C. nardosmia.*
		Crocidium	*C. multicaule.*
		Doronicum	*D. orientale, D. pardalianches.*
		Erechtites	*E. hieraciifolius (P-EX).*
		Jacobaea	*J. vulgaris (P-I).*
		Luina	*L. hypoleuca.*

		Packera	*P. aurea (P-N), P. cana (P-N), P. conterminal (P-N), P. crocata, P. glabella, P. heterophylla (P-N), P. hyperborealis (P-EX), P. indecora (P-N), P. macounii, P. obovata, P. ogotorukensis, P. pauciflora (P-N), P. paupercula (P-N), P. plattensis (P-N), P. pseudaurea (P-N), P. schweinitziana, P. streptanthifolia (P-N), P. subnuda (P-N), P. tridenticulata (P-EX), P. werneriifolia.*
		Petasites	*P. frigidus (P-N), P hybridus, P. japonicus.*
		Senecio	*S. elmeri, S. eremophilus (P-N), S. fremontii (P-N), S. hydrophiloides (P-N), S. hydrofilus, S. integerrimus (P-N), S. lugens (P-N), S. megacephalus (P-N), S. pseudoarnica, S. serra, S. sheldonensis, S. squalidus, S. sylvaticus, S. triangularis (P-N), S. viscosus (P-I), S. vulgaris (P-I).*
		Sinosenecio	*S. newcombei.*
		Tephroseris	*T. frigida, T. kjellmanii, T. lindstroemii, T. palustris (P-N), T. yukonensis.*
		Tetradymia	*T. canescens.*
		Tussilago	*T. farfara.*
	Tageteae	*Dyssodia*	*D. papposa (P-I).*
		Tagetes	*T. erecta, T. minuta.*
Carduoideae	Cardueae	*Amberboa*	*A. moscata.*
		Arctcium	*A. lappa (P-I), A. minus (P-I), A. tomentosum (P-I), A. mixtum, A. nothum.*
		Carduus	*C. acanthoides, C. crispus, C. nutans (P-I), C. orthocephalus.*
		Carthamus	*C. criticus, C. tinctorius (P-I).*
		Centaurea	*C. benedicta, C. calcitrapa, C. cyanus (P-I), C. diffusa (P-I), C. jacea, C. macrocephala, C. melitensis, C. montana, C. nigra, C. nigrescens, C. scabiosa, C. solstitialis (P-I), C. stoebe (P-I), C. moncktonii, C. psammogena.*
		Cirsium	*C. arvense (P-I), C. brevistylum, C. canescens, C. discolor (P-N), C. drummondii (P-N), C. edule, C. flodmanii (P-N), C. foliosum (P-N), C. helenioides, C. hookerianum (P-N), C. muticum (P-N), C. palustre, C. pitcheri, C. pumilum, C. scariosum (P-N), C. undulatum (P-N), C. vulgare (P-I), C. vancouverense.*
		Echinops	*E. exaltatus, E. sphaerocephalus (P-EP).*
		Onopordum	*O. acanthium (P-EX).*
		Rhaponticum	*R. repens (P-I)*
		Saussurea	*S. amara (P-EX), S. Americana (P-N), S. angustifolia, S. nuda (P-N)*
		Silybum	*S. marianum (P-I).*
Cichorioideae	Cichorieae	*Agoseris*	*A. aurantiaca (P-N), A. glauca (P-N), A. grandiflora, A. heterophylla, A. parviflora (P-EX), A. agrestis (P-EX), A. elata.*
		Arnoseris	*A. minima.*
		Askellia	*A. elegans (P-N), A. pygmaea (P-N).*
		Chondrilla	*C. juncea.*
		Cichorium	*C. endivia (P-EX), C. intybus (P-I).*
		Crepis	*C. acuminata, C. atribarba (P-N), C. biennis, C. capillaris (P-I), C. intermedia (P-N), C. modocensis (P-EX), C. nicaeensis, C. occidentalis (P-N), C. pulchra, C. runcinate (P-N), C. tectorum (P-I), C. vesicaria.*

		Helminthotheca	*H. echioides (P-I).*
		Hieracium	*H. albiflorum (P-N), H. alpinum, H. groenlandicum, H. gronovii, H. lachenalii, H. laevigatum, H. longiberbe, H. longipilum, H. murorum, H. paniculatum, H. prenanthoides, H. robinsonii, H. sabaudum, H. scabrum, H. scouleri (P-N), H. triste (P-N), H. umbellatum (P-N), H. venosum, H. vulgatum, H. fassettii, H. grohii, H. marianum.*
		Hypochaeris	*H. glabra, H. radicata.*
		Krigia	*K. biflora (P-N), K. dandelion, K. virginica.*
		Lactuca	*L. biennis, L. canadensis (P-EX), L. floridana (P-N), L. hirsuta, L. ludoviciana (P-N), L. saligna, L. sativa (P-EX), L. serriola (P-I), L. virosa (P-EX).*
		Lapsana	*L. communis (P-I).*
		Leontodon	*L. hispidus, L. saxatilis.*
		Lygodesmia	*L. juncea (P-N).*
		Microseris	*M. bigelovii, M. borealis, M. nutans (P-N).*
		Mulgedium	*M. pulchellum (P-N).*
		Mycelis	*M. muralis.*
		Nabalus	*N. alatus (P-N), N. albus (P-N), N. altissimus, N. asper, N. racemosus (P-N), N. sagittatus (P-N), N. trifoliolatus, N. mainensis.*
		Nothocalais	*N. cuspidate (P-N), N. troximoides.*
		Picris	*P. hieracioides.*
		Pilosella	*P. aurantiaca (P-I), P. caespitosa (P-I), P. flagellaris, P. glomerata, P. lactucella, P. officinarum, P. piloselloides, P. floribunda.*
		Scorzoneroides	*S. autumnalis.*
		Shinnersoseris	*S. rostrate (P-N).*
		Sonchus	*S. arvensis (P-I), S. asper (P-I), S. oleraceus (P-I), S. palustris.*
		Stephanomeria	*S. lactucina, S. runcinate (P-N), S. tenuifolia (P-N).*
		Taraxacum	*T. alaskanum, T. carneocoloratum, T. ceratophorum (P-N), T. erythrospermum (P-I), T. holmenianum, T. hyparcticum, T. lapponicum (P-EX), T. latilobum (P-EX), T. laurentianum, T. officinale (P-I), T. phymatocarpum, T. scopulorum (P-N), T. palustre.*
		Tragopogon	*T. dubius (P-I), T. mirus, T. porrifolius (P-I), T. pratensis (P-I), T. crantzii, T. mirabilis, T. neohybridus.*
		Uropappus	*U. lindleyi.*
	Vernonieae	*Vernonia*	*V. fasciculata (P-N), V. gigantea, V. missurica.*
Mutisioideae	Mutisieae	*Adenocaulon*	*A. bicolor (P-N).*

1.2 Sesquiterpene lactones

1.2.1 Chemistry and biosynthesis of sesquiterpene lactones

Sesquiterpene lactones (SLs) are compounds with a 15-carbon backbone that includes a lactone group. They are products of the secondary metabolism of plants. Its biosynthesis starts from the union of three isoprene units, which are 5-carbon derivatives of the mevalonic acid, creating an acyclic farnesyl pyrophosphate (FPP), the simplest sesquiterpene structure (Seaman, 1982). This FPP can cyclize to produce one of the main precursors of the SLs: a ten-membered ring with an isopropyl sidechain called germacrane. The process of lactonization occurs as a consequence of two chemical reactions: first, an oxidation of the germacrane sidechain creates a carboxyl function in C-12. Second, a hydroxylation at either C-6 or C-8 of the ten-membered ring subsequently forms an ester between the carboxyl and the hydroxyl groups, introducing an α-methylene-γ-lactone to the compound now called SL (**Figure 1**) (Seaman, 1982). However, not every SL contains the α-methylene group. Examples of SLs lacking this group include cadinane, isocedrene, or eremophilane-derived SLs (Seaman, 1982). In germacrane-derived SLs, the most relevant SLs for this thesis, the basic structure formed after lactonization is the C-6 or C-8 germacranolide (depending on the site of lactonization) and from it, a large number of diverse SLs can be made. Guaianolides, pseudoguaianolides, and eudesmanolides, together with the precursor germacranolide are the main classes of SLs (**Figure 2**). Eudesmanolides have two fused 6-membered rings, guaianolides have a 7 and a 5-membered ring and a methyl group at C-4, and pseudoguaianolides have the same 7 and 5-membered rings but the methyl group is at C-5. All contain a fused 5-membered lactone group (Chadwick et al., 2013).

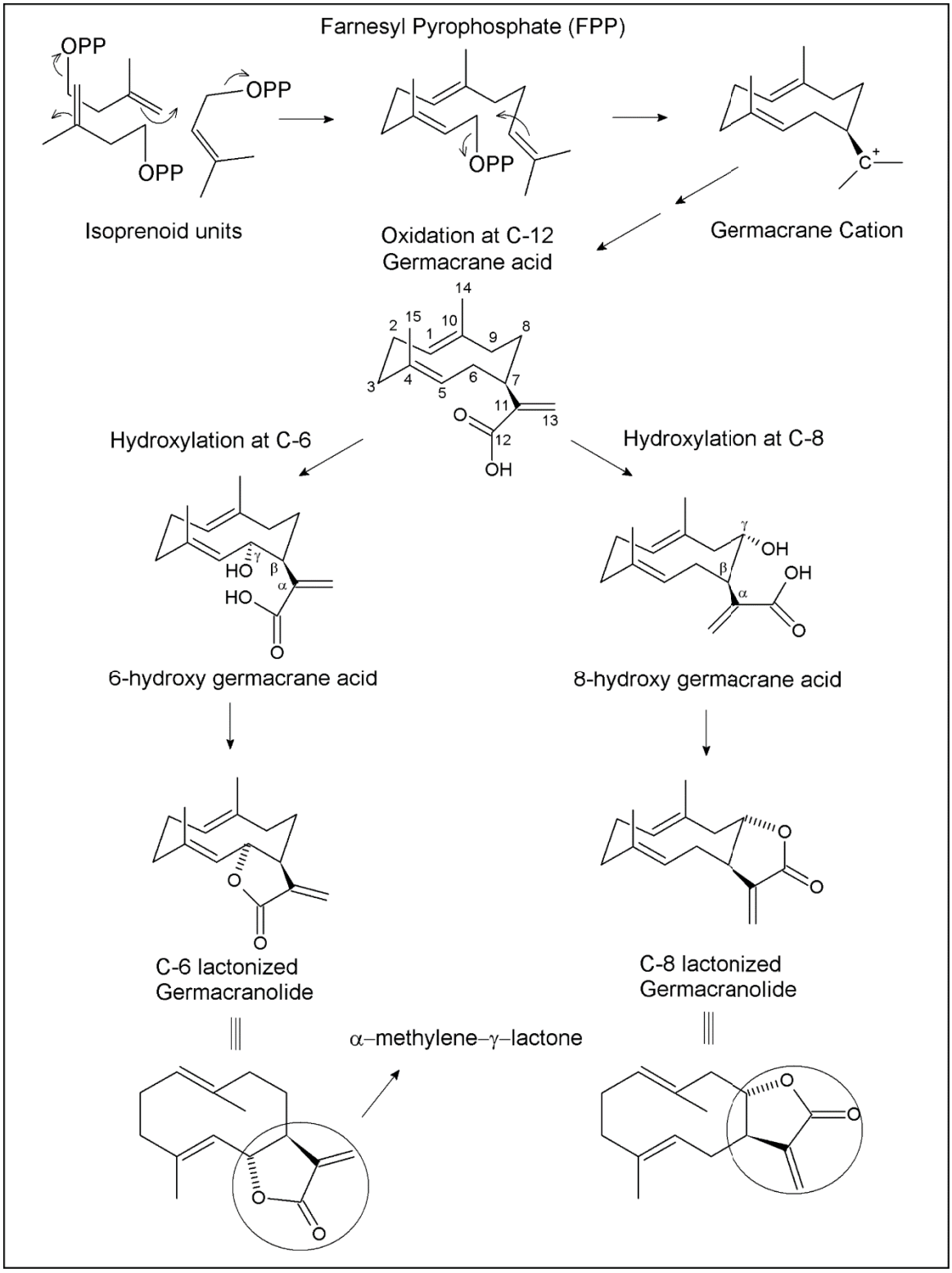

Figure 2. Sesquiterpene lactones biogenesis from isoprenoid pyrophosphate (OPP) units using the germacrane precursor (from Seaman, 1986).

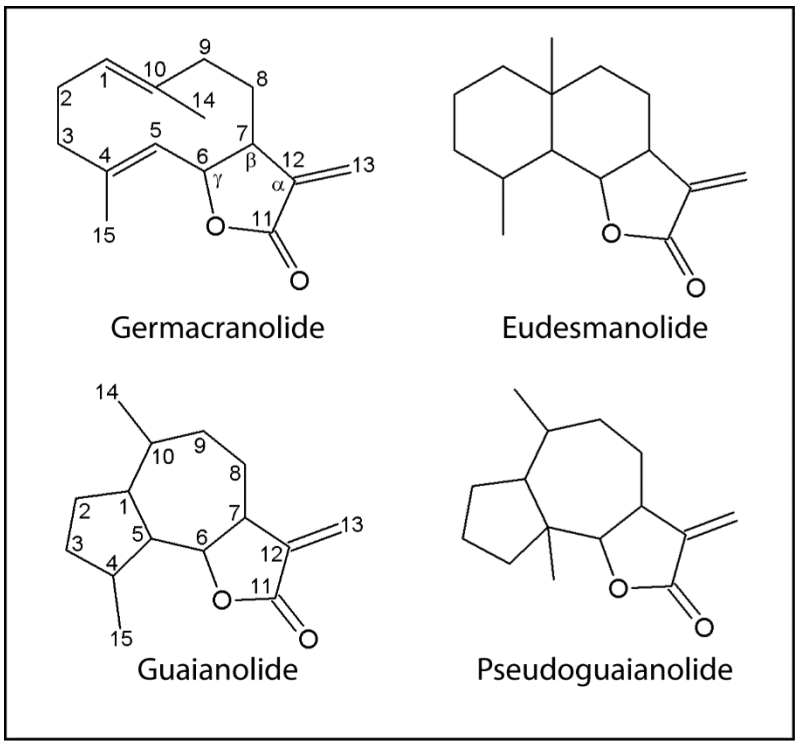

Figure 3. Main classes of sesquiterpene lactone structures.

1.2.2 Biological activities in plants and other organisms

Sesquiterpene lactones have been reported to be present in many plant families such as Apiaceae, Magnoliaceae, Acanthaceae, Solanaceae, Araceae, Euphorbiaceae, amongst others (Rodriguez et al., 1976; Chadwick et al., 2013), but they can be found almost ubiquitously in the Asteraceae family. SLs are found predominantly in tissues attractive to herbivores, such as leaves, phyllaries, and achenes, stored in glandular trichomes or laticifers to be secreted in the surface of these organs (Seaman, 1982; Chadwick et al., 2013). A range of biological activities has been attributed to them, from plant-plant interactions, insect feeding deterrent, antibiotic, antifungal, and antiparasitic, to allergenic, toxic, and antiproliferative effects in animal and human cells. An example of interaction of these compounds with other plants was observed with several SLs from the *Helianthus*

genus, which were shown to negatively influence the root and shoot length and decrease the germination rate of *Lactuca sativa, Lepidium sativum and Lycopersicon esculentum* (Macías et al., 1996). The anti-feedant capacity, as an herbivory defense response, has been shown in diverse studies. In a study performed with six different species of moth, researchers observed that the feeding behaviour of these moths was reduced greatly and proportionally after exposure to media containing increasing amounts of the germacranolide glaucolide-A, the major SL of *Vermonia* species (Burnett et al., 1974). Regarding the inhibition of infective organisms it has been demonstrated, for example, that the germacranolides mikanolide and dihydromikanolide inhibit the growth of bacterium *Staphylococcus aureus* and yeast *Candida albicans*; the helenanolide helenalin exhibits activity against the fungi *Trichophyton mentagrophytes*, *T. acriminatum* and *Epidermophyton* sp.; and artemisinin has the capacity to incapacitate or kill the parasite *Plasmodium falciparum* (Rodriguez et al., 1976). In vertebrates, it is well documented the poisonous effects in livestock foraging in plants from the Asteraceae family containing SL, such as the bitterweed *Hymenoxys odorata* with its toxic hymenovin or the *Geigeria* species containing vermeerin (Hardy et al., 1931) (Anderson et al., 1967). It has been reported that many plants or plant products containing SLs cause contact dermatitis in humans. Examples of this effect are the weeds from *Parthenium* genus with its major allergen the pseudoguianolide parthenin, or the reported allergies from the horticultural plant Chrysanthemum, the vegetable Chicory, or perfumes using *Saussurea* extracts (Rodriguez et al., 1976).

All these effects in microorganisms, insects, and mammals are evidence that sesquiterpene lactones are compounds with a great ability to influence the physiology of other organisms in contact with them.

To understand how these compounds can exert their activities, researchers have tested SLs with different chemical structures in cytotoxic assays. Here, the proportion of death cells after treatment with SLs is measured and compared among the different structures. This allows scientists to have a better insight of the chemical groups that are required to cause cytotoxicity or that can increase or decrease the toxicity.

1.4.3 Structure-Activity Relationship of Sesquiterpene Lactones

Early studies from Hartwell and Abbott (1969) linked SLs' activity to the α-methylene-γ-lactone (αMγL) group in the structure. Later, it was proposed that the required group for cytotoxic effects was the unsaturated carbonyl moiety (O=C–C=CH_2), whether it is present in a lactone or ketone group, because SLs containing α-β-unsaturated ketones were about equally active to α-β-unsaturated lactones (Lee et al., 1971). It was also suggested that presence of secondary functionalities, such as α-β-unsaturated carbonyl groups, as well as increase of lipophilicity in the molecule were related to an enhanced cytotoxic effect (Kupchan et al., 1971b). Because of the chemical resonance in the α-β-unsaturated carbonyl, one carbon becomes electrophilic and can alkylate nucleophilic groups, such as sulfhydryl groups in cysteine amino acids of proteins, in a reaction called Michael-type addition (Kupchan et al., 1970). Posterior analysis supported the idea that secondary substitutions might be important for the activity. For example, esters of helenalin and mexicanin I, having two alkylating centers, were more toxic (i.e. IC_{50} = 1.3 – 5.4 μM) than dihydrohelenalins and chamissonolides (IC_{50} = 19 – 128 μM), which only have one alkylating site (Beekman et

al., 1997). In this study, the authors also presented a relationship between the size and position of the ester groups and the cytotoxicity. In SLs having ester groups far from the alkylating center, it appeared that cytotoxicity was directly proportional to the size of the ester, possibly by means of facilitated membrane penetration with higher lipophilicity (Beekman et al., 1997). However, they found that in SLs with an ester group close to an alkylating center there is an optimum size for the ester that will increase the activity. Acetyl and isobutyryl derivatives of helenalin presented an IC_{50s} of 1.3 μM, showing a higher cytotoxicity than the unesterified parent helenalin, with an IC_{50} of 2.4 μM. Larger acyl groups, such as tigloyl or isovaleryl exhibited a decreased cytotoxicity, with IC_{50} of 5.3 and 3.2 μM, respectively (Beekman et al., 1997). Beekman et al. (1997) claimed that this effect in cytotoxicity was due to steric hindrance of the exocyclic methylene that affects its accessibility to the reactive site responsible for the biological activity. Additionally, SLs bioactivity can increase by means of noncovalent interactions such as hydrogen bonds between oxygen atoms in the SLs and amino acids residues in the proximity of the reactive cysteine of a target protein (Schmidt, 1999). A study using cells derived from human carcinoma of the nasopharynx (KB) looked for structural descriptors of the activity in 37 related SLs. By comparing their relative cytotoxicities, they found that guaianolides and pseudoguaianolides were the most active SLs, and found that a double bond at C-3 in the cyclopentane ring or at C-10 in the 7-membered ring, as well as the hydroxyl group at C-5 and an angeloyloxy group at C-8 were important for the cytotoxic activity of the subset of SLs analyzed (Scotti et al., 2007) (see **Figure 2** for carbon positions in SL chemical structure). Another critical aspect in the SLs' activity might be their conformational flexibility. Flexible helenalin with a *cis*-fused lactone ring presented a slightly higher cytotoxicity (i.e. IC_{50} 0.39 μM) than the more rigid stereoisomer mexicanin I (IC_{50} 0.56

μM) with *trans*-fused lactone ring (Beekman et al., 1997). Moreover, analysis of related SLs structures showed that an iso-seco-tanapartholide SL with a β-OH group displayed an enhanced potency over its stereoisomer containing an α-OH group (Ghantous et al., 2009), confirming the importance of SL stereochemistry for the bioactivity.

Often, SL cytotoxic activity is related to the protein complex Nuclear Factor Kappa B (NF-κB) (Bork et al., 1997; Siedle et al., 2004), which regulates DNA transcription of genes involved in programmed cell death (Dutta et al., 2006) and oncogenesis (Basseres & Baldwin, 2006). This nuclear factor regulates the response to apoptosis and proliferation and it is regarded as a cell survival factor because numerous of its targets have anti-apoptotic functions (Lin et al., 2010). It is comprised of a p50 and a p65 subunit and is regulated by interaction with the inhibitor IκB, which sequesters the NF-κB dimer in the cytosol. When there is an inflammatory stimulus, phosphorylation of IκB enables its ubiquitination and subsequent degradation, releasing the NF-κB dimer. The free NK-κB translocate to the nucleus and induce gene transcription. (Gilmore, 2006). SLs can inhibit NF-κB in two ways: directly alkylating key amino acids in the p65 subunit required for DNA-binding (Lyss et al., 1998) or alkylating the IκB that prevents its recognition for degradation, hence, maintaining the inhibitory effect of IκB on NF-κB (Hehner et al., 1998). Therefore, a possible explanation of SLs cytotoxic effects can be via inhibition of this nuclear factor with the consequent sensitization to apoptosis.

1.2.3 Anti-mitotic activities

Recently, our laboratory found that the sesquiterpene lactone pulchelloid A was the active compound in the Asteraceae species *Gaillardia aristata,* which caused cancer cells to arrest in mitosis (Bosco, 2017). This anti-mitotic activity is of scientific interest since it might

directly impact cancer cell division and survival. During mitosis, intricate signaling pathways are activated or silenced, and a gross reorganization of the cellular structure occurs. These tightly coordinated changes that determine the fidelity of the nuclear division makes mitosis the most fragile phase of the cell cycle, during which it is susceptible to cell death if exposed to certain insults (Rieder & Maiato, 2004). Different types of anti-mitotic agents have been developed and are used in cancer therapy or are undergoing clinical trials for this use (Chan et al., 2012). They can affect the mitotic process in a variety of ways that we explain in the next part of this chapter. An anti-mitotic compound could be used to develop a drug for cancer therapy or as a research tool for a diversity of cell cycle studies. Notwithstanding, very little research has been done regarding SLs potential anti-mitotic activity. From more than 5000 SLs described (Chadwick et al., 2013), only a few have been reported to induce a mitotic arrest effect on cells. Our laboratory collected the information about previous research made with SLs reporting a cell cycle arrest and a compilation can be found in the review from Bosco & Golsteyn (2017).

6-O-Angeloylplenolin (6-OAP), a SL isolated from the Asteraceae plant *Centipeda minima*, induced a mitotic arrest in lung cancer cells characterized by increased levels of cyclin B, decreased levels of Tyr15-phosphorylated Cdk1, increased levels of phospho-histone H3 (PH3), presence of mitotic spindles, and activation of the spindle assembly checkpoint proteins BubR1 and Mad2 (Liu et al., 2011b). More recently, it was found that 6-OAP suppresses the S-phase kinase-associated protein 2 (Skp2), a component of the E3 ligase Skp1-Cullin-F-box protein (SCF) complex, by inhibiting the transcription factor Signal Transducer and Activator 3 (STAT3) and decreasing the interaction Skp2-Skp1. This causes dissociation and proteolysis of E3 ligase complexes and leads to an

accumulation of their substrates cyclin B, p27, and E-cadherin (Liu et al., 2015) (Cheng et al., 2017). Another SL, the compound coronopilin, was reported to induce an arrest of 52% of the cells in the G2/M phase, demonstrated by flow cytometry and characterized by an activated Cdk1/Cyclin B complex, sustained levels of cyclin B, and increased levels of PH3. It was also shown by western blot analysis that coronopilin-treated cells exhibited hyper-polymerized tubulin and γ-H2AX protein accumulation (Cotugno et al., 2012b). In 2015, Tang et al. found that parthenolide, a SL from the Asteraceae species *Tanacetum parthenium*, elicited a G2/M phase arrest together with downregulation of survivin in glioblastoma cells (Tang et al., 2015). In a different study, it was found that parthenolide inhibited the tubulin carboxypeptidase (TCP) (Fonrose et al., 2007). Tubulin tyrosination regulates microtubule interactions with cytoskeleton-associated proteins that bind to the microtubules plus ends (CAP-Gly). The TCP enzyme removes the tyrosine residue in the α-tubulin subunit, and detyrosinated tubulin, with associated mislocalization of CAP-Gly, was correlated with defects in spindle positioning, which in turn favoured tumour invasiveness (Mialhe et al., 2001) (Peris et al., 2006). This effect of reducing detyrosinated tubulin activity was also observed after 6 hours of treatment with 25 μM of the SL costunolide in Bt-549 and MDA-MB-157 cancer cells. Presence of detyrosinated tubulin is correlated with aberrant microtubule stability that can facilitate formation of microtentacles, proliferation, migration, and reattachment in cancer cells (Whipple et al., 2013). In a different study, costunolide induced modulation of Chk2/Cdc25c/Cdk1/cyclin B1 signaling and a mitotic arrest as shown by flow cytometry with the PH3 mitotic marker and by presence of immuno-stained mitotic spindles in liver cancer cells (Liu et al., 2011a). The SLs psilostachyin A and C inhibited the G2/M checkpoint and blocked cells in mitosis with aberrant mitotic spindles (Sturgeon et al., 2005). In this study, MCF-7 cells were

submitted to ionizing radiation and treated with different drugs after 16 hours, when 90% of cells were arrested at the G2/M checkpoint. After 8 extra hours, cell collection, fixation, and nuclear staining allowed to count the percentage of cells that overcame the checkpoint and entered mitosis. At 50 μM, psilostachyin A and C overrode the G2/M checkpoint in 40 and 50% of the cells, respectively (Sturgeon et al., 2005). The authors analyzed by flow cytometry the cell cycle progression after psilostachyin treatment without irradiation and found that these compounds increased the percentage of cells in mitosis to 24% after 6 hours, percentage that decreased to 15 % at 12 hours. Mitotic cells examined presented unaligned condensed chromosomes and disorganized mitotic spindles (Sturgeon et al., 2005).

From the scarce studies showing an M-phase arrest induced by SL treatment, very few studies have indicated a possible mechanism of action. Knowledge of the specific cellular responses to SL treatment and possible pathways involved in the activity, plus the research of SLs structure-activity relationship, can lead to the development of a specific and potent anti-mitotic agent by enhancing the biochemical properties of these natural compounds. To discern the possible modes of action of the SLs on human cells, it is necessary to first understand how a normal mitosis occurs in the cell cycle and how some anti-mitotic agents can interfere with this process.

1.3 Overview of the cell cycle

The eukaryotic cell cycle comprises a series of highly controlled events that allow cells to accurately duplicate their hereditary material and segregate the copies into two genetically identical daughter cells. It is composed of two major phases separated by two gap phases. The two major phases in the cell cycle are the synthesis phase (S phase), in which DNA is

replicated, and the mitotic phase (M phase), in which both mitosis and cytokinesis occur. The intervals between these two events are the gap phase 1 (G1) and gap phase 2 (G2). Right after M phase and before S phase, in G1, protein synthesis leads cell growth and the cell monitors intra and extracellular conditions that determine the commitment for DNA duplication. After S phase and before M phase, in G2, a control system verifies that the previous process was properly executed and there is no DNA damage to assure that the cell is ready for division. All phases different from M phase are commonly referred as interphase (i.e. G1, S, and G2). In a typical cultured mammalian cell, the cell cycle lasts an average of 24 hours. The longest time is spent on interphase with about 11 hours in G1, 8 hours in S phase, and 4 hours in G2, that represent approximately a 46%, 33%, and 17% of the cell cycle, respectively. Despite its complexity, the mitotic phase is the shortest period and lasts about 1 hour, representing 4% of the cell cycle. When extracellular conditions are unfavorable, cells can delay the G1 phase or they can enter a resting or quiescent state called G0. They can remain in this resting phase for days or years before resuming proliferation or remain permanently until cell death.

Before DNA replication occurs, human cells contain a 2c amount of DNA that is double the content of a gamete (haploid) cell. After S phase, the cell has a 4c amount of DNA in one pair of sister chromatids, which are considered one chromosome. Although the number of chromosomes stays the same (i.e. 2n), the DNA content doubles in each cell. This can be measured by flow cytometry, in which cells of a population are stained with a fluorescent dye and then counted and individually measured for their DNA content. Using only a DNA dye, cells can be assigned to G1 phase if they contain 2c amount of DNA, to G2/M phase if they contain 4c amount of DNA, or to S phase if they have intermediate amounts. G2 and

M phases cannot be distinguished by flow cytometry unless a second dye that binds to a mitotic marker is added because in both stages the cell has the same DNA content.

The cell cycle process is rigorously regulated by distinct control systems called checkpoints (Hartwell & Weinert, 1989). First, the restriction point in the G1/S transition serves to certify whether cells are ready to duplicate depending on internal and external factors. Later, in the G2/M checkpoint, the cell verifies that each chromosome was correctly duplicated during S phase and does not contain damaged DNA. Finally, the spindle assembly checkpoint (SAC) during M phase assures the proper attachment and alignment of each chromosome in the mitotic spindle equator, determining the readiness to proceed to mitotic exit and cytokinesis. To execute successfully the sequential phases that define the cell cycle, a myriad of proteins coordinates their functions in a precise manner. Cyclic synthesized proteins called cyclins pair to and activate their corresponding cyclin-dependent kinases (Cdks) to start waves of phosphorylation events that lead every other downstream event required on each phase (Nigg, 2001). A system of protein degradation called the Ubiquitin-Proteasome Pathway (UPP) works in parallel with these cyclic events to regulate protein activity (Glickman & Ciechanover, 2002).

In the present study, the focus will be in the M phase of the cell cycle, particularly in the nuclear division or mitosis, which will be described in more detail to provide an insight of how an anti-mitotic compound can interfere with this complex and tightly regulated cell cycle phase.

1.4 Mitosis and its inhibitors

The M phase of the cell cycle starts when the G2/M checkpoint is satisfied, and the cells are ready to commit with the following events: a first event called mitosis that ends with the division of the nuclear content, and a second event called cytokinesis in which the rest of the cellular content is divided and equally distributed in the two daughter cells by cleavage of the cell membrane.

Mitosis is further divided into 5 phases that follow in an orderly manner: prophase, prometaphase, metaphase, anaphase, and telophase. Before metaphase, the correct execution of the early mitotic events in prophase, and the spindle dynamics and chromosome movements during prometaphase will determine if, in the metaphase-to-anaphase transition, the mitotic checkpoint is silenced to proceed with mitotic exit in the latest mitotic phases of anaphase and telophase.

Cellular susceptibility in mitosis makes this phase an excellent target to stop cell division and inhibit proliferation. Small molecules developed to block one or more mitotic events, here referred to as anti-mitotic agents, will be introduced in this section together with the description of the mitotic processes that they can modify.

1.4.1 Early mitotic events – Mitotic kinase inhibitors

The activation of the complex Cdk1/Cyclin B sets the beginning of mitosis. Cyclin B levels fluctuate whereas Cdk1 levels remain constant during the cell cycle. At the onset of mitosis, cyclin B levels reach a peak that partially activates its Cdk1 partner, which is fully activated by the removal of two inhibitory phosphates (Nurse, 1990). Prophase starts with chromosome condensation and centrosome separation and maturation. The replicated

chromosomes from S phase become highly condensed to prevent breaks and allow an equal segregation into the daughter cells. This process requires the phosphorylation of histone H3 at its serine 10 residue (Wei et al., 1999), and aurora B kinase appears to be responsible at least in part for this post-translational modification (Hsu et al., 2000). Concomitantly, with the required Plk1 protein, centrosomes mature by recruiting additional γ-tubulin ring complexes, which increases microtubule nucleation activity (Lane & Nigg, 1996). The dynamic structure that holds the duplicated centrosomes together is degraded and motor proteins separate them to opposite spindle poles. Eg5, member of the kinesin family, has a prominent role on this separation and its phosphorylation by the mitosis-driver Cdk1/Cyclin B complex is required for Eg5 centrosomal localization (Blangy et al., 1995). Importantly, the kinase aurora A localizes in the poles and also plays key roles in centrosome maturation, separation, and organization (Barr & Gergely, 2007). Finally, the end of prophase is marked by nuclear envelope breakdown that permits mixing between cytoplasm and nuclear compartments and promotes a complete reorganization of the cellular structure. A partial disassembly of the envelope occurs as a consequence of phosphorylation of nuclear pore complexes, dependent on Cdk1/Cyclin B (Laurell et al., 2011), but the mechanisms that cause the complete envelope breakdown remain poorly understood, with F-actin recently shown to be involved (Mori et al., 2014).

As noted above, the different events that drive the early mitotic events of chromosome condensation, centrosome maturation and separation, and nuclear envelope breakdown are controlled by essential kinases (**Figure 3**). For this reason, an anti-mitotic approach is to inhibit the activity of these mitotic-driver kinases (Chan et al., 2012). The most prominent activity so far is attributed to the Cdk1/Cyclin B complex; however, members of aurora,

polo-like, and NIMA kinase families have been importantly implicated in diverse mechanisms of mitotic progression (Nigg, 2001). Several non-selective pan-Cdk inhibitors have been developed after the alkaloid flavopiridol and roscovitine showed high antiproliferative and cytotoxic effects in many cancer cell lines (Law et al., 2015). However, they inhibit different Cdks that act at different stages of the cell cycle and cause many off-target effects (i.e. effects different from mitotic arrest). Researchers keep working on the development of more specific Cdk inhibitors: dinaciclib, although it still acts by inhibiting several kinases including Cdk1, does not inhibit Cdk4, Cdk6, or Cdk7 (Law et al., 2015). RO-3306 is a specific ATP-competitive Cdk1 inhibitor that arrests cells at the G2/M transition inhibiting mitotic entrance (Vassilev et al., 2006). Among the Plk1 inhibitors, wortmannin and BI2536 are also ATP competitors, and ON01910 binds at or near the peptide-binding site without competing with ATP (Strebhardt & Ullrich, 2006). Plk1 inhibition arrests cancer cells in mitosis with monopolar mitotic spindles (Marcel et al., 2004). ZM447439 inhibits aurora A and B by binding in the ATP pocket of the enzymes (Ditchfield et al., 2003). Phosphorylation of histone H3 is abolished in ZM447439-treated cells and, although a normal bipolar spindle is formed and kinetochores attach to microtubules, chromosomes do not align properly at the metaphase plate. Furthermore, ZM447439 does not affect localization of aurora kinases but it markedly reduces levels of BubR1, Mad2, and CENP-E at kinetochores (proteins involved in the spindle assembly checkpoint) (Ditchfield et al., 2003). Another aurora B inhibitor is the small molecule hesperadin, which also inhibits other kinases to some degree. Hesperadin-treated cells presented an increase in syntelic chromosome attachments. The authors argued that aurora B is required to ensure bipolar attachments and has an important involvement in the spindle assembly checkpoint (Hauf et al., 2003).

Another anti-mitotic agent that acts by blocking an early mitotic event but does not inhibit a mitotic kinase is monastrol. It was demonstrated that the small molecule monastrol inhibits centrosome separation by binding to and inhibiting Eg5, the plus-end directed motor protein required for the early mitotic centrosome migration (Blangy et al., 1995). This causes monoastral spindles and chromosomes to arrange in a ring shape where erroneous microtubule attachments are abundant. Presence of the checkpoint component Mad2 in many of these chromosomes indicate the activity of the spindle assembly checkpoint that impede mitotic exit (Kapoor et al., 2000).

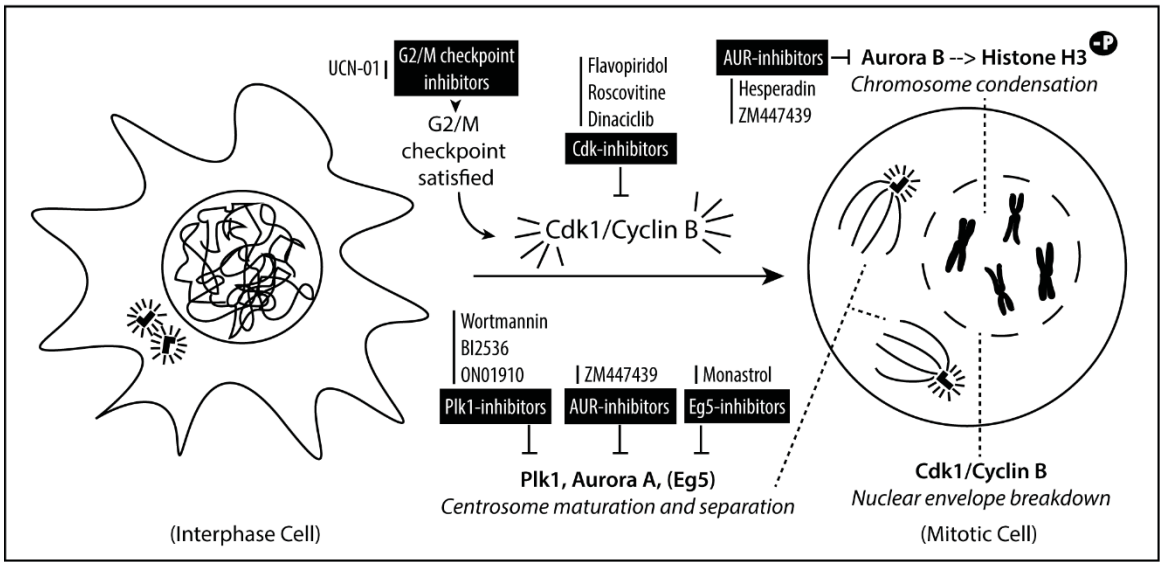

Figure 4. Early mitotic events and its inhibitors. Interphase cells start mitosis once the G2/M checkpoint is satisfied. Chromosome condensation, centrosome maturation and separation, and nuclear envelope breakdown are controlled by mitotic kinases (e.g. Cdk1, Plk1, Aurora A and B). The motor kinesin Eg5 is also involved in centrosome separation. Diverse anti-mitotic agents that act at this level are shown in black boxes.

1.4.2 The mitotic spindle assembly – Tubulin poisons

Microtubules are polymers of α-β-tubulin dimers characterized by their dynamics; they use the hydrolysis of GTP to add or remove tubulin subunits at one or both of their ends,

resulting in growing or shortening of the fibers (Mitchison, 1988). An active Cdk1/Cyclin B complex increases the rate of microtubules disassembly from interphase to M-phase as a result of phosphorylation of microtubule-associated proteins. In addition, the number of microtubules emanating from the centrosomes, now located at opposite sides, increases. This leads to the formation of the mitotic spindle, a specialized bipolar apparatus that moves chromosomes during mitosis (Dumont & Mitchison, 2009). It consists of three types of microtubules emerging from each of the two opposite centrosomes: one set of short astral microtubules that radiate outward from the centrosomes towards the cell membrane and are important for spindle positioning, and two sets of microtubules that radiate towards the middle of the cell (Prosser & Pelletier, 2017). Polar or non-kinetochore microtubules overlap with one another in the center of the cell (e.g. the spindle equator) providing stability and contributing to separate the poles, and kinetochore microtubules attach to the chromosomes and ultimately lead them to align in the metaphase plate (Prosser & Pelletier, 2017) (**Figure 4**).

Anti-mitotic agents that target microtubules bind to different parts of the tubulin dimer or at different positions within the microtubule inducing different disrupting effects on their dynamics (Jordan & Wilson, 2004). The *Vinca* alkaloids bind to β-tubulin at a specific region called *Vinca*-binding domain and directly at the ends of microtubules. At high concentrations it depolymerizes microtubules; but at low, clinically relevant concentrations, it suppresses the dynamics and has potent anti-mitotic activity without depolymerizing effects (Jordan et al., 1991). The loss of dynamics has at least two effects in mitosis: the inability to assemble a mitotic spindle and the reduction of tension between kinetochores and microtubules. Paclitaxel and docetaxel bind directly and strongly to β-

tubulin in the inside surface of the microtubules, in a place known as the taxane-binding site (Rowinsky & Donehower, 1995). High concentrations of them stimulate microtubule polymerization, likely by inducing a conformational change that increases tubulin-tubulin affinity; however, lower concentrations stabilize microtubules with no increase in polymer mass (Jordan & Wilson, 2004). Therefore, taxanes are able to form a highly stable but dysfunctional mitotic spindle (Rowinsky & Donehower, 1995). Colchicine, another anti-mitotic agent, presents yet a different mechanism that inhibits microtubules dynamics: it binds to and induces a conformational change in soluble tubulin, then this colchicine-tubulin complex copolymerizes in the microtubule ends together with other free tubulin molecules rendering the microtubules non-dynamic (Skoufias & Wilson, 1992). Independent of their specific mode of action, all tubulin poisons suppress the normal kinetics of the mitotic spindle, leading to a prolonged activation of the spindle assembly checkpoint and mitotic arrest (Jordan & Wilson, 1998).

1.4.3 Chromosome congression – Motor kinase inhibitors

In tight coordination with the cytoskeletal network provided by the mitotic spindle, chromosomes now are moved to the spindle equator, a process known as chromosome congression. Chromosomes possess a proteinaceous structure at the centromere of each sister chromatid called a kinetochore. Kinetochores can establish end-on or lateral attachments with microtubules influenced by the chromosome position at the moment of nuclear envelope breakdown (NEB) and determining the mechanism of congression of individual chromosomes (Maiato et al., 2017). Chromosomes close to the center of the spindle are able to bi-orient soon after NEB and use a direct congression. In this mechanism, opposite kinetochore-pulling forces, resulting from the tight regulation of

microtubule dynamics and length at the kinetochores, in coordination with polar ejection forces along chromosome arms, drive chromosome oscillations until net force is zero near the equator (Rieder et al., 1986; Inoue & Salmon, 1995). Peripheral (polar) chromosomes that are unable to bi-orient at NEB use a second mechanism where the minus-end directed motor protein dynein captures and transports these chromosomes near spindle poles (Li et al., 2007). Here, aurora A activity prevents stabilization of end-on attachments and activate the plus-end directed motor CENP-E, which will laterally attach kinetochores to microtubules and transport the chromosomes towards the spindle equator (Maiato et al., 2017) (**Figure 4**). At the equator the chances of bi-orientation are maximal, and members of other plus-end directed motors kinesin 4 and 10 promote conversion from lateral to end-on stable attachments (Drpic et al., 2015). Coordination of kinetochore-pulling forces and polar ejection forces together with participation of additional factors will determine the maintenance of an aligned metaphase plate. When all kinetochores are properly attached at kinetochore microtubules and are under a stable tension in the metaphase plate, the spindle assembly checkpoint will be satisfied and the cell will turn to a metaphase-to-anaphase transition point (Joglekar, 2016).

With the success of the microtubule-interfering agents to arrest cells in mitosis and induce cell death, new strategies were formulated to manipulate the spindle dynamics aimed to halt cancer cell proliferation. This is how the mitotic kinesins, essential motor proteins responsible for the interactions between chromosomes and microtubules, became important anti-mitotic agents (Chan et al., 2012).

Centromeric protein E (CENP-E) is a motor protein from the kinesin family localized at the kinetochores and required for proper chromosome congression (Wood et al., 1997).

When its expression is reduced by antisense oligonucleotides, the tension at the kinetochores also decreases, as well as the number of stable microtubule attachments at kinetochores, and leads to mitotic arrest (Yao et al., 2000; Putkey et al., 2002). It was also demonstrated that it binds to and stimulate BubR1 (Weaver et al., 2003), a key effector of the mitotic checkpoint that forms complexes with the checkpoint proteins Cdc20, Bub3, and Mad2 to inhibit the ubiquitin ligase activity of the APC/C (see UPP section). Therefore, CENP-E might act as a link between microtubule attachments and the mitotic checkpoint signaling cascade (Yao et al., 2000; Weaver et al., 2003). Two types of CENP-E inhibitors have been described to date: ATPase antagonists of the motor domain and Farnesyl Transferase Inhibitors (FTIs) (Schmidt & Bastians, 2007). The compound GSK923295 represents the first group. It binds allosterically to the CENP-E motor domain and reduces its ATPase activity by inhibiting the release of inorganic phosphate. This causes a more stable and tight interaction with microtubules and leads to improper chromosome congression and mitotic arrest (Wood et al., 2010). A FTI named Lonafarnib inhibits the required post-translational modification known as farnesylation of the CENP-E, perturbing its normal assembly with microtubules and also inducing defects in the chromosomes' alignment (Schafer-Hales et al., 2007). After treatment with this FTI, the proteins CENP-E as well as CENP-F were absent at the kinetochores during what was defined as a pseudo-metaphase state, where lagging chromosomes were present near the spindle poles. Inhibition of the farnesyl transferase causes the activation of the BubR1 checkpoint and, opposite from the ATPase antagonism of CENP-E motor domain, the FTI lonafarnib creates a weak kinetochore-microtubule interaction (Schafer-Hales et al., 2007).

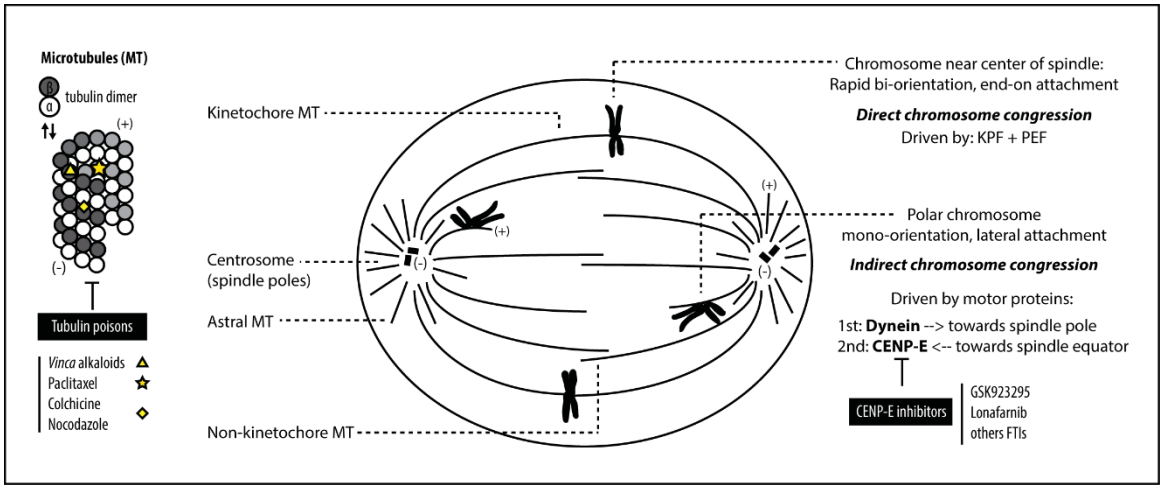

Figure 5. Mitotic spindle and chromosome congression and their inhibitors. Binding sites of tubulin poisons are shown with yellow figures. KPF: kinetochore-pulling forces. PEF: polar ejection forces. FTI: farnesyl transferase inhibitor.

1.4.4 The metaphase-to-anaphase transition and mitotic exit – Inhibitors of the Ubiquitin-Proteasome Pathway

When the chromosomes have established stable attachments with the kinetochore microtubules and have congressed to the spindle equator, the mitotic checkpoint is satisfied, and a cascade of cell signals enables the cell to proceed with anaphase, starting the mitotic exit (Joglekar, 2016). If cell division occurs in the presence of unattached kinetochores, chromosome loss or missegregation would occur during the late phases of M phase, leading to aneuploidy and chromosome instability (Joglekar, 2016). To avoid this, the mitotic checkpoint, called spindle assembly checkpoint (SAC), is activated by different erroneous microtubule-kinetochore interactions and prevents anaphase to take place if chromosomes are not ready for segregation. High rates of microtubule depolymerization (e.g. during nocodazole treatment), stabilization of microtubule dynamics (e.g. paclitaxel treatment), absence of sufficient tension on kinetochore microtubules (e.g. CENP-E inhibitors treatment), or the presence of unattached kinetochores will cause activation of the SAC

(McIntosh, 1991; Rieder et al., 1994; Jordan & Wilson, 1998). The SAC signal is mainly comprised of members of mitotic-arrest-deficient proteins, such as Mad2 (Li & Benezra, 1996); budding uninhibited by benzimidazole proteins, such as Bub3 or BubR1 (Hoyt et al., 1991; Zeng et al., 2010); and the cell division cycle protein Cdc20 (Hwang et al., 1998). Cdc20 is an activator of the ubiquitin proteasome pathway member APC/C (anaphase-promoting complex/cyclosome); therefore, its sequestration by interaction with SAC proteins leads to inactivation of APC/C (Sudakin et al., 2001). Once the SAC is silenced by properly attached and aligned chromosomes, the APC/C mediates degradation of its substrates cyclin B and securin (Thornton & Toczyski, 2003) enabling anaphase onset. Cyclin B degradation inactivates the mitotic driver Cdk1 while securin degradation unleashes the protease separase to degrade the cohesin complex that holds the sister chromatids together (Kirschner et al., 1991; Uhlmann et al., 1999).

The route of destruction of cyclin B and securin enables mitotic exit and occurs via the Ubiquitin Proteasome Pathway (UPP). This pathway uses a ligase complex called APC/C to add ubiquitin polypeptides to proteins to mark them to be degraded by the proteasome (Ciechanover, 1998). Another strategy used by anti-mitotic agents is to interfere with the UPP, which should arrest cells at the metaphase-to-anaphase transition. UPP inhibitors can act in two parts of this system: inhibiting the ubiquitination of key proteins or inhibiting their degradation by the proteasome (Chan et al., 2012). Ubiquitination is a three-step process that requires the activity of three types of enzymes named E1, E2, and E3. In a first step, E1 activates the ubiquitin molecule by forming a thiol ester at the C-terminus of ubiquitin, a process dependent on ATP. After ubiquitin is activated, the enzyme E2 can recognize it and conjugates ubiquitin to the substrate or to E3, a ligase enzyme that will

finally transfer the ubiquitin molecule to a lysine residue of the substrate or to another ubiquitin molecule to make a polymeric chain (Pickart, 2001). APC/C is an E3 ligase multiprotein complex that in mitosis requires the coactivator subunit Cdc20 to recognize and recruit cyclin B and securin to start the ubiquitination reaction of these substrates (Peters, 2002). A prodrug of TAME (tosyl-L-arginine methyl ester) was reported to perturb the APC/C binding with its activator Cdc20 causing a mitotic arrest with no spindle irregularities that was dependent on SAC activation (Zeng et al., 2010).

The 26S proteasome is a large multi-subunit that degrades proteins into small peptides in an ATP-dependent manner. It is composed of a 20S core where proteolysis occurs, and one or two 19S regulatory parts, used for ubiquitylated-substrates recognition and preparation. The 20S core is a hollow cylindrical structure with different subunits that carry catalytic residues that represent the place for proteolysis. The hydroxyl group of N-terminal threonine functions as the catalytic nucleophile responsible for the protein cleavage caused by the proteasome sites (Groll & Huber, 2004). There are a variety of proteasome inhibitors acting through the formation of bonds, covalent or not, with this N-terminal threonine of the proteolytic sites. Peptide aldehydes (e.g. MG132), boronates (e.g bortezomib), α-β-epoxiketones (e.g carfilzomib), ketoaldehydes, β-lactones (e.g omuralide), syrbactins, and oxatiazol-2-ones bind to the active site through different chemical reactions and cause more or less potent inhibition with different specificities for the different catalytic sites of the proteasome (Kisselev et al., 2012).

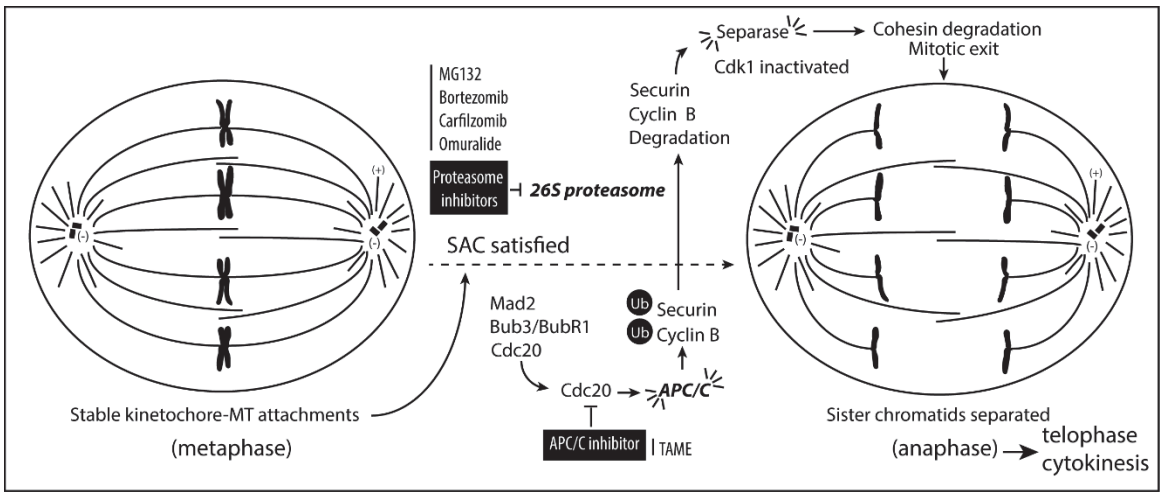

Figure 6. Metaphase-to-Anaphase transition and the Ubiquitin Proteasome Pathway inhibitors. When stable kinetochore-microtubules attachments are achieved, the spindle assembly checkpoint (SAC) is satisfied, which releases Cdc20 and allows activation of the E3 ligase anaphase promoting complex/cyclosome (APC/C). APC/C ubiquitinates securin and cyclin B, marking them for proteasome degradation. When securin is degraded, separase is released and activated to degrade cohesin complexes to allow sister chromatid separation and mitotic exit.

1.4.5 G2/M transition – Checkpoint kinases inhibitors

Another therapy aimed to induce a prolonged mitotic arrest and following mitotic cell death consists in abrogating the checkpoint that exists between G2 and M phases. Although G2/M checkpoint inhibitors do not directly interfere with mitotic processes, they cause cells to enter mitosis with damaged DNA, which in turn causes them to arrest in mitosis. To assure the genomic stability of the next generation of cells, by giving time for DNA repair, a checkpoint system at the G2 phase halts mitotic entrance if a signal of DNA damage is received from the DNA damage response pathway (O'Connell et al., 2000). Initiation of mitosis is marked by the activation of the Cdk1/Cyclin B complex. The cyclin-dependent kinase 1 (Cdk1) requires several modifications to be activated, including the removal from its structure of two inhibitory phosphates by the phosphatase Cdc25 (Nurse, 1990). When DNA damage occurs in G2, different sensor complexes are recruited, and ATM (ataxia-

telangiectasia mutated) and ATR (ATM and Rad 3-related) kinases get activated. They can afterwards phosphorylate a variety of downstream targets including the effector checkpoint kinases Chk1 and Chk2, which ends with the phosphorylation and inactivation of Cdc25 phosphatases (Kastan & Bartek, 2004). Without Cdc25 activity, no activation of Cdk1 is possible and the cell arrests in G2. Another ATM and ATR substrate relevant to this thesis is the histone H2AX, which becomes phosphorylated at its Ser 139 residue upon DNA damage to become γ-H2AX (Rogakou et al., 1998; Furuta et al., 2003).

An anti-mitotic approach that abrogates the G2/M checkpoint started after the observation that p53-deficient cancer cells tend to rely more in the G2/M checkpoint to repair damaged DNA than in the p53-dependent G1 checkpoint (Kawabe, 2004). This strategy combines the use of Chk1 and/or Chk2 inhibitors with DNA-damaging therapies to force mitotic entrance with an amount of damage that a mitotic cell cannot repair, leading to mitotic arrest followed by a type of cell death called mitotic catastrophe (Kawabe, 2004). There are overlaps in the activation process and substrates of Chk1 and Chk2; although, Chk2 has a bigger impact in the G1/S checkpoint and Chk1 in the G2/M checkpoint, which might explain why inhibition of Chk1 kinase have shown better results in clinical trials (Matthews et al., 2013). The majority of the G2/M checkpoint inhibitors, like isogranulatimide or the staurosporine derivative UCN-01, bind to different amino acids in the kinase domain of Chk1 and/or Chk2 with variable specificities competing with ATP and inhibiting the kinase capacity to phosphorylate their substrates (Wang et al., 1996) (Jiang et al., 2004).

In our experimental model, we are able to observe the main pathways in which anti-mitotic agents can block the normal cell division. To date, however, the capacity of sesquiterpene lactones to arrest cancer cells in mitosis has not been widely studied.

Through the Prairie to Pharmacy Program, our laboratory investigates plants from the Canadian prairies for novel bioactivities. A recent project from this program found that the Asteraceae plant *Gaillardia aristata* induced an anti-mitotic activity on cancer cells thanks to its active compound the sesquiterpene lactone pulchelloid A (Bosco, 2017). To investigate if this activity is common to other Canadian plant species from this sesquiterpene lactone-containing family, the following six Asteraceae species were studied:

1.5 Canadian prairie species under investigation

1.5.1 Liatris punctata (Hooker)

The commonly named Dotted Blazing Star (Darbyshire et al., 2000), is a member of the Asteraceae family, tribe Eupatorieae, and is native in Canada according to the database of vascular plants of Canada. In 1946, Gaiser gathered information of different herbaria for a taxonomic revision of the *Liatris* genus. He considered *L. punctata* as the most broadly spread species of this genus, distributed from northern Mexico and Texas to the prairies of southern Canada (Gaiser, 1946a, 1946b).

It was first characterized by Joseph Hooker in 1833 in the Flora Borealis Americana and described in Gaiser's revision of *Liatris* by presenting numerous glabrous and striate stems, 15-80 cm long, from an elongate mostly branched rootstock; glabrous punctate leaves, with 8-15 long and 1.5-6 mm wide basal leaves; a spicate inflorescence 6-30 cm long and 2-3 cm wide of usually crowded heads that contains 4-8 flowers; herbaceous, thick, and punctate phyllaries of 10-14 mm long and 1.5-2 mm wide; a purple corolla 9-12 mm long with the tube inside and filaments of quite pilose stamens; a distinctly plumose pappus 9-11 mm long; and a ribbed and hairy achene 6-7 mm long (Gaiser, 1946a, 1946b).

In our research for sesquiterpene lactone content in *L. punctata,* we only found reported the presence of the germacranolides liatripunctin, punctaliatrin (Herz & Sharma, 1975), and punctatin (Herz & Wahlberg, 1973b). However, within the *Liatris* genus many other sesquiterpene lactones, mainly of the germacranolide, but also guaianolide types, have been isolated. They include, but are not limited to: eleganin from *Liatris elegans*; liscundin and liscundritin from *L. secunda* (Herz & Sharma, 1975); provincialin from *L. provincialis,* which was reported to have cytotoxic activities (Herz & Wahlberg, 1973a); Liatrin from *L. chapmanii*, attributed to induce an antileukemic activity (Kupchan et al., 1971a); graminiliatrin, deoxygraminiliatrin, and graminichlorin from *L. graminifolia*; and spicatin and epoxyspicatin from *L. pycnostachya* and *L. spicata* (Herz et al., 1975).

1.5.2 Hymenoxys richardsonii (Hooker) Cockerell

Commonly known as Colorado (pingue) rubberweed or Richardson's bitterweed (Bain et al., 2014), *Hymenoxys richardsonii* belongs to the Asteraceae family, tribe Helenieae, subtribe Tetraneurinae, subgenera Picradenia (Baldwin & Wessa, 2000; Bierner, 2001). Baldwin et al. (2002) carried out phylogenetic analysis using DNA sequences of Helenieae species and found that origins of this tribal group were based in North America (northwest of Mexico, southwest of United States) and diversified from it. In agreement with these studies, Bierner (2001) claimed that *H. richardsonii* habitat corresponds to Colorado, Utah, Wyoming, Montana, and North Dakota in United States, and Alberta and Saskatchewan in Canada, where this plant has a native status according to the database of vascular plants of Canada (Brouillet et al., 2010).

H. richardsonii's first botanical description is attributed to Joseph Hooker, who called it *Picradenia richardsonii* and it is found in the Flora Borealis Americana from 1833, and a

first description as *Hymenoxys richardsonii*, made by Theodore Cockerell, is available in Latin in the digitized version of the Bulletin of the Torrey Botanical Club from 1904. A more recent English version of the botanical description made by Bierner in 2001 characterizes this plant species as having 1-10 stems of 7-24 cm, sparsely pubescent and dotted with sessile glands; long-villous-woolly moderately pubescent leaves simple or divided into 3-7 segments; 5-35 heads per plant; pubescent peduncles of 1-5 cm; 9-13 outer lanceolate phyllaries with acuminate apices, pubescent abaxial faces, and dotted with sessile glands; 9-18 inner phyllaries with pubescent abaxial faces; 8-14 ray florets with yellow ligules; disc florets with corollas of 3-5 x 0.7-1 mm, eglandular or sparsely dotted with sessile glands; receptacles of 2-3.5 x 3-4 mm; and cypselae of 2-3 x 0.7-1 mm, with 5-6 pappus scales, usually lanceolate-aristate of 2-3.5 x 0.5-0.8 mm (Bierner, 2001).

Some members of the *Hymenoxys* genus, including *H. richardsonii*, have been reported as toxic to livestock (Hardy et al., 1931; Aanes, 1961). Several sesquiterpene lactones of the type guaianolides, pseudoguaianolides, and modified pseudoguaianolides that are considered characteristic of this genus (Spring et al., 1994) have been described in *Hymenoxys* species. Examples of these are the sesquiterpene lactones hymenoxynin, hymenolide, paucin in *H. odorata*; anthemoidin, themoidin, vermerin in *H. anthemoides*; floribundin in *H. greenei* and *H. anthemoides* (Herz et al., 1970); hymenovin in *H. odorata* and *Dugaldia hoopesi* (Ivie et al., 1975); or Biennin A, 3 and 4-methyl hymenoxon in *H. subintegra* (Ahmed et al., 1995). Specifically in *H. richardsonii*, the following sesquiterpene lactones have been described: floribundin and vermerin (Herz et al., 1970), hymenoratin, hymenograndin, hymenolide, isohymenoloide, 2α-tiglinoyloxydugaldiolide (Ahmed et al., 1995), and hymenovin (Ivie et al., 1976).

Hymenovin, also called hymenoxon (Kim & Pattersen, 1976), is the only sesquiterpene lactone from this species that has been associated with a biological activity. It was established that hymenovin was the major toxic compound found in *H. odorata* responsible for high toxicity in sheep and hamsters and for inhibiting *in vivo* C3H mouse mammary carcinoma (Ivie et al., 1975). A later study showed that hymenovin formed adducts with guanine residues in DNA and the NMR spectra indicated that the reaction included at least two guanines per hymenovin molecule, suggesting that this compound might cross-link DNA, also supported by the higher cytotoxicity of this compound in DNA cross-link repair-deficient Chinese hamster ovary cells (Sylvia et al., 1987). In addition, mutagenic activities of hymenovin were reported for *Salmonella typhimurium* (MacGregor, 1977; Manners et al., 1978), *Bacillus subtilis* (Jones et al., 1981), and *Bacillus thuringiensis* (Norman et al., 1976).

1.5.3 Arnica cordifolia (Hooker)

Described by Hooker in 1834, *Arnica cordifolia*, better known as Heart-leaved Arnica, belongs to the Asteraceae family, Madieae tribe, subgenus *Austromontana* (Wolf, 2006). It is widespread in western North America, from the Yukon Territory to New Mexico and California, representing the ancestral species of the *Austromontana* subgenus from where the rest of the Arnica subgenera originated (Maguire, 1938; Wolf & Denford, 1983).

A. cordifolia plants are from 10 to 40 cm high, with simple or sometimes branched stems; 2-4 pairs of cauline petiolate leaves characterized by cordate or sub-cordate to ovate blades 3-10 x 2-10 cm long, dentate margins, acute to rounded apices, and sparsely villous faces; 1 or 3-5 heads; campanulate involucres; 10-20 narrowly ovate to lanceolate phyllaries; 6-

13 ray florets of yellow corollas; densely hirsute, sometimes glandular dark gray cypselae of 5-10 mm long; and white pappi with barbellate bristles (Wolf, 2006).

Regarding the chemical content of sesquiterpene lactones, the pseudoguaianolides carabrone, 2,3-dihydroaromaticin, and the *cis*-isomer of 2,3-dihydroaromaticin were identified in *A. cordifolia* (Merfort & Wendisch, 1993). Other SLs have been reported in related *Arnica* species. Schmidt and Wilhum in 2000 investigated the chemical differences between *A. angustifolia* subspecies to encourage revision of the classification. They reported that *A. angustifolia* spp. *attenuata* contained in its flower heads the helenanolides chamissonolide, 6-deoxychamissonolide, 2-deacetyl-4-tigloylchamissonolide, and 11α,13-dihydroarnifolin. However, in flower heads of *A. angustifolia* spp. *angustifolia* no helenanolide or guianolide type of SL was found, and the only SL obtained by the authors was the eudemanolide ivalin, also present in *A. nevadensis* and *A. chamissonis* (Schmidt & Willuhn, 2000).

It had been described in *Arnica angustifolia* ssp. *attenuata* nine helenanolides, and two 1,5-*trans*-guaianolides, including the first 7(12),6-*trans*-lactonized pseudoguaianolide isolated from a natural source: 4-*O*-tigloylarnicalpin (Schmidt et al., 1995). In *Arnica montana* different SLs have been described, mainly helenalin and 11α, 13-dihydrohelenalin. They are thought to be responsible for the anti-inflammatory properties of this widely used medicinal plant (Petrova et al., 2012).

1.5.4 Balsamorhiza sagittata (Pursh) Nuttall

This plant from the *Heliantheae* tribe of the Asteraceae family is better known as Arrow-leaved Balsamroot. *B. sagittata* is also a native species in Canada and can be found in the provinces of Alberta and British Columbia (Brouillet et al., 2010).

It is a plant of 15 to 65 cm high with silvery or gray-green basal leaves of 5-25 x 3-15 cm. The leaves are described as having rounded-deltate or triangular-deltate blades, with cordate bases, entire margins, acute to attenuate apices, and sericeous or tomentose faces, sometimes glabrescent. Its heads are usually borne singly. Presents hemispheric to turbinate involucres of 12 to 25 mm of diameter; lanceolate or linear outer phyllaries, 15 to 30 mm long, with acute apices; and ray laminae of 20 to 40 mm long (Weber, 2006).

Aboriginal Canadians ate the starchy roots and tender young shoots, used the powdered leaves in wounds to prevent infections, and the whole plant for stomachache, headache, colds, fever, insect bites, swellings, among others (Matsuura et al., 1996; Turner et al., 2000). Interested in this ethnobotanical information, Matsuura studied and isolated the antibacterial tiophene from this plant (Matsuura et al., 1996). With respect to SLs content, the aerial parts of *B. sagittata* afforded 12 sesquiterpene lactones, including the heliangolides epinobilin and zoapatanolide, the germacranolide montafrusin, and the guaianolide 8-acetylpumilin (Bohlmann et al., 1985). Later, purification and analysis of the resinous exudate from *B. sagittata* yielded four sesquiterpene lactones related to the guaianolide pumilin (Mohamed et al., 2006).

1.5.5 Helianthus species and Helianthus annuus

From the tribe *Heliantheae*, the *Helianthus* genus is well-known as the Sunflower group. Most species of the *Helianthus* genus are native in North America and *H. annuus*, the Common Sunflower, is considered native in Canada (Schilling, 2006; Brouillet et al., 2010).

By 1991, the genus *Helianthus* L. was classified into four sections that included 49 North American species. Series *Corona-solis* and series *Microcephali* were characterized by yellow disc flowers and lack of a basal rosette of leaves, with the former series having larger heads than the latter. Series *Angustifolii* and series *Atroburentes* were described as usually presenting a basal rosette of leaves and were distinguished by whether the phyllaries were appressed and the leaves serrate, as in the case of series *Atrorubentes*, or the phyllaries were loose and the leaves entire, case of series *Angustifolii*. Following this organization, Spring and Schilling, after analyzing 31 species of *Helianthus,* summarized the SL profile of this genus. They found that *Corona-solis*, *Atrorubentes* and *Microcephali* species predominantly produce germacrolide compounds of the eupaserrin type, particularly frequent were desacetyleupaserrin and mollisorin B. Species of series *Angustifolii* were characterized by synthesis of eudesmanolides and heliangolide compounds, especially of the budlein and niveusin types, and the single species *H. microcephalus* presented guaianolide compounds (Spring & Schilling, 1991).

Previously, another analysis in the resinous content of capitate glandular trichomes from the leaves of the common sunflower *Helianthus annuus* yielded six SL: the heliangolides niveusin C, 15-hydroxy-3-dehydrodesoxyfruticin and argophyllin B, and three germacranolides of the niveusin-A type (Spring et al., 1989).

The identification of *Helianthus* species has been problematic due to a combination of factors such as ecological plasticity, frequency of hybridization, and presence of polyploidy characteristic of this genus (Schilling, 2006) (Kantar et al., 2014). The use of their chemical profiles, mainly by their SL content has been suggested to be useful to classify sunflower species (Prasifka et al., 2015).

Based on the study made with the plant species *G. aristata* in our laboratory and on the literature research of the Asteraceae family and SL biological activities, the present project poses the following hypothesis and objectives:

1.6 Hypothesis

Canadian prairie plants from the Asteraceae family synthesize sesquiterpene lactone molecules with anti-mitotic effects upon cancer cells.

1.7 Objectives

- To determine if the Asteraceae species *Liatris punctata*, *Helianthus* sp., *Hymenoxys richardsonii*, *Arnica cordifolia*, *Balsamorhiza sagittata*, and *Helianthus* annuus elicit an anti-mitotic activity upon the cancer cell lines HT29 or M059K.
- To characterize the anti-mitotic activity of the bioactive crude extract(s) upon the cancer cell line HT29.
- To isolate the compound(s) responsible for the anti-mitotic activity from the bioactive(s) Asteraceae plant(s) via biology-guided fractionation.

CHAPTER 2

Materials and Methods

2.1 Plant collection

Aerial plant parts of the species listed in **Table 2** were collected with a sustainable practice at the dates, GPS coordinates, and altitudes shown in **Table 3**. *Helianthus* sp. plant parts were collected by an external source in the Blood Reserve (west of Lethbridge, AB). Plant taxonomy was confirmed to species based on documents of the flora of Southern Alberta (Kuijt, 1982; Moss & Packer, 1983; Bain et al., 2014) and verified by Prof. John Bain, the director of the University of Lethbridge Herbarium. Information including collection date, site description, associated species and location were stored with a voucher specimen in the Herbarium database. A molecular voucher consisting of plant tissue was stored in silica gel for future analysis of DNA.

Table 2. Canadian prairie species from the Asteraceae family under investigation.

Plant scientific name	Common name	Tribe	Lab Code
Liatris punctata Hooker	Dotted gayfeather, plains blazing-star	Eupatorieae	PP060
Helianthus sp.	Prairie sunflower	Heliantheae	PP210-β
Hymenoxys richardsonii (Hooker) Cockerell	Colorado bitterweed, pingue rubberweed	Helenieae	PP360
Arnica cordifolia Hooker	Heart-leaved arnica	Madieae	PP420
Balsamorhiza sagittata (Pursh) Nuttall	Arrow-leaf balsam	Heliantheae	PP480
Helianthus annuus Linnaeus	Common sunflower	Heliantheae	PP490

Table 3. Plant collection dates, location information, and amounts obtained.

Plant Code	Harvesting Date	Location (GPS coordinates)		Location Elevation (m.a.s.l.)	Amount (g)	
		Latitude	Longitude		Wet	Dry
PP060	31/08/14	49°40.516	112°51.642	908	4000	122
PP210-β	05/08/15	unknown	unknown	unknown	unknown	78
PP360	05/06/16	49°41.004	112°52.122	904	313	73
	31/05/17	49°41.004	112°52.122	922	1230	436
PP420	22/06/16	49°28.753	114°23.232	1646	256	53
PP480	30/06/16	49°27.932	114°20.974	1370	702	176
PP490	08/07/16	49°40.293	112°54.504	938	10500	570

2.2 Plant extraction

Following the harvest, plants were dried at room temperature for the first day and then in an oven at 40°C for three or four days. The different plant parts (flower heads, stems, and leaves) were separated and stored in paper bags in a dry environment at room temperature until extraction. Plant extracts were prepared by grinding dried material with a mortar and pestle or a blender to a fine powder. The powder was suspended to 10% (w/v), with either dichloromethane (DCM), 75% ethanol (EtOH), or water, and stirred overnight at room temperature. The suspension was filtered to collect the soluble fraction, which was dried in a convection oven at 40°C for 1-2 days. The dried material was collected, weighed, labeled, given a code number, and stored in darkness at room temperature until use. Letter A was assigned to denote ethanolic extracts and added at the end of the code number and letter B was assigned to denote dichloromethane extracts. Samples were dissolved in dimethyl

sulfoxide (DMSO) (Sigma-Aldrich; D2438) to a concentration of 50 mg/mL, centrifuged at 10,000 x g for 10 minutes, and the supernatant was used in biological assays. Solutions were stored at -20°C in small aliquots to avoid freeze-thaw cycles.

2.3 Cell culture

The human cell lines HT29 (ATCC HTB-38), M059K (ATCC CRL-2365), and WI38 (ATCC CCL-75) were obtained from the American Type Culture Collection (ATCC). HT29 cells were maintained in RPMI 1640 medium (ThermoFisher; 21870-092) supplemented with 10% (v/v) heat inactivated fetal bovine serum (FBS) (ThermoFisher; 12484028) and 2 mM GlutaMAX (ThermoFisher; 35050-061). M059K cells were maintained in Dulbecco's Modified Eagle Medium/F-12 (ThermoFisher; 11320-082) supplemented with 10% (v/v) heat inactivated FBS, 2 mM Modified Eagle Medium non-essential amino acids (ThermoFisher; 11140050) and 15 mM HEPES (4-(2-hydroxyethyl)-1-piperazineethanesulfonic acid), pH 7.4. WI38 cells were maintained in DMEM/High glucose (Sigma; D6546) supplemented with 10% heat inactivated FBS, 2 mM Modified Eagle Medium non-essential amino acids, and 2 mM GlutaMAX. Cells were grown at 37°C in 5% CO_2 and the media were changed every 3-4 days. HT29 cells were plated at a density of 3.0 x 10^5 cells/25 cm^2 or 1.0 x 10^6 cells/75 cm^2 flask and cultured for 48-72 h prior to treatment. M059K and WI38 cells were plated at a density of 1.5 x 10^5/25 cm^2 flask and cultured for 24-48 h prior to treatment. The compounds nocodazole (Sigma-Aldrich; M1404), paclitaxel (Sigma, T7402), camptothecin (Sigma; 7689-03-4), and hymenoratin were dissolved in dimethyl sulfoxide (DMSO) (Sigma-Aldrich; D2438) to a concentration of 200 μg/mL, 100 μM, 10mM, and 10 μg/mL, respectively, and stored at -20°C. In non-

treated cells, DMSO was added as a solvent vehicle control in a volume equal to the highest volume of plant extract or compound tested, and never adding more than 1% (v/v).

2.4 Cytotoxicity assay

Plant extract cytotoxicity was measured by the MTT (3-((4,5)-dimethylthiazol-2-yl)-2,5-diphenyl-tetrazolium) assay (Sigma-Aldrich; M2128-1G). HT29 cells were plated at 4.0 x 10^5 cells/96 well culture plate and cultured at 37°C for 72 h prior to treatment. M059K and WI38 cells were plated at 2.5 x 10^5 cells/96 well culture plate and cultured at 37°C for 48 h prior to treatment. All treatments were run in triplicate at 96 h and experiments were performed at least three times. After the specified treatment time, 20 µl of MTT solution (5 mg/ml MTT in phosphate buffered saline (PBS) (137 mM NaCl, 3 mM KCl, 100 mM Na_2HPO_4, 18 mM KH_2PO_4) was added to the media in each well and the plates were incubated at 37°C for 3.5 h. The media were then aspirated and 150 µl of MTT solvent (4 mM HCl, 0.1% (v/v) octyl-phenoxy-polyethoxy-ethanol, in isopropanol) was added to each well. Plates were placed on a shaker for 30 min in the dark, and absorbance was measured at 590 nm using an Epoch microplate spectrophotometer (BioTek Instruments, USA) powered by Gen5 software. Results were expressed as IC_{50} concentrations; the concentration of the compound or plant extract that reduced the absorbance of MTT by 50 %, by comparison to 0.1% (v/v) DMSO-treated cells. The normalized percent absorbance was calculated as shown:

Normalized percent absorbance = (absorbance/DMSO absorbance) x 100

The log concentrations of the compound were plotted against the normalized percent absorbance using Microsoft Excel software. Analysis was performed with GraphPad Prism

5 software, using non-linear regression (log (inhibitor) versus normalized response), to estimate the IC_{50} concentrations. Standard curves were plotted using the equation:

$Y = maximum + (maximum – minimum)/ (1+10(X-LogIC_{50}))$

Where maximum is the percentage of viable cells after treatment with 0.1% DMSO, minimum is the percentage of viable cells after treatment with the highest concentration of the genotoxic molecule and X is the log10 value of the treatment concentration.

2.5 Cell rounding morphology assay

HT29 cells were seeded at 5.0 x 10^4/well in a 12 well culture plate and incubated for 48 or 72 h prior to treatment and M059K and WI38 cells were seeded at 2.5 x 10^4/well in a 12 well culture plate and incubated for 24-48 h prior to treatment to reach a cell confluency of 50-70%. DMSO was used as a negative control in a volume equal to the highest volume added of treatment under investigation, and nocodazole 200 ng/mL was included as a positive control for cell rounding. Images were captured after 24 h of treatment with either an Infinity 1 camera powered by Infinity Capture imaging software (Lumenera Corporation) on an Olympus CKX41 inverted microscope or with a Cytation™ 5 Cell Imaging Multi-Mode Reader using Gen5 software (BioTek Instruments, USA). Images were processed using Adobe Photoshop (CC 2015 16.0). Flat (interphase) cells and rounded cells were manually counted using Image J (1.47v) software and the percentage of rounded cells in the total sample was determined. Each experiment was performed at least three times and the mean and standard error of the mean of the percentage of rounded cells were calculated.

2.6 Immunofluorescence microscopy

HT29 cells were seeded at a density of 5.0 x 10^4/well in 12 well culture plates or on glass coverslips at 1.0 x 10^5/well in 6 well culture plates and incubated at 37°C for 48 or 72 h prior to treatment. After 24 hours of treatment, cells were fixed at room temperature for 20 min in 3% (v/v) paraformaldehyde (Fisher Scientific; 30525-89-4), diluted in PBS. Fixation was quenched with 50 mM NH_4Cl in PBS and cells were permeabilized for 5 min using 0.2% (v/v) Triton X-100 in PBS and blocked for 30 minutes with 3% (w/v) BSA in PBS-T (0.1% (v/v) Tween-20 diluted in PBS). Cells were then incubated at 4°C overnight with the primary antibodies anti-phospho-Ser10 histone H3 (Millipore; 06-570(CH) in a 1:1000 dilution, anti-α-tubulin (Santa Cruz Biotechnology; sc-53030) in a 1:200 dilution, or anti-histone γ-H2AX (Millipore; 05-636; 1:400) in a 1:400 dilution. After washing with PBS-T, cells were incubated with secondary antibodies for 2 h at room temperature as follows: Alexa Fluor 488 rabbit anti-rat IgG (ThermoFisher; A11006; 1:400) for anti-α-tubulin, Alexa Fluor 594 AffiniPure goat anti-rabbit IgG (Jackson ImmunoResearch; 111-585-003; 1:400) for anti-phospho-Ser10 histone H3, and Alexa Fluor 488 rabbit anti-mouse IgG (ThermoFisher; A11059; 1:400) for anti-histone γ-H2AX. Nuclei were stained with 300 nM DAPI (4′, 6-diamidino-2-phenylindole) (Fisher; LSD1306) in PBS for 15 min and coverslips were mounted onto microscope slides using ProLong Gold Antifade reagent (ThermoFisher; P36934). Cells were observed and recorded with either a Cytation™ 5 Cell Imaging Multi-Mode Reader using Gen5 software (BioTek Instruments, USA) or with an Olympus BX41 microscope using an Infinity 3 camera operated by Infinity Capture imaging software (Lumenera Corporation). Images were prepared using Adobe Photoshop (CC 2015 16.0) software. Cells positive for phospho-Ser10 histone H3 and total number of

cells (DAPI stained) were counted with Gen5 software using exposure settings from non-treated cells as the threshold for fluorescent signal. A minimum of 200 cells were counted for each treatment and the mean and standard error of the mean percentage of PH3-positive cells of at least three independent experiments were calculated. For the analysis of the mitotic spindles, at least three independent experiments were performed and a minimum of 50 mitotic cells per treatment were observed in total to evaluate whether their mitotic spindles were distorted or not. DMSO-treated mitotic cells were used as a reference for normal, non-distorted mitotic spindle morphology. To distinguish signals from those of background histone γ-H2AX staining, the signal from not treated cells was set to zero using exposure settings on the microscope camera (Borgne et al., 2006)

2.7 Cell extraction

HT29 cells were plated at 1 x 10^6 cells/75 cm^2 flask and incubated at 37°C for 48-72 h prior to treatment. After 24 hours of treatment, cells were either trypsinized or collected by mechanical shake-off and washed with ice cold PBS. Cells were resuspended in ice cold lysis buffer (50 mM HEPES, pH 7.4, 50 mM NaF, 10 mM EGTA, 50 mM β-glycerophosphate, 1 mM ATP, 1 mM DTT, 1% Triton X-100 (v/v), 10 µg/ml RNase A (Sigma-Aldrich; R6513), 0.4 U/ml DNase I (ThermoFisher, AM2222) and protease inhibitor cocktail (Roche; 11836170001)) at a concentration of 20,000 cells/µl, passed through a 26-gauge needle five times and incubated on ice for 30 min. The suspension was centrifuged at 10,000 x g for 10 min at 4°C, aliquoted into 1.5 ml microcentrifuge tubes and stored at -80°C. Extracts were either used for electrophoresis after being boiled for 5 min in the presence of 2x SDS (sodium dodecyl sulphate) sample buffer (20% (v/v) glycerol, 10% (v/v) DTT, 6% (w/v) SDS, 500 mM Tris, pH 6.8) or used for the detection

of Cdk1 activity. The concentration of proteins in each extract was quantified using the Agilent 2100 Bioanalyzer and samples were prepared using the Agilent Protein 230 kit: 4 µl of protein sample and 2 µl denaturing solution were mixed in a 0.5 ml microcentrifuge tube and incubated at 95°C for 5 min. The samples were then briefly centrifuged and 84 µl deionized water was added. Samples were mixed by vortexing and loaded onto the Agilent Protein 230 chip which was loaded into the Agilent 2100 Bioanalyzer. Samples were analyzed using Agilent Expert 2100 software to quantify the amount of protein present.

2.8 Mechanical shake-off

HT29 cells were plated at 1 x 106 cells/75 cm2 flask and incubated at 37°C for 48-72 h prior to treatment. After 24 hours of treatment, media were aspirated and cells were gently washed with PBS. Fresh medium was added at 1 ml/25 cm2 and the flask was tapped with medium force on all edges to extract rounded cells from flattened cells (Swift & Golsteyn, 2016).

2.9 Electrophoresis and western blot analysis

Cell extracts were separated on 10% (v/v) SDS-PAGE (poly-acrylamide gel electrophoresis) gels with 4% (v/v) stacking gels. Precision Plus Protein Dual Colour Standard (BioRad; 161-0394) was used to determine molecular weight in kilodaltons (kDa). Proteins were transferred onto nitrocellulose membranes by semi-dry transfer (BioRad) for 45 minutes at 25 volts. Membranes were blocked with either 5% (w/v) low fat milk or 2% (w/v) BSA in Tris buffered saline with Tween-20 (TBS-T) (50 mM Tris base, 150 mM NaCl and 0.1% (v/v) Tween-20, pH 7.6) for 2 h. Membranes were then incubated with the following primary antibodies at 4°C overnight: anti-Cdk1/Cdc2

(Signalway Antibodies; 21236-2; 1:500); anti-phospho-tyr15 Cdk1/Cdc2 (Signalway Antibodies; 11244-2; 1:500); anti-cyclin B1 (Santa Cruz Biotechnology; sc-245; 1:100); anti-actin (Santa Cruz Biotechnology; sc-58673; 1:200); anti-cyclin A (Santa Cruz Biotechnology; sc-271682; 1:500), anti-cyclin E (BD Pharmingen; 551159; 1:2000) , anti-plk1 (ThermoFisher; 33-1700; 1:300), anti-phospho-thr210 plk1 (BD Pharmingen; 558400; 1:30000). The membranes were then washed with TBS-T and incubated with the following secondary antibodies for 1 h at room temperature: alkaline phosphatase coupled anti-mouse IgG (Promega; PRS3721; 1:2500) or alkaline phosphatase coupled anti-rabbit IgG (Promega; PRS3731; 1:2500). The membranes were washed with TBS-T and developed using an alkaline phosphatase conjugate substrate kit (BioRad; 172-1063). Development was stopped with Tris-EDTA (ethylenediaminetetraacetic acid) buffer (10 mM Tris base, 1 mM EDTA, pH 8.0). Western blot analyses were performed three times.

2.10 Cdk1 assay

The Cdk1 assay was performed by the method of Lewis et al. (2013), with changes as noted. Cdk1 phosphorylation reactions (20 µl total volume) were prepared as follows: 10 µl 2x Cdk1 phosphorylation buffer (50 mM β-glycerophosphate pH 7.4, 10 mM $MgCl_2$, 10 mM NaF, 1 mM DTT) with 200 µM ATP and 5 µl of either 40 ng/µl glutathione S-transferase (GST) or GST-PP1C-S artificial substrates. Reactions were initiated by adding 5 µl of whole cell extracts diluted in cold lysis buffer (50 mM HEPES, pH 7.4, 50 mM NaF, 10 mM EGTA, 50 mM β-glycerophosphate, 1 mM ATP, 1 mM DTT, 1% Triton X-100 (v/v), 10 µg/ml RNase A (Sigma-Aldrich; R6513), 0.4 U/ml DNase I (ThermoFisher, AM2222) and protease inhibitor cocktail (Roche; 11836170001)) to 200 lysed cells/µl. Reactions were incubated for 5 min at 30°C and were stopped by adding an equal volume of 2x SDS

sample buffer and heating at 95°C for 5 min. Reaction mixtures were separated on 12% (v/v) SDS-PAGE gels. Proteins were transferred to nitrocellulose membranes with a semi-dry electroblotter system (BioRad) for 45 min at 25 volts. The membranes were blocked with either 5% (w/v) low fat milk or 5% (w/v) BSA in TBS-T and incubated overnight at room temperature with either anti-phospho-Thr320 PP1Cα (Abcam; Ab62334; 1:50,000) or anti-GST (Sigma-Aldrich; G7781; 1: 50,000) primary antibodies (Lewis et al., 2013). After washing with TBS-T, the membranes were incubated with alkaline phosphatase coupled anti-rabbit IgG (Fisher; PRS3731; 1:2500). The membranes were washed with TBS-T and developed using an alkaline phosphatase conjugate substrate kit (BioRad; 172-1063). Development was stopped using Tris-EDTA buffer. Cdk1 assays were performed three times.

2.11 Time-lapse video microscopy

HT29 cells were plated in 6 well culture plates at a density of 1 x 10^5/well and incubated at 37°C for 48 h prior to treatment. The time-lapse video microscopy experiment was set in a Cytation^{TM} 5 Cell Imaging Multi-Mode Reader using Gen5 software (BioTek Instruments, USA) to collect phase contrast images every 10 min for 24 or 48 h post-treatment using the 10x objective in a controlled chamber at 37°C and 5% CO_2. Cells were manually scored for a rounded or flat morphology between 0 and 24 or 48 h. At least 100 HT29 cells were counted per treatment. Experiments were performed at least three times.

2.12 Thymidine-synchronization time-lapse video microscopy

HT29 cells were plated in 6 well culture plates at a density of 1 x 10^5/well and incubated at 37°C. After 48 h of incubation, cells were either treated with 2 mM thymidine (Sigma;

T1895) or not treated. After 18 h, the S-phase block was released washing the thymidine-containing media twice with warm PBS and adding fresh media. Following the S-phase release, cells were treated with either DMSO, nocodazole 200 ng/mL, or PP360-A 50 µg/mL. The time-lapse microscopy experiment was set in a Cytation™ 5 Cell Imaging Multi-Mode Reader using Gen5 software (BioTek Instruments, USA) to collect phase contrast images every 15 min for 24 h using the 10x objective in a controlled chamber at 37°C and 5% CO_2. Cells were manually scored for a rounded or flat morphology between 0 and 24 h post-treatment. At least 100 HT29 cells were counted for each treatment and experiments were performed three times.

2.13 Flow cytometry

HT29 cells were plated at 0.3 x 10^6 cells/25 cm^2 flask and incubated at 37°C for 48-72 h prior to treatment. Total cell cultures were collected by trypsinization and rounded mitotic cells were collected by mechanical shake-off. Cells were washed with PBS containing 1% bovine serum albumin (BSA) and 1 mM EDTA and fixed in ice cold absolute ethanol for at least 24 h. Fixed samples were stored at -20°C until analysis. The staining and analysis of the samples were performed at the Flow Cytometry Facility of the Cumming School of Medicine of the University of Calgary as follows: cell suspensions were transferred to 12x75 mm FACS reading tubes (BD Falcon™) and centrifuged at 200 g for 10 minutes. Cell pellets were then resuspended in 1 mL PBS containing 1 % BSA. The centrifugation step was repeated, and the final cell pellets were re-suspended in 500 µL of FxCycle™ PI/RNase Staining Solution (Invitrogen F10797). After 1 hour of incubation at room temperature, samples were analyzed on a BD LSR 11 Flow Cytometer (BD Biosciences) using the PE channel.

2.14 Biology-guided fractionation

The chemical fractionation was performed by Dr. Andersen and his colleagues at the Department of Chemistry, University of British Columbia, Vancouver, BC as follows: 98.87 g of dried plant material was extracted twice with 200 mL methanol (MeOH) overnight at room temperature. The combined MeOH extracts were dried and partitioned between water (1: 300) and ethyl acetate (EtOAc) (3:75). The EtOAc extracts were combined, dried, and given the laboratory code RA164. Approximately 1/4 of the EtOAc soluble material was chromatographed on Sephadex LH20 using a 86 x 2.6 cm column with 80 % MeOH/CH_2Cl_2 as eluent. The fractions were labelled RA163-RA171 and analyzed in our laboratory with the cell rounding assay using concentrations of 15 and 50 µg/mL. The bioactive fraction obtained was then purified by C-18 reverse-phase HPLC using an InertSustain 25 x 1 cm column with 80% H2O/MeCN as eluent with a flow rate of 2 mL/min to give 26.8 mg of hymenoratin (labelled RA173). The structure of hymenoratin was confirmed by analysis of 1D and 2D Nuclear Magnetic Resonance (NMR) spectra and Low-Resolution Electrospray Ionization Mass Spectrometry (LRESIMS).

2.15 Statistical analysis

Data were analyzed using Microsoft Excel 2010 and GraphPad Prism 5 software. Data were plotted as means from three independent experiments ± standard error of the mean. One-way analysis of variance (ANOVA) with Tukey's or Dunnett's post hoc test were used to analyze results from light microscopy and immunofluorescence microscopy assays. Two-way repeated measures ANOVA was used for the analysis of the time-lapse microscopy. Differences were considered significant when $p < 0.05$.

CHAPTER 3

Investigation of the biological activity of six Asteraceae species extracts

To understand if the anti-mitotic activity recently found by our laboratory in *Gaillardia aristata* is common to other Asteraceae species, we tested and compared the Canadian Asteraceae species *Liatris punctata, Helianthus* sp.*, Hymenoxys richardsonii, Arnica cordifolia, Balsamorhiza sagittata* and *Helianthus annuus*. They had been previously collected by members of the laboratory, and we tested their capacity to induce cytotoxicity and anti-mitotic effects measured by cell rounding activity, phosphorylation of histone H3, and morphology of the mitotic spindles.

3.1 Cytotoxic effect of extracts prepared from six Asteraceae species upon HT29 and M059K cell lines

To detect and compare cytotoxic properties of the six species under study (**Table 2**) we performed the MTT assay. HT29 cells were treated with either DMSO (solvent) as a non-toxic control, camptothecin (CPT, a genotoxic agent) as a toxic control, or treated with concentrations of the extracts ranging from 0.3 to 1000 µg/mL for 96 hours. We determined the half maximum inhibitory concentration (IC_{50}) of CPT and the extracts as described in the materials and methods. CPT presented an IC_{50} of 15.8 ± 0.8 nM, as expected. Among the extracts, the most cytotoxic was PP420-B with an IC_{50} of 10.2 ± 0.8 µg/mL and the least cytotoxic extract was PP360-A with an IC_{50} of 123.7 ± 15.7 µg/mL. The following IC_{50} values were determined for the other extracts: 44.0 ± 2.1 µg/mL (PP060-B); 20.5 ± 1.6 µg/mL (PP210-β-B), 22.7 ± 1.6 µg/mL (PP480-B), and 56.9 ± 1.9 µg/mL (PP490-B) (**Table 4**).

M059K cells were treated using similar conditions to HT29 cells for the cytotoxicity assay. PP420-B showed the lowest IC_{50} of 4.5 ± 0.2 µg/mL and PP360-A had the highest IC_{50} of 56.1 ± 6.0 µg/mL. PP060-B and PP480-B also presented relatively low IC_{50} values of 5.6 ± 1.3 µg/mL and 4.7 ± 0.4 µg/mL, respectively. Intermediate cytotoxic values were found for PP210-β-B with an IC_{50} of 24.6 ± 1.9 µg/mL and for PP490-B with an IC_{50} of 13.7 ± 1.4 µg/mL. With these first results, compared in **Figure 8**, we could observe that there are differences in the level of toxicity exerted by the six species, suggesting different biological activities.

3.2 Asteraceae plant extracts differ from each other in their capacity to induce a rounded morphology when applied to HT29 or M059K cells

We wanted to compare the percentage of rounded cells after treatment with the extracts to identify which one(s) might have a mitotic arrest activity. When cells are committed to mitosis, they adopt a rounded morphology that is known to be crucial for chromosome capturing by the kinetochore microtubules, mitotic spindle bipolarity, and positioning of the division axis to achieve a proper and symmetrical segregation of the chromosomes in the two daughter cells (Cadart et al., 2014). Cells also round up when they die by apoptosis, but this type of cell death is also characterized by other morphological changes, including some that are visible with light or fluorescent microscopy such as membrane blebbing or condensed pyknotic nuclei (Kerr et al., 1972; Häcker, 2000), that can be used to distinguish them from mitotic cells. Two types of extracts, ethanolic (distinguished by the letter A in their code name) and dichloromethane (distinguished by letter B), were prepared from each of the six Asteraceae species, giving a total of twelve extracts for testing. The extracts were examined in a cell rounding assay where HT29 or M059K cell lines were treated with the

different extracts in a range of concentrations from 5 µg/mL to 500 µg/mL. DMSO was added in a volume identical to the highest volume added of extract as a negative control, whereas nocodazole, which arrests cells in mitosis, was used as a positive control for cell rounding. After 24 hours, three photos were taken per treatment and cells were manually scored for their rounded or flat morphology. The percentage of rounded cells was determined for each concentration of each extract and the mean and standard error of the mean of at least three independent experiments were calculated.

As expected, DMSO-treated cells had a mean percentage of 5.2 ± 0.6% of rounded cells in HT29 cells and 5.3 ± 0.7% in M059K cells. HT29 cells treated with nocodazole were rounded after 24 hours, obtaining a mean percentage of 98.6 ± 0.7% rounded cells, whereas in M059K this percentage was 50.7 ± 3.0%. A representative photo was selected for the DMSO and nocodazole treatments in HT29 and M059K cells from all the experiments performed and is presented in the figures of all the extracts tested.

In a first experiment, HT29 cells were treated with either DMSO, nocodazole, or with one of two plant extracts of *Liatris punctata* (PP060-A and PP060-B) at concentrations ranging from 5 to 500 µg/mL. Photos of treatments were taken by light microscopy at 24 hours and the percentages of rounded cells were compared with DMSO and nocodazole treatments (Panels A and C in **Figure 9**). PP060-A treated cells revealed an increasing number of rounded cells starting at 5 µg/mL with the greatest number at 150 µg/mL. The mean percentages of rounded cells from three experiments at each concentration were: 9.3 ± 1.7% at 5 µg/mL, 10.7 ± 1.3% at 15 µg/mL, 20.3 ± 4.1% at 50 µg/mL, and 28.3 ± 3.2% at 150 µg/mL. At 500 µg/mL treatment, the cells were no longer rounded or adherent and were considered to be dead. For PP060-B, the corresponding mean percentages of rounded cells

at each treatment were: 9.3 ± 0.3% at 5 µg/mL, 13.0 ± 1.7% at 15 µg/mL, 19.3 ± 3.7% at 50 µg/mL, and toxicity (dead cells) at both 150 and 500 µg/mL treatments. These values were compared to those from DMSO-treated cells and we found that treatment with 150 µg/mL of PP060-A induced a statistically significantly higher percentage of rounded cells.

Experiments to identify cell rounding activity of *L. punctata* extracts were performed in a second cell line, M059K. After treating M059K cells for 24 hours with either DMSO, nocodazole, or increasing concentrations from 5 to 500 µg/mL of ethanolic (PP060-A) and dichloromethane (PP060-B) extracts of *L. punctata*, we scored cell morphologies (flat or rounded) and determined the percentages of rounded cells per each of these treatments. The mean percentage of rounded cells for PP060-A were 7.7 ± 3.2% rounded cells at 5 µg/mL, and 13.0 ± 2.6% at 15 µg/mL. The extract was toxic at 50 µg/mL and above. For PP060-B we obtained an 8.3 ± 2.0% rounded cells at 5 µg/mL, 25.0 ± 3.6% at 15 µg/mL, and toxicity again at the three highest concentrations of 50, 150, and 500 µg/mL (Panels B and D in **Figure 9**). No significant difference was found when comparing the values of the extracts with the DMSO treatment in M059K cells. Even though there was no induction of cell rounding in M059K cells after treatment with any PP060 extracts, the assay in HT29 cells showed us that the ethanolic extract PP060-A is able to induce a cell rounding activity in this cell line.

We proceeded to investigate the possible rounded cell activity in *Helianthus* sp. extracts. For this purpose, we first used HT29 cells and treated them for 24 hours with either DMSO as a negative control, nocodazole as a positive control, or increasing concentrations from 5 to 500 µg/mL of *Helianthus* sp. ethanolic and dichloromethane extracts (PP210-β-A and PP210-β-B). After three independent experiments we calculated the mean percentage of

rounded cells. We found that treatment with PP210-β-A caused 13.0 ± 2.9% of rounded cells when using at a concentration of 5 μg/mL, 11.7 ± 1.3% with 15 μg/mL, and 21.5 ± 6.1% with 50 μg/mL. Treatments with 150 and 500 μg/mL showed an accumulation of dead cells and were considered toxic for HT29 cells. Extract PP210-β-B exerted an activity that caused accumulation of 20.0 ± 5.0% rounded cells at 5 μg/mL, and 24.0 ± 5.3% at 15 μg/mL. At higher concentrations (i.e. 50, 150, and 500 μg/mL), extract PP210-β-B was toxic to HT29 cells. No statistical difference was found between DMSO-treated cells and PP210-β-A or PP210-β-B-treated cells at any of the concentrations tested (Panels A and C in **Figure 10**).

Similarly, we tested PP210-β-A and PP210-β-B extracts in M059K cells and determined the mean percentage of rounded cells of three experiments using DMSO as a negative control, nocodazole as a positive control, and concentrations ranging from 5 to 500 μg/mL of the mentioned *Helianthus* sp. extracts. As observed in panels B and D of **Figure 10**, the ethanolic extract PP210-β-A induced 18.3 ± 9.5% at 5 μg/mL, 17.0 ± 3.1% at 15 μg/mL, 16.0 ± 2.1% at 50 μg/mL, and toxicity at 150 and 500 μg/mL. The dichloromethane extract PP210-β-B induced 20.0 ± 8.0% rounded cells at 5 μg/mL and a high percentage of 71.0 ± 2.0% of rounded cells at 15 μg/mL. When PP210-β-B was used at 50, 150, or 500 μg/mL, we observed toxicity. The 15 μg/mL treatment with PP210-β-B induced a significantly higher number of rounded cells than DMSO treatment and was not statistically different from the nocodazole treatment. These data presented the extract PP210-β-B as positive for cell rounding activity in M059K cells and negative, together with PP210-β-A, for this activity in HT29 cells.

We proceeded to determine the rounded cell activity of *Hymenoxys richardsonii* ethanolic extract, PP360-A, and dichloromethane extract, PP360-B, by the same protocol as described for extracts PP060 or PP210-β. Representative photos of these experiments are shown in **Figure 11,** where panels A and C present the results obtained in HT29 cells and panels B and D present the results in M059K cells. In HT29, we observed toxicity when using 500 µg/mL of PP360-A and 150 µg/mL or 500 µg/mL of PP360-B. PP360-A induced an accumulation of 11.3 ± 1.2% rounded cells at 5 µg/mL, 14.7 ± 1.2% at 15 µg/mL, 39.3 ± 7.7% at 50 µg/mL, and 36.3 ± 4.3% at 150 µg/mL, whereas PP360-B induced 16.7 ± 1.5% of rounded cells at 5 µg/mL, 30.7 ± 0.8% at 15 µg/mL, and 37.0 ± 0.6% at 50 µg/mL upon HT29 cells. Statistical analysis confirmed that PP360-A treatment at 50 and 150 µg/mL and PP360-B treatment at 15 and 50 µg/mL induced a significantly higher number of rounded cells than DMSO.

In M059K cells, control treatments DMSO and nocodazole presented the expected number of rounded cells. Treatments with 150 or 500 µg/mL of PP360-A and with 50, 150, or 500 µg/mL of PP360-B were toxic to this cell line, causing detached cells that were no longer rounded and presumably dead. For the ethanolic extract PP360-A, the percentages of rounded cells obtained were 10.3 ± 2.9% at 5 µg/mL, 14.0 ± 3.6% at 15 µg/mL, and 51.2 ± 7.1% at 50 µg/mL. For the dichloromethane extract PP360-B, the corresponding values were 9.3 ± 1.5% at 5 µg/mL, and 12.7 ± 1.2% at 15 µg/mL. The percentage of rounded cells after 50 µg/mL of PP360-A was significantly higher than that observed after DMSO treatment. These results show a cell rounding activity elicited by PP360 extracts at different concentrations and present in the two cell lines tested.

Subsequently, we tested *Arnica cordifolia* extracts PP420-A and PP420-B under the same conditions used for the previous extracts for cell rounding activity. As represented in panel A and C of **Figure 12**, PP420-A induced an increasing number of rounded cells in HT29 causing a 13.0 ± 2.3% of rounded cells at 5 µg/mL, 18.0 ± 2.1% at 15 µg/mL, 22.0 ± 4.1% at 50 µg/mL, and 36.3 ± 5.9% at 150 µg/mL. At 500 µg/mL, this extract was toxic to the cells. PP420-B caused an 18.7 ± 2.4% rounded cells at 5 µg/mL, 38.7 ± 1.2% at 15 µg/mL, and toxicity at the higher concentrations tested. Treatments with PP420-A at 150 µg/mL and PP420-B at 15 µg/mL had a significantly higher number of rounded cells when compared to treatment with DMSO. Using M059K cells, we determined a percentage of rounded cells of 7.7 ± 3.2% at 5 µg/mL, 14.3 ± 9.4% at 15 µg/mL, and 15.3 ± 2.6% at 50 µg/mL with PP420-A and 37.3 ± 6.1% at 5 µg/mL with PP420-B. Higher concentrations were toxic to M059K cells (panel B and D of **Figure 12**). The rounded cell percentage obtained with the 5 µg/mL treatment of PP420-B was significantly higher than that obtained with DMSO treatment in M059K cells. Therefore, we could find a rounding cell activity in extracts from *A. cordifolia* in both HT29 and M059K cell lines.

In the *Balsamorhiza sagittata* analysis of rounding cell activity presented in **Figure 13**, we observed relatively low percentages of rounded cells of 7.3 ± 0.7% at 5 µg/mL, 6.0 ± 0.6% at 15 µg/mL, 13.7 ± 3.0% at 50 µg/mL, and 13.3 ± 6.8% at 150 µg/mL when using the PP480-A extract in HT29 cells. PP480-B induced a 17.3 ± 1.5% at 5 µg/mL, and 23.0 ± 4.5% rounded cells at 15 µg/mL. The concentrations of 50, 150, and 500 were toxic to HT29 cells. When the extracts were tested in M059K cells, we found that treatment with PP480-A elicited 8.7 ± 2.2% rounded cells at 5 µg/mL, 8.7 ± 1.7% at 15 µg/mL, 23.7 ± 5.0% at 50 µg/mL, and toxicity at 150, and 500 µg/mL. PP480-B induced 15.7 ± 5.4%

rounded cells at 5 µg/mL and was toxic to M059K cells at higher concentrations. These results were not statistically different from DMSO treatment, showing our *B. sagittata* extracts negative for rounding cell activity in HT29 and M059K cells at the concentrations tested.

We obtained similar results to *B. sagittata* when analyzing the mean percentages of rounded cells from the *Helianthus annuus* cell rounding assay. As shown in **Figure 14**, HT29 cells treated with PP490-A presented a percentage of rounded cells of 9.0 ± 1.5% at 5 µg/mL, 16.0 ± 2.1% at 15 µg/mL, and 18.0 ± 4.4% at 50 µg/mL and were dead at 150 or 500 µg/mL treatments. When the cell line was treated with PP490-B, 14.3 ± 4.4% rounded cells accumulated at the 5 µg/mL treatment, 18.0 ± 3.5% at 15 µg/mL, and 16.7 ± 2.7% at 50 µg/mL and toxicity was present at 150 and 500 µg/mL treatments.

In M059K cells, the mean percentage of rounded cells was 8.3 ± 1.2% at 5 µg/mL and 15.7 ± 1.5% at 15 µg/mL for PP490-A, and 23.0 ± 6.7% at 5 µg/mL for PP490-B. Higher concentrations of PP490-A or PP490-B were toxic to the cells. No statistically significant differences were found when these values were compared to the DMSO treatment of each cell line. This shows the extracts tested of *Helianthus annuus* as inactive for cell rounding in HT29 and M059K cells.

The results of the cell rounding assay of the twelve extracts are summarized in **Figure 15**. Using HT29 cells, the DMSO-treated cells contained a mean of 5.2 ± 0.6% rounded cells, whereas the nocodazole-treated cells contained 98.6 ± 0.7% rounded cells, as expected. The plant extracts that showed a statistically significant difference in the number of rounded cells compared with DMSO were PP060-A at 150 µg/mL (28.3 ± 3.2%), PP360-A at 50 (39.3 ± 7.7%) and 150 µg/mL (36.3 ± 4.3%), PP360-B at 15 (30.7 ± 0.8%) and 50 µg/mL

(37.0 ± 0.6%), PP420-A at 150 µg/mL (36.3 ± 5.9%), and PP420-B at 15 µg/mL (38.7 ± 1.2%). All plant extracts had a lower cell rounding activity than the nocodazole treatment. Regarding toxicity, all twelve extracts were toxic to the cells after 24 hours of treatment with 500 µg/mL; PP060-B, PP210-β-A, PP210-β-B, PP360-B, PP420-B, PP480-B, PP490-A, and PP490-B caused toxicity when added at 150 µg/mL; and PP210-β-B, PP420-B, and PP480-B were toxic at 50 µg/mL. With M059K cells, the mean percentage of rounded cells in the DMSO-treated cells was 5.3 ± 0.7% whereas in the nocodazole-treated cells this percentage was 50.7 ± 3.0%. Of the twelve extracts, treatment with three of them presented a significant higher percentage of rounded cells compared with DMSO: PP210-β-B at 15 µg/mL (71.0 ± 2.0%), PP360-A at 50 µg/mL (51.2 ± 7.1%), and PP420-B at 5 µg/mL (37.3 ± 6.1%). These three treatments, together with PP060-B at 15 µg/mL, were not statistically different from nocodazole treatment. These data reveal that cell rounding activity, which is suggestive of a mitotic arrest effect, is present only in a subset of Asteraceae species.

3.3 Extracts prepared from different Asteraceae species vary in their capacity to induce mitosis

The cell rounding assay identified extracts prepared from Asteraceae species that are candidates for having chemicals that arrest cells in mitosis. Even though two Asteraceae species did not show a statistical difference in their cell rounding activity compared to DMSO treatment, we decided to investigate all six species in a specific assay for mitosis. We selected only the most active type of extract for each plant species, either dichloromethane or ethanolic extract. In the case of PP360, there was no difference between the two types of extracts, so the ethanolic extract was selected. We studied their capacity

to induce the phosphorylation of histone H3 at serine 10, an event that drives chromosome condensation when cells are in mitosis (Gurley et al., 1978; Hendzel et al., 1997).

HT29 cells were treated for 24 hours with either DMSO in a volume identical to the highest volume added of extract as a negative control; nocodazole 200 ng/mL as a positive control for mitotic arrest activity, or 5, 15, and 50 µg/mL of the selected extracts. Following the time of treatment, an immunofluorescence microscopy protocol was performed using anti-phospho-histone H3 (anti-PH3) antibody to detect cells undergoing mitosis and DAPI to stain the DNA. Three sets of photos, each including one of the targeted PH3 and one of the DAPI staining, were taken per treatment and the mitotic indices were calculated. We determined mitotic indices of all treatments using the percentage of cells positive for PH3 in the total number of cells given by DAPI staining. In the case that an extract presented a mitotic index statistically higher than that of DMSO treatment, we considered that extract positive to induce an anti-mitotic activity. Representative photos of every extract treatment are presented in **Figure 16-Figure 21** and mitotic indices of all treatments are compared in **Figure 22**. The control treatments, DMSO and nocodazole, were added every time a new experiment was carried out and were always consistent with the expected number of HT29 cells positive for PH3. On average, DMSO induced 5.0 ± 0.5% of mitotic cells and nocodazole induced 84.4 ± 2.3%. Only one representative set of photos for each of them was selected and is presented at the top of every extract figure.

To investigate if *Liatris punctata* extracts possessed an anti-mitotic activity, HT29 cells were treated for 24 hours with either DMSO, nocodazole, or the selected dichloromethane extract PP060-B at the concentrations of 5, 15, and 50 µg/mL. We observed cells by immunofluorescence microscopy with anti-PH3 antibody and DAPI staining and analyzed

three sets of photos taken per treatment to determine the percentage of PH3-positive cells present on each of them. This experiment was performed three times and **Figure 16** shows a representative photo of these PP060-B treatments. We observed fewer PH3-positive cells at the three concentrations tested when compared to nocodazole; however, PP060-B at 50 µg/mL presented more cells in mitosis (PH3-positive) than the DMSO treatment. We found that treatment with PP060-B at 5 µg/mL induced 5.0 ± 0.6% of PH3-positive cells, at 15 µg/mL 9.6 ± 1.5%, and at 50 µg/mL, consistent with our initial observations, PP060-B induced a 17.2 ± 1.7% of PH3-positive cells. The mitotic index of PP060-B at 50 µg/mL was statistically higher than that of DMSO.

We performed an immunofluorescence microscopy assay of *Helianthus* sp. extract under the same conditions that we used to test *L. punctata* extract to target the phospho-histone H3 (PH3) present only in mitotic cells. Using the required antibodies and DAPI staining, we could observe and determine the percentage of PH3-positive HT29 cells after a 24-hour treatment with either DMSO, nocodazole or PP210-β-B at 5, 15, and 50 µg/mL (**Figure 17).** The mean percentages of PH3-positive cells were calculated and analyzed from three independent experiments, we found that cells treated with PP210-β-B at 5 µg/mL presented 6.0 ± 0.7% PH3-positive cells, at 15 µg/ml 5.8 ± 0.6%, and at 50 µg/mL 11.3 ± 2.1%. None of these values were statistically significant when compared to DMSO treatment. Hence, no anti-mitotic activity was associated with *Helianthus* sp. extract PP210-β-B.

We proceeded to analyze the ethanolic extract of *Hymenoxys richardsonii,* PP360-A. We treated HT29 cells for 24 hours with 5, 15, and 50 µg/mL of PP360-A and analyzed them as we did with PP060-B and PP210-β-B (**Figure 18**). We determined the mean percentage of mitotic cells based on the number of PH3-positive cells present in the total number of

cells stained with DAPI and analyzed them statistically obtaining the following results: 5 and 15 μg/mL of PP360-A caused 5.4 ± 0.5%, and 4.8 ± 0.5% of PH3-positive cells, respectively, having a similar effect to DMSO treatment. Importantly, however, when PP360-A was used at 50 μg/mL, a 31.3 ± 3.6% of mitotic cells accumulated in the treated HT29 cells. This was a significantly higher number of PH3-positive cells when compared to DMSO treatment. The *H. richardsonii* extract PP360-A at 50 μg/mL elicits an anti-mitotic activity upon HT29 cell line.

The next extract to be tested for anti-mitotic activity by immunofluorescence microscopy was the dichloromethane extract of *Arnica cordifolia,* PP420-B. We performed the analysis following the steps described above. With the images obtained from these experiments, represented in **Figure 19**, we could observe an accumulation of PH3-positive cells at the 15 μg/mL treatment of PP420-B and no accumulation of mitotic cells at 5 or at 50 μg/mL treatment. The number of PH3-positive cells in the images of the 15 μg/mL treatment was lower than that of nocodazole but was higher than DMSO treatment. Moreover, the DAPI staining showed highly condensed DNA in cells treated with 50 μg/mL of PP420-B, suggesting the presence of apoptotic cells. We found that PP420-B treatment induced, respectively, 11.9 ± 1.2%, 18.0 ± 3.5%, and 3.6 ± 0.9% of PH3-positive cells at 5, 15, and 50 μg/mL. The concentration of 15 μg/mL of PP420-B induced a significantly higher number of PH3-positive cells than DMSO.

An illustration of typical results obtained in *Balsamorhiza sagittata* analysis for anti-mitotic activity is shown in **Figure 20**. Here, HT29 cells were treated for 24 hours with 5, 15, or 50 μg/mL of PP480-B and analyzed by the immunofluorescence microscopy analysis described for the previous extracts. The mean percentages of PH3-positive cells of the

treatment were 9.7 ± 1.3% for the 5 μg/mL treatment, 13.4 ± 3.2% for 15 μg/mL, and 2.4 ± 0.6% for 50 μg/mL treatment. None of these values were significantly different from DMSO-treated cells, which presented the *B. sagittata* extract PP480-B as an inactive extract for mitotic arrest effect.

Lastly, we investigated the ability of *Helianthus annuus* extract, PP490-B, to induce mitotic arrest in HT29 cells. As we did with all the other five species, an immunofluorescence microscopy analysis was carried out after a 24-hour treatment with 5, 15, or 50 μg/mL of PP490-B to target the mitotic marker PH3 and staining DNA with DAPI to determine the percentage of PH3-positive cells in the cells submitted to these treatments. DMSO and nocodazole treatments were included and showed the expected numbers of PH3-positive cells. We obtained a mean percentage of PH3-positive cells of 4.6 ± 1.0% after the 5 μg/mL treatment, 10.3 ± 1.3% after 15 μg/mL treatment, and 9.7 ± 2.0% after treatment with 50 μg/mL of PP490-B. Statistical analysis showed no significant difference in any of these results when compared with DMSO treatment. Hence, *Helianthus annuus* extract PP490-B was also considered negative for anti-mitotic activity. Representative photos of these experiments are shown in **Figure 21**.

To compare the ability of the Asteraceae extracts under investigation to induce a mitotic arrest activity, **Figure 22** shows representative images of the best activity of each extract and graph in **Figure 23** presents a comparison of all values obtained in these assays based on the mean percentages of PH3-positive cells. Treatment with PP060-B or PP360-A at 50 μg/mL and PP420-B at 15 μg/mL showed a significantly higher activity than the DMSO treatment, activity that was also different from that elicited by the positive control treatment nocodazole. Together these data support our previous finding that the anti-mitotic activity

is specific to a subset of plant species. In the present study, *H. richardsonii* extract PP360-A was able to elicit the highest anti-mitotic effect among the group of six species tested.

3.4 Mitotic spindle morphology of HT29 cells after treatment with six Asteraceae plant extracts.

We identified extract PP360-A from *Hymenoxys richardsonii* as the extract with the highest activity of the six Asteraceae extracts to induce mitosis based on cell rounding and phospho-histone H3 observations. Mitosis is characterized by several cellular and biochemical features; therefore, we pursued our investigation of mitotic arrest using other criteria. Several mitosis-arresting compounds, such as nocodazole that we use here, affect spindle organization; thus, we examined whether PP360-A or PP060-B, PP210-β-B, PP420-B, PP480-B, or PP490-B influenced the organization of the mitotic spindle. We used the technique of immunofluorescence microscopy to observe cells stained with anti-α-tubulin antibodies. We performed this analysis after 24 hours of treatment with extracts from the six species at 5, 15, and 50 µg/mL, and with four different controls. The entire assay was carried out at least three independent times.

We used DMSO treatment to represent a non-treated population where a symmetrical bipolar mitotic spindle morphology was expected. For abnormal mitotic spindle morphologies, we used two anti-mitotic compounds that have opposite effects: nocodazole and paclitaxel. Nocodazole at 200 ng/mL prevents the formation of the mitotic spindle whereas paclitaxel at 100 nM stabilizes the mitotic spindle. We included a third control treatment: PP006 at 50 µg/mL, an extract from the previously studied *Gaillardia aristata*, which induces an anti-mitotic arrest with mitotic spindle distortion. These treatments were included in every experiment performed for each plant extract. Only the control treatments

DMSO and nocodazole are included in **Figure 24-Figure 29**, illustrating results of individual extracts. A summary of the best activities displayed by each of the six extracts under investigation plus the four control treatments are presented in **Figure 30**.

The first extract to be analyzed was PP060-B from *Liatris punctata.* HT29 cells were treated for 24 hours with this extract at increasing concentrations of 5, 15 and 50 μg/mL and with DMSO, nocodazole, paclitaxel, and *G. aristata* extract, following an immunofluorescence microscopy analysis of α-tubulin. **Figure 24** shows representative photos obtained by this analysis. We could observe the expected morphologies within DMSO and nocodazole-treated cells: bipolar mitotic spindles and no spindles, respectively. When treating cells with 5 μg/mL of PP060-B we observed that 17.0 ± 11.2% of the mitotic spindles were distorted (i.e. the spindle had a different morphology than that observed in DMSO-treated cells). The number of distorted spindles increased to 27.8 ± 11.4% when cells were treated with 15 μg/mL and was lowered to 3.5 ± 3.5% at 50 μg/mL. The rest of mitotic cells had symmetrical bipolar spindles, similar to those observed in DMSO-treated cells. The percentage of distorted mitotic spindles after 15 μg/mL treatment of PP060-B was significantly higher when compared with DMSO treatment, which only rarely (1.6 ± 1.6%) induced a distortion of the spindle in HT29 mitotic cells. These observations indicate an ability of PP060-B to distort the spindles of a portion of the mitotic cells in a concentration-dependent manner that is different from nocodazole and paclitaxel.

Next, we investigated *Helianthus* sp. extract PP210-β-B. With the purpose of observing the mitotic spindles after treatment with this extract, we used immunofluorescence microscopy to target α-tubulin in HT29 cells treated for a period of 24 hours with either the control treatments DMSO, nocodazole, paclitaxel, and PP006, or with 5, 15, and 50 μg/mL of

PP210-β-B. The control treatments caused the expected responses in the treated cells: symmetric bipolar spindles with DMSO, absence of mitotic spindles with nocodazole, highly polymerized mitotic spindles with paclitaxel, and mitotic spindle distortion with PP006. HT29 cells treated with PP210-β-B presented only normal bipolar mitotic spindles (**Figure 25**). We then counted the total of mitotic spindles observed in photos taken in three experiments and calculated the percentage of distorted mitotic spindles to compare with a non-treated population represented by DMSO, where only a 1.6 ± 1.6% of mitotic cells present a distortion on their spindle apparatus. PP210-β-B-treated cells presented 5.8 ± 2.5% of distorted mitotic spindles at 5 μg/mL treatment, 3.1 ± 1.3% at 15 μg/mL, and 6.6 ± 3.3% at 50 μg/mL. These values were not statistically different from those of DMSO-treated cells. PP210-β-B, hence, does not induce distortion in HT29 mitotic spindles at the concentrations tested.

Remarkable results were observed with *Hymenoxys richardsonii* extract PP360-A when HT29 cells were analyzed as described for PP060-B and PP210-β-B. After 24 hours of treatment with either DMSO, nocodazole, paclitaxel, PP006, or 5, 15, and 50 μg/mL of PP360-A and analysis by immunofluorescence microscopy, we could see a striking distortion in a large number of mitotic cells at the 50 μg/mL treatment with PP360-A (**Figure 26**). To quantitatively evaluate this effect, we determined the percentage of mitotic spindles that were distorted and obtained a 5.4 ± 2.1% of distorted mitotic spindles at 5 μg/mL and a 4.6 ± 2.2% at the 15 μg/mL treatment with PP360-A that were similar to the DMSO treatment. Consistent with our observations, treatment with PP360-A induced distortion in 72.0 ± 4.4% of the mitotic spindles of HT29 cells when added at 50 μg/mL.

Therefore, PP360-A at 50 μg/mL was considered to elicit a clear activity of mitotic spindle distortion in mitotic HT29 cells that accumulate after 24 hours post-treatment.

We tested the *Arnica cordifolia* dichloromethane extract PP420-B for its ability to influence microtubule organization. As with the preceding assays, when HT29 cells were treated for 24 hours with the control treatments, they caused the normal responses. We observed mitotic spindles similar to those obtained after DMSO treatment with all the concentrations tested of PP420-B (**Figure 27**). More precisely, the 5 μg/mL treatment of PP420-B only caused 5.6 ± 1.6% of distorted mitotic spindles, the 15 μg/mL, caused 5.0 ± 1.1%, and at 50 μg/mL no distorted mitotic spindles were detected. This means that approximately 95% of the mitotic spindles were bipolar and not distorted as those presented in DMSO-treated cells. PP420-B did not affect the morphology of the mitotic spindles different from a non-treated population in HT29 cells at the conditions tested.

The *Balsamorhiza sagittata* extract PP480-B was investigated for its capacity to affect the mitotic spindle organization. As it is illustrated in **Figure 28**, the majority of the mitotic spindles presented in PP480-B-treated cells were normal (i.e. bipolar and symmetrical, as in DMSO treated-cells) at the 5 and 15 μg/mL treatments. Nonetheless, some mitotic spindles were distorted in the 15 μg/mL treatment. We did not detect mitotic spindles in cells treated with 50 μg/mL of PP480-B. We determined that there was an 8.9 ± 3.2% of distorted mitotic spindle after treatment with 5 μg/mL of PP480-B, and a 19.3 ± 4.7%, with the 15 μg/mL treatment. However, these percentages were not significantly higher when statistically compared to DMSO treatment; hence, we considered PP480-B as not having a distorting activity in mitotic spindles of HT29 cells.

The last extract investigated was the *Helianthus annuus* extract PP490-B. As we did with the other five Asteraceae extracts, we analyzed HT29 cells after treatment with PP490-B at 5, 15, and 50 μg/mL or with DMSO, nocodazole, paclitaxel, or PP006 by immunofluorescence microscopy targeting α-tubulin. We could observe, as represented in **Figure 29**, the expected effects after DMSO and nocodazole treatment and a distortion effect in mitotic spindles after PP490 treatment. The percentages of distorted mitotic spindles found were: 7.0 ± 2.5% when treating with PP490-B at 5 μg/mL, 14.7 ± 4.3% at 15 μg/mL, and 21.0 ± 8.0% at 50 μg/mL. Even though treatments with 15 and 50 μg/mL of PP490-B seemed to contain an abnormal number of distorted spindles, none of these values resulted significantly different from DMSO treatment when statistically analyzed.

To compare the percentages of distorted mitotic spindles obtained in these assays of the six Asteraceae extracts, refer to graph in **Figure 31**. We noticed that only two treatments, PP360-A and PP060-B were able to cause a significant distortion in the mitotic spindles of HT29 cells.

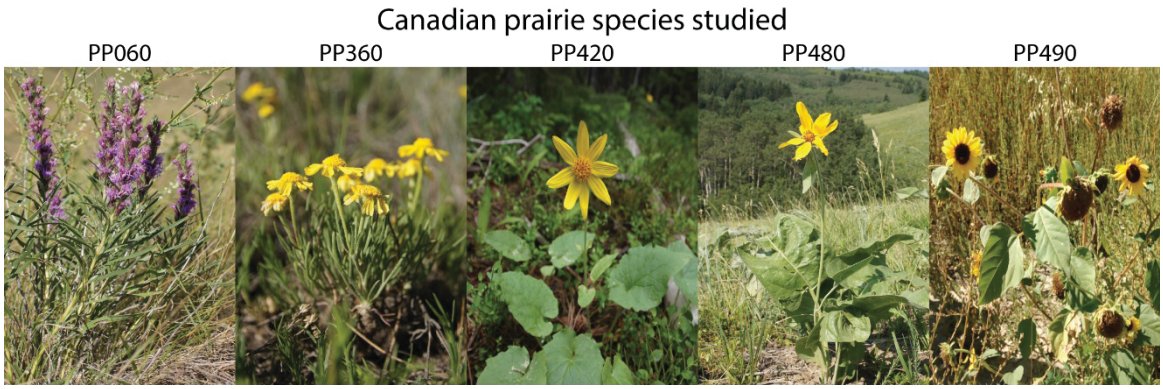

Figure 7. Canadian prairie species under investigation. PP060: *Liatris punctata*, PP360: *Hymenoxys richardsonii*, PP420: *Arnica cordifolia*, PP480: *Balsamorhiza sagitatta*, PP490: *Helianthus annuus*. PP210-β: *Helianthus* sp. was collected by an external source and photo is not available.

Table 4. Half maximum inhibitory concentration (IC_{50}) of the six Asteraceae plant extracts in HT29 and M059K cells after 96 hours of treatment.

Cell line	Control (nM)	Plant extract (µg/mL)					
	CPT	PP060-B	PP210-beta-B	PP360-A	PP420-B	PP480-B	PP490-B
HT29	15.8 ± 0.8	44.0 ± 2.1	20.5 ± 1.6	123.7 ± 15.7	10.2 ± 0.8	22.7 ± 1.6	56.9 ± 1.9
M059K	5.0 ± 0.5	15.6 ± 1.3	24.6 ± 1.9	56.1 ± 6.0	4.5 ± 0.2	4.7 ± 0.4	13.7 ± 1.4

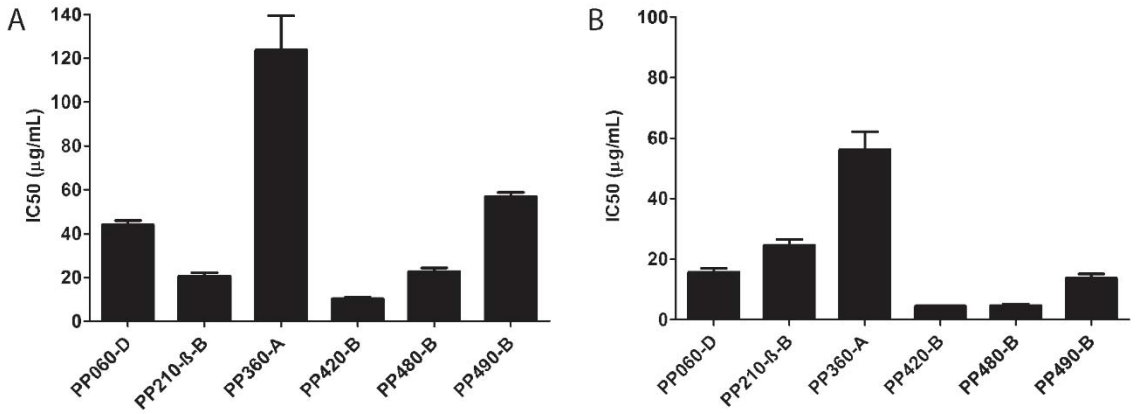

Figure 8. Half maximum inhibitory concentration (IC_{50}) of the six Asteraceae plant extracts in HT29 (A) and M059K cells (B) after 96 hours of treatment. Error bars represent the SEM of at least three independent experiments.

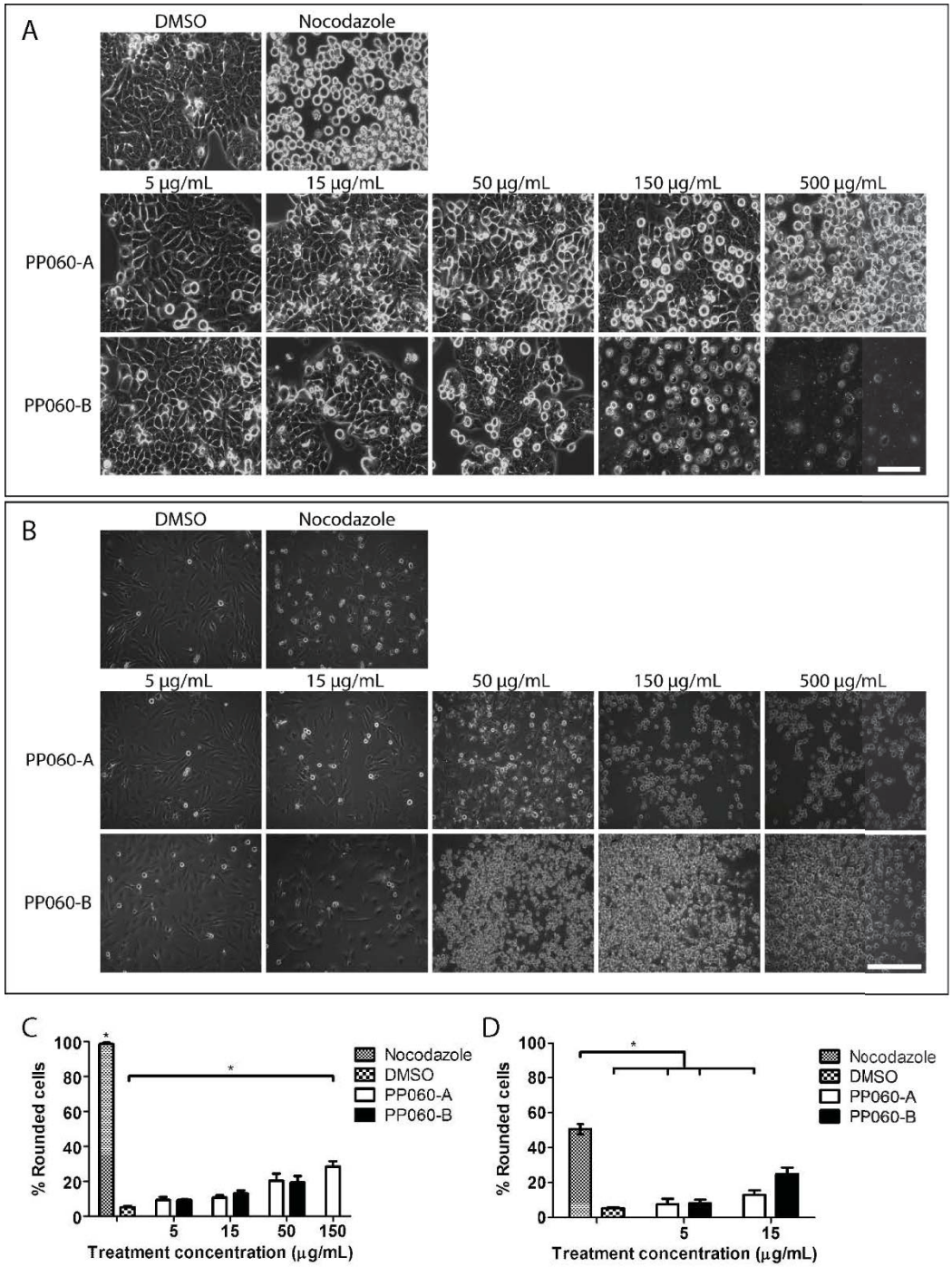

Figure 9. Cell rounding assay after treatment with PP060 plant extracts at a range of concentrations from 5 to 500 µg/mL in HT29 (**A**) and M059K (**B**) cell lines. Negative control: DMSO. Positive control: nocodazole 200 ng/mL. Scale bars: A: 100 µm. B: 200 µm. Mean percentage of rounded cells determined after manually scoring HT29 (**C**) and M059K (**D**) morphologies. Error bars represent the SEM of at least three independent experiments. Statistical significance was determined using one-way ANOVA followed by Tukey's post hoc test ($p < 0.05$).

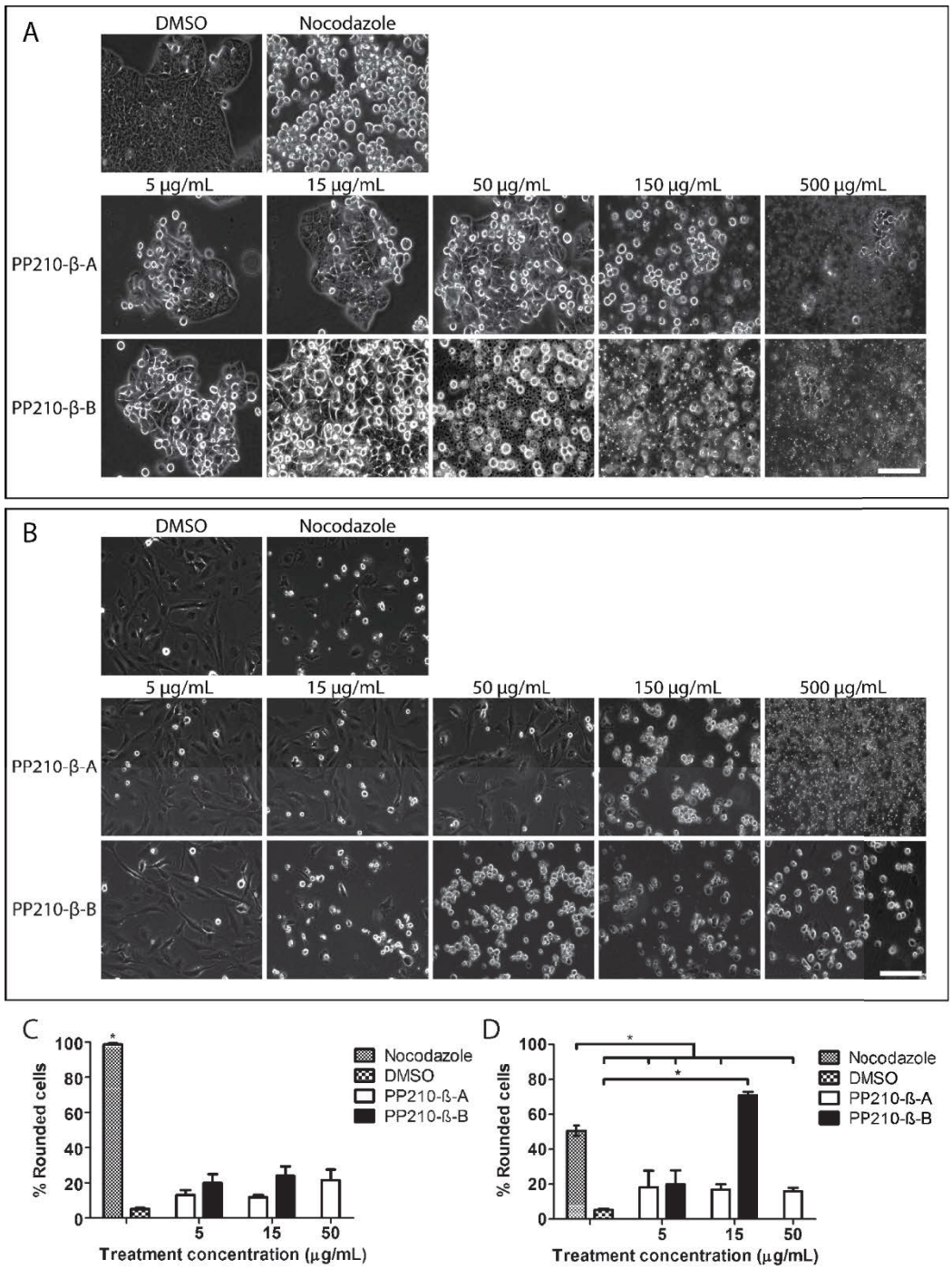

Figure 10. Cell rounding assay after treatment with PP210-β plant extracts at a range of concentrations from 5 to 500 µg/mL in HT29 (**A**) and M059K (**B**) cell lines. Negative control: DMSO. Positive control: nocodazole 200 ng/mL. Scale bars A and B: 100 µm. Mean percentage of rounded cells determined after manually scoring HT29 (**C**) and M059K (**D**) morphologies. Error bars represent the SEM of at least three independent experiments. Statistical significance was determined using one-way ANOVA followed by Tukey's post hoc test ($p < 0.05$).

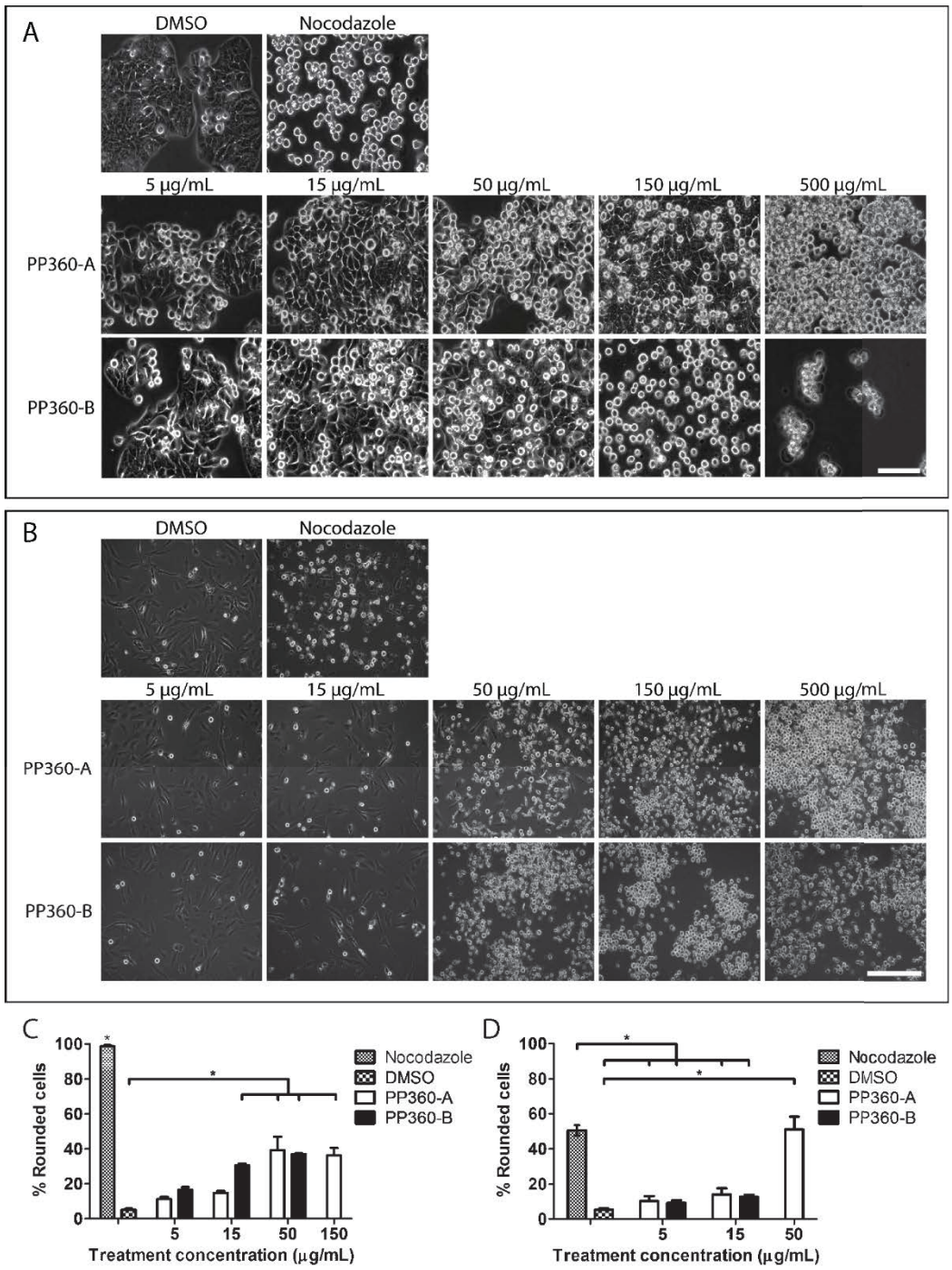

Figure 11. Cell rounding assay after treatment with PP360 plant extracts at a range of concentrations from 5 to 500 µg/mL in HT29 (**A**) and M059K (**B**) cell lines. Negative control: DMSO. Positive control: nocodazole 200 ng/mL. Scale bars: A: 100 µm. B: 200 µm. Mean percentage of rounded cells determined after manually scoring HT29 (**C**) and M059K (**D**) morphologies. Error bars represent the SEM of at least three independent experiments. Error bars represent the SEM. Statistical significance was determined using one-way ANOVA followed by Tukey's post hoc test ($p < 0.05$).

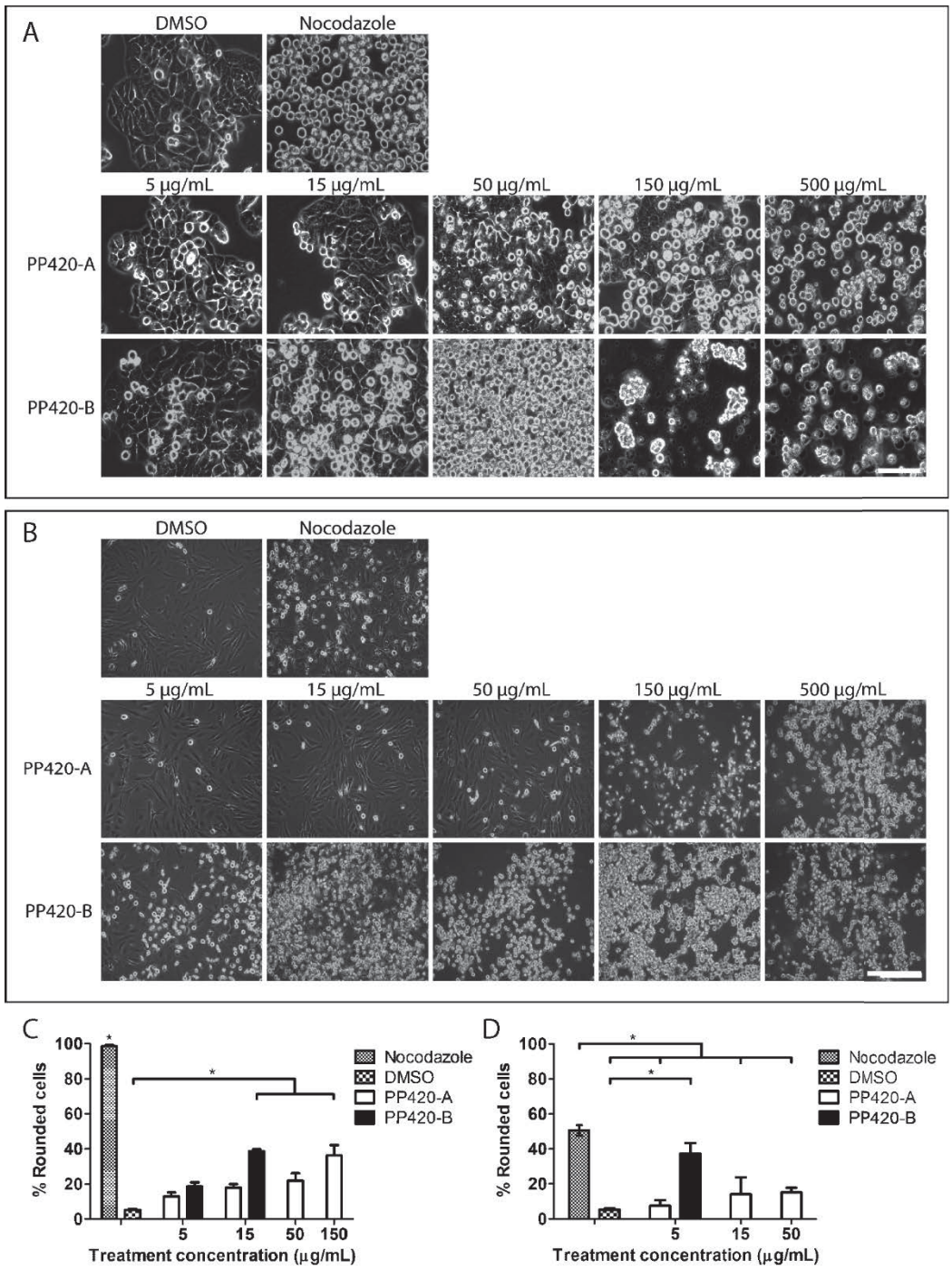

Figure 12. Cell rounding assay after treatment with PP420 plant extracts at a range of concentrations from 5 to 500 µg/mL in HT29 (**A**) and M059K (**B**) cell lines. Negative control: DMSO. Positive control: nocodazole 200 ng/mL. Scale bars: A: 100 µm. B: 200 µm. Mean percentage of rounded cells determined after manually scoring HT29 (**C**) and M059K (**D**) morphologies. Error bars represent the SEM of at least three independent experiments. Error bars represent the SEM. Statistical significance was determined using one-way ANOVA followed by Tukey's post hoc test ($p < 0.05$).

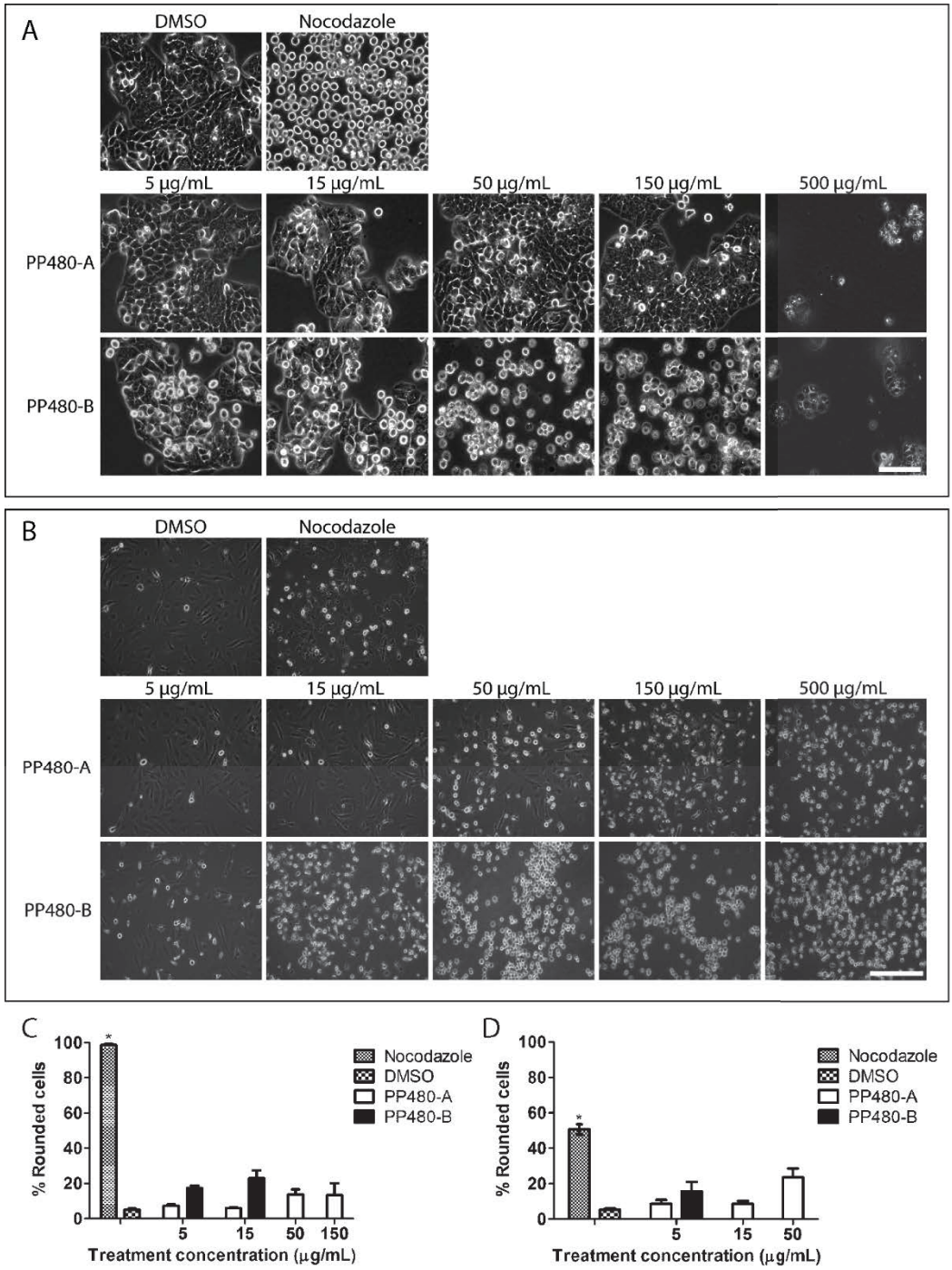

Figure 13. Cell rounding assay after treatment with PP480 plant extracts at a range of concentrations from 5 to 500 µg/mL in HT29 (**A**) and M059K (**B**) cell lines. Negative control: DMSO. Positive control: nocodazole 200 ng/mL. Scale bars: A: 100 µm. B: 200 µm. Mean percentage of rounded cells determined after manually scoring HT29 (**C**) and M059K (**D**) morphologies. Error bars represent the SEM of at least three independent experiments. Error bars represent the SEM. Statistical significance was determined using one-way ANOVA followed by Tukey's post hoc test ($p < 0.05$).

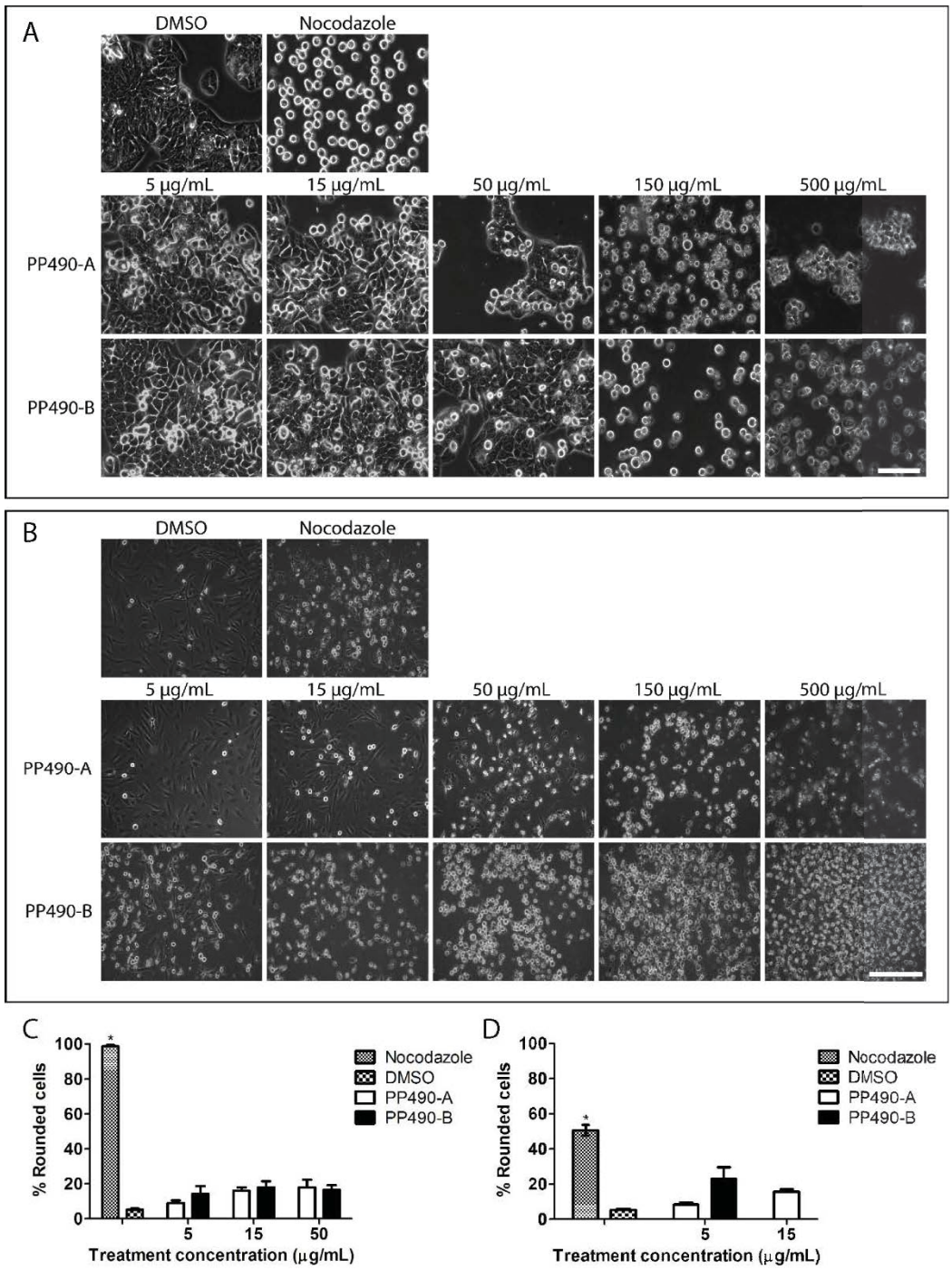

Figure 14. Cell rounding assay after treatment with PP490 plant extracts at a range of concentrations from 5 to 500 µg/mL in HT29 (**A**) and M059K (**B**) cell lines. Negative control: DMSO. Positive control: nocodazole 200 ng/mL. Scale bars: A: 100 µm. B: 200 µm. Mean percentage of rounded cells determined after manually scoring HT29 (**C**) and M059K (**D**) morphologies. Error bars represent the SEM of at least three independent experiments. Error bars represent the SEM. Statistical significance was determined using one-way ANOVA followed by Tukey's post hoc test ($p < 0.05$).

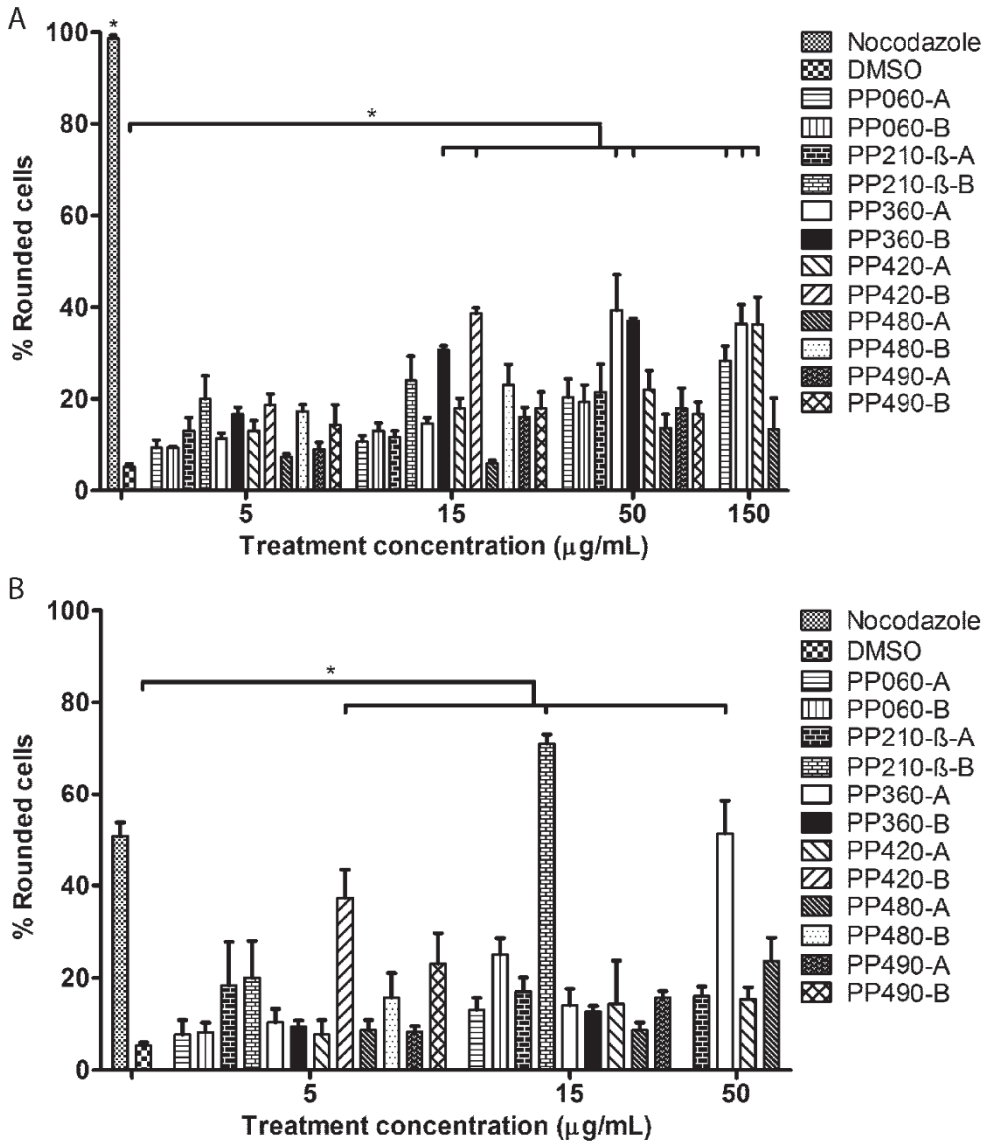

Figure 15. Mean percentage of rounded cells after treatment with 12 Asteraceae extracts in cancer cells HT29 (**A**) and M059K (**B**). Ethanolic and dichloromethane extracts of each plant were added at a range of concentrations from 5 to 500 µg/mL. Negative control: DMSO. Positive control: nocodazole 200 ng/mL. Note: percentage was not determined when the extract was toxic to cells. Error bars represent the SEM of at least three independent experiments. Statistical significance was determined using one-way ANOVA followed by Tukey's post hoc test ($p<0.05$).

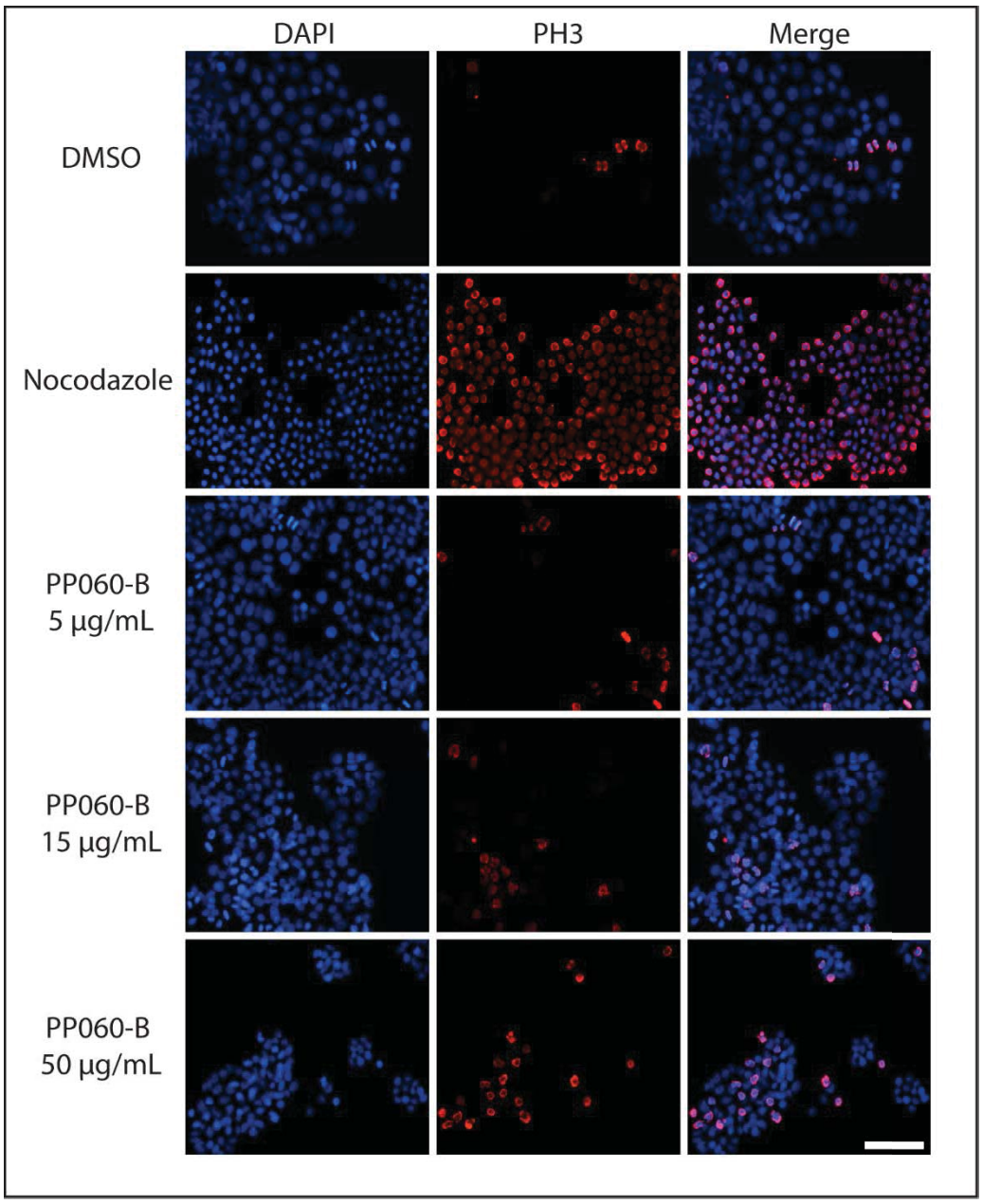

Figure 16. Mitotic cells accumulated after treatment with PP060-B at 5, 15, and 50 µg/mL. Negative control: DMSO. Positive control: nocodazole 200 ng/mL. Analysis by immunofluorescence microscopy. Red: phospho-histone H3 (mitotic cells). Blue: DAPI (DNA). Scale bar: 100 µm.

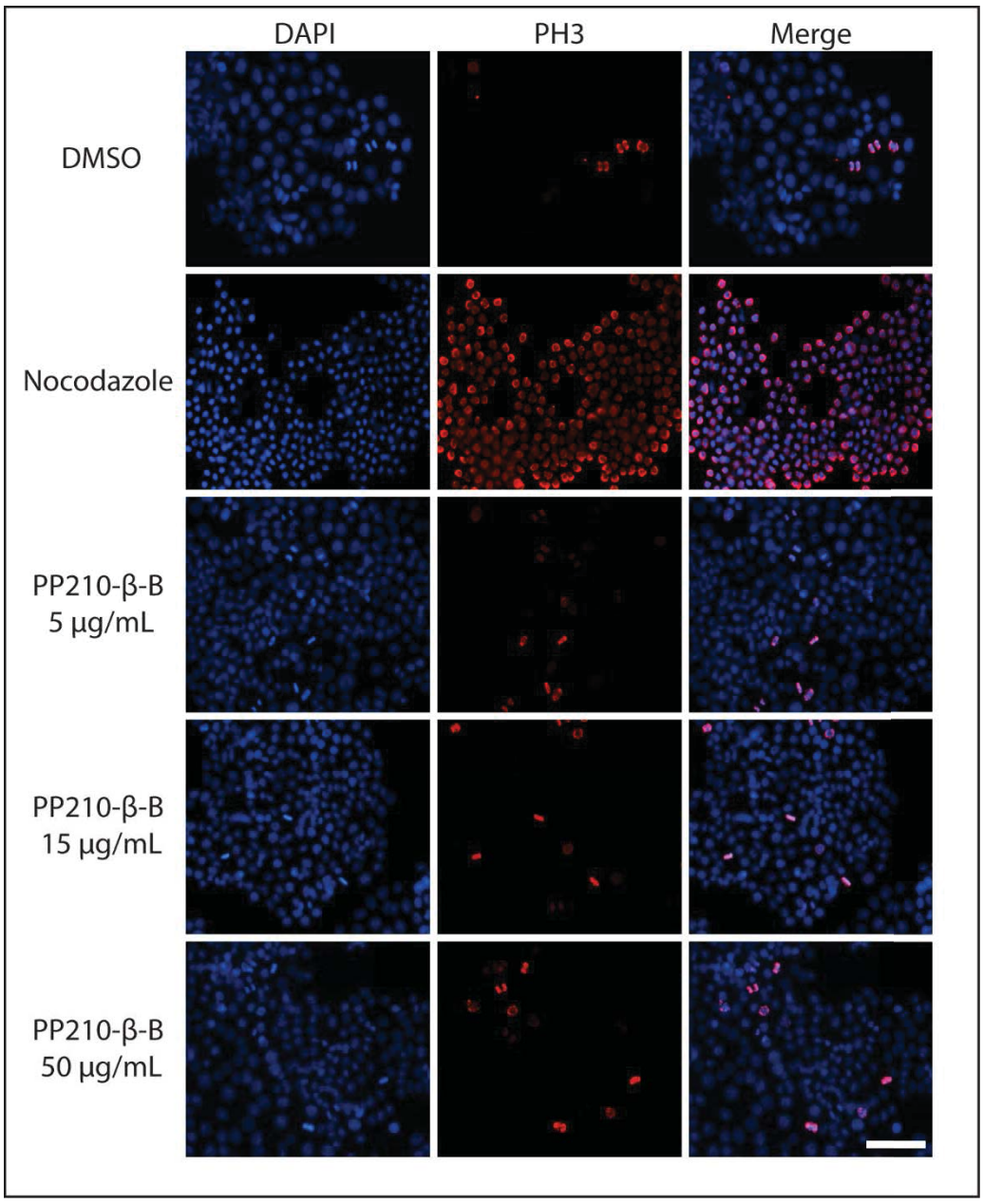

Figure 17. Mitotic cells accumulated after treatment with PP210-β-B at 5, 15, and 50 µg/mL. Negative control: DMSO. Positive control: nocodazole 200 ng/mL. Analysis by immunofluorescence microscopy. Red: phospho-histone H3 (mitotic cells). Blue: DAPI (DNA). Scale bar: 100 µm.

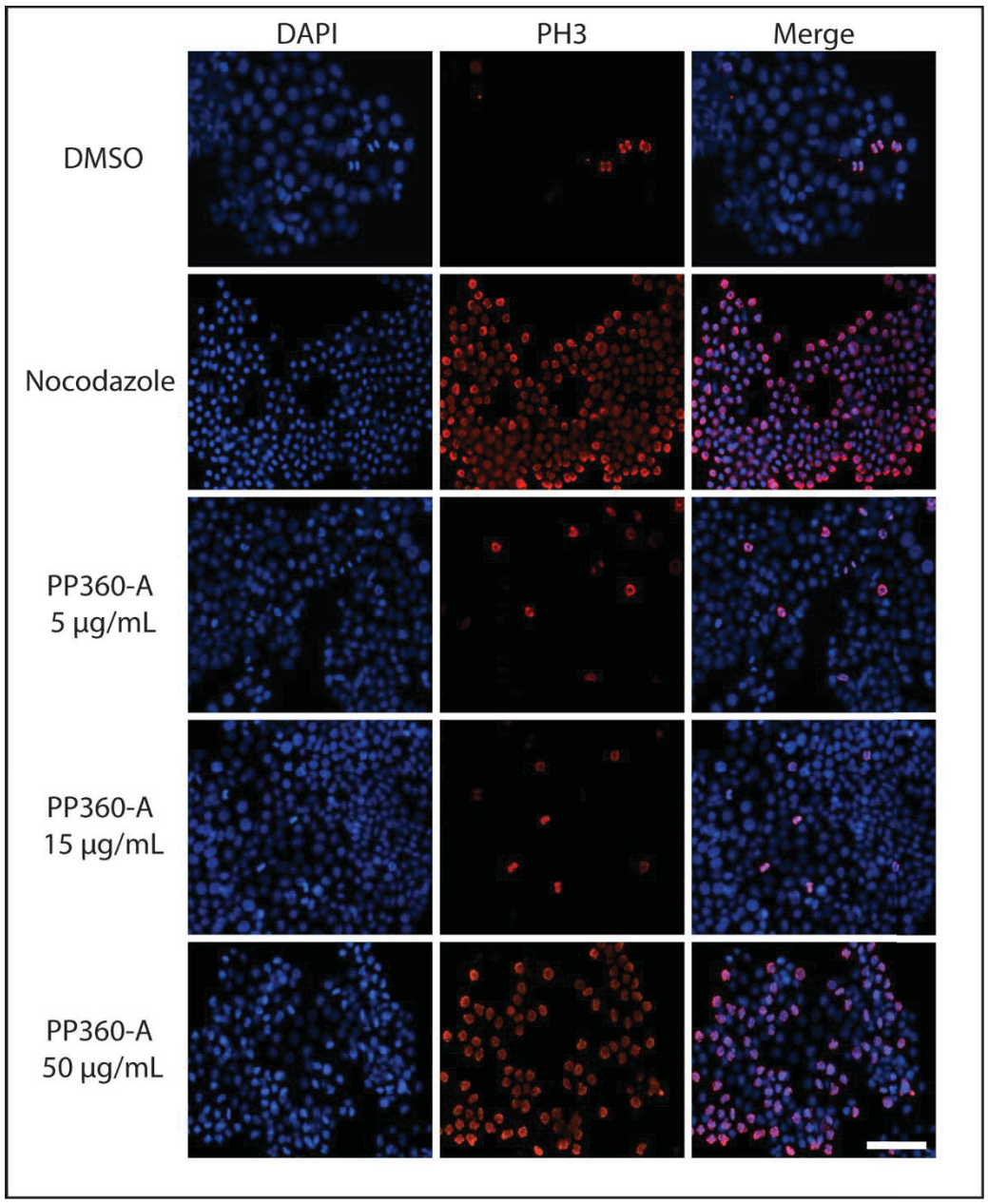

Figure 18. Mitotic cells accumulated after treatment with PP360-A at 5, 15, and 50 µg/mL. Negative control: DMSO. Positive control: nocodazole 200 ng/mL. Analysis by immunofluorescence microscopy. Red: phospho-histone H3 (mitotic cells). Blue: DAPI (DNA). Scale bar: 100 µm.

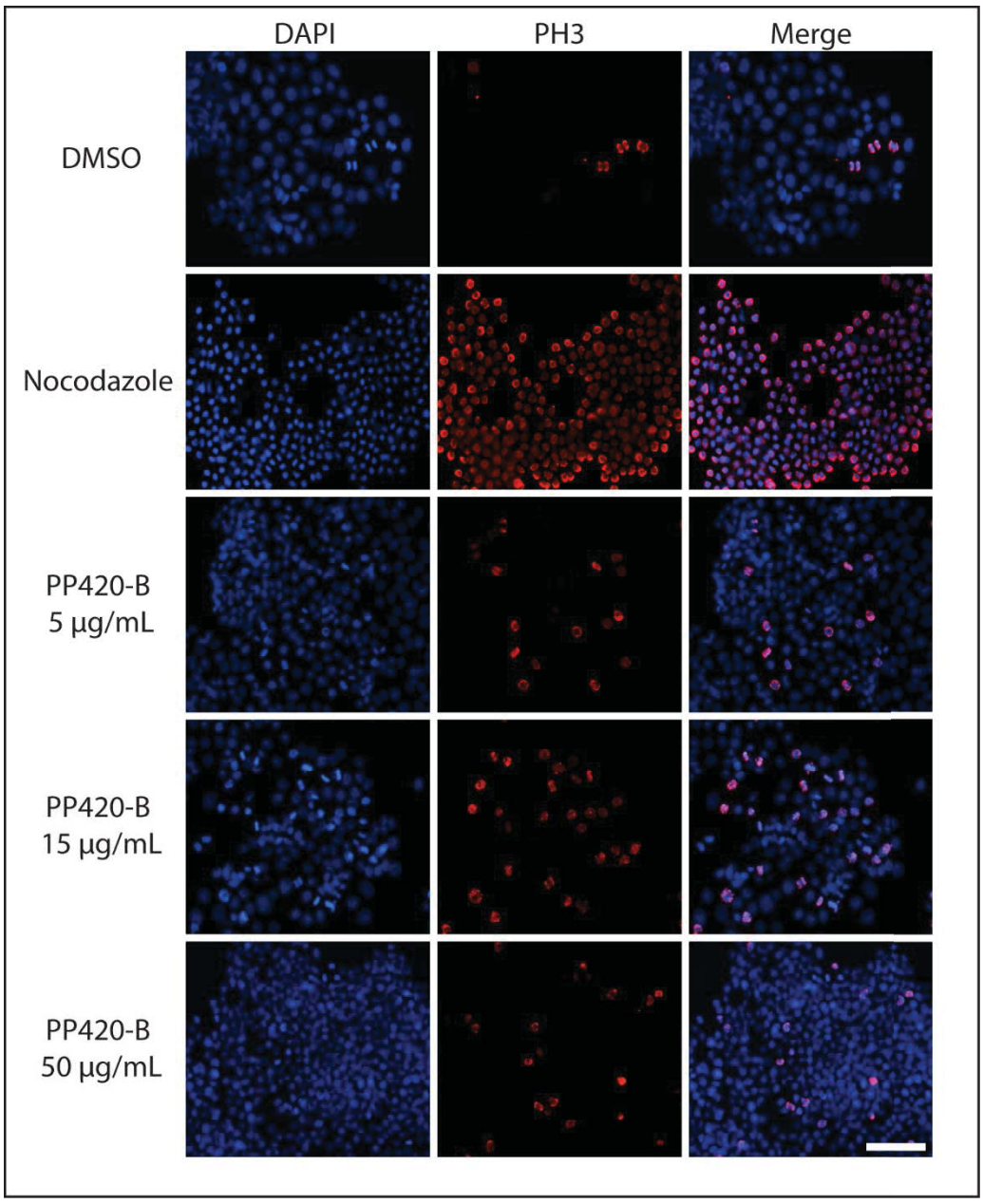

Figure 19. Mitotic cells accumulated after treatment with PP420-B at 5, 15, and 50 µg/mL. Negative control: DMSO. Positive control: nocodazole 200 ng/mL. Analysis by immunofluorescence microscopy. Red: phospho-histone H3 (mitotic cells). Blue: DAPI (DNA). Scale bar: 100 µm.

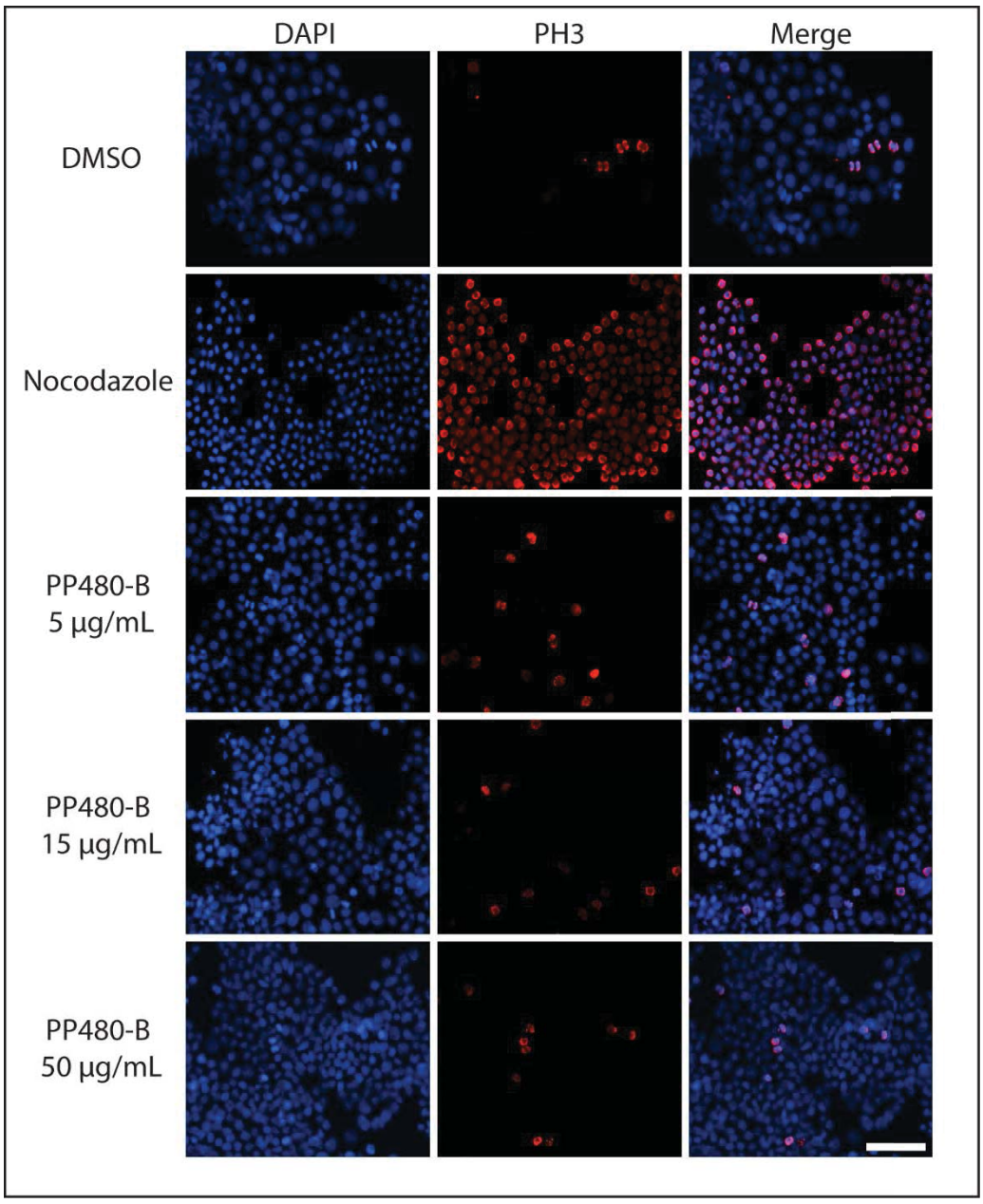

Figure 20. Mitotic cells accumulated after treatment with PP480-B at 5, 15, and 50 µg/mL. Negative control: DMSO. Positive control: nocodazole 200 ng/mL. Analysis by immunofluorescence microscopy. Red: phospho-histone H3 (mitotic cells). Blue: DAPI (DNA). Scale bar: 100 µm.

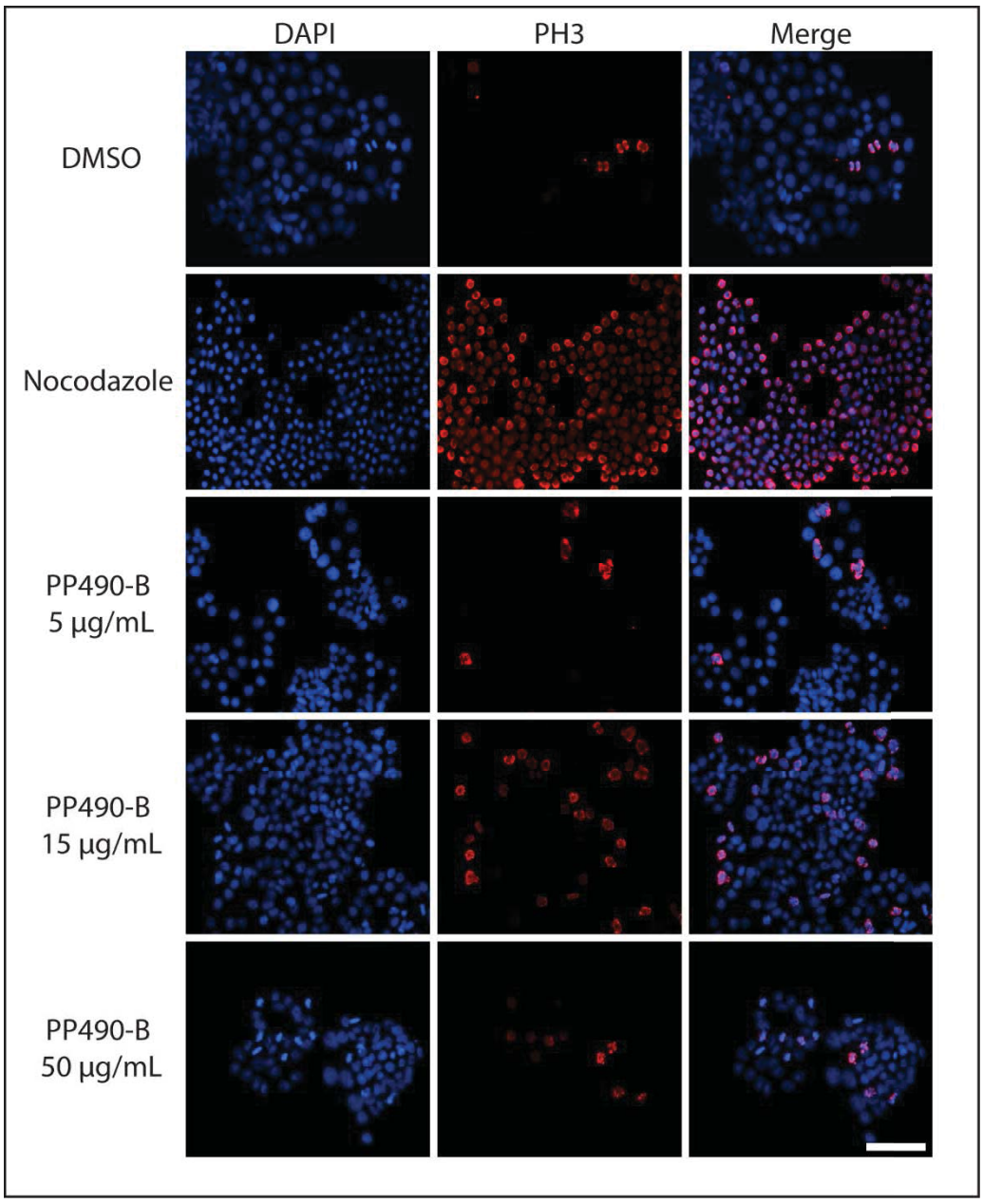

Figure 21. Mitotic cells accumulated after treatment with PP490-B at 5, 15, and 50 µg/mL. Negative control: DMSO. Positive control: nocodazole 200 ng/mL. Analysis by immunofluorescence microscopy. Red: phospho-histone H3 (mitotic cells). Blue: DAPI (DNA). Scale bar: 100 µm.

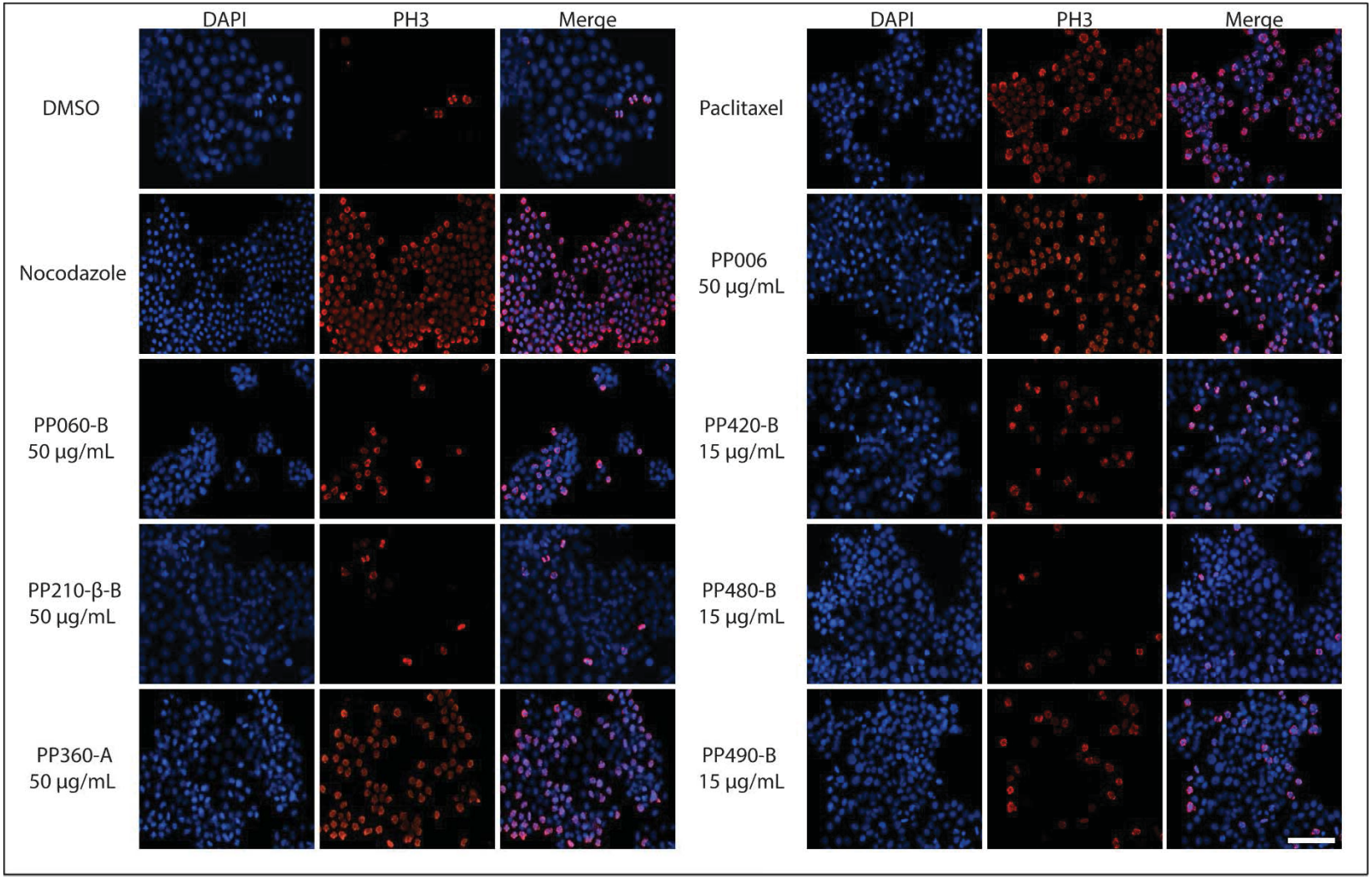

Figure 22. Mitotic HT29 cells accumulated after treatment with six Asteraceae plant extracts. Negative control: DMSO. Positive controls: nocodazole 200 ng/mL, paclitaxel 100 nM, and PP006 50 µg/mL. Analysis by immunofluorescence microscopy. Red: phospho-histone H3 (mitotic cells). Blue: DAPI (DNA). Representative images of the concentration that caused the highest activity for each extract are shown. Scale bar: 100 µm.

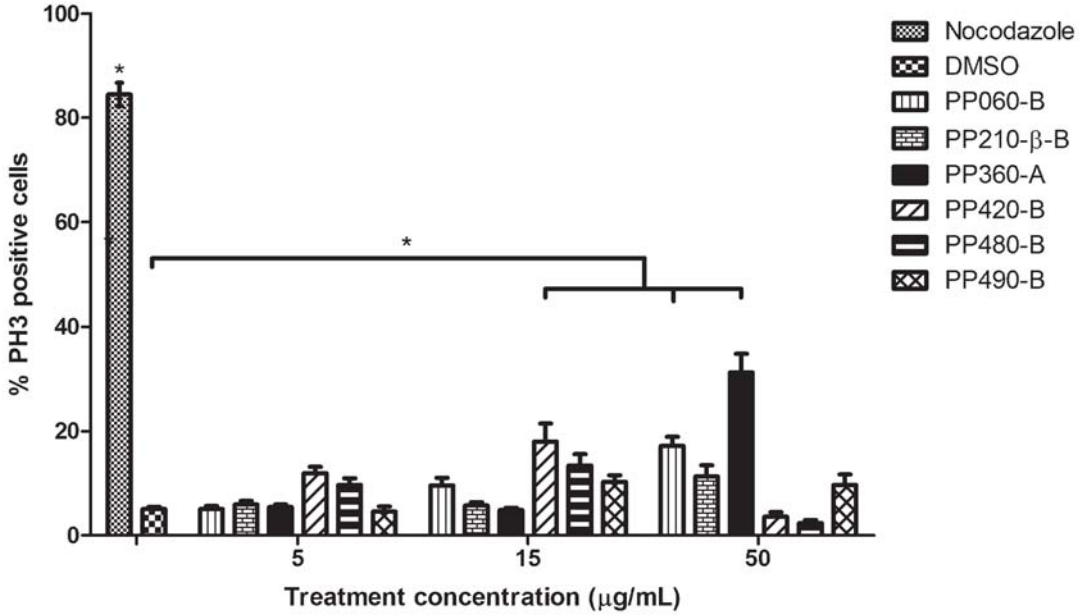

Figure 23. Mitotic indices based on mean percentages of PH3-positive HT29 cells after treatment with six Asteraceae plant extracts at 5, 15, and 50 μg/mL. Negative control: DMSO. Positive control: nocodazole 200 ng/mL. Error bars represent the SEM of at least three independent experiments. Statistical significance was determined using one-way ANOVA followed by Dunnett's post hoc test ($p < 0.05$).

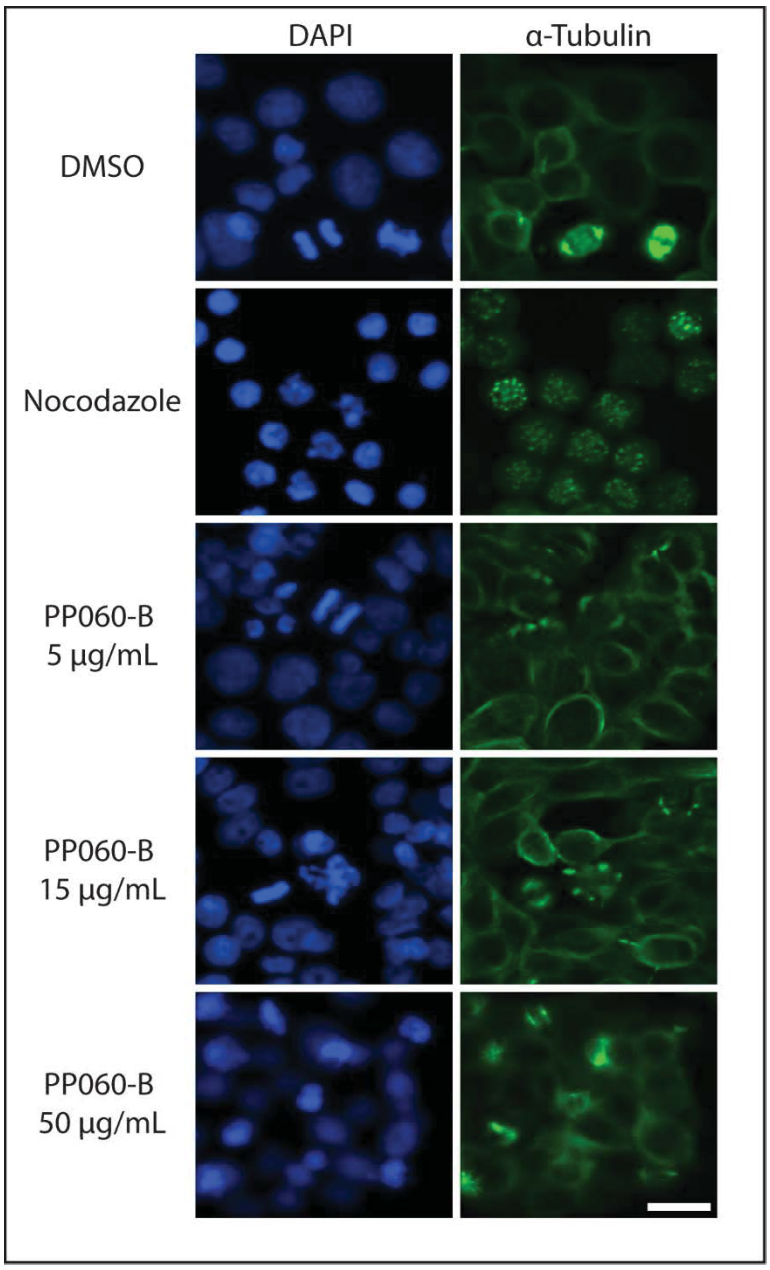

Figure 24. Mitotic spindles in HT29 cells after treatment with PP060-B at 5, 15, and 50 µg/mL. Controls: DMSO and nocodazole 200 ng/mL. Analysis by immunofluorescence microscopy. Green: α-tubulin (microtubules/mitotic spindles). Blue: DAPI (DNA). Scale bar: 20 µm.

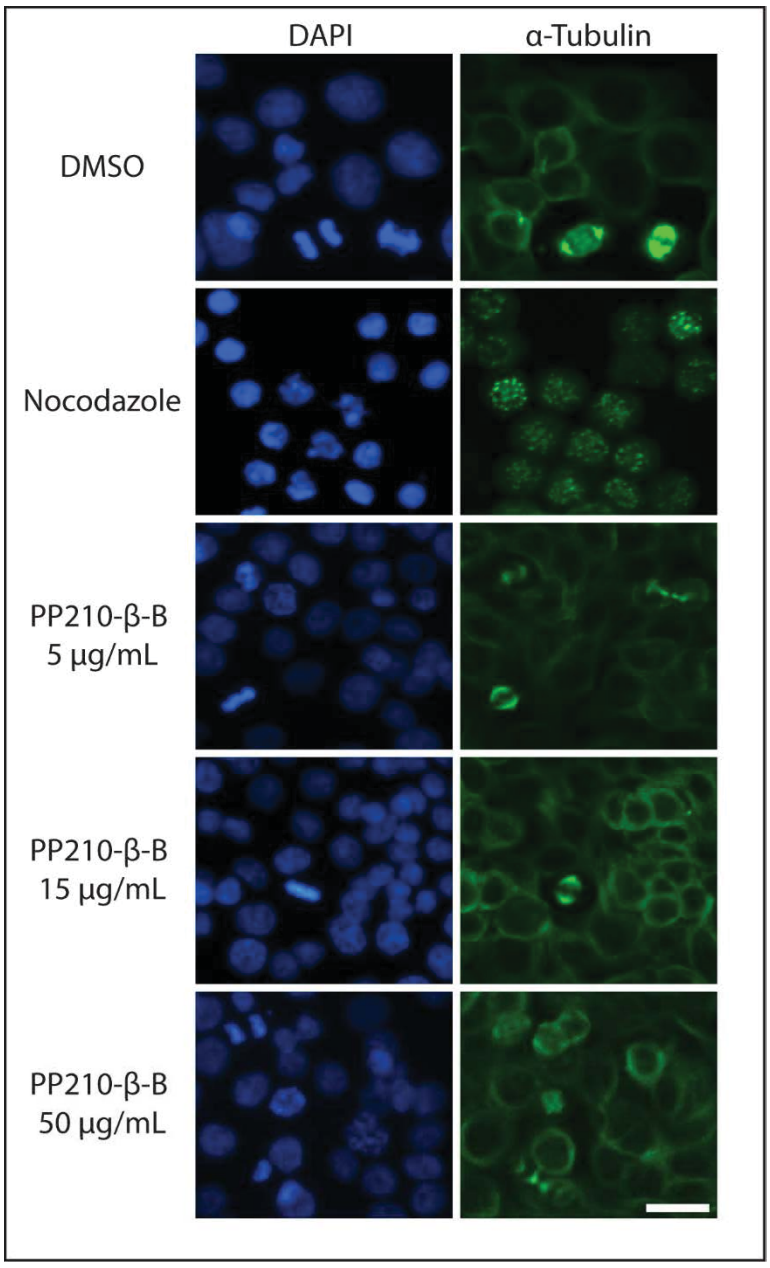

Figure 25. Mitotic spindles in HT29 cells after treatment with PP210-β-B at 5, 15, and 50 µg/mL. Controls: DMSO and nocodazole 200 ng/mL. Analysis by immunofluorescence microscopy. Green: α-tubulin (microtubules/mitotic spindles). Blue: DAPI (DNA). Scale bar: 20 µm.

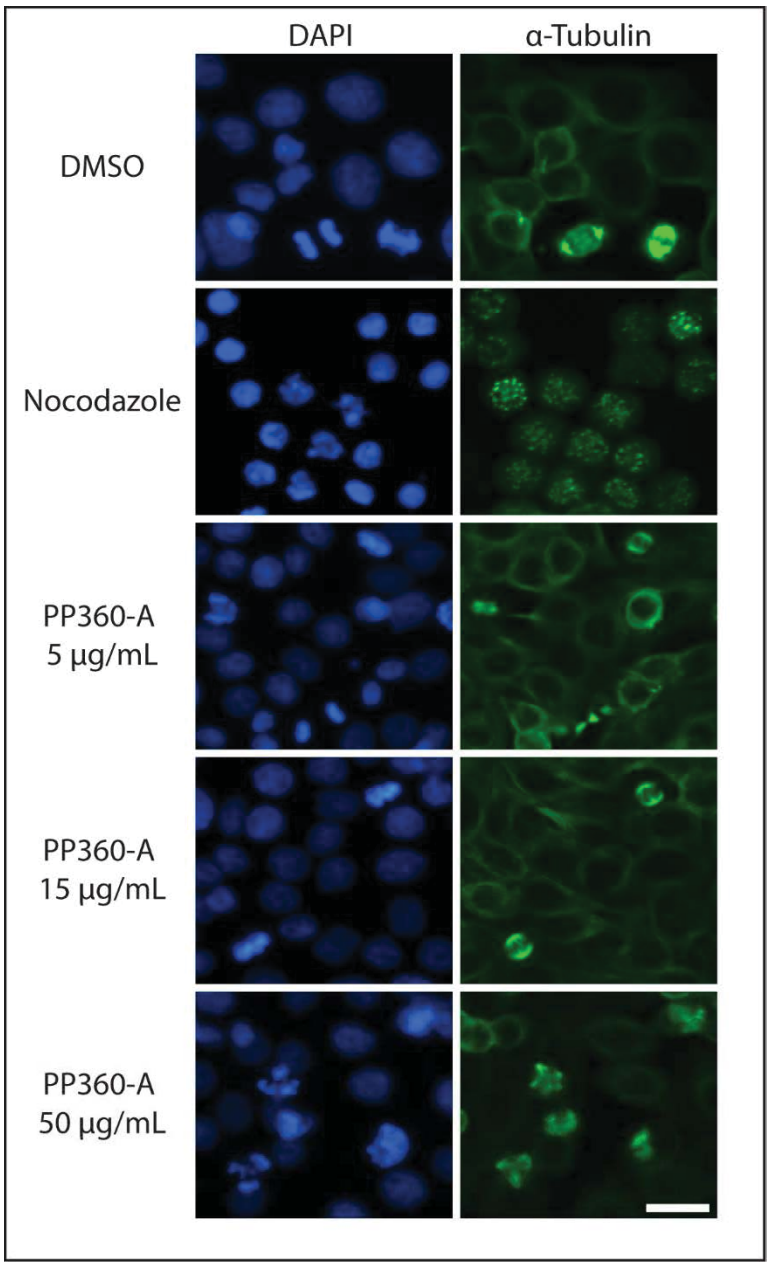

Figure 26. Mitotic spindles in HT29 cells after treatment with PP360-A at 5, 15, and 50 µg/mL. Controls: DMSO and nocodazole 200 ng/mL. Analysis by immunofluorescence microscopy. Green: α-tubulin (microtubules/mitotic spindles). Blue: DAPI (DNA). Scale bar: 20 µm.

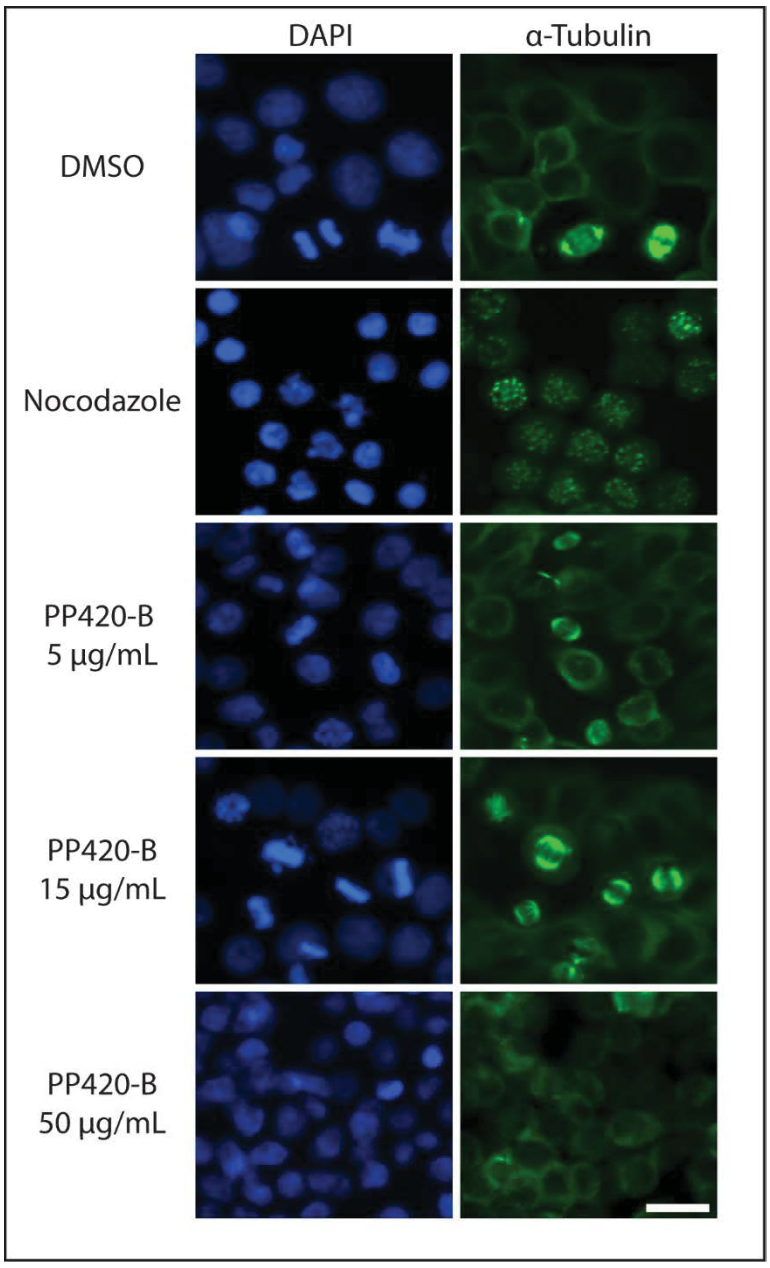

Figure 27. Mitotic spindles in HT29 cells after treatment with PP420-B at 5, 15, and 50 µg/mL. Controls: DMSO and nocodazole 200 ng/mL. Analysis by immunofluorescence microscopy. Green: α-tubulin (microtubules/mitotic spindles). Blue: DAPI (DNA). Scale bar: 20 µm.

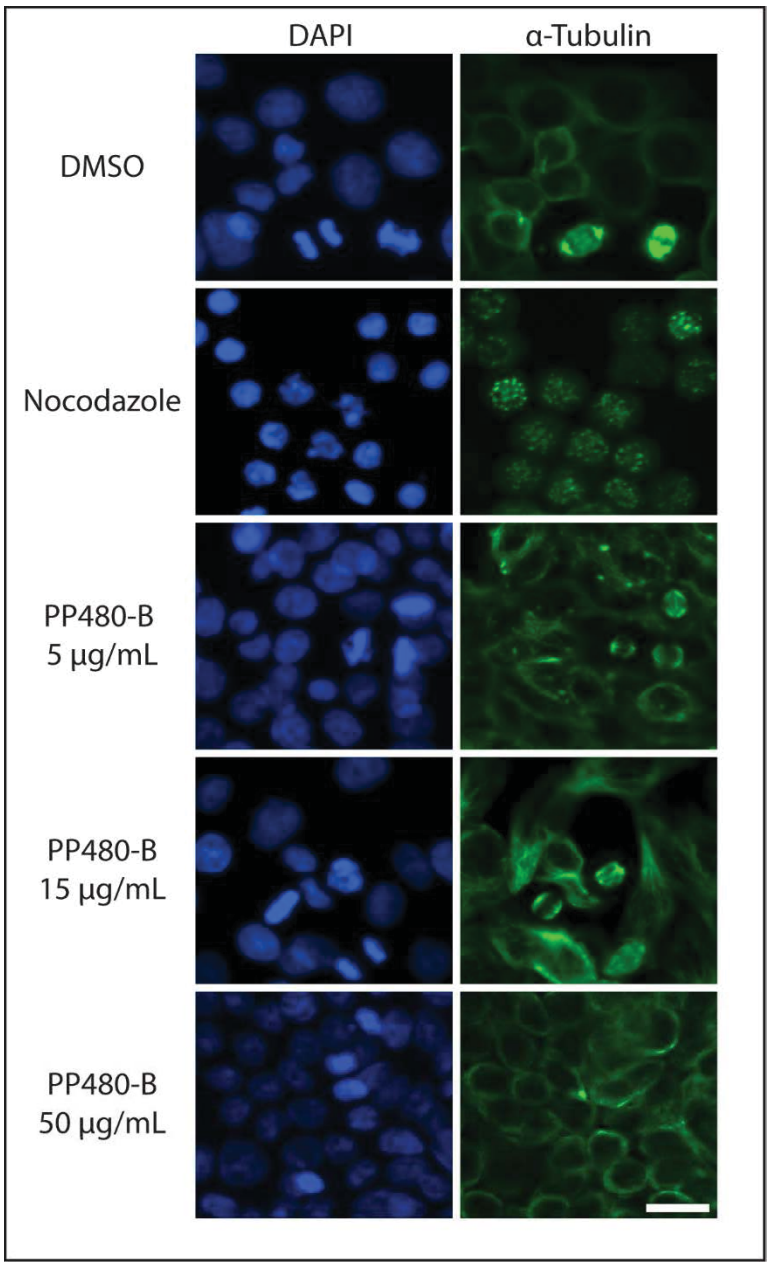

Figure 28. Mitotic spindles in HT29 cells after treatment with PP480-B at 5, 15, and 50 µg/mL. Controls: DMSO and nocodazole 200 ng/mL. Analysis by immunofluorescence microscopy. Green: α-tubulin (microtubules/mitotic spindles). Blue: DAPI (DNA). Scale bar: 20 µm.

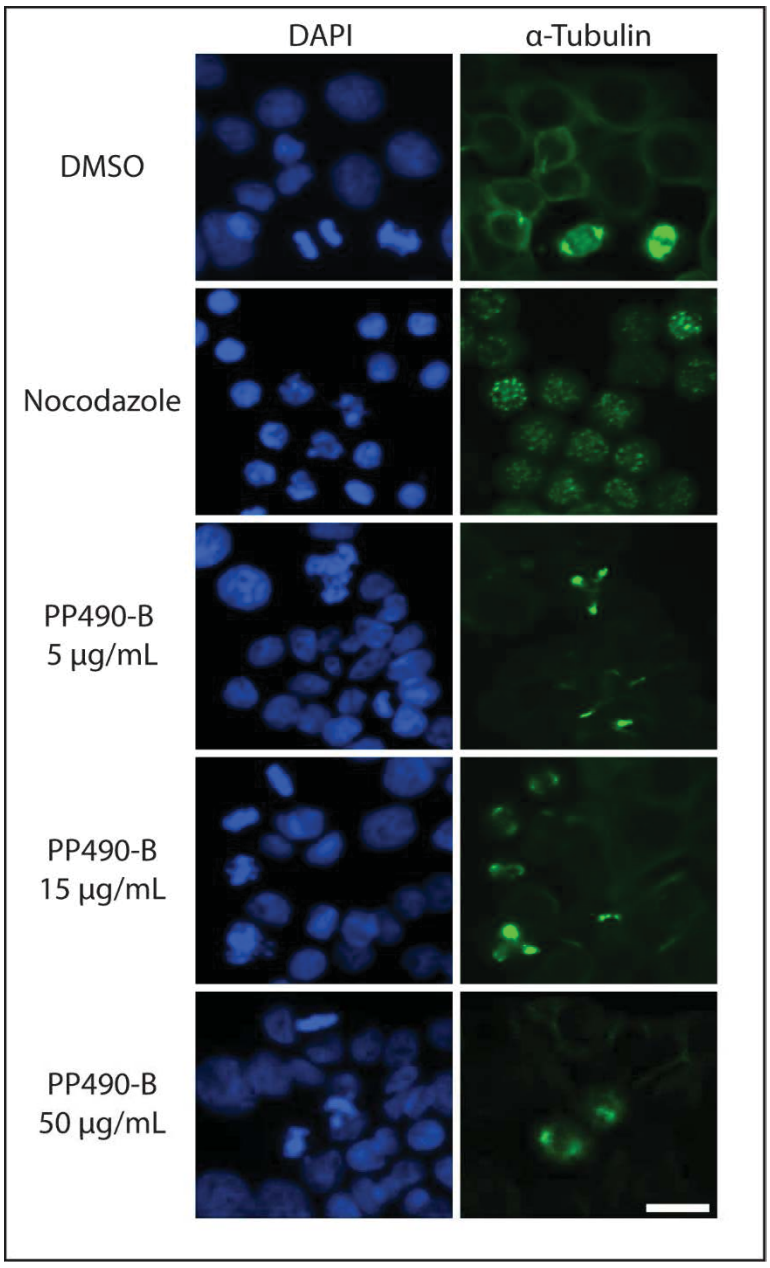

Figure 29. Mitotic spindles in HT29 cells after treatment with PP490-B at 5, 15, and 50 µg/mL. Controls: DMSO and nocodazole 200 ng/mL. Analysis by immunofluorescence microscopy. Green: α-tubulin (microtubules/mitotic spindles). Blue: DAPI (DNA). Scale bar: 20 µm.

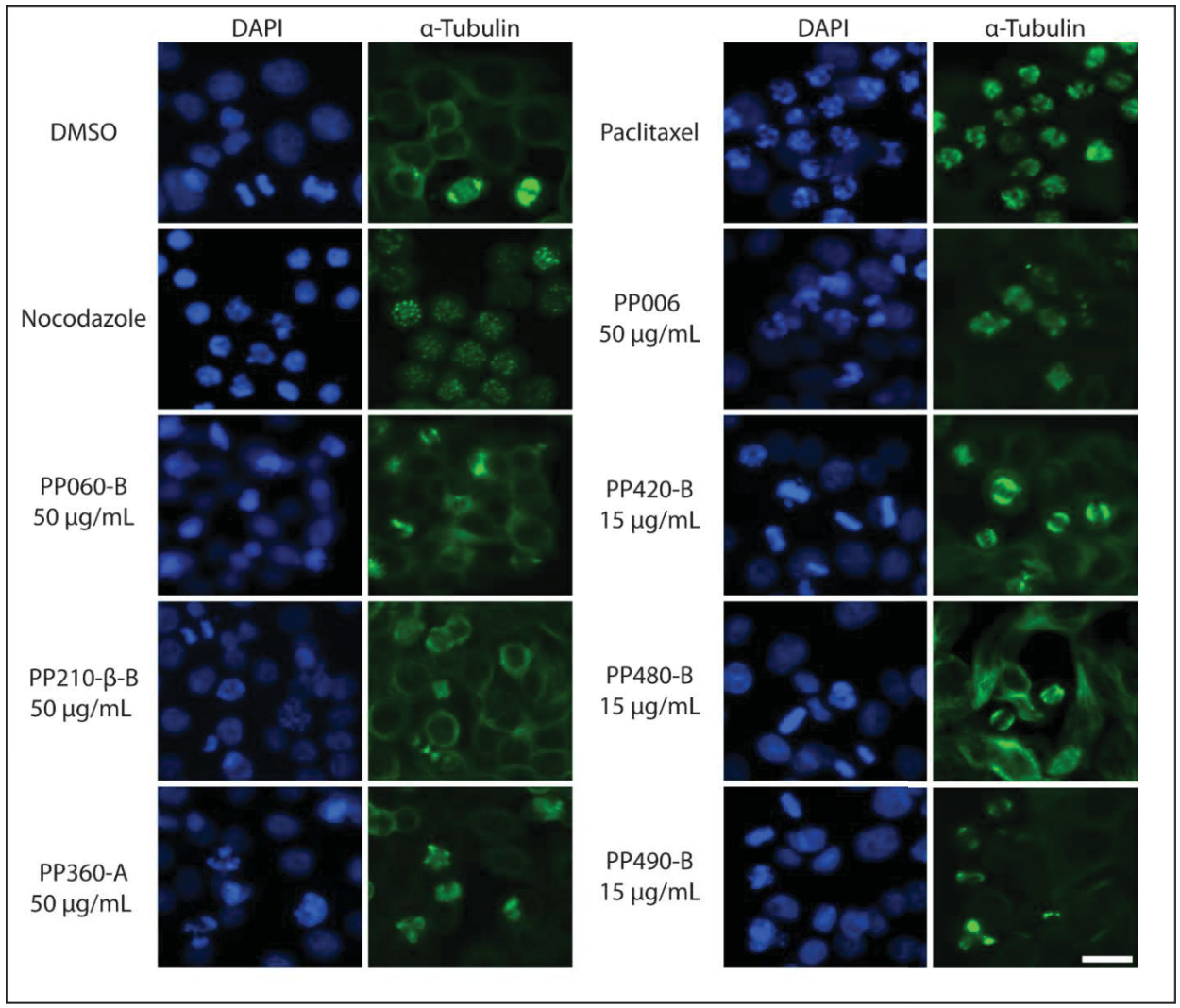

Figure 30. Mitotic spindles in HT29 cells after treatment with six Asteraceae plant extracts. Controls: DMSO, nocodazole 200 ng/mL, paclitaxel 100 nM and PP006 50 µg/mL. Analysis by immunofluorescence microscopy. Green: α-tubulin (microtubules/mitotic spindles). Blue: DAPI (DNA). Representative images of the concentration that caused the highest activity for each extract are shown. Scale bar: 20 µm.

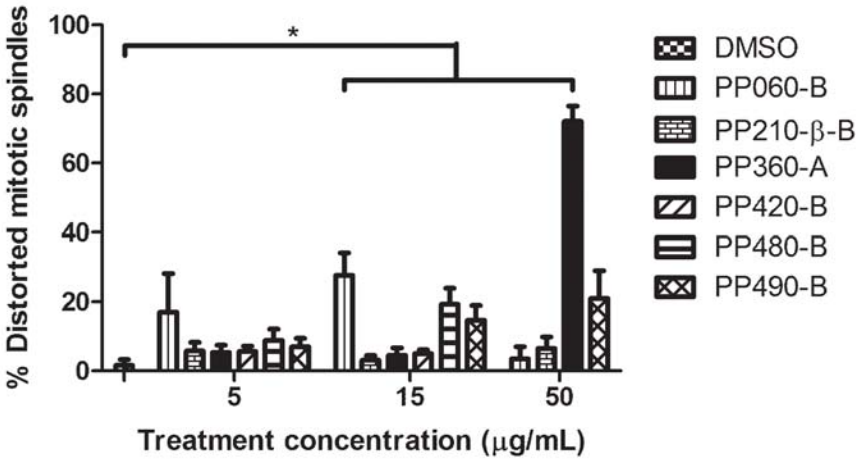

Figure 31. Mean percentages of distorted mitotic spindles in HT29 cells after treatment with six Asteraceae plant extracts at 5, 15, and 50 μg/mL. Analysis by immunofluorescence microscopy targeting α-tubulin. Negative control: DMSO. Error bars represent the SEM of at least three independent experiments. Statistical significance was determined using one-way ANOVA followed by Tukey's post hoc test ($p < 0.05$).

CHAPTER 4

Identification and characterization of PP360-A anti-mitotic activity

We selected *Hymenoxys richardsonii* for further analysis amongst the group of six Asteraceae species. It was the best source of mitotic arrest activity and it induced an interesting distortion of the mitotic spindle. We focused on characterizing the cellular features of the mitotic arrest and on isolating the active compound(s) from the plant extract. Before performing further experiments, we wanted to investigate the different *H. richardsonii* plant parts, extraction methods, or plant collections from different years to ensure that we had a reliable source of material for this research.

4.1 Leaves/stems have the highest relative anti-mitotic activity amongst *H. richardsonii* plant parts

Due to the morphology of *H. richardsonii*, where acicular leaves were difficult to separate from the stems, we prepared three plant parts: roots, flower heads, and the combination of leaves and stems. These three plant parts were separately ground and extracted with ethanol and these extracts were prepared for testing as described in the materials and methods section. To compare the activity of each extract, HT29 cells were treated with either DMSO as a negative control, nocodazole as a positive control, or with one of the three extract preparations. At 24 hours post-treatment, three photos were taken by light microscopy for us to score the morphology of the cells. The percentage of rounded cells was then calculated, and each extract was compared to DMSO and to each other. In **Figure 32** we could see that control treatments induced the expected effects: DMSO presented a normal number of rounded cells in a non-treated population (4.6 ± 0.8%) whereas nocodazole

caused nearly every cell to become rounded. Root and flower extracts elicited responses similar to that of DMSO. More precisely, cells treated with the root extract presented a 7.0 ± 0.9% of rounded cells and treated with the flower extract showed a 9.2 ± 0.9% of rounded cells. The leaves plus stem extract induced a percentage of rounded cells significantly higher than DMSO treatment, with a 28.8 ± 2.9% of rounded cells after the 24-hour treatment. Hence, we determined that the rounding cell activity was present in the leaves and or stems of the *H. richardsonii* plant species.

4.2 The cell rounding activity can be extracted from *H. richardsonii* by either 75% ethanol or dichloromethane but not with water

Next, we tested the effect of three extraction solvents in PP360 activity. Under the same conditions, we prepared extracts from the leaves/stems of *H. richardsonii* using either 75% ethanol, pure dichloromethane, or water, and compared them in a cell rounding assay. HT29 cells were treated for 24 hours with DMSO, nocodazole, or the three extracts, and we then scored the cell morphologies to evaluate the cell rounding activity. As shown in **Figure 33**, DMSO and nocodazole-treated cells presented the expected number of rounded cells after these treatments: about 5% in DMSO and about 100% in nocodazole treatment. We found no difference between the ethanolic and dichloromethane extracts activity, which in both cases was significantly higher than that elicited by DMSO treatment. The ethanolic extract caused 29.0 ± 2.5% of rounded cells and the dichloromethane extract caused 30.7 ± 1.4% of rounded cells. In contrast, the water extract of *H. richardsonii* did not present a rounded cell activity on HT29 cells and only a 7.6 ± 0.7% of cells were rounded, similar to that of DMSO treatment. We chose 75% ethanol to extract the cell rounding activity from the leaves/stems of *H. richardsonii* for further experiments.

4.3 Anti-mitotic activity of *H. richardsonii* is maintained in two different years

Synthesis of secondary metabolites by plants might have variations when environmental conditions change (Pavarini et al., 2012). We wanted to check that *H. richardsonii* plant species collected in different years elicited a similar activity upon cancer cells. In June 2016 and May 2017, we collected *H. richardsonii* from the same location and prepared ethanolic extracts from ground leaves/stems from both collections under similar conditions. We then tested the two extracts in a cell rounding assay using light microscopy photos to count the percentage of rounded cells induced by each extract in HT29 cells after 24 hours of treatment. We treated HT29 cells with DMSO or nocodazole and observed the expected responses as shown in **Figure 34**. Cells treated with PP360 extract from 2016 or 2017 collections presented 24.0 ± 4.1% and 27.7 ± 1.4% of rounded cells, respectively. When these values were compared to each other and to the percentage of rounded cells obtained from DMSO treatment (4.6 ± 1.8%), we found that PP360 extracts from 2016 and 2017 had a similar cell rounding activity.

We demonstrated that *H. richardsonii* activity was found in the leaves plus stems and could be extracted by ethanolic or dichloromethane solvents. Furthermore, the activity was present in two different years of collection. Hence, we decided to use the ethanolic extract of leaves plus stems of *H. richardsonii* from 2016 collection, referred as PP360-A, for further studies of its biological effects upon cells.

4.4. Non-cancer lung fibroblastic cells WI38 do not accumulate rounded cells after 24 hours of treatment with PP360-A

We were interested in testing PP360-A on a non-cancer cell line in addition to the two cancer cell lines. We treated WI38 cells, which are normal, non-transformed lung fibroblastic cells, for 24 hours with either DMSO, nocodazole, or PP360-A at a range of concentrations from 5 μg/mL to 500 μg/mL and performed a cell rounding assay. Using light microscopy photos, we observed the treated cells and scored them for their rounded or flat morphology. **Figure 35** illustrates the results obtained where DMSO treatment, as expected, did not induce a rounding cell activity and presented a normal 4.3 ± 0.3% of rounded cells, and nocodazole treatment caused an accumulation of 40.1 ± 2.0% of rounded cells, which was lower than in HT29 cells but similar to the M059K cells. Interestingly, the cell rounding activity previously observed with cancer cell lines HT29 and M059K after treatment with PP360-A was not present in WI38 cells at any of the concentrations tested. PP360-A treatment only caused 2.7 ± 0.3% rounded cells at 5 μg/mL, 3.3 ± 1.2% at 15 μg/mL, 3.7 ± 1.2% at 50 μg/mL, and 5.7 ± 1.2% at 150 μg/mL. None of these values were statistically different from the percentage of rounded cells obtained after DMSO treatment. When WI38 cells were treated with PP360-A at 150 μg/mL, even though we did not find many rounded cells, we noticed a change in cell morphology where WI38 cells seemed less adherent to the culture plate surface. At the relatively high concentration of 500 μg/mL, the treatment caused cell death. These data indicated that PP360-A did not have a cell rounding activity in the non-cancer cell line WI38.

4.5 PP360-A has a relatively low cytotoxic effect in WI38 cell line

We determined the half maximum inhibitory concentration (IC_{50}) of extract PP360-A in the non-cancer cell line WI38 after 96 hours of treatment using the MTT assay. Extract PP360-A had an IC_{50} of 96.4 ± 23.7 μg/mL for WI38 cells. This was a similar value to the IC_{50} obtained for HT29 cells (123.7 ± 15.7 μg/mL) and suggests that PP360-A still affects WI38 cells at relatively high concentrations but does not induce a mitotic arrest, as demonstrated in the cell rounding assay.

4.6 Cell cycle protein levels after 24 hours of treatment with PP360-A

A series of Western Blot analyses were performed to observe the levels of proteins involved in the cell cycle of cells treated with PP360-A. HT29 cells were treated with either DMSO, nocodazole, or 50 μg/mL of PP360-A. After 24 hours of treatment, a mechanical shake-off was carried out in the nocodazole and in one of two flasks of PP360-A treatment to separate the rounded cells (mitotic cells, MC). Adherent cells from all flasks were collected by trypsinization and proteins were extracted following the cell extraction protocol described in the materials and methods. PP360-A-treated and adherent cells remaining after mechanical shake-off were labeled as interphase cells (IC). A second treatment with PP360-A and no mechanical shake-off was included to represent a total population of cells (TC) (i.e. mitotic plus interphase cells). Proteins present in the five samples (DMSO, nocodazole, TC, IC, and MC) were separated by electrophoresis with polyacrylamide gels, and the western blotting technique was carried out using different antibodies of interest.

We aimed to analyze the effects of PP360-A upon levels of the cell cycle proteins cyclin B1, cyclin A, and cyclin E in HT29 cells. The results are shown in panel A of **Figure 36**.

Cyclin B1 levels were higher in nocodazole-treated cells and in PP360-A-treated MC when compared with DMSO treatment and with TC and IC from PP360-A treatment, where the bands corresponding to cyclin B1 were lighter. Because cyclin B1 protein is required for mitotic entrance, when its levels reach a peak, these results confirmed the state in mitosis of those rounded cells accumulated after PP360-A treatment. Cyclin A levels were higher in DMSO treatment and in TC and IC from PP360-A treatment. Interestingly however, we detected lower levels of cyclin A in MC from PP360-A treatment relative to nocodazole treatment, suggesting that the timing for the mitotic arrest caused by PP360-A extract might be later than the arrest caused by nocodazole treatment. Cyclin E protein was detected in samples from DMSO treatment, as well as in TC and IC from PP360-A treatment, and no bands were present either in nocodazole treatment or in MC from PP360-A treatment. These results supported our observations that PP360-A has an activity that affects the mitotic phase of the cell cycle.

Together with cyclin B1, Cdk1 protein is essential for cells to enter mitosis. It is always present throughout the cell cycle, but it requires post-translational modifications, such as dephosphorylation of tyrosine 15 residue (i.e. Y15), to be active. We performed a western blot analysis using the anti-Cdk1-Y15 antibody and an antibody that targets all Cdk1 proteins. The pan-anti-Cdk1 antibody revealed a steady level of Cdk1 protein in all the samples, as expected. By contrast, we observed low levels of the Y15-phosphorylated form of Cdk1 in nocodazole samples and higher levels in DMSO, TC, and IC protein samples. MC from PP360-A treatment were similar to nocodazole treatment (panel B in **Figure 35**). This result showed that rounded cells obtained from PP360-A treatment have low levels of Y15-Cdk1, consistent with cells in mitosis. We also investigated the effects of PP360-A

treatment in the levels of threonine 320-phosphorylated form of Plk1 protein (i.e. Plk1 pT210), which is involved in the mitotic processes. Using a pan-anti-Plk1 antibody, we observed low levels of Plk1 in DMSO and higher levels in nocodazole sample. From PP360-A treatment, TC and IC were similar to DMSO, whereas MC, like nocodazole, had higher levels of Plk1 protein. The specific anti-Plk1-pT210 antibody revealed no band in DMSO-treated cells and a band in nocodazole-treated cells. The only sample from PP360-A treatment with a band corresponding to T210-phosphorylated form of Plk1 was the MC sample. No Plk1-pT210-band was detected in TC or IC from PP360-A treatment. (Panel B in **Figure 36**). Again, this result is consistent with rounded cells from PP360-A treatment undergoing mitosis.

4.7 Rounded cells accumulated after PP360-A treatment have an active Cdk1

Having shown that cyclin B and dephosphorylated Cdk1 are present in PP360-A-treated rounded cells, we then asked if Cdk1 was enzymatically active by performing an enzyme assay. This activity can be measured by detecting the levels of one of the Cdk1 substrates, the protein phosphatase 1 catalytic subunit alpha (PP1Cα), which is phosphorylated in its threonine 320 residue by Cdk1. GST-PP1Cα is an artificial Cdk1 substrate that contains the Cdk1 consensus sequence found in PP1Cα. The protein GST alone does not have the Cdk1 phosphorylation site and is used as a negative control substrate (Lewis et al., 2013). The artificial Cdk1 substrate and the GST protein were used to carry enzymatic in vitro reactions with HT29 cell extracts from DMSO, nocodazole, and PP360-A treatments. A purified Cdk1 protein and the extraction buffer were used as positive and negative controls of the enzymatic reaction, respectively, showing that the artificial Cdk1 substrate was phosphorylated by purified Cdk1 protein and was not phosphorylated by the extraction

buffer. Cells extracted from DMSO treatment had a light band of phosphorylated PP1Cα, whereas cells from nocodazole treatment had a strong band of this protein, indicating low and high Cdk1 activities, respectively. TC and IC extracts from PP360-A treatment presented bands with similar intensity to that of the DMSO extract, reflecting low levels of Cdk1 activity. By contrast, MC exhibited a strong band of the phosphorylated PP1Cα, in agreement with our hypothesis of an active Cdk1 protein in the rounded cells collected after 24 hours of treatment with PP360-A (**Figure 37**).

4.8 Characterization of the cell cycle arrest induced by PP360-A treatment by time-lapse video microscopy

To understand better the mitotic arrest activity elicited by the plant extract PP360-A, we performed time-lapse video microscopy experiments (**Figure 38**). HT29 cells were treated with either DMSO or PP360-A at 50 µg/mL and immediately observed in a Cytation^{TM} 5 Image Reader with light microscopy photos taken every 10 minutes for 24 or 48 hours.

4.8.1 Percentage of rounded cells fluctuate over 24 hours of treatment with PP360-A

Light microscopy photos of DMSO and PP360-A-treated cells were manually counted at every hour time point from 0 to 24 hours in 5 independent videos to determine the percentage of rounded cells over time. A non-treated population, here represented by the DMSO-treated cells, do not accumulate rounded cells over time. It contains approximately 5% of cells undergoing mitosis at any time. Interestingly, we found that the percentage of rounded cells from PP360-A treatment was statistically different at the 6-hour time point with a 13.2 ± 1.6% of rounded cells, then it reached a peak of 27.0 ± 2.2% rounded cells at

the 13-hour time point and finally decreased over time. By 24 hours, 15.6 ± 1.3% of rounded cells were present in the PP360-A-treatment (n=5, panel A of **Figure 38**).

4.8.2 Duration of mitotic arrest in HT29 cells treated with PP360-A

In the video microscopy analysis of HT29 cells treated with DMSO, we noticed that a normal mitotic phase had a duration of 30 minutes on average. We considered the start of mitosis the moment when a cell rounded, and the end of mitosis the moment when it underwent cytokinesis. We then measured the duration of mitosis in PP360-A-treated cells. Early on, we noticed that the timing was variable, therefore, we classified the timing into two groups: the first consisting of cells with a rounded morphology lasting less than 2 hours and the second consisting of cells with a rounded morphology lasting 2 or more hours. Importantly, as shown in panel B of **Figure 38**, we obtained that there was a 25.3 ± 4.5% of cells falling into the second category and staying in the mitotic phase for more than 2 hours (n=300). The remaining 74.7 ± 4.5% of cells, however, underwent mitosis in what seemed to be a normal time of less than 2 hours.

4.8.3 HT29 cell fate after treatment with PP360-A

We observed the fate of a total of 300 cells treated with PP360-A at 50 µg/mL from 3 time-lapse videos to determine if they exited the rounded state or not. A first observation was that 99% of the cells entered mitosis and only 1% of cells did not enter mitosis during our analysis. Furthermore, 80% of the cells that entered mitosis could exit it and undergo cytokinesis and returned to a flat, adherent morphology (Panel C of **Figure 38**). From the remaining cells that entered mitosis, 8% of them divided into more than two parts and returned to a flat morphology, which we termed abnormal cell division. This group

belonged to cells that arrested in mitosis for periods of about 20 hours or more, according to the information gathered in the previous analysis. We could not determine the fate of 12% of the cells because they moved from the visible field during observation. However, we decided to still consider them for this analysis because they had been arrested in mitosis for abnormal times, in agreement with the observation that cells dividing abnormally had arrested in mitosis for long periods. Possibly, there is about a 20% of PP360-A-treated cells that delays or arrests in mitosis for more than 2 hours and might end in an abnormal cell division or cell death.

4.8.4 Relationship between time of mitotic entrance and duration of arrest

We decided to record the precise time point at which every cell entered mitosis and the duration of this mitotic phase, considered as the interval of time since the moment the cell became rounded until it underwent cytokinesis. We noticed an interesting pattern than we could then reflect on panel D of **Figure 38**. 74% of the cells that entered mitosis in the first 8 hours post-treatment stayed arrested for more than 2 hours. In contrast, 93% of the cells that entered mitosis after 8 hours of treatment could exit this phase in less than 2 hours (n=300).

These results further confirm that PP360-A induces an accumulation of rounded cells, representing delayed or arrested mitotic cells. Based on the decrease of the percentage of rounded cells during the second half of the 24-hour treatment and the number of cells that exit mitosis, these data also suggest that PP360-A-treated cells might either overcome the mitotic defect and exit mitosis or, depending on time, a group is not affected by the treatment and do not arrest in the first place.

4.9 Investigation of a second cell cycle arrest in HT29 cells after treatment with PP360-A

Based on our observations, treatment with PP360-A arrested a maximum of thirty percent of the cells in mitosis, whereas nocodazole or paclitaxel could arrest nearly a hundred percent of the treated cells. To understand better why PP360-A-treated cells never reached a higher percentage of mitotic arrested cells, we investigated if cells were being arrested in another phase of the cell cycle.

4.9.1 No difference in mitotic entrance timing between PP360-A and control treatment in synchronized HT29 cells suggests no cell cycle arrest prior to mitotic arrest

HT29 cells were partially synchronized at the G1/S checkpoint by treating them with thymidine at 2 mM for 15 hours. After removing thymidine, which permits cells to continue the cell cycle, they were treated with either DMSO or PP360-A at 50 μg/mL and observed by time-lapse video microscopy for the next 24 hours. Photos at every hour time point from 0 to 24 hours after the DMSO and PP360-A treatments were manually scored for their rounded or flat cell morphology and the percentage of rounded cells was determined over time. We found, as expected, an accumulation of mitotic cells with the PP360-A treatment. We also found that both DMSO-treated and PP360-A-treated cells entered mitosis in a period of 3 hours starting at the same time of 7 hours post-treatment (**Figure 39**). These data suggest that treatment with PP360-A causes an arrest in mitosis and not elsewhere in the cell cycle.

4.9.2 Sensitivity to nocodazole re-treatment after mitotic exit of PP360-A-treated cells suggests absence of a different type of cell cycle arrest following the mitotic arrest

After investigating the possibility of an arrest prior to the mitotic arrest, we wanted to investigate if cells treated with PP360-A that are able to exit mitosis and continue viable stayed arrested in another phase of the following cell cycle. To answer this question, we designed an experiment in which HT29 cells were first treated with PP360-A at 50 μg/mL for 24 hours and then re-treated with either DMSO or nocodazole at 200 ng/mL for another 24 hours. We observed that interphase cells from the 24-hour treatment with PP360-A could re-enter mitosis and arrest with the nocodazole re-treatment (**Figure 40**). By 24 hours of nocodazole re-treatment, PP360-A-treated cells, presented a similar percentage of rounded cells than that observed in a normal 24-hour treatment with nocodazole (i.e. nearly 100% of rounded cells). These results support the notion that there is no cell cycle arrest after PP360-A-induced mitotic arrest.

4.10 Analysis of HT29 cells treated with PP360-A by flow cytometry

To confirm if PP360-A treatment arrested cells at different cell cycle phases, such as M phase, we analyzed PP360-A-treated cells in a cell cycle analysis by flow cytometry. We cultured HT29 cells in eight 25 cm^2 flasks, treated them with PP360-A at 50 μg/mL, and then collected and fixed the cells every 3 hours, during the first 24 hours post-treatment, completing a total of eight time points. We also treated HT29 cells with DMSO, in an equal volume to that added of PP360-A, to represent a non-treated population; nocodazole 200 ng/mL for G2/M arrest; and CPT 50 nM for S-phase arrest. These cells were collected after 24 hours of treatment and fixed with ethanol under the same conditions that PP360-A-treated cells. DNA was then stained with propidium iodide and analyzed with flow

cytometry. The results of three independent experiments are represented in **Figure 41**. Control treatments presented the expected percentage of cells on every phase of the cell cycle: DMSO-treated cells presented 6.6 ± 2.5% of cells in the G2/M phases, 62.8 ± 0.4% in G1 phase, and 30.6 ± 2.2% in S phase; nocodazole-treated cells presented 95.7 ± 1.3% in G2/M, 0.5 ± 0.2% in G1, and 3.8 ± 1.2% in S phase; and CPT presented 4.6 ± 4.6% in G2/M, 0.5 ± 0.5% in G1, and 94.8 ± 5.2% in S phase. PP360-A treatment showed a similar pattern in the percentages of cells arrested in the G2/M phase to that observed in our time-lapse video microscopy. The percentage of cells arrested in G2/M was 12.51 ± 1.73% after 3 hours of treatment with PP360-A, increasing over time to reach a peak of 34.6 ± 11.9% at 12 hours and then decreased progressively. According to this analysis, by 24 hours post-treatment, there is a 7.8 ± 6.0% of G2/M-arrested cells.

4.11 Treatment with PP360-A damages DNA in mitotic cells as measured by phosphorylation of histone H2AX

To characterize further the biological activity of our extract, we wanted to determine if the treatment with PP360-A extract could induce damage in the DNA and, if so, observe its characteristics. We treated HT29 cells for 24 hours with either DMSO, CPT 50 nM as a positive control for genotoxicity, or PP360-A at 50 μg/mL and then performed an immunofluorescence microscopy assay using anti-histone-γ-H2AX antibody. This histone is phosphorylated when the DNA damage pathway is activated after treatment with ionizing radiation or with a genotoxic agent (Rogakou et al., 1998; Furuta et al., 2003). DMSO-treated cells were also used as a control to set the threshold of the fluorescent signal. As shown in **Figure 42**, HT29 cells treated with DMSO did not show γ-H2AX signal, whereas cells treated with CPT presented a strong signal showing clearly damaged DNA. CPT

interferes with DNA synthesis and arrests cells in S phase; therefore, a characteristic pan-nuclear γ-H2AX signal is observed in interphase-arrested cells. Surprisingly, PP360-A-treated cells had γ-H2AX foci in the mitotic cells that accumulated after 24 hours. We did not observe this signal in interphase cells. When looking at the DAPI staining of PP360-A-treated and γ-H2AX positive cells, we commonly noticed a morphology where mitotic cells appeared to have an abnormal chromosome congression. A small percentage of the mitotic cells seemed to have a normal mitotic morphology and those cells did not contain γ-H2AX foci.

The experiments performed with PP360-A showed that this ethanolic extract of the leaves/stems of *H. richardsonii* induced a mitotic arrest in HT29 cells that was determined by a 4c content of DNA and rounded PH3-positive cells with an active Cdk1/Cyclin B complex and T210-phosphorylated Plk1. The accumulation of mitotic cells could be observed after 3 hours of treatment, peaked at 12-13 hours with approximately 30% of mitotic cells, and afterwards decreased. About 20% of PP360-A treated HT29 cells delayed or arrested for abnormal times and possibly underwent an aberrant cell division. Mitotic cells from PP360-A treatment are characterized by the presence of distorted mitotic spindles, defects in chromosome congression, and damaged DNA. In addition, no cell cycle arrest different from mitotic arrest was observed. The non-transformed WI38 cell line did not accumulated rounded cells after 24 hours of PP360-A treatment.

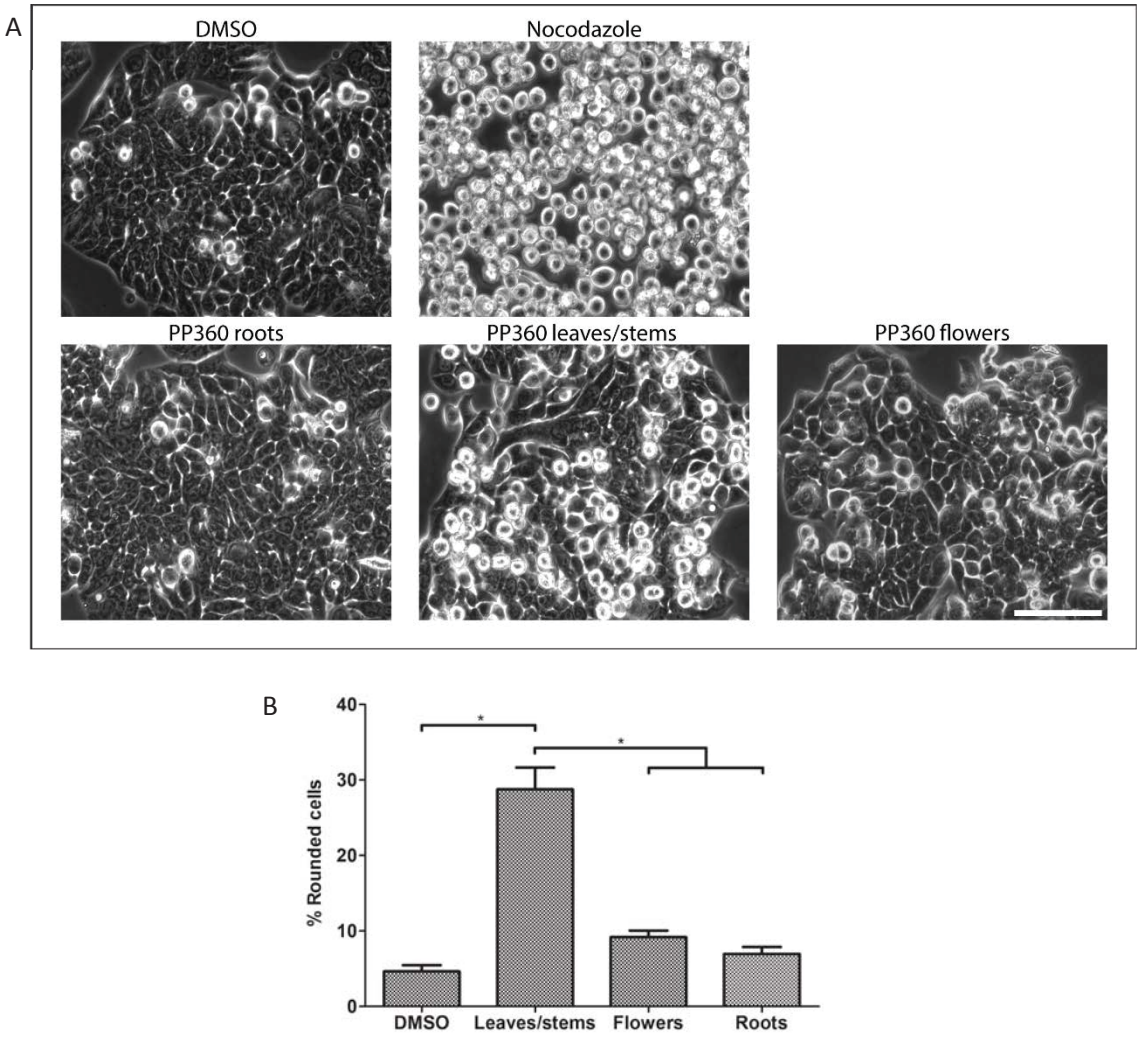

Figure 32. Leaves/stems extract from *H. richardsonii* causes the highest percentage of rounded cells when compared with the flower or root extracts. Analysis by light microscopy in HT29 cells after 24 hours of treatment with the three different plant extracts at 50 µg/mL. Negative control: DMSO. Positive control: nocodazole 200 ng/mL. Scale bar: 100 µm (A). Mean percentage of rounded cells after counting of light microscopy photos. Error bars represent the SEM of two independent experiments. Statistical significance was determined with one-way ANOVA followed by Tukey's post hoc test ($p < 0.05$) (B).

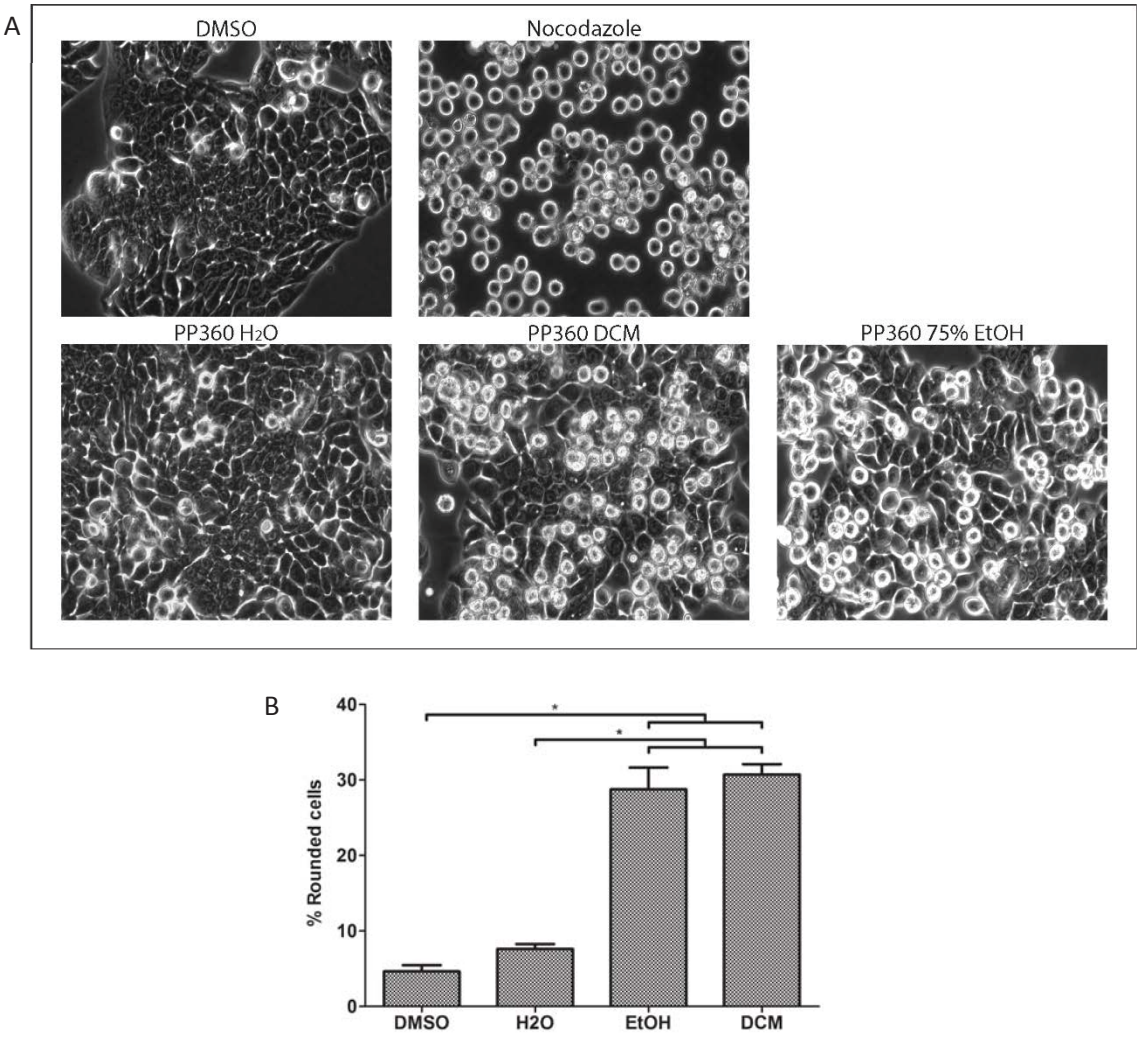

Figure 33. Ethanol and dichloromethane extracts from *H. richardsonii* induce a similar percentage of rounded cells. Water extract of *H. richardsonii* is not different from negative control. Analysis by light microscopy in HT29 cells after 24 hours of treatment with the three different plant extracts at 50 μg/mL. Negative control: DMSO. Positive control: nocodazole 200 ng/mL. Scale bar: 100 μm (**A**). Mean percentage of rounded cells after counting of light microscopy photos. Error bars represent the SEM of two independent experiments. Statistical significance was determined with one-way ANOVA followed by Tukey's post hoc test ($p < 0.05$) (**B**).

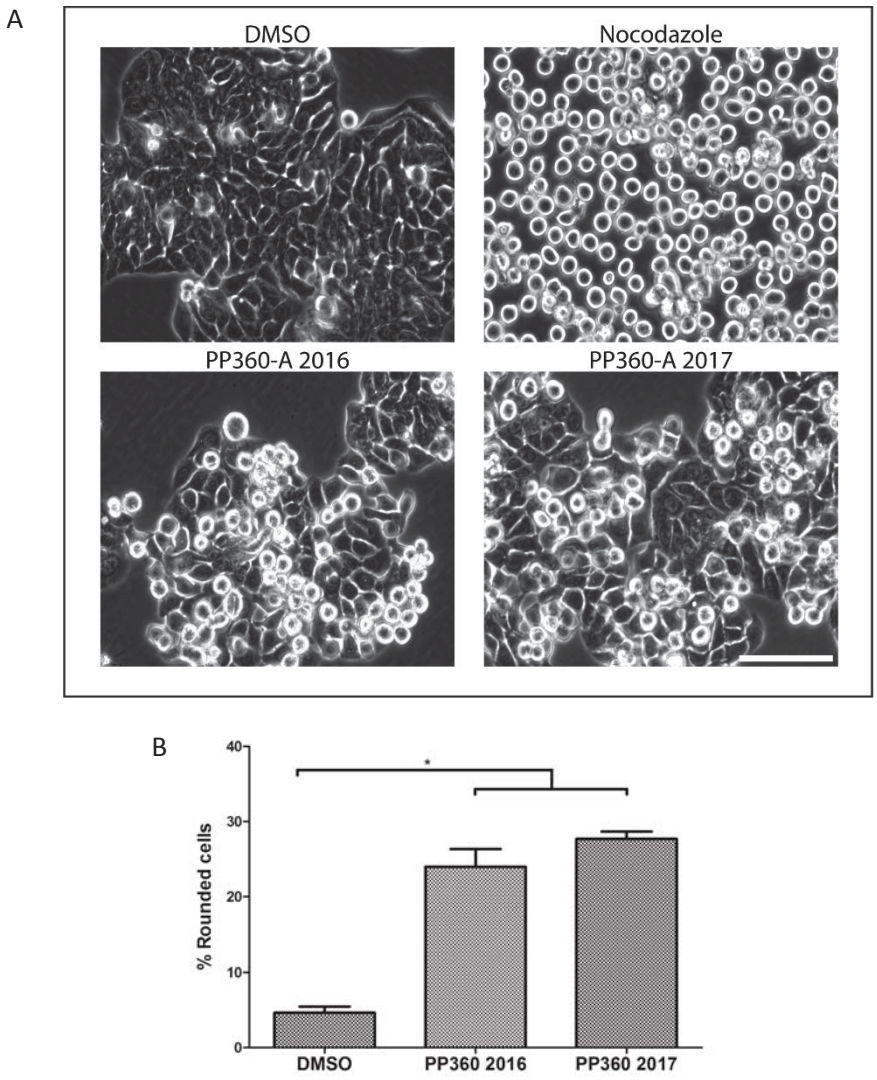

Figure 34. *H. richardsonii* extracts from two different years induce a similar percentage of rounded cells. Analysis by light microscopy in HT29 cells after 24 hours of treatment with the three different plant extracts at 50 μg/mL. Negative control: DMSO. Positive control: nocodazole 200 ng/mL. Scale bar: 100 μm (**A**). Mean percentage of rounded cells after counting of light microscopy photos. Error bars represent the SEM of two independent experiments. Statistical significance was determined with one-way ANOVA with Tukey's post hoc test ($p < 0.05$) (**B**).

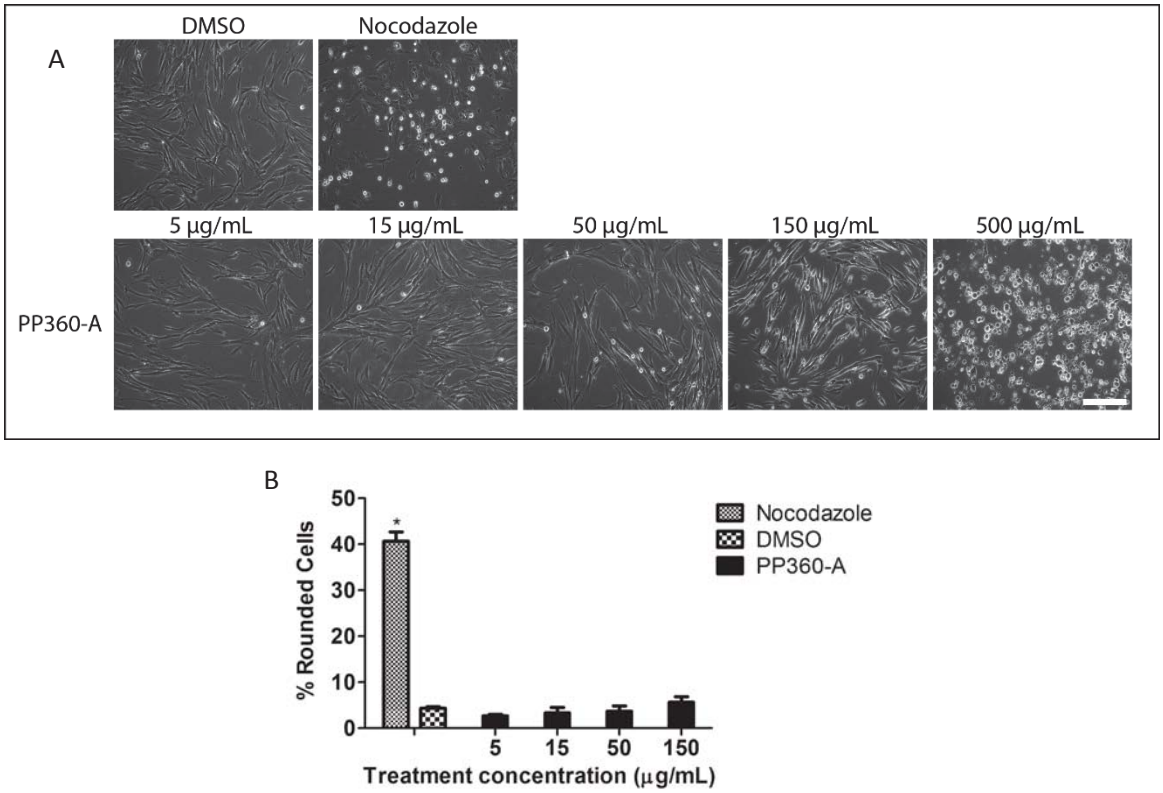

Figure 35. Cell rounding assay in WI38 cell line after treatment with PP360-A at a range of concentrations from 5 to 500 µg/mL. Positive control: nocodazole 200 ng/mL. Negative control: DMSO. Scale bar: 100 µm (**A**). Mean percentage of rounded cells determined after manually scoring WI38 cell morphologies from light microscopy assay. Error bars represent the SEM of at least three independent experiments. Statistical significance was determined using one-way ANOVA followed by Tukey's post hoc test ($p < 0.05$) (**B**).

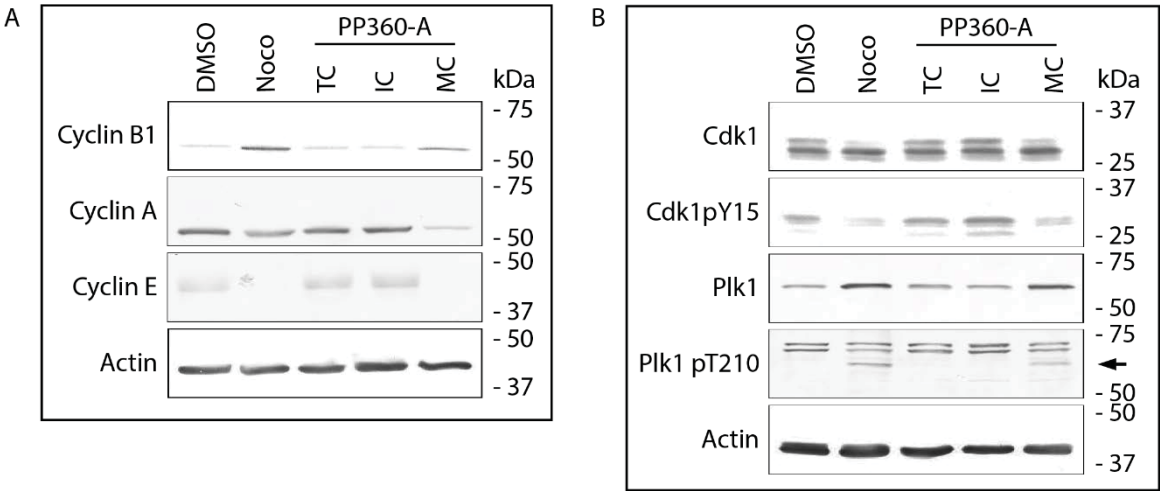

Figure 36. Cell cycle proteins in HT29 cells after treatment with PP360-A. After 24 hours of treatment with PP360-A at 50 µg/mL, mitotic cells (MC) were separated from total cells (TC) with a mechanical shake-off, remaining the interphase cells (IC). Cell extracts from controls DMSO and nocodazole and MC, TC, and IC were separated by SDS-PAGE and analyzed by western blotting for cyclin B1, cyclin A, and cyclin E (**A**); Cdk1, Cdk1 pY15, Plk1, and Plk1 pT320 (**B**). Protein levels loaded were standardized with actin.

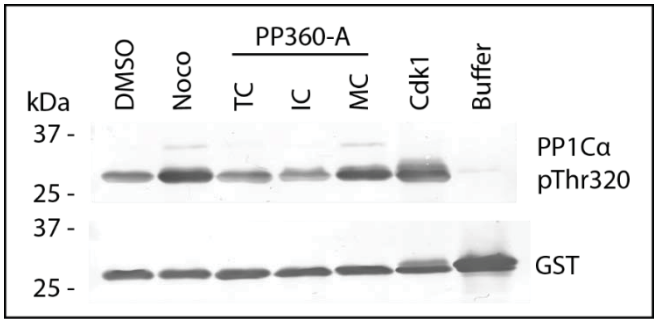

Figure 37. Cdk1 assay in HT29 cells treated with PP360-A. After 24 hours of treatment with PP360-A at 50 µg/mL, mitotic cells (MC) were separated from total cells (TC) with a mechanical shake-off, leaving the interphase cells (IC). Enzymatic reactions were carried out using GST protein and GST-PP1Cα as negative and positive Cdk1 substrates, respectively, and analyzed by western blotting. Controls: DMSO, nocodazole 200 ng/mL, purified Cdk1, extraction buffer.

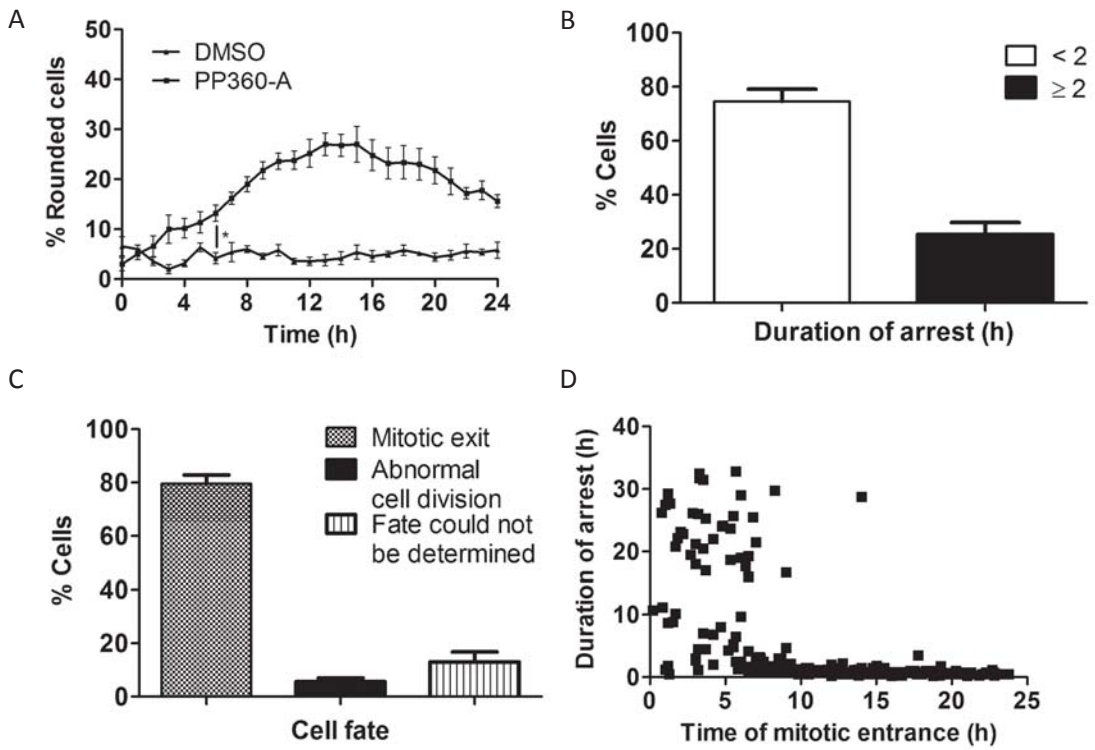

Figure 38. Time-lapse video microscopy of HT29 cells treated PP360-A at 50 µg/mL. Percentage of rounded cells over time (**A**), duration of arrest (rounded cell morphology) (**B**), cells fate (**C**), and relationship between time of mitotic entrance and duration of arrest (**D**). Light microscopy photos were taken every 10 minutes for 24-48 hours and were manually analyzed. Error bars represent the SEM of at least three independent experiments (n=300). Statistical significance between PP360-A and control treatment in **A** was determined using repeated measures mixed ANOVA ($p < 0.05$).

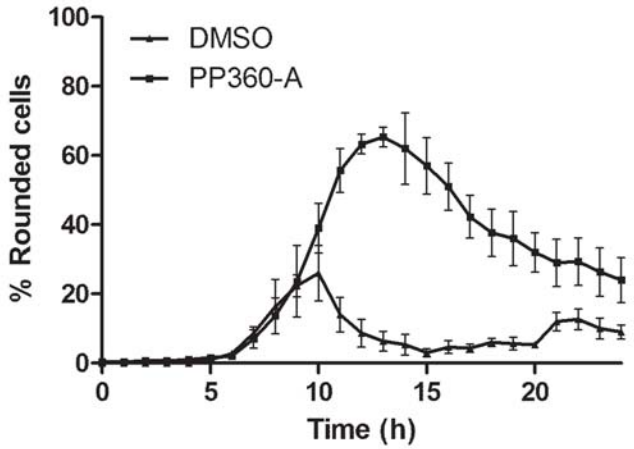

Figure 39. Comparison of PP360-A-induced cell cycle arrest with control in synchronized HT29 cells. HT29 cells were partially synchronized at G1/S checkpoint with thymidine 2mM and then treated for 24 hours with either PP360-A 50 µg/mL or DMSO. Analysis by time-lapse video microscopy. Percentage of rounded cells was determined by manual counting of images at every hour time point.

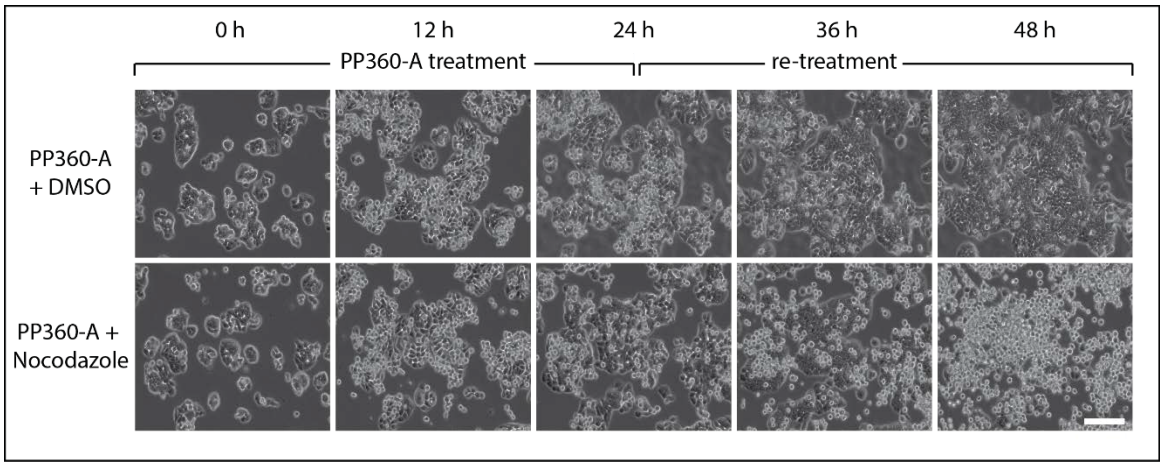

Figure 40. Effect of nocodazole re-treatment in HT29 cells after treatment with PP360-A 50 µg/mL. Analysis by time-lapse video microscopy. Negative control: DMSO re-treatment after 24-hour treatment with PP360-A. Scale bar: 100 µm.

A

Timepoint after PP360-A treatment (h)	% cells in cell cycle phases ± SEM		
	G1	S	G2/M
24	47.59 ± 10.40	44.20 ± 12.93	8.20 ± 2.63
21	50.48 ± 2.05	37.48 ± 1.65	12.05 ± 1.96
18	32.88 ± 9.32	46.61 ± 4.65	20.51 ± 7.69
15	25.79 ± 12.40	43.36 ± 4.65	30.76 ± 14.82
12	21.78 ± 12.00	42.26 ± 4.23	35.96 ± 13.13
9	29.73 ± 8.05	41.96 ± 3.90	28.30 ± 4.95
6	39.82 ± 2.85	44.60 ± 4.22	15.58 ± 3.12
3	44.06 ± 1.92	43.43 ± 0.23	12.51 ± 1.73
Controls at 24 h	G1	S	G2/M
DMSO	61.91 ± 1.27	32.06 ± 1.06	6.03 ± 1.92
Nocodazole	0.38 ± 0.17	4.22 ± 1.13	95.41 ± 1.30
CPT	0.53 ± 0.53	94.83 ± 5.17	4.62 ± 4.62

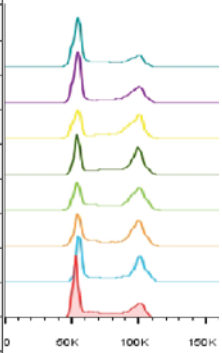

B

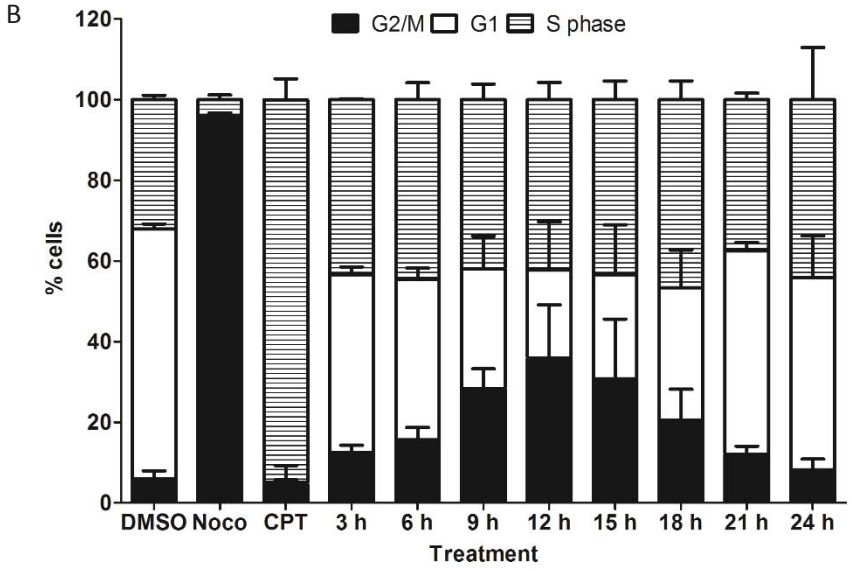

Figure 41. G2/M arrest of HT29 cells treated with PP360-A extract by flow cytometry. HT29 cells were treated with PP360-A at 50 µg/mL and collected every 3 hours for 24 hours. Controls: DMSO (normal cell cycle distribution), nocodazole 200 ng/mL (G2/M arrest), camptothecin (CPT) 50 nM (S-phase arrest). Mean cell percentages at different cell cycle phases obtained after different treatments. Curves shown are from a single experiment (**A**). Graph of cell distribution in each cell cycle phase after different treatments (**B**) Data shown represent the mean ± SEM of three independent experiments.

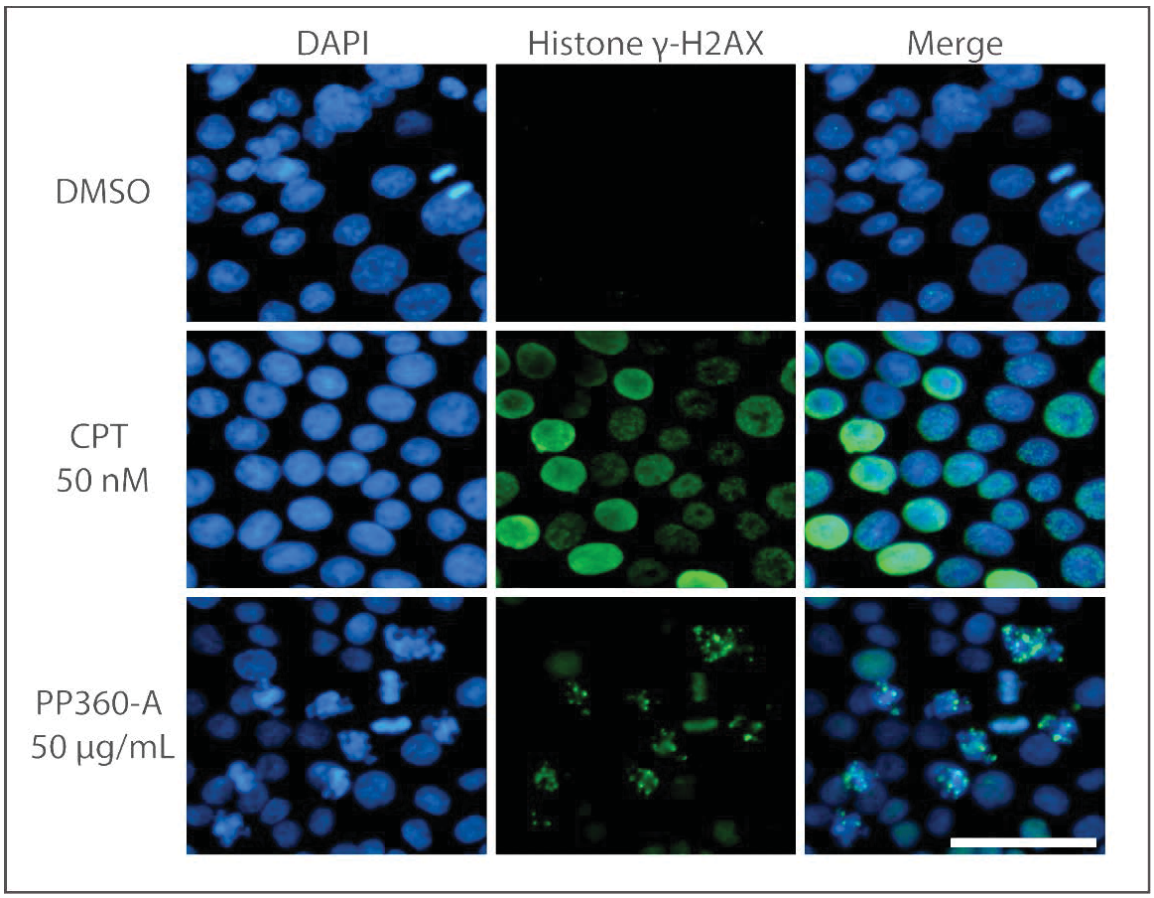

Figure 42. Treatment with PP360-A extract damages DNA in mitotic cells.Analysis by immunofluorescence microscopy using anti-γ-histone-H2AX antibody in HT29 cells after a 24-hour treatment with PP360-A at 50 µg/mL. Negative control: DMSO. Positive control: camptothecin 50 nM. Green: γ-histone H2AX. Blue: DAPI. Scale bar: 50 µm.

CHAPTER 5

Biology-guided fractionation of *H. richardsonii* extract and anti-mitotic activity of purified sesquiterpene lactone hymenoratin

After we confirmed and characterized the anti-mitotic activity of PP360-A and determined that *H. richardsonii* was a reliable source capable to induce a similar activity in two different years of collection, we wanted to know the chemical identity of the active compound(s). In collaboration with Dr. Raymond Andersen, from the University of British Columbia, we decided to pursue the identification and isolation of the anti-mitotic compound(s) by biology-guided fractionation of *H. richardsonii* crude extract.

5.1 Rounded cell activity in fractions from *H. richardsonii* extract

We collected 1.2 Kg of *H. richardsonii* and confirmed its rounded cell activity. The new plant material was extracted and fractionated as described in the materials and methods obtaining nine fractions labelled RA163 to RA171. These fractions were then tested in a cell rounding assay in HT29 cells using light microscopy. Cells were treated with either DMSO, nocodazole at 200 ng/mL, or the fractions at concentrations of 15 and 50 μg/mL. At 24 hours post-treatment, light microscopy images were taken, and the percentage of rounded cells elicited by each treatment was determined (**Figure 43**).

DMSO and nocodazole treatments presented the expected percentages of rounded cells: DMSO treatment caused 2.9 ± 1.6% of rounded cells, whereas nocodazole caused nearly 100% of the cells to be rounded. As described in the materials and methods, *H. richardsonii* leaves/stems were extracted with methanol and then partitioned between water and ethyl acetate. RA164 represents that ethyl acetate partition of the extracted plant, which preceded

the chromatographic fractionation. After treatment with 15 µg/mL of this fraction, 27.3 ± 2.9% of the cells were rounded. This activity increased to 40.2 ± 2.0% rounded cells when RA164 was added at 50 µg/mL. Either treatments with RA164 induced a statistically higher number of rounded cells than the DMSO treatment, showing that the first purification step successfully extracted the cell rounding activity from *H. richardsonii* plant parts.

We also observed a cell rounding activity with fractions RA166 and RA167. With fraction RA166, we observed an increase of the activity when increasing the concentration of the treatment, finding 10.2 ± 2.4% of rounded cells at 15 µg/mL and 39.3 ± 9.9% rounded cells at 50 µg/mL. Cells treated with fraction RA167 at 15 µg/mL presented the highest percentage of rounded cells of 47.75 ± 6.3%, and at 50 µg/mL we found a mixture of rounded cells (presumably mitotic) and dead cells. Treatment with the remaining fractions RA165, RA168, RA169, RA170, and RA171 did not elicit a rounded cell activity at any of the two concentrations tested. RA165 induced a 4.6 ± 1.1% of rounded cells at 15 µg/mL and 4.8 ± 2.5% at 50 µg/mL. Treatment with RA168 presented 12.9 ± 5.4% of rounded cells at 15 µg/mL and caused cell death at 50 µg/mL. When added at 15 µg/mL, RA169, RA170, and RA171 caused similar responses with low rounded cell percentages of 0.5 ± 0.5%, 4.4 ± 0.2 %, and 6.2 ± 3.5%, respectively. At 50 µg/mL the percentages of rounded cells were 2.5 ± 2.5% for RA169, 2.1 ± 0.4% for RA170, and 2.9 ± 1.4% for RA171, but these fractions caused a type of toxicity characterized by small vacuoles and shrunk edges in the HT29 cells. The only two treatments from the eight fractions obtained from RA164 able to elicit a cell rounding activity were RA166 at 50 µg/mL and RA167 at 15 µg/mL.

5.2 Purification of the sesquiterpene lactone hymenoratin from fraction RA167

Knowing that fraction RA167 was the fraction with the most potent mitotic activity, we aimed to isolate the compound(s) that induced this activity. The major compound present in this fraction was isolated by high performance liquid chromatography (HPLC). The chemical structure was determined by nuclear magnetic resonance (NMR) analysis and low-resolution electrospray ionization mass spectrometry (LRESIMS) spectra and the sesquiterpene lactone hymenoratin (**Figure 44**) was identified. Isolation of hymenoratin from RA167 using HPLC yielded 26.8 mg of the pure compound, which represents approximately 0.03% of the plant material used (i.e. 98.87 g).

5.3 Anti-mitotic activity of purified compound hymenoratin presents similar characteristics as PP360-A when applied to HT29 cells

Our next goal was to determine if the purified compound hymenoratin, which was given the code RA173, maintained the activity found in the crude extract PP360-A upon HT29 cells. We aimed to observe the morphology induced by this compound in a cell rounding assay with light microscopy, observe phospho-histone H3, α-tubulin, and γ-H2AX signal by immunofluorescence microscopy, and measure DNA content in a cell cycle analysis by flow cytometry.

5.3.1 Testing RA173 concentrations for rounded cell activity

As a first analysis to compare the activities of PP360-A and hymenoratin, we performed a cell rounding assay. HT29 cells were either treated with DMSO, nocodazole 200 ng/mL, PP360-A at 50 µg/mL, or RA173 at a range of concentrations from 1.5 µg/mL to 150 µg/mL. After 24 hours of treatment, light microscopy photos were taken, and the

percentages of rounded cells induced by each treatment were determined. Control treatments caused the usual responses in HT29 cells: no cell rounding activity in DMSO-treated cells, with a normal 3.0 ± 1.6% of rounded cells; a cell rounding activity with almost 100% of rounded cells in nocodazole-treated cells; and 28.0 ± 0.6% rounded cells after PP360-A treatment. Importantly, two of the RA173 treatments also induced a similar anti-mitotic activity to that of PP360-A in HT29 cells. We noticed that the number of rounded cells increased with concentration from 1.5 µg/mL to 15 µg/mL, obtaining a mean value of 7.3 ± 0.8% rounded cells at 1.5 µg/mL, 13.5 ± 2.0% at 5 µg/mL, and a 25.0 ± 3.8 % at 15 µg/mL. With higher concentrations we did not perceive a higher activity. At 50 µg/mL, we found a 24.3 ± 0.7% of rounded cells, a similar number to the one obtained with the 15 µg/mL treatment; however, at this concentration we found what seemed to be a mixture of mitotic and dead cells. Finally, when RA173 was added at 150 µg/mL, it was evident that this concentration was toxic to HT29 cells. We statistically analyzed the results obtained and found that 15 µg/mL and 50 µg/mL of RA173 induced a higher percentage of rounded cells than that of DMSO treatment, consistent with a cell rounding activity. The number of rounded cells accumulated after 24 hours of treatment with 15 µg/mL or 50 µg/mL of RA173 is similar to that elicited by the crude extract PP360-A at 50 µg/mL. This indicated that the sesquiterpene lactone hymenoratin was responsible for the rounding cell activity found in *H. richardsonii* plant extract. This was the first time that this compound was shown to induce a biological activity upon cancer cells. We decided to use the concentration of 15 µg/mL of RA173, instead of the possibly toxic 50 µg/mL, for the next experimental tests.

5.3.2 Mitotic index of RA173 based on HT29 PH3-positive cells

The next step was to confirm the state in mitosis of those rounded cells accumulated after RA173 treatment. We included a 12-hour time point because in the analysis of PP360-A we found a peak of activity after 12 hours of treatment. HT29 cells were treated for 12 or 24 hours with either DMSO, nocodazole at 200 ng/mL, PP360-A at 50 µg/mL, or RA173 at 15 µg/mL. We then performed an immunofluorescence microscopy assay using anti-phospho-histone H3 (PH3) antibodies and DAPI to stain DNA and we took pictures to determine the mitotic index based on the percentage of PH3-positive cells. As illustrated in **Figure 46**, DMSO treatment did not show an accumulation of PH3-positive cells whereas nearly all nocodazole-treated cells were positive for PH3 at both 12 and 24-hour time points. Addition of 50 µg/mL of PP360-A induced the accumulation of 33.3 ± 3.2% of PH3-positive cells after 12 hours of treatment and 30.1 ± 5.0% after 24 hours. When RA173 was added at 15 µg/mL, we found a slightly smaller percentage of rounded cells accumulated when compared to PP360-A treatment. We determined an 18.0 ± 1.5% and 14.5 ± 1.3% of PH3-positive cells at 12 and 24 hours, respectively, after treatment with RA173. These values showed a statistically significant mitotic arrest activity when compared to DMSO.

5.3.3 Distorted mitotic spindles after treatment with 15 µg/mL of RA173

A characteristic of the PP360-A anti-mitotic activity was the distortion of the mitotic spindles. We wanted to confirm that this effect was also maintained with the purified compound RA173. We submitted HT29 cells to treatment with DMSO, nocodazole at 200 ng/mL, PP360-A at 50 µg/mL, or RA173 at 15 µg/mL. At 12 and 24 hours post-treatment, an immunofluorescence microscopy protocol was carried out using anti-α-tubulin antibody

to target the microtubules and observe the mitotic spindles in the mitotic cells and DAPI to stain DNA. DMSO-treated mitotic cells presented normal bipolar spindles and nocodazole-treated mitotic cells were unable to form mitotic spindles at 12 and 24 hours. We observed the expected distortion of the mitotic spindles by 24 hours of treatment with PP360-A at 50 µg/mL. Significantly, treatment with RA173 at 15 µg/mL also induced distortion of the mitotic spindles (**Figure 47**). We observed that already at 12 hours the majority of the spindles were distorted after both PP360-A and RA173 treatments. With these results we could further state that RA173 have a similar activity than PP360-A.

5.3.4 Flow cytometric analysis of HT29 cells after 12 and 24 hours of treatment with 15 µg/mL of RA173

We performed a cell cycle analysis using flow cytometry at 12 and 24 hours post-treatment with RA173 and compared it with PP360-A. HT29 cells were treated with either DMSO to represent a non-treated population, nocodazole 200 ng/mL for G2/M arrest, PP360-A 50 µg/mL, or RA173 15 µg/mL. After 12 or 24 hours of treatment, we collected and fixed the cells and they were posteriorly analyzed by flow cytometry. Control treatments presented the expected percentage of cells on every phase of the cell cycle after 24 hours of treatment: DMSO-treated cells presented 6.0 ± 1.9% of cells in the G2/M phases, and nocodazole-treated cells presented 95.4 ± 1.3% in G2/M. Respectively, 12 and 24 hours of PP360-A treatment induced an accumulation of 35.96 ± 13.13 and 8.20 ± 2.63% in G2/M. Regarding RA173 15 µg/mL, we found a 6.6 ± 4.4% in G2/M phase after 12 hours of treatment and a 7.4 ± 1.8% of cells in G2/M after 24 hours. However, it is possible that there are errors in the analysis of the data due to the choice of parameters used to calculate the number of cells in the G2/M area. In the figures obtained after the analysis, we could observe a higher

percentage of cells accumulated close to the established G2/M area (**Figure 48**). No other cell cycle arrest was found with RA173 15 µg/mL treatment of HT29 cells.

5.3.5 DNA-damage foci in mitotic cells after hymenoratin treatment

We then tested if compound RA173 induced γ-histone-H2AX foci as the crude extract PP360-A. HT29 cells were treated with either DMSO, camptothecin 50 nM as a positive control for genotoxicity, PP360-A 50 µg/mL, or RA173 15 µg/mL for 24 hours. Cells were then examined for γ-H2AX foci by immunofluorescence microscopy. HT29 cells treated with DMSO did not show γ-H2AX signal, whereas cells treated with CPT presented a strong signal showing damaged DNA. Using the fluorescent signal of DMSO-treated cells as a threshold for background signal, we observed γ-H2AX foci in mitotic cells of both PP360-A and RA173 treatments and only a higher γ-H2AX signal than DMSO in few interphase cells. A few number of mitotic cells with what seemed to be a normal mitotic DNA morphology were negative for γ -H2AX. We could observe the same characteristics of DNA damage in RA173-treated cells and PP360-A-treated cells (**Figure 49**). The genotoxic activity found in mitotic cells after treatment with the *H. richardsonii* crude extract PP360-A was confirmed to be also present after treatment with the purified compound RA173.

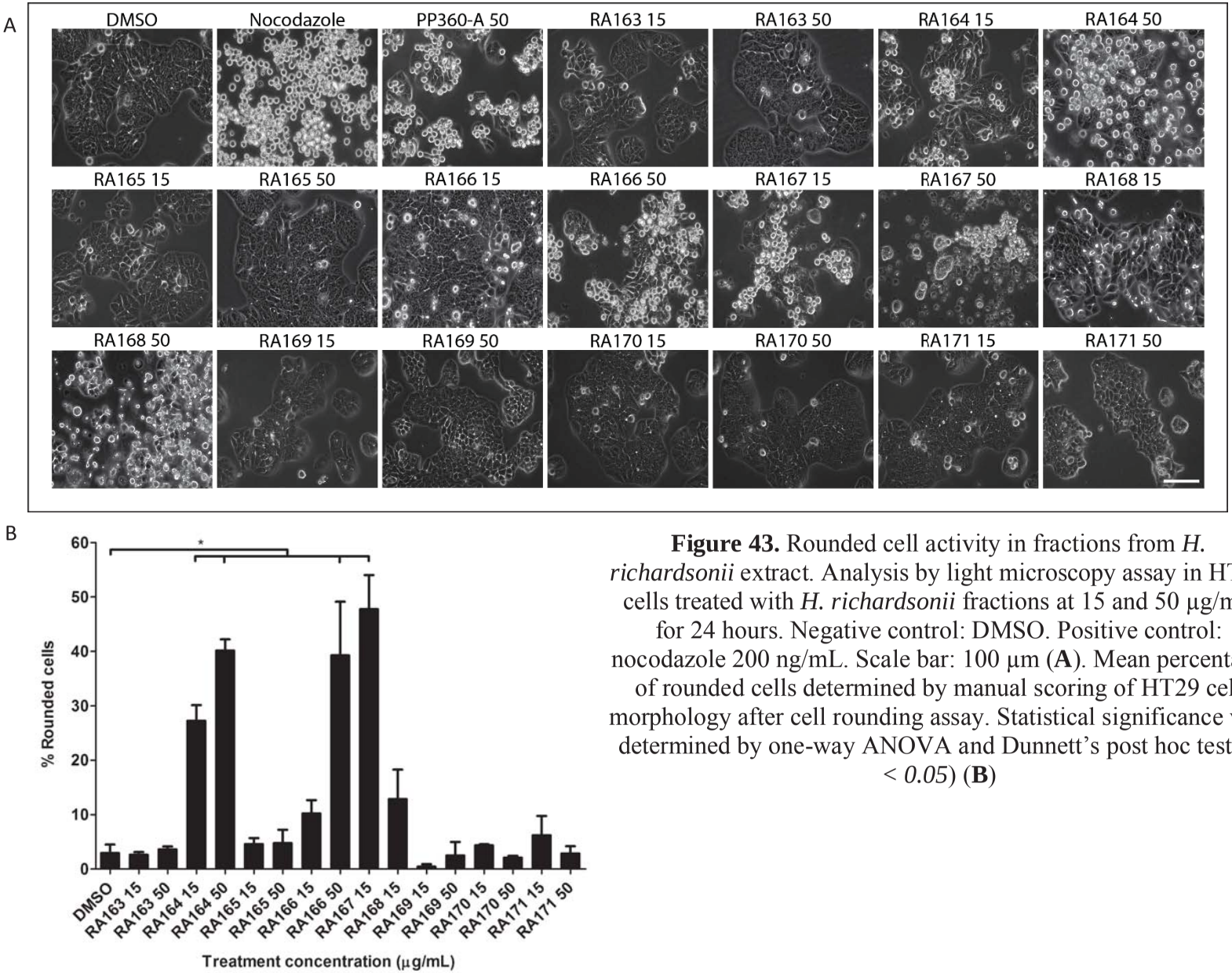

Figure 43. Rounded cell activity in fractions from *H. richardsonii* extract. Analysis by light microscopy assay in HT29 cells treated with *H. richardsonii* fractions at 15 and 50 µg/mL for 24 hours. Negative control: DMSO. Positive control: nocodazole 200 ng/mL. Scale bar: 100 µm (**A**). Mean percentage of rounded cells determined by manual scoring of HT29 cell morphology after cell rounding assay. Statistical significance was determined by one-way ANOVA and Dunnett's post hoc test ($p < 0.05$) (**B**)

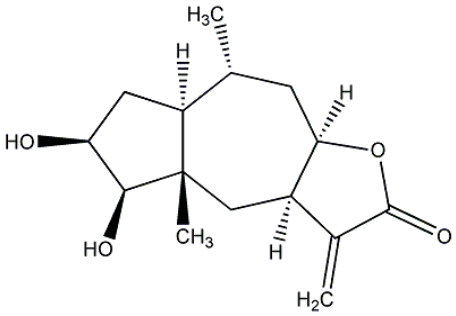

Figure 44. Structure of the sesquiterpene lactone hymenoratin (RA173), isolated from of *H. richardsonii* plant extract.

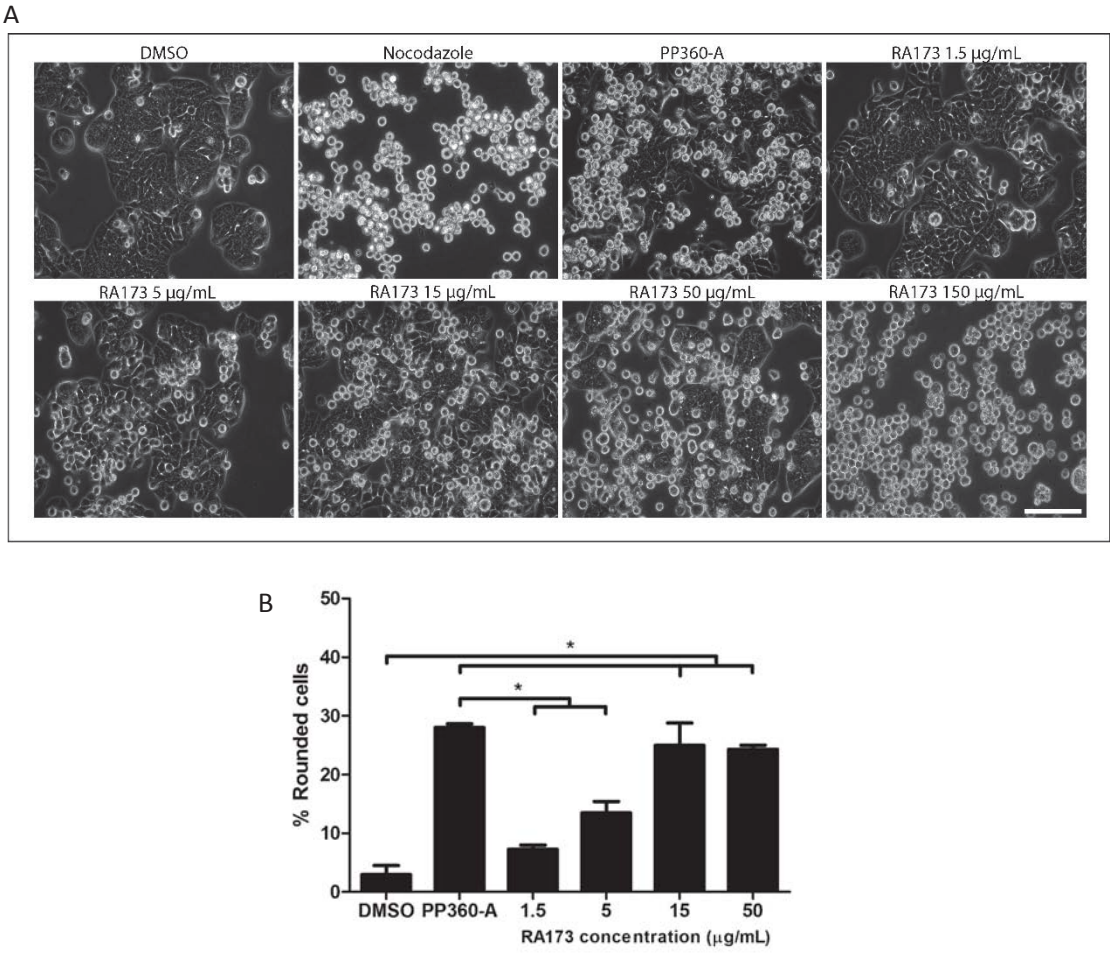

Figure 45. Rounded cell activity of RA173 upon HT29 cells. Analysis by light microscopy in HT29 cells treated for 24 hours with RA173 at a range of concentrations from 1.5 to 150 µg/mL. Negative control: DMSO. Positive control: nocodazole 200 ng/mL, PP360-A 50 µg/mL. Scale bar: 100 µm (**A**). Mean percentage of rounded cells determined by manual scoring of HT29 cell morphology after cell rounding assay. Error bars represent the SEM of three independent experiments. Statistical significance was determined using one-way ANOVA followed by Dunnett's post hoc test ($p < 0.05$) (**B**).

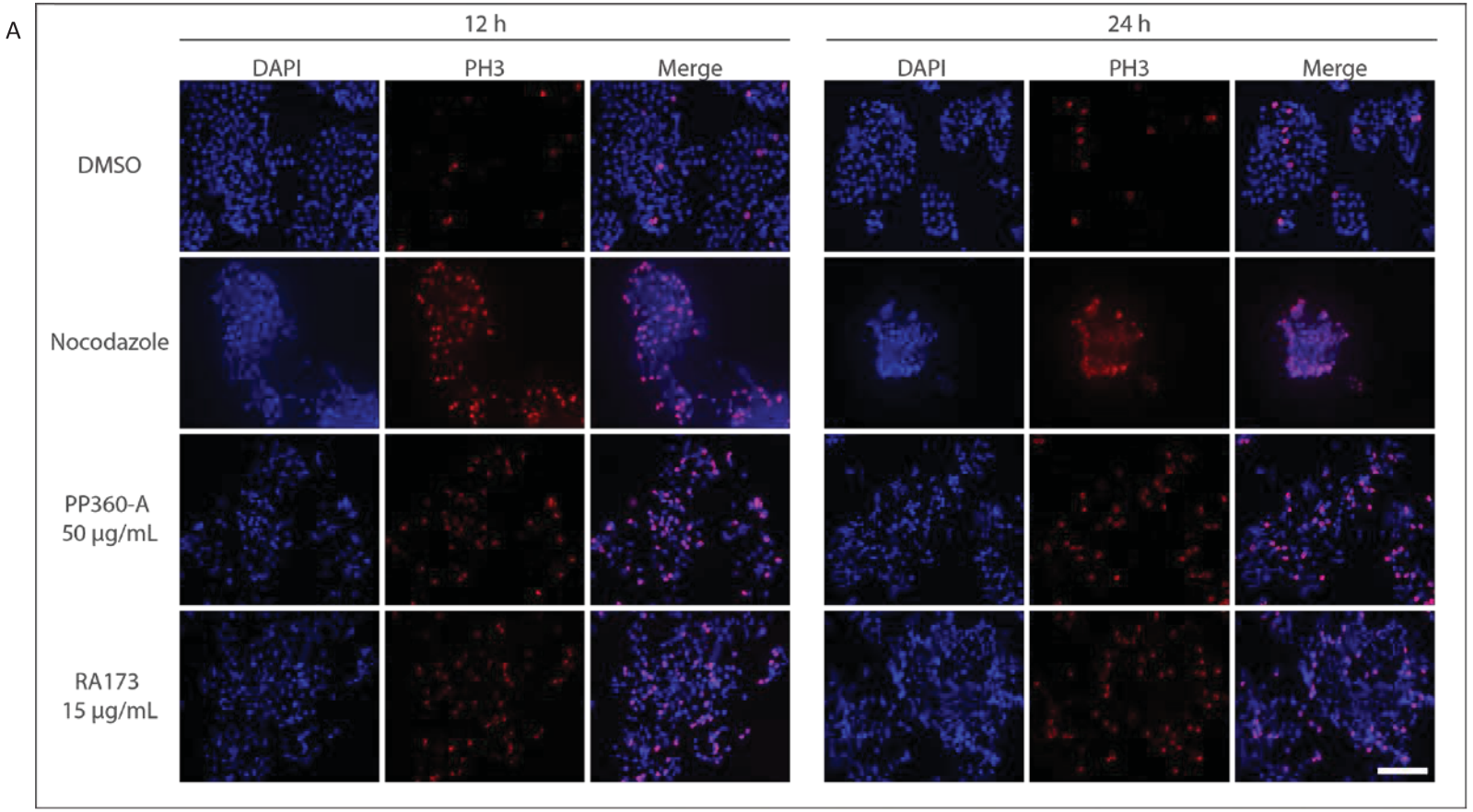

Figure 46. Mitotic cells accumulated after 12 and 24 hours of treatment with RA173 at 15 µg/mL and PP360-A at 50 µg/mL. Negative control: DMSO. Positive control: nocodazole 200 ng/mL. Analysis by immunofluorescence microscopy. Red: phospho-histone H3 (mitotic cells). Blue: DAPI (DNA). Scale bar: 100 µm (**A**). Mean percentage of PH3-positive cells determined after counting immunofluorescence microscopy images. Error bars represent the SEM of three independent experiments. Statistical significance was determined using one-way ANOVA followed by Dunnett's post hoc test ($p < 0.05$) (**B**).

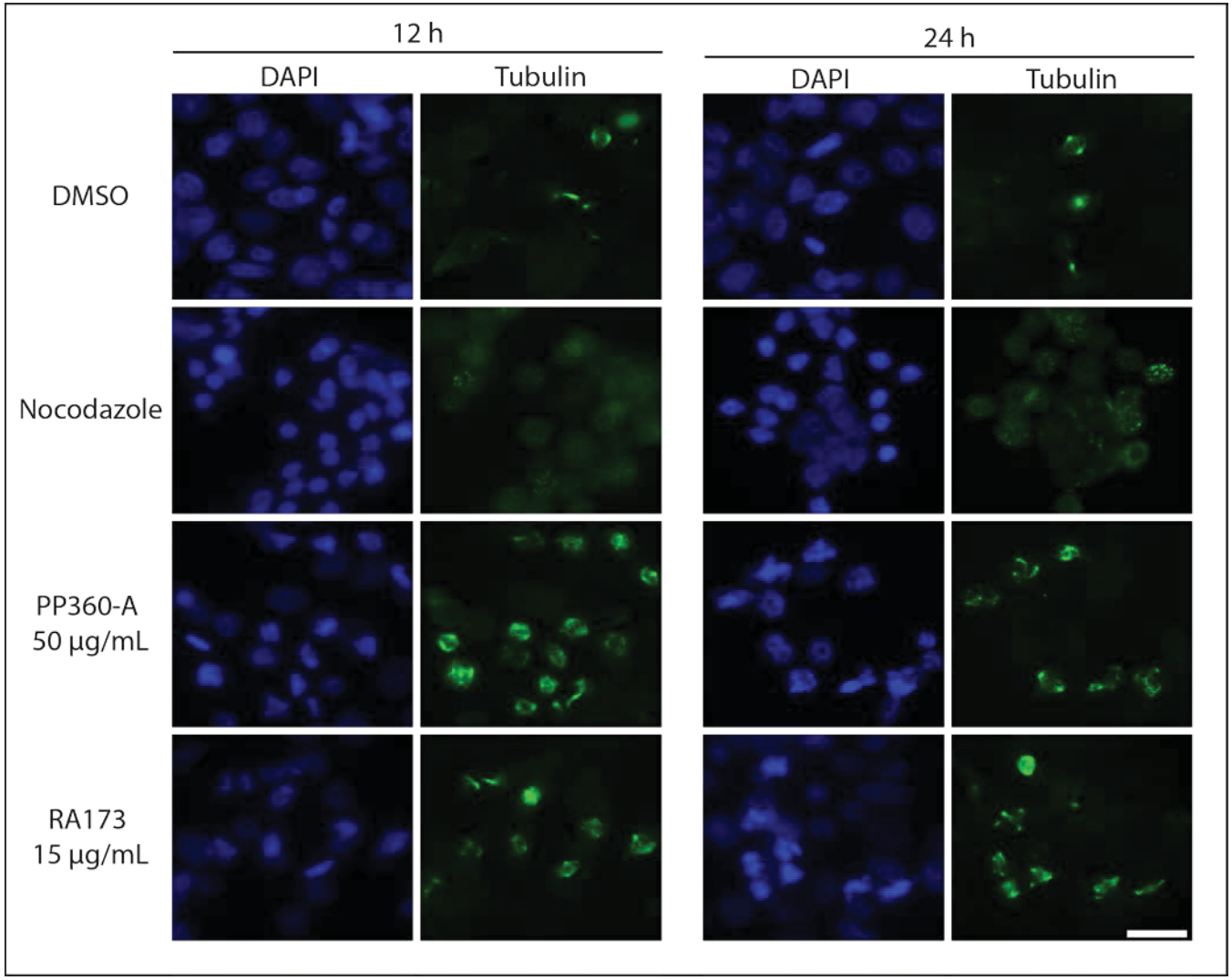

Figure 47. Mitotic spindles in HT29 cells after 12 and 24 hours of treatment with RA173 at 15 µg/mL and PP360-A at 50 µg/mL. Controls: DMSO, nocodazole 200 ng/mL. Analysis by immunofluorescence microscopy. Green: alpha-tubulin (microtubules/mitotic spindles). Blue: DAPI (DNA). Scale bar: 20 µm.

A

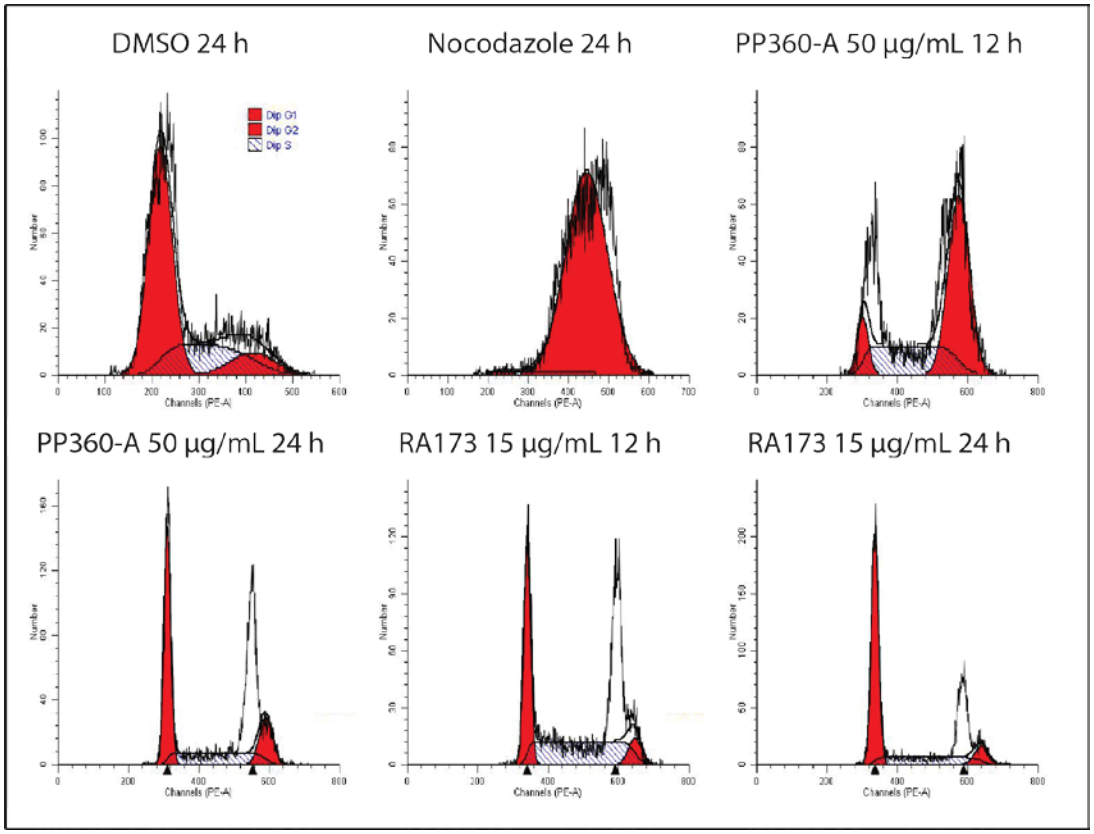

B

	% Cells in cell cycle phases ± SEM		
Treatment (time)	**G1**	**S**	**G2/M**
DMSO 24 h	59.4 ± 4.6	33.9 ± 3.5	6.7 ± 2.6
Nocodazole 24 h	0.4 ± 0.2	4.3 ± 1.4	95.3 ± 1.6
PP360-A 12 h	24.0 ± 14.6	41.4 ± 6.9	34.6 ± 16.8
PP360-A 24 h	47.6 ± 12.5	44.0 ± 17.1	8.4 ± 7.4
RA173 12 h	35.0 ± 13.6	58.3 ± 18.0	6.7 ± 4.4
RA173 24 h	62.2 ± 1.9	30.4 ± 3.7	7.4 ± 1.8

Figure 48. G2/M arrest of HT29 cells treated for 12 and 24 hours with RA173 at 15 µg/mL and PP360-A at 50 µg/mL. Cell cycle analysis by flow cytometry using propidium iodide nuclear staining. Controls: DMSO (normal cell cycle distribution), nocodazole 200 ng/mL (G2/M arrest). Curves shown are from a single experiment (**A**). Mean cell percentages ± SEM at cell cycle phases obtained from three independent experiments (**B**).

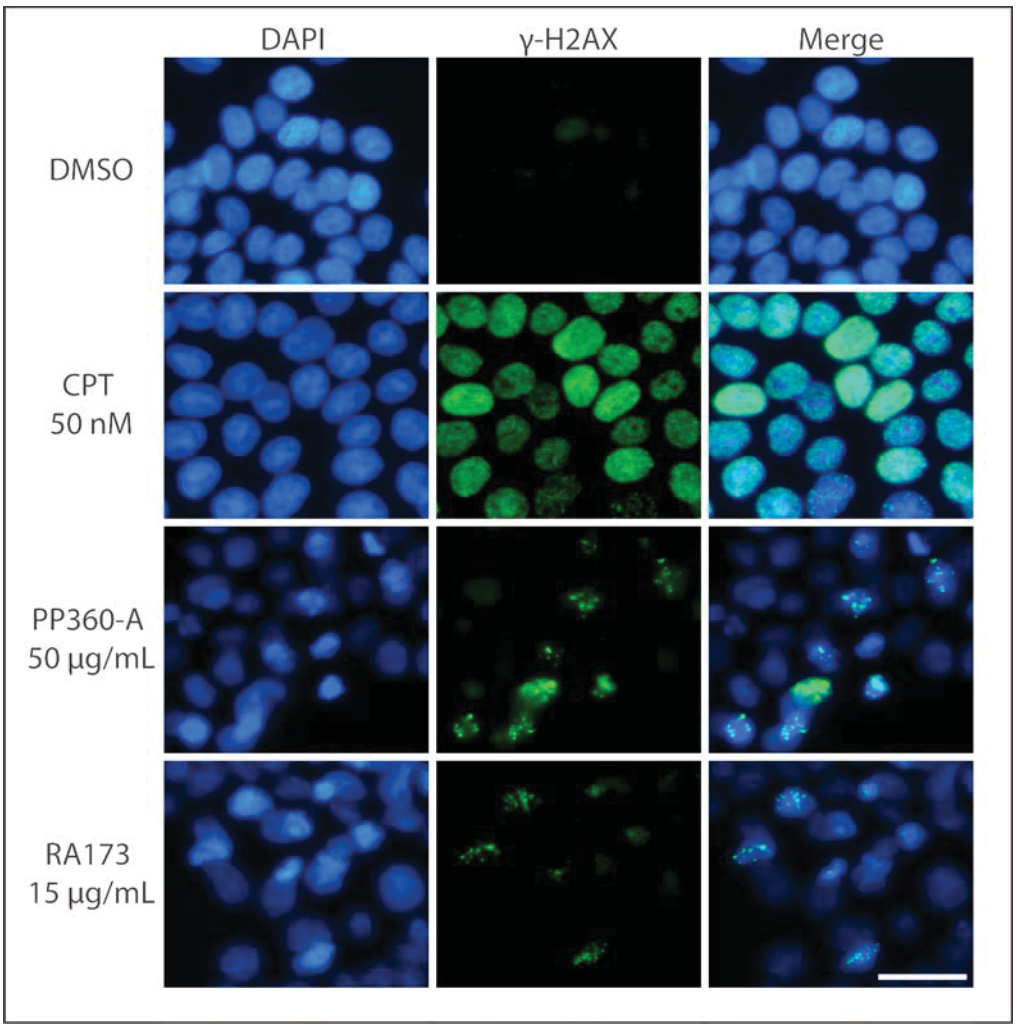

Figure 49. RA173 at 15 µg/mL damages DNA in mitotic cells. Analysis by immunofluorescence microscopy using anti-γ -histone H2AX antibody in HT29 cells after a 24-hour treatment. Positive control: camptothecin 50 nM. Negative control: DMSO. Green: γ-histone H2AX (damaged DNA). Blue: DAPI (DNA). Scale bar: 20 µm.

CHAPTER 6

Discussion

When I started my research project in Fall 2016, the laboratory had recently isolated an anti-mitotic chemical from a plant species of the Asteraceae family. At that time, there were few previously reported anti-mitotic chemicals from members of the Asteraceae family (Bosco & Golsteyn, 2017). We realized there was an opportunity to fill a knowledge gap about the relationship between Asteraceae species and natural products inhibitors of mitosis. Therefore, to characterize better the biological activities of prairie plants and to find chemicals that arrest cells in mitosis, we studied six species from the Asteraceae family. This was the first time that a hypothesis-driven approach had been applied in the Prairie to Pharmacy program, which prior to this had used a discovery-based approach. In addition, my goal was to isolate another chemical with anti-mitotic properties so that we would understand better the relationship between the chemical structure and the mitotic arrest. My project then was to investigate whether plant species from the Asteraceae family generally harbour chemicals with anti-mitotic activity, which chemical(s) is responsible for this activity, and what are the characteristics of the mitotic arrest.

I was able to undertake this project because the laboratory had already collected six species from the Asteraceae family and had developed a simple cell rounding assay (Kubara et al., 2012) to screen for potential anti-mitotic agents. Nonetheless, this was the first project in which one person was investigating six plants species instead of one species per project. By our investigation, we found that extracts from Asteraceae species elicit different effects upon cancer cells, and not all of them contain chemicals with anti-mitotic properties. Importantly, we discovered that the plant species *Hymenoxys richardsonii* can arrest human

cancer cells in mitosis. In collaboration with Dr. Raymond Andersen's laboratory at University of British Columbia, we performed biology-guided fractionation and identified the sesquiterpene lactone hymenoratin as the source of the anti-mitotic activity. This is the first time that either *H. richardsonii* extracts, or hymenoratin have been reported to arrest human cells in mitosis. Furthermore, we were able to characterize several aspects of the anti-mitotic activity and we related them to the chemistry of sesquiterpene lactones.

6.1 Asteraceae family as a source of anti-mitotic sesquiterpene lactones

The Asteraceae family is known for the production of a class of secondary metabolites called sesquiterpene lactones (Seaman, 1982), which have been shown to have cytotoxic effects in cancer cells (Picman, 1986; Ghantous et al., 2010); however, little research has been done regarding their effects upon mitosis. Only seven sesquiterpene lactones (SLs) extracted from this plant family were found to induce an anti-mitotic activity (Bosco & Golsteyn, 2017). These are: 6-O-angeloylplenolin from *Centipeda minima*, coronopilin from *Ambrosia arborescens*, costunolide and dehydrocostuslactone from *Saussurea costus,* psilostachyins A and C from *Ambrosia artemisifolia,* and pulchelloid A from *Gaillardia aristata*. In addition, six SLs isolated from Asteraceae species can potentially have an anti-mitotic activity, although they have been only reported to accumulate cells in G2/M phase. These are: parthenolide from *Tanacetum parthenium,* 9-β-acetoxycostunolide and santamarine from *Cyathocline purpurea*; artesunate and dihydroartemisinin, synthetic derivatives of artemisinin from *Artemisia annua*; and dehydroleucodine from *Artemisia douglasiana*. We believe that the anti-mitotic activity of SLs has been underestimated, and that some of those that have only been reported to be cytotoxic to cancer cells act by interfering with mitotic processes.

6.2 Comparison of six Asteraceae species activity upon cancer cells

To understand better if the anti-mitotic activity is common to Asteraceae species, we tested and compared the Canadian Asteraceae species *Liatris punctata, Helianthus* sp., *Hymenoxys richardsonii, Arnica cordifolia, Balsamorhiza sagittata* and *Helianthus annuus*. We first compared their cytotoxic effects and afterwards their anti-mitotic effects measured by cell rounding activity, phosphorylation of histone H3, and morphology of the mitotic spindles.

Values of the half maximal inhibitory concentration (IC_{50}) obtained from the MTT assay revealed that *A. cordifolia* extract was the most toxic extract, requiring only approximately 10 and 5 µg/mL to reduce HT29 and M059K cell viability by half after 96 hours of treatment, respectively. In contrast, the least toxic extract was that of *H. richardsonii* with an IC_{50} of 124 µg/mL for HT29 and 56 µg/mL for M059K cells. The other plants presented intermediate values, occasionally including a relatively high cytotoxicity for M059K cells. Remarkably, the cell rounding assay and immunofluorescence microscopy assay targeting the mitotic marker phospho-histone H3 (PH3) showed that *H. richardsonii* extract induced about 30% of cells to arrest in mitosis. *A. cordifolia* and *L. punctata* extracts also had an anti-mitotic activity and caused the accumulation of a significant number of rounded cells and PH3-positive cells. However, extracts from *B. sagittata* and the *Helianthus* species did not present an anti-mitotic activity upon HT29 cells. When evaluating the possible effects upon mitotic spindles induced by extracts from these plant species, a striking distortion of about 72% of the mitotic spindles was found after treatment with *H. richardsonii* extract. This phenotype was reminiscent of the *G. aristata* effect on mitotic spindles and was also similar to that observed after treatment with *L. punctata* extract, which affected about 28%

of mitotic spindles. Surprisingly, HT29 cells treated with *A. cordifolia* at the same concentration that induced an accumulation of mitotic cells did not display distorted mitotic spindles, which instead appeared symmetric as in DMSO-treated mitotic cells. Neither *B. sagittata*, nor *Helianthus* species induced a significant mitotic spindle distortion.

We could observe that extracts obtained from species of the same family have different degrees of toxicity and that the anti-mitotic activity is not widely present in Asteraceae species. Although it remains possible that a potential anti-mitotic activity is masked in a crude extract, we observed that it is limited to a subset of species. Furthermore, the anti-mitotic activity could be elicited with a range of potencies (e.g. *H. richardsonii* exhibited a higher activity compared to *L. punctata*) and possibly through different mechanisms, as we saw with *A. cordifolia* that arrested cells in mitosis but did not affect the mitotic spindle morphology as did *L. punctata* and *H. richardsonii*.

These differences found in the cytotoxic and anti-mitotic activities of the Asteraceae species tested are potentially due to the synthesis of different secondary metabolites. As a result of biotic and abiotic pressures, plant species can modify their biosynthetic routes to produce different metabolites (Pavarini et al., 2012). In the Asteraceae family, there are examples of closely related taxa that shift the emphasis of their biosynthetic pathways from one type of terpenoid to another (Seaman, 1982). In the tribe Astereae, the synthesis of the ubiquitous SLs is replaced by a predominant production of a broad array of active diterpenes (Seaman, 1982). Even minor differences in the substitution pattern of SLs molecules could translate on different cellular effects. For instance, Beekman et al. (1997) found that a higher lipophilicity due to presence of certain ester groups in SL molecules

resulted in a higher cytotoxicity if the size of these groups was not large enough to block the access of the alkylating site to the target.

We chose *H. richardsonii* for further research and purification of its active compound because it disclosed a high cell rounding activity, the highest mitotic index and a conspicuous effect in the mitotic spindles. Moreover, the characteristics and proportions of *H. richardsonii* effects upon cancer cells resembled those of *G. aristata,* a plant with anti-mitotic activity that belongs to the same tribe that *H. richardsonii*: Helenieae tribe (Biddulph, 1944; Baldwin & Wessa, 2000). This close relationship within the Asteraceae plant family might indicate a greater possibility to find similar secondary metabolites (Seaman, 1982) and activities that we aimed to explore in more depth.

6.3 Comparison of chemical structure of sesquiterpene lactone in Hymenoxys richardsonii with other anti-mitotic SLs

The biology-guided fractionation of *H. richardsonii* led to the identification of the SL hymenoratin. We confirmed that hymenoratin induced a mitotic arrest with the characteristics originally found in *H. richardsonii* extract. This secondary metabolite is closely related to *G. aristata* anti-mitotic compound pulchelloid A. Both are SLs of the pseudoguaianolide type, with the α-methylene-γ-lactone at C-8 and hydroxyl groups in the molecule, including one hydroxyl group at C-4. The main differences are that pulchelloid A has an angeloyloxy group at C-2, and two other hydroxyl groups at C-6 and C-9, whereas hymenoratin has another hydroxyl group (i.e. different from the one at C-4 that they both contain) at C-3 (**Table 5**).

It has been demonstrated that the α-β-unsaturated carbonyl group present in the lactone moiety of SLs is required for their biological activities; for example, the anti-mitotic activity of psilostachyin A and C, as well as that of coronopilin, is dependent on this chemical group (Sturgeon et al., 2005; Cotugno et al., 2012a). The biological effects of SLs are associated with the capacity of the electrophilic α-β-unsaturated carbonyl to react and form adducts with nucleophilic cysteine residues of key enzymes (Kupchan et al., 1970). However, other chemical characteristics of the SL molecules influence their capacity to induce a specific activity. In our literature research of the SLs with anti-mitotic effects (refer to **Table 5** for chemical structures and references), we found that the pseudoguaianolide class of SLs is one of the most common type of structures that can elicit this biological activity, independently of the lactonization site (i.e. C-6 or C-8). Hymenoratin, pulchelloid A, 6-O-angeloylplenolin, the psilostachyins A and C, coronopilin, and dehydroleucodine belong to this class. From the group of SLs shown to arrest cells in M phase, only costunolide is a germacranolide. Costunolide's derivative 9-β-acetoxycostunolide and parthenolide are also germacranolides that potentially have an anti-mitotic activity, but only a G2/M phase-arrest was reported. Similarly, only a G2/M arrest effect was reported for the eudesmanolide santamarine and the SL derivatives artesunate and dihydroartemisinin, and their specific anti-mitotic activity has not been investigated yet. Another SL relevant to this project is the 8-acetyl arteminolide, which also belongs to the pseudoguaianolide class. Its anti-mitotic activity has not been studied but it induces a biological effect that might be important in the understanding of hymenoratin's mode of action for reasons discussed later in this chapter. According to Kupchan et al. (1971) and Beekman et al. (1997), presence of the angeloyloxy group in pulchelloid A and 6-OAP would translate in an enhanced cytotoxicity due to a higher lipophilicity. Similarly,

presence of a second alkylating group, such as the second α-β-unsaturated carbonyl in dehydroleucodine, would also increase the cytotoxicity (Kupchan et al., 1971b; Beekman et al., 1997). Hymenoratin does not contain lateral chains or secondary alkylating groups; nonetheless, hydroxyl groups present in the molecule, as well as its *cis* conformation might increase the biological activity. Hydroxyl groups can form noncovalent interactions with amino-acids and a *cis* conformation is more flexible than the *trans* counterpart; these factors can enhance the interaction with the target protein(s) (Beekman et al., 1997). Using structure-activity-relationship studies, we can determine the relevant groups for the anti-mitotic activity observed in hymenoratin by blocking individual groups in the molecule and evaluating its activity. These studies are recommended for future research to discern what are the requirements, besides the α-β-unsaturated carbonyl, for the mitotic arrest effect caused by SLs. This knowledge may help uncover the target of SLs and help develop an optimized molecule with higher specificity and potency.

Table 5. Sesquiterpene lactones from Asteraceae family that cause a cell cycle arrest. It is provided the tribal classification of the plant species from which these compounds were extracted; their chemical structure and description of the main characteristics; and the reported anti-mitotic activity.

Name	**Plant source**	**Taxonomy**	**Structure**	**Type of SL**	**Anti-mitotic activity**	**Characteristics or possible mode of action**
Pulchelloid A	*Gaillardia aristata*	Helenieae	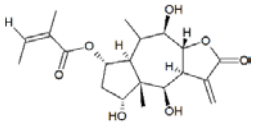	Pseudoguaianolide *trans*-C-8 lactonized. Angeloyloxy and hydroxyl groups. Two α-β unsaturated carbonyl groups.	M-phase arrest confirmed by: cell rounding, Cdk1 activity, high levels of cyclin B and securin, PH3, MS.	MS distortion and γ-H2AX foci in MC. (Bosco, 2017).
Hymenoratin	*Hymenoxys richardsonii*	Helenieae	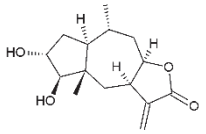	Pseudoguaianolide *cis*-C-8 lactonized. Hydroxyl groups.	M-phase arrest confirmed by: cell rounding, Cdk1 activity, high levels of cyclin B and Plk1, PH3, MS, flow cytometry.	MS distortion, γ-H2AX foci and chromosome congression defects in MC. No other cell cycle arrest.
6-O-Angeloylplenolin	*Centipeda minima*	Athroismeae	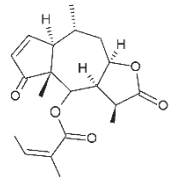	Pseudoguaianolide *cis*-C-8 lactonized. Angeloyl group. Two α-β unsaturated carbonyl groups.	M-phase arrest confirmed by: Cdk1 activity, PH3.	Active SAC. Failed activation of APC/C (low cyclin B-ubiquitinated levels). (Liu et al., 2011b, Liu et al., 2015, Cheng et al., 2017).
Coronopilin	*Ambrosia arborescens*	Heliantheae	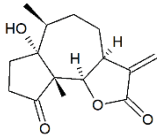	Pseudoguaianolide *cis*-C-6 lactonized. Hydroxyl group.	M-phase arrest confirmed by: high cyclin B levels, PH3.	Covalent interaction with tubulin causing hyperpolymerization. (Cotugno et al., 2012b).

Dehydroleucodine	*Artemisia douglasiana*	Anthemideae	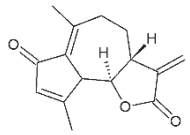	Guaianolide *trans*-C-6 lactonized. Two α-β unsaturated carbonyl groups.	M-phase delay measured by PH3 levels.	Delay in mitotic entry. Temporary M-phase arrest followed by accumulation in G1 phase. γ-H2AX signal by WB. (Constantino et al., 2013).
Psilostachyin A	*Ambrosia artemisifolia*	Heliantheae	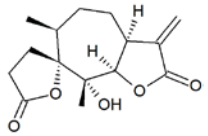	Modified pseudoguaianolide *cis*-C-6 lactonized. Hydroxyl group.	M-phase arrest confirmed by: flow cytometry, condensed chromosomes, MS.	Chromosome congression defects. Distorted MS. Tubulin polymerization not affected *in vitro*.
Psilostachyin C	*Ambrosia artemisifolia*	Heliantheae	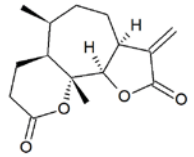	Modified pseudoguaianolide *cis*-C-6 lactonized.	M-phase arrest confirmed by: flow cytometry, condensed chromosomes, MS.	Ídem to Psilostachyin A. (Psilostachyin A and B: Sturgeon et al., 2005).
8-acetyl-arteminolide	*Artemisia sylvatica*	Anthemideae	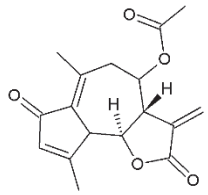	Guaianolide *trans*-C-6 lactonized.	Not studied.	Inhibits Farnesyl Transferase. Inhibits cell proliferation. (Lee et al., 2000; Lee et al., 2003).
Costunolide	*Saussurea costus*	Cardueae	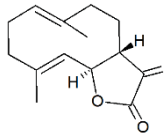	Germacranolide *trans*-C-6 lactonized.	M-phase arrest confirmed by: MS and flow cytometry measuring PH3.	TCP inhibition. Short and dense MT fibers. (Whipple et al., 2013; Liu et al., 2011a).

Parthenolide	*Tanacetum parthenium*	Anthemideae	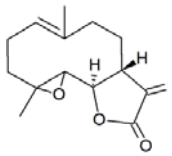	Germacranolide *trans*-C-6 lactonized.	G2/M phase arrest.	TCP inhibition. (Fonrose et al., 2007; Tang et al., 2015).
9-β-acetoxycostunolide	*Cyathocline purpurea*	Astereae	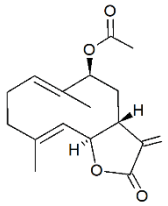	Germacranolide *trans*-C-6 lactonized. Acyl group.	G2/M phase arrest.	Not studied. (Ma et al., 2009).
Santamarine	*Cyathocline purpurea*	Astereae	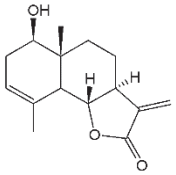	Eudesmanolide *trans*-C-6 lactonized.	G2/M phase arrest.	Not studied. (Ma et al., 2009).
Artesunate (artemisinin synthetic derivative)	*Artemisia annua*	Anthemideae		SL derivative. No lactone or α-β unsaturated carbonyl.	G2/M phase arrest.	Multiple centrosomes/spindles. Cytokinesis defect. (Steinbruck et al., 2010).
Dihydroartemisinin (artemisinin synthetic derivative)	*Artemisia annua*	Anthemideae		SL derivative. No lactone or α-β unsaturated carbonyl.	G2/M phase arrest.	High levels of cyclin B and decreased levels of Wee1. (Luo et al., 2013).

MS= mitotic spindle, PH3= phospho-histone H3, SAC= Spindle assembly checkpoint, TCP= tubulin carboxypeptidase, MT= microtubules, WB= western blotting.

6.4 Anti-mitotic activity of *Hymenoxys richardsonii*

6.4.1 No cell-rounding effect in non-cancer cell line

At concentrations of *H. richardsonii* extract that induced a cell rounding activity upon HT29 and M059K cell lines, the lung fibroblastic non-cancer cell line WI38 did not seem to have any reaction. Only at relatively high concentrations of 150 and especially 500 µg/mL we found a directly toxic effect of *H. richardsonii* extract upon this cell line; therefore, no cell rounding activity was ever noticed. Cancer cells are characterized by a series of hallmarks that are not present in normal, non-cancer cells (Hanahan & Weinberg, 2011). It is possible that the biological pathway affected by the treatment investigated here is essential for the proliferation of cancer cells, where proliferative signals are altered, and unnecessary to support cell division in non-cancer cells, where the mitotic process is tightly coordinated and controlled through different pathways.

6.4.2 Mitotic state of H. richardsonii-treated cells by enzymatic assays

We predict that the mitotic entrance occurs in a normal fashion based on the protein levels analyzed, with high levels of threonine 320-phosphorylated Plk1 and cyclin B, low levels of tyrosine 15-phosphorylated Cdk1, enzymatically active Cdk1, low levels of cyclin A, and no cyclin E. We could see a difference in cyclin A levels between nocodazole-treated cells and *H. richardsonii*-treated mitotic cells. Mitotic cells induced by treatment with *H. richardsonii* extract presented a lighter band of cyclin A than nocodazole-treated cells in a western blot assay, indicating a possible timing for the mitotic arrest. Nocodazole arrest occurs at the beginning of mitosis due to the inability to polymerize tubulin and form a mitotic spindle (Jordan & Wilson, 2004). Proteasome-mediated degradation of cyclin A

starts after nuclear envelope breakdown early in mitosis and its levels are almost zero in metaphase (den Elzen & Pines, 2001). If levels of cyclin A are lower with *H. richardsonii* extract treatment compared to nocodazole treatment, we can infer that mitotic cells from the former treatment are arrested at a later time in mitosis than mitotic cells from the latter treatment. Results of the other proteins analyzed were expected in cells undergoing the mitotic phase of the cell cycle and allowed us to confirm the state of mitosis of the rounded cells obtained after *H. richardsonii* treatment. We can also predict that hymenoratin is interfering with downstream mitotic events and not disturbing the normal levels of the main regulatory mitotic proteins mentioned (Cdk1/Cyclin B and Plk1).

6.4.3 Not more than 35% of cells arrest in mitosis but there is no other cell cycle arrest

An interesting characteristic of the activity observed in cancer cells after treatment with *H. richardsonii* is that the number of mitotic cells never reaches 100%, as with nocodazole or paclitaxel treatments, but ranges from 25 to 35% at 24 hours post-treatment. This might lead to believe that the active compound has different targets that induce other effects in cells such as an arrest in other cell cycle phases before mitosis. However, several tests revoked this initial hypothesis. First, with the exception of 1% of multinucleated cells, every cell analyzed by video microscopy entered mitosis in the first 24 hours. Second, when cells were synchronized at the G1/S checkpoint, both *H. richardsonii*-treated and DMSO-treated populations entered mitosis at the same time, no delay was noticed with our treatment. Third, cyclin E levels, which peak at the entrance of S phase, were similar in DMSO-treated cells and *H. richardsonii*-treated interphase cells, possibly indicating that adherent cells were normally distributed in the three phases of interphase and not accumulated in late G1 or S-phase. Finally, cell cycle analysis by flow cytometry showed

no cellular arrest in any other cell cycle phase other than mitosis. We could confirm those previous observations that were supporting the absence of a different arrest.

The characteristic of a maximum of 35% percent of mitotic cells was accompanied with the detection of a great percentage of cells undergoing mitosis at normal times, notably in the last two thirds of the 24 hours of treatment tested. By time-lapse video microscopy, we discovered that the rounding cell activity induced by *H. richardsonii* treatment was in a nonlinear fashion and the graph plotting the percentage of rounded cells over time of exposure resulted in a parabola. After treatment of HT29 cells with *H. richardsonii,* there was an initial increase in the rounding cell activity over time, but this trend reached a peak of about 30% rounded cells at 12-15 hours, followed by a decrease in the percentage of rounded cells at later hours post treatment. Moreover, in the first 24 hours of treatment, 25% of treated cells presented a mitotic delay or arrest for more than 2 hours, and the remaining 75% exited mitosis in what seemed to be a normal cell division (i.e. they divided in two and adopted an adherent flat morphology). The vast majority of cells that arrested in mitosis were those that entered this phase in the first 8 hours post-treatment. One explanation for these observations could be that the active compound in *H. richardsonii* binds covalently to the target and after 8 hours of treatment its levels start to get depleted in the media, causing the new cells undergoing mitosis to find fewer or no restrictions to face cell division. For instance, cells that are in G1 phase at the moment of treatment would require more than 8 hours to enter M phase because they have to undergo S and G2 phases before committing to divide. If the active compound, now bound to a target protein in 25% of the cells, were depleted from the media by that moment, this group of cells and cells entering mitosis later would not be affected by it. In agreement with this hypothesis and as

described in chapter 1, SLs have shown to form Michael-type additions with cysteines. This type of reaction involves the addition of a nucleophilic group, such as a sulfhydryl group, to the α-β-unsaturated carbonyl leading to the formation of a thioether bond, which is a covalent bond (Kupchan, 1970). Therefore, the apparently normal cell division of the unaffected remaining cells, together with the possible cell death of some of the mitotic-arrested cells, would explain why the percentage of mitotic cells decreases over time.

6.4.4 Possible mode of action of hymenoratin

From our western blotting results, we were able to assume that hymenoratin did not inhibit several known anti-mitotic targets such as the kinases Cdk1 or Plk1. This is also supported by the observation that HT29 cells treated with PP360-A and hymenoratin seemed to undergo normal early mitotic events such as chromosome condensation, centrosome separation, and formation of the mitotic spindle. Hymenoratin-treated cells separated the centrosomes, indicating that this compound does not inhibit the motor protein Eg5, which is required for this step. In addition, the degradation of cyclin A, which depends on APC/C ubiquitination and proteolysis by the 26S proteasome, suggests that the ubiquitin-proteasome system might not be inhibited by our treatment. Literature research led to a possible explanation that accounts for the chemical characteristics of SLs and for the main three characteristics detected in the mitotic arrest of HT29 cells after PP360-A and hymenoratin treatment: chromosome congression defects, mitotic spindle distortion, and damaged DNA in mitotic-arrested cells.

Observations of DNA morphology using DAPI staining in the mitotic-arrested cells from treatment with *H. richardsonii* extract or hymenoratin revealed lagged chromosomes close to the spindle poles that failed to align in the metaphase plate. One of the main drivers of

chromosome congression to the spindle equator is the plus-end directed centromeric protein E (CENP-E) that allows kinetochores of polar chromosomes to slide along the microtubules and align at the spindle equator (Yen et al., 1992; Wood et al., 1997; Kapoor et al., 2006). CENP-E is an integral component of the corona fibers in the outer layer of kinetochores that link centromeres with microtubules (Yao et al., 1997). It has been described that following suppression of this protein many chromosomes congress and form a metaphase plate but a subset remain trapped close to the spindle poles (Putkey et al., 2002). It was also found that CENP-E inhibition reduces tension at the kinetochores and reduces the binding stability with microtubules, activating the SAC and causing cells to arrest in mitosis with high levels of cyclin B (Yao et al., 2000). A related protein, CENP-F has been shown to be important to maintain levels of kinetochore-bound CENP-E and dynactin (cofactor of another motor protein: dynein) and its repression by RNA interference led to chromosome misalignments in a similar manner than CENP-E suppression (Holt et al., 2005; Yang et al., 2005). Both CENP-E and CENP-F proteins possess in their carboxyl terminus the consensus sequence CAAX (C= cysteine, A=aliphatic amino acid, and X=methionine, serine, alanine, glutamic acid, or cysteine) and are farnesylated (Ashar et al., 2000). Farnesylation of CENP-F is required for its localization in the kinetochores (Hussein & Taylor, 2002). Holland et al. (2015) demonstrated that farnesylation of CENP-E was required for chromosome congression and timely mitotic progression. In addition, a study using the farnesyl transferase inhibitor lonafarnib suggested that farnesylation is required for a normal maintenance of chromosome alignment. In that study, metaphase CENP-E and CENP-F-depleted kinetochores leave the spindle equator and move towards the poles as lagged chromosomes causing a mitotic delay (Schafer-Hales et al., 2007). The farnesylation process that affects CENP-E and CENP-F function is a type of post-translational

modification in which farnesyltransferase catalyzes the covalent thioether attachment between the farnesyl pyrophosphate and the cysteine sulfhydryl present in proteins with the CAAX consensus sequence (Rando, 1996). Because the farnesyl pyrophosphate that the farnesyl transferase transfers to the CENP-E and CENP-F terminus is a sesquiterpene structure, it is possible that the SL hymenoratin can interfere with this process forming Michael-type adducts with the cysteines present at the CAAX sequence of these motor proteins.

A mitotic spindle distortion was also observed in studies in which CENP-E or CENP-F were suppressed. Yao et al. (2000) described the presence of flattened bipolar spindles and some apparent fragmentation of spindle poles observed as multipolar spindle arrays after depletion of CENP-E. The authors believed that the flattening could be a consequence of the reduced tension between the poles, but they suggested as another factor the reduced amount of kinetochore-bound dynein after suppression of CENP-E. The centrosomal dynein-mediated release of the dynein-dynactin-NuMA complex is required for tethering of polar microtubules (Merdes et al., 2000). Competition between the motor proteins CENP-E and dynein was suggested then to be important for an appropriate release of their cargos so that normal dynein functions might be affected by suppression of CENP-E levels (Yao et al., 2000). A separate study investigating functions of CENP-F also illustrated problems in proper mitotic spindle assembly after CENP-F silencing. Their observations and quantitation of tubulin fluorescent signal in CENP-F-deficient cells supported the idea that there is a slightly lower microtubule density in the region close to the poles, which often presented a cone shape, and a higher density at the midzone when compared to controls, with spindle microtubules often extending beyond the midzone (Holt et al., 2005).

They also found multipolar spindles, but they could not explain the mechanism of action by which CENP-F suppression led to it. However, they considered unlikely a direct interaction of this protein with the microtubules since it did not sediment with taxol-stabilized microtubules. They suggested that an anaphase-mimicking response, with variation in microtubules flux, sliding in the midzone, and elongation, may be activated when there are separated sister chromatids near the spindle poles, which was a characteristic of CENP-F inhibition (Holt et al., 2005). The α-tubulin and DAPI staining from these studies is comparable with our results, having a morphology of aberrant chromosome congression and distorted mitotic spindles that often appear to be multipolar.

Lastly, regarding damaged DNA, Holt and colleagues showed that CENP-F depletion weakens centromeric cohesion, consistent with their finding of kinetochores with no sisters near the spindle poles, suggesting premature separation of sister chromatids (Holt et al., 2005). They also affirmed that the characteristics observed in their study were strikingly similar to those obtained in studies after repression of Sgo1 protein (Holt et al., 2005), such as that from Salic et al in 2004 or McGuiness et al in 2005, where they stated that Sgo1 has a key role in protection of centromere cohesion and stabilization of kinetochore-microtubules. This possible involvement of CENP-F in centromeric cohesion might account for the γ-H2AX foci detected in mitotic-arrested cells after *H. richardsonii* and hymenoratin treatment since it was demonstrated that knockdown of the related motor protein Sgo1 caused telomeres dysfunction with increased γ-H2AX signal and activation of the DNA-damage pathway (Hayashi et al., 2012). In the same study it was shown that telomere dysfunction was also observed after treatment with the tubulin-poison colcemid and the authors proposed a model where the mitotic arrest *per se* induces, in a time-

dependent manner, telomere deprotection by destabilization of a telomere binding protein called TRF2 (Hayashi et al., 2012). This is consistent with different studies describing formation of γ-H2AX foci during mitotic arrest induced by treatment with nocodazole or even specifically with a CENP-E inhibitor (Dalton et al., 2007; Quignon et al., 2007; Guerrero et al., 2010; Tu et al., 2013; Colin et al., 2015) or with the SL dehydroleucodine (Bailon-Moscoso et al., 2015).

Importantly for our research, SLs isolated from *Artemisia sylvatica* species, called arteminolides, were shown to be inhibitors of the farnesyl transferase (Lee et al., 2000) and although they were not investigated for an anti-mitotic activity, they inhibited cancer cell growth (Lee et al., 2003). This indicates that these SLs, which are closely related to hymenoratin structure (**Table 5**), are able to interact with farnesyltransferase, raising the possibility that their biological effects in cancer cells are due to the inhibition of CENP-E/CENP-F farnesylation with the consequent induction of mitotic arrest.

Recently, another protein called Spindly has been shown to be involved in the chromosome congression failure after treatment with farnesyl transferase inhibitors (FTIs). Spindly, like CENP-E and CENP-F, localizes in the fibrous corona of the kinetochores, where it functions as an adaptor of dynein (Griffis et al., 2007). It is removed from the kinetochores when they attach to microtubules and dynein mediates transport to the spindle poles, possibly as part of a mechanism that coordinates microtubules attachments with the SAC (Barisic et al., 2010). After CENP-E and CENP-F were considered the only mitotic proteins that are FTase substrates, Spindly now represents a third mitotic protein that interacts with the FTase (Holland et al., 2015). Spindly farnesylation was shown to be required for its localization at the kinetochores (Barisic et al., 2010). Preventing farnesylation of Spindly

resulted in a delay in chromosome congression and a similar mitotic phenotype to that observed after FTIs treatment (Holland et al., 2015; Moudgil et al., 2015).

Additionally, a factor that influences chromosome congression is the tyrosinated state of tubulin. One of tubulin post-translational modifications is the detyrosination carried by tubulin carboxypeptidase (TCP) at the C-terminus of the α-subunit, which can be retyrosinated by another enzyme called tyrosine ligase (Contin et al., 1999). Whereas dynein has an affinity for tyrosinated astral microtubules, CENP-E has a preference for detyrosinated spindle microtubules and it is important to guide chromosome movements ultimately towards the spindle pole (Barisic et al., 2014; Barisic et al., 2015). The SLs parthenolide and costunolide were shown to inhibit TCP and caused chromosome congression defects (Whipple et al., 2013; Barisic et al., 2015). Whether hymenoratin interferes with FTase-dependent farnesylation of CENP-E, CENP-F, and/or Spindly, or with TCP detyrosination of tubulin, the outcome of the inhibition of both post-translational modifications would be the inability of motor proteins, notably CENP-E, to move polar chromosomes to the spindle equator. This defect in chromosome congression is accompanied with a weakened tension in the kinetochore-microtubules attachments and activation of the spindle assembly checkpoint that keeps cells arrested in mitosis.

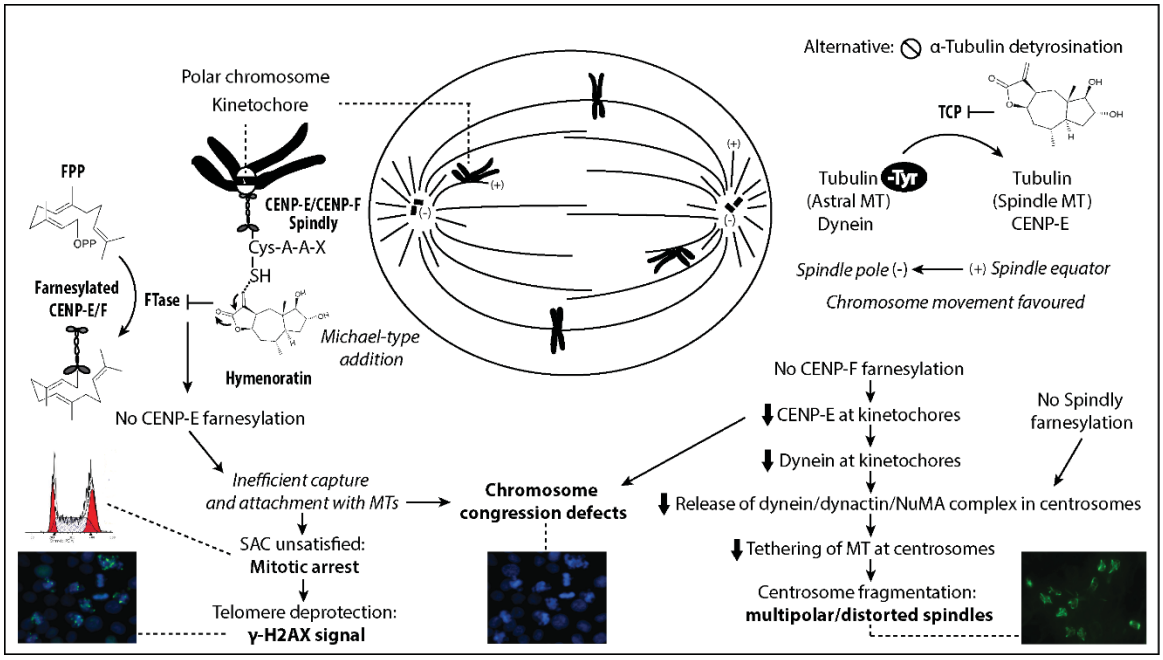

Figure 50. Proposed mode of action of hymenoratin. Hymenoratin, related to the sesquiterpene farnesyl pyrophosphate (FPP), interferes with farnesylation of motor proteins such as CENP-E, CENP-F, or Spindly, causing defects in kinetochore-microtubule (MTs) attachments of polar chromosomes and chromosome congression failure. The spindle assembly checkpoint (SAC) is not silenced and cells stay arrested in mitosis. Prolonged arrest leads to telomere deprotection, wich damages DNA. Abnormal levels of CENP-E-Dynein in kinetochores end with decrease of MT tethering at centrosomes which causes mitotic spindle defects. An alternative or additional mode of action might be the inhibition of tubulin carboxypeptidase (TCP), which removes the tyrosine residue in α-tubulin, important to guide chromosome movements during mitosis. Chromosomes movement is favoured towards the spindle poles when MTs are tyrosinated.

6.5 Future directions

Future research with hymenoratin or other SLs should include analysis of kinetochore-microtubule attachments, centromere cohesion, and other analysis to measure levels of CENP-E/CENP-F/Spindly farnesylation or microtubule tyrosination state. They could prove or disprove whether all of these similarities in the cellular features between our results and previous research are due to hymenoratin acting as a farnesyl transferase

inhibitor that interferes with the function of motor proteins driving chromosome congression.

A cell-permeable small molecule like hymenoratin with the capacity to inhibit, directly or indirectly, a key mitotic protein can be a useful probe to understand the complexity of many cellular processes involved in mitosis that are poorly understood. In addition, although there are many anti-mitotic agents, their use as anticancer therapies is limited because their *in vitro* activity cannot be translated to clinical efficacy or they induce strong side effects or resistance (Chan et al., 2012). Insight into the structure-activity relationship of SLs and anti-mitotic effects might lead to the development of a more specific and potent anti-mitotic agent that might be clinically efficient to inhibit cancer cell proliferation.

This project has contributed to a better approach in the selection of plant species from the Asteraceae family to look for biologically active SLs. Three out of six species of this family studied in this project were found to arrest cancer cells in mitosis. Our data from chapter 3 support that although Asteraceae family is characterized for the production of SLs, plants from different taxa in this family synthesize more or less complex sesquiterpenoids leading to different biological effects upon cells. *H. richardsonii* and *G. aristata* belong to the Helenieae tribe and this taxonomical proximity may be a reason for the similar secondary metabolism and anti-mitotic activity. Nevertheless, during the course of this research, we started a new project to select species from different Asteraceae tribes and investigate if they have anti-mitotic activity upon cells. We found that this activity might be even specific to certain genera because the plant *Tetraneuris acaulis*, which belongs to the same tribe and subtribe as *H. richardsonii* (i.e. Helenieae, Tetraneurinae), did not induce a cell rounding effect. Literature research of secondary metabolism of these two plants showed

that *T. acaulis* is unable to synthesize modified pseudoguaianolides whereas *H. richardsonii* can produce them. The biosynthetic complexity of each taxa might lead to the production of a specific type of SL that has the chemical structure requirements that allow interaction with specific targets within the cell and elicit an anti-mitotic effect. Even though this could be specific for certain taxa, our results suggest that taxonomic proximity among plant species increases chances to find biologically active SLs. We recommend for future studies of anti-mitotic activities in Canadian prairie plants, the analysis of *Arnica* genus from Madieae tribe, *Liatris* from Eupatorieae, *Helenium* from Helenieae tribe, *Artemisia* and *Tanacetum* genera from Anthemideae tribe, *Ambrosia* genus from Heliantheae, and even the *Saussurea* genus from the farther Cardueae tribe, which produces the SLs costunolide and dehydrocostuslactone.

New questions are now open for future research in this field regarding the possible target(s) of these related molecules and the structure-activity relationship between SLs and mitotic arrest. New anti-mitotic compounds with different chemical structures can help elucidate the mechanisms controlling certain biological pathways by inhibition of mitotic proteins whose functions are sometimes largely unexplored. Continuous investigation of the mitotic arrest capacity of certain types of SLs produced by a subset of Canadian prairie plants can be used for future models in the development of effective anti-mitotic drugs.

References

Aanes, W. A. (1961). Pingue (*Hymenoxys richardosnii*) poisoning in sheep. *American Journal of Veterinary Research, 22*, 47-52.

Ahmed, A. A., Spring, O., Abd El-Razek, M. H., Hussein, N. S., & Mabry, T. J. (1995). Sesquiterpene lactones and other constituents from *Hymenoxys richardsonii* and *H. subintegra*. *Phytochemistry, 39*, 1127-1131.

Anderson, L. A. P., de Kock, W. T., Pachler, K. G. R., & Brink, C. v. d. M. (1967). The structure of vermeerin : A sesquiterpenoid dilactone from *Geigeria africana* gries. *Tetrahedron, 23*, 4153-4160.

Ashar, H. R., James, L., Gray, K., Carr, D., Black, S., Armstrong, L., et al. (2000). Farnesyl transferase inhibitors block the farnesylation of CENP-E and CENP-F and alter the association of CENP-E with the microtubules. *Journal of Biological Chemistry, 275*, 30451-30457.

Bailon-Moscoso, N., Gonzalez-Arevalo, G., Velasquez-Rojas, G., Malagon, O., Vidari, G., Zentella-Dehesa, A., et al. (2015). Phytometabolite dehydroleucodine induces cell cycle arrest, apoptosis, and DNA damage in human astrocytoma cells through p73/p53 regulation. *Plos One, 10*, e0136527.

Bain, J. F., Flanagan, J., & Kuijt, J. (2014). *Common coulee plants of Southern Alberta* (2nd ed.). Lethbridge, Alberta: University of Lethbridge.

Baldwin, B. G., & Wessa, B. L. (2000). Phylogenetic placement of *Pelucha* and new subtribes in Helenieae sensu stricto (Compositae). *Systematic Botany, 25*, 522-538.

Barisic, M., Aguiar, P., Geley, S., & Maiato, H. (2014). Kinetochore motors drive congression of peripheral polar chromosomes by overcoming random arm-ejection forces. *Nature Cell Biology, 16*, 1249.

Barisic, M., Sohm, B., Mikolcevic, P., Wandke, C., Rauch, V., Ringer, T., et al. (2010). Spindly/ccdc99 is required for efficient chromosome congression and mitotic checkpoint regulation. *Molecular Biology of the Cell, 21*, 1968-1981.

Barisic, M., Sousa, R. S. E., Tripathy, S. K., Magiera, M. M., Zaytsev, A. V., Pereira, A. L., et al. (2015). Microtubule detyrosination guides chromosomes during mitosis. *Science, 348*, 799-803.

Barr, A. R., & Gergely, F. (2007). Aurora-A: The maker and breaker of spindle poles. *Journal of Cell Science, 120*, 2987-2996.

Basseres, D. S., & Baldwin, A. S. (2006). Nuclear factor-kappa B and inhibitor of kappa B kinase pathways in oncogenic initiation and progression. *Oncogene, 25*, 6817-6830.

Beekman, A. C., Woerdenbag, H. J., vanUden, W., Pras, N., Konings, A. W. T., Wikstrom, H. V., et al. (1997). Structure-cytotoxicity relationships of some helenanolide-type sesquiterpene lactones. *Journal of Natural Products, 60*, 252-257.

Biddulph, S. F. (1944). A revision of the genus *Gaillardia*. *State College of Washington, 12*, 195-256.

Bierner, M. W. (2001). Taxonomy of *Hymenoxys* subgenus *Picradenia* and a conspectus of the subgenera of *Hymenoxys* (Asteraceae: Helenieae: Tetraneurinae). *Lundellia*, 37-63.

Blangy, A., Lane, H. A., dHerin, P., Harper, M., Kress, M., & Nigg, E. A. (1995). Phosphorylation by p34(cdc2) regulates spindle association of human Eg5, a kinesin-related motor essential for bipolar spindle formation in vivo. *Cell, 83*, 1159-1169.

Bohlmann, F., Misra, L. N., Jakupovic, J., King, R. M., & Robinson, H. (1985). Guaianolides, heliangolides, diterpenes and cycloartenol derivatives from *Balsamorhiza sagittata*. *Phytochemistry, 24*, 2029-2036.

Borgne, A., Versteege, I., Mahe, M., Studeny, A., Leonce, S., Naime, I., et al. (2006). Analysis of cyclin B1 and cdk activity during apoptosis induced by camptothecin treatment. *Oncogene, 25*, 7361-7372.

Bork, P. M., Schmitz, M. L., Kuhnt, M., Escher, C., & Heinrich, M. (1997). Sesquiterpene lactone containing mexican indian medicinal plants and pure sesquiterpene lactones as potent inhibitors of transcription factor Nf-κB. *FEBS Letters, 402*, 85-90.

Bosco, A., & Golsteyn, R. M. (2017). Emerging anti-mitotic activities and other bioactivities of sesquiterpene compounds upon human cells. *Molecules, 22*, 459.

Bosco, A. (2017). *A novel anti-mitotic activity on human cells by pulchelloid A, a compound isolated from the Prairie plant Gaillardia aristata.* (master's thesis), University of Lethbridge, Alberta, Canada.

Briskin, D. P. (2000). Medicinal plants and phytomedicines. Linking plant biochemistry ad physiology to human health. *Plant Physiology, 124*, 507.

Brouillet L, Desmet P, Coursol F, Meades SJ, Favreau M, Anions M, et al. (2010+). Database of vascular plants of Canada (VASCAN). Retrieved 2018-03-14 http://data.canadensys.net/vascan

Burnett, W. C., Jones, S. B., Mabry, T. J., & Padolina, W. G. (1974). Sesquiterpene lactones — insect feeding deterrents in *Vernonia*. *Biochemical Systematics and Ecology, 2*, 25-29.

Cadart, C., Zlotek-Zlotkiewicz, E., Le Berre, M., Piel, M., & Matthews, Helen K. (2014). Exploring the function of cell shape and size during mitosis. *Developmental Cell, 29*, 159-169.

Carlson, E. E. (2010). Natural products as chemical probes. *ACS Chemical Biology, 5*, 639.

Chadwick, M., Trewin, H., Gawthrop, F., & Wagstaff, C. (2013). Sesquiterpenoids lactones: benefits to plants and people. *International Journal of Molecular Sciences, 14*, 12780-12805.

Chan, K. S., Koh, C. G., & Li, H. Y. (2012). Mitosis-targeted anti-cancer therapies: where they stand. *Cell Death & Disease, 3*, e411.

Chang, J., & Kwon, H. J. (2016). Discovery of novel drug targets and their functions using phenotypic screening of natural products. *Journal of Industrial Microbiology & Biotechnology, 43*, 221-231.

Cheng, X., Liu, Y. Q., Wang, G. Z., Yang, L. N., Lu, Y. Z., Li, X. C., et al. (2017). Proteomic identification of the oncoprotein STAT3 as a target of a novel Skp1 inhibitor. *Oncotarget, 8*, 2681-2693.

Ciechanover, A. (1998). The ubiquitin-proteasome pathway: on protein death and cell life. *The EMBO Journal, 17*, 7151-7160.

Clardy, J., & Walsh, C. (2004). Lessons from natural molecules. *Nature, 432*, 829-837.

Colin, D. J., Hain, K. O., Allan, L. A., & Clarke, P. R. (2015). Cellular responses to a prolonged delay in mitosis are determined by a DNA damage response controlled by Bcl-2 family proteins. *Open Biology, 5*, 140156-140156.

Contin, M. A., Sironi, J. J., Barra, H. S., & Arce, C. A. (1999). Association of tubulin carboxypeptidase with microtubules in living cells. *The Biochemical Journal, 339*, 463-471.

Cotugno, R., Fortunato, R., Santoro, A., Gallotta, D., Braca, A., De Tommasi, N., et al. (2012b). Effect of sesquiterpene lactone coronopilin on leukaemia cell population growth, cell type-specific induction of apoptosis and mitotic catastrophe. *Cell Proliferation, 45*, 53-65.

Dalton, W. B., Nandan, M. O., Moore, R. T., & Yang, V. W. (2007). Human cancer cells commonly acquire DNA damage during mitotic arrest. *Cancer Research, 67*, 11487-11492.

Darbyshire, S. J., Favreau, M., & Murray, M. (2000). *Common and scientific names of weeds in Canada*. Ottawa, Ontario: Canadian Government Publishing.

den Elzen, N., & Pines, J. (2001). Cyclin A is destroyed in prometaphase and can delay chromosome alignment and anaphase. *The Journal of Cell Biology, 153*, 121-136.

Ditchfield, C., Johnson, V. L., Tighe, A., Ellston, R., Haworth, C., Johnson, T., et al. (2003). Aurora B couples chromosome alignment with anaphase by targeting Bubr1, Mad2, and Cenp-E to kinetochores. *The Journal of Cell Biology, 161*, 267-280.

Drpic, D., Pereira, António J., Barisic, M., Maresca, Thomas J., & Maiato, H. (2015). Polar ejection forces promote the conversion from lateral to end-on kinetochore-microtubule attachments on mono-oriented chromosomes. *Cell Reports, 13*, 460-468.

Dumont, S., & Mitchison, T. J. (2009). Force and length in the mitotic spindle. *Current Biology, 19*, 749-761.

Dutta, J., Fan, Y., Gupta, N., Fan, G., & Gelinas, C. (2006). Current insights into the regulation of programmed cell death by Nf-kB. *Oncogene, 25*, 6800-6816.

Ecological Stratification Working Group (1996). *A national ecological framework for Canada*. Ottawa, Ontario: Agriculture and Agri-Food Canada.

Flora of North America Editorial Committee (1993 +). *Flora of North America. North of Mexico*. New York, NY: Oxford University Press.

Fonrose, X., Ausseil, F., Soleilhac, E., Masson, V., David, B., Pouny, I., et al. (2007). Parthenolide inhibits tubulin carboxypeptidase activity. *Cancer research, 67*, 3371-3378.

Funk, V. A., Sussana, A., Stuessy, T. F., Bayer, R. J. (2009). *Systematics, evolution, and biogeography of Compositae*. Vienna, Austria: International Association for Plant Taxonomy, Institute of Botany, University of Vienna.

Furuta, T., Takemura, H., Liao, Z.-Y., Aune, G. J., Redon, C., Sedelnikova, O. A., et al. (2003). Phosphorylation of histone H2AX and activation of Mre11, Rad50, and Nbs1 in response to replication-dependent DNA double-strand breaks induced by mammalian DNA topoisomerase I cleavage complexes. *Journal of Biological Chemistry, 278*, 20303-20312.

Gaiser, L. O. (1946a). The genus *Liatris*. *Rhodora, 48*, 165-183.

Gaiser, L. O. (1946b). The genus *Liatris* (continued). *Rhodora, 48*, 331-382.

Ghantous, A., Gali-Muhtasib, H., Vuorela, H., Saliba, N. A., & Darwiche, N. (2010). What made sesquiterpene lactones reach cancer clinical trials? *Drug Discovery Today, 15*, 668-678.

Ghantous, A., Nasser, N., Saab, I., Darwiche, N., & Saliba, N. A. (2009). Structure–activity relationship of seco-tanapartholides isolated from *Achillea falcata* for inhibition of hacat cell growth. *European Journal of Medicinal Chemistry, 44*, 3794-3797.

Gilmore, T. D. (2006). Introduction to Nf-kB: players, pathways, perspectives. *Oncogene, 25*, 6680-6684.

Glickman, M. H., & Ciechanover, A. (2002). The ubiquitin-proteasome proteolytic pathway: destruction for the sake of construction. *Physiological Reviews, 82*, 373-428.

Griffis, E. R., Stuurman, N., & Vale, R. D. (2007). Spindly, a novel protein essential for silencing the spindle assembly checkpoint, recruits dynein to the kinetochore. *The Journal of Cell Biology, 177*, 1005-1015.

Groll, M., & Huber, R. (2004). Inhibitors of the eukaryotic 20s proteasome core particle: A structural approach. *BBA - Molecular Cell Research, 1695*, 33-44.

Guerrero, A. A., Gamero, M. C., Trachana, V., Fütterer, A., Pacios-Bras, C., Díaz-Concha, N. P., et al. (2010). Centromere-localized breaks indicate the generation of DNA damage by the mitotic spindle. *Proceedings of the National Academy of Sciences of the United States of America, 107*, 4159-4164.

Gurley, L. R., D'Anna, J. A., Barham, S. S., Deaven, L. L., & Tobey, R. A. (1978). Histone phosphorylation and chromatin structure during mitosis in Chinese hamster cells. *European Journal of Biochemistry / FEBS, 84*, 1-15.

Häcker, G. (2000). The morphology of apoptosis. *Cell and Tissue Research, 301*, 5-17.

Hanahan, D., & Weinberg, R. (2011). Hallmarks of cancer: the next generation. *Cell, 144*, 646-674.

Hardy, W. T., Cory, V. L., Schmidt, H., & Dameron, W. H. (1931). *Bitterweed poisoning in sheep*. Texas: Texas Agricultural Experiment Station.

Hartmann, T. (1996). Diversity and variability of plant secondary metabolism: a mechanistic view. *Entomologia Experimentalis et Applicata, 80*, 177-188.

Hartwell, L. H., & Weinert, T. A. (1989). Checkpoints: controls that ensure the order of cell cycle events. *Science, 246*, 629-634.

Hauf, S., Cole, R. W., LaTerra, S., Zimmer, C., Schnapp, G., Walter, R., et al. (2003). The small molecule hesperadin reveals a role for aurora B in correcting kinetochore-microtubule attachment and in maintaining the spindle assembly checkpoint. *The Journal of Cell Biology, 161*, 281-294.

Hayashi, M. T., Cesare, A. J., Fitzpatrick, J. A. J., Lazzerini-Denchi, E., & Karlseder, J. (2012). A telomere-dependent DNA damage checkpoint induced by prolonged mitotic arrest. *Nature Structural & Molecular Biology, 19*, 387-394.

Hehner, S. P., Heinrich, M., Bork, P. M., Vogt, M., Ratter, F., Lehmann, V., et al. (1998). Sesquiterpene lactones specifically inhibit activation of NF-kappa B by preventing the degradation of I kappa B-alpha and I kappa B-beta. *Journal of Biological Chemistry, 273*, 1288-1297.

Hendzel, M. J., Wei, Y., Mancini, M. A., Van Hooser, A., Ranalli, T., Brinkley, B. R., et al. (1997). Mitosis-specific phosphorylation of histone H3 initiates primarily within pericentromeric heterochromatin during G2 and spreads in an ordered fashion coincident with mitotic chromosome condensation. *Chromosoma, 106*, 348-360.

Herz, W., Aota, K., Holub, M., & Samek, Z. (1970). Sesquiterpene lactones and lactone glycosides from *Hymenoxys* species. *The Journal of Organic Chemistry, 35*, 2611-2624.

Herz, W., Poplawski, J., & Sharma, R. P. (1975). Constituents of *Liatris* species. VI. New guaianolides from *Liatris* species. *The Journal of Organic Chemistry, 40*, 199-206.

Herz, W., & Sharma, R. P. (1975). New germacranolides from *Liatris* species. *Phytochemistry, 14*, 1561-1567.

Herz, W., & Wahlberg, I. (1973a). Constituents of *Liatris* species. III. Provincialin, a cytotoxic germacradienolide from liatris provincialis with unusual ester side chain. *The Journal of Organic Chemistry, 38*, 2485-2489.

Herz, W., & Wahlberg, I. (1973b). Punctatin: a new germacradienolide from *Liatris punctata*. *Phytochemistry, 12*, 1421-1426.

Ho, L. K., & Nodwell, J. R. (2016). David and Goliath: Chemical perturbation of eukaryotes by bacteria. *Journal of Industrial Microbiology & Biotechnology, 43*, 233-248.

Holland, A. J., Reis, R. M., Niessen, S., Pereira, C., Andres, D. A., Spielmann, H. P., et al. (2015). Preventing farnesylation of the dynein adaptor Spindly contributes to the mitotic defects caused by farnesyltransferase inhibitors. *Molecular Biology of the Cell, 26*, 1845-1856.

Holt, S. V., Vergnolle, M. A. S., Hussein, D., Wozniak, M. J., Allan, V. J., & Taylor, S. S. (2005). Silencing Cenp-F weakens centromeric cohesion, prevents chromosome alignment and activates the spindle checkpoint. *Journal of Cell Science, 118*, 4889-4900.

Hoyt, M. A., Totis, L., & Roberts, B. T. (1991). *Saccharomyces-cerevisiae* genes required for cell-cycle arrest in response to loss of microtubule function. *Cell, 66*, 507-517.

Hsu, J. Y., Sun, Z. W., Li, X. M., Reuben, M., Tatchell, K., Bishop, D. K., et al. (2000). Mitotic phosphorylation of histone H3 is governed by Ipl1/Aurora kinase and Glc7/PP1 phosphatase in budding yeast and nematodes. *Cell, 102*, 279-291.

Hussein, D., & Taylor, S. S. (2002). Farnesylation of Cenp-F is required for G2/M progression and degradation after mitosis. *Journal of Cell Science, 115*, 3403-3414.

Hwang, L. H., Lau, L. F., Smith, D. L., Mistrot, C. A., Hardwick, K. G., Hwang, E. S., et al. (1998). Budding yeast cdc20: A target of the spindle checkpoint. *Science, 279*, 1041-1044.

Inoue, S., & Salmon, E. D. (1995). Force generation by microtubule assembly disassembly in mitosis and related movements. *Molecular Biology of The Cell, 6*, 1619-1640.

Ivie, G. W., Witzel, D. A., Herz, W., Kannan, R., Norman, J. O., Rushing, D. D., et al. (1975). Hymenovin. Major toxic constituent of western bitterweed (*Hymenoxys odorata* dc.). *Journal of Agricultural and Food Chemistry, 23*, 841-845.

Ivie, G. W., Witzel, D. A., Herz, W., Sharma, R. P., & Johnson, A. E. (1976). Isolation of hymenovin from *Hymenoxys richardsonii* (pingue) and *Dugaldia hoopesii* (orange sneezeweed). *Journal of Agricultural and Food Chemistry, 24*, 681-682.

Ji, H.-F., Li, X.-J., & Zhang, H.-Y. (2009). Natural products and drug discovery. Can thousands of years of ancient medical knowledge lead us to new and powerful drug combinations in the fight against cancer and dementia? *EMBO Reports, 10*, 194-200.

Jiang, X., Zhao, B., Britton, R., Lim, L. Y., Leong, D., Sanghera, J. S., et al. (2004). Inhibition of Chk1 by the G2 DNA damage checkpoint inhibitor isogranulatimide. *Molecular Cancer Therapeutics, 3*, 1221.

Joglekar, A. (2016). A cell biological perspective on past, present and future investigations of the spindle assembly checkpoint. *Biology, 5*, 44.

Jones, D. H., Kim, H. L., & Donnelly, K. C. (1981). DNA damaging effects of three sesquiterpene lactones in repair-deficient mutants of *Bacillus subtilis*. *Research Communications in Chemical Pathology and Pharmacology, 34*, 161.

Jordan, M., & Wilson, L. (2004). Microtubules as a target for anticancer drugs. *Nature Reviews Cancer, 4*, 253-265.

Jordan, M. A., Thrower, D., & Wilson, L. (1991). Mechanism of inhibition of cell proliferation by *Vinca* alkaloids. *Cancer Research, 51*, 2212.

Jordan, M. A., & Wilson, L. (1998). Microtubules and actin filaments: dynamic targets for cancer chemotherapy. *Current Opinion in Cell Biology, 10*, 123-130.

Jung, H. J., Shim, J. S., Lee, J., Song, Y. M., Park, K. C., Choi, S. H., et al. (2010). Terpestacin inhibits tumor angiogenesis by targeting uqcrb of mitochondrial complex III and suppressing hypoxia-induced reactive oxygen species production and cellular oxygen sensing. *The Journal of Biological Chemistry, 285*, 11584-11595.

Kantar, M. B., Baute, G. J., Bock, D. G., & Rieseberg, L. H. (2014). Genomic variation in *Helianthus*: Learning from the past and looking to the future. *Briefings in Functional Genomics, 13*, 328-340.

Kapoor, T. M., Lampson, M. A., Hergert, P., Cameron, L., Cimini, D., Salmon, E. D., et al. (2006). Chromosomes can congress to the metaphase plate before biorientation. *Science, 311*, 388-391.

Kapoor, T. M., Mayer, T. U., Coughlin, M. L., & Mitchison, T. J. (2000). Probing spindle assembly mechanisms with monastrol, a small molecule inhibitor of the mitotic kinesin, Eg5. *The Journal of Cell Biology, 150*, 975-988.

Kastan, M. B., & Bartek, J. (2004). Cell-cycle checkpoints and cancer. *Nature, 432*, 316-323.

Kawabe, T. (2004). G2 checkpoint abrogators as anticancer drugs. *Molecular Cancer Therapeutics, 3*, 513-519.

Keeler, R. F., & Baker, D. C. (1990). Myopathy in cattle induced by alkaloid extracts from *Thermopsis montana*, *Laburnum anagyroides* and a *Lupinus* sp. *Journal of Comparative Pathology, 103*, 169-182.

Kernéis, S., Swift, L. H., Lewis, C. W., Bruyère, C., Oumata, N., Colas, P., et al. (2015). Natural product extracts of the Canadian Prairie plant, *Thermopsis rhombifolia*, have anti-cancer activity in phenotypic cell-based assays. *Natural Product Research, 29*, 1026-1034.

Kerr, J. F., Wyllie, A. H., & Currie, A. R. (1972). Apoptosis: A basic biological phenomenon with wide-ranging implications in tissue kinetics. *British Journal of Cancer, 26*, 239.

Kim, H. L., & Pattersen, R. C. (1976). X-ray structures of hymenoxon and hymenolane : pseudoguaianolides isolated from *Hymenoxys odorata* dc. (bitterweed) *Journal of Chemistry Society, Perkin Transaction 2*, 1399-1403.

Kindscher, K. (1992). *Medicinal wild plants of the Prairie. An ethnobotanical guide*: University Press of Kansas.

Kirschner, M. W., Murray, A. W., & Glotzer, M. (1991). Cyclin is degraded by the ubiquitin pathway. *Nature, 349*, 132-138.

Kisselev, Alexei F., van der Linden, W. A., & Overkleeft, Herman S. (2012). Proteasome inhibitors: an expanding army attacking a unique target. *Chemistry & Biology, 19*, 99-115.

Kubara, P. M., Kerneis-Golsteyn, S., Studeny, A., Lanser, B. B., Meijer, L., & Golsteyn, R. M. (2012). Human cells enter mitosis with damaged DNA after treatment with pharmacological concentrations of genotoxic agents. *Biochemical Journal, 446*, 373-381.

Kuijt, J. (1982). *A flora of Waterton lakes national park*. Edmonton: University of Alberta Press.

Kupchan, S. (1970). Recent advances in the chemistry of tumor inhibitors of plant origin. *Transactions of the New York Academy of Sciences, 32*, 85.

Kupchan, S. M., Davies, V. H., Fujita, T., Cox, M. R., & Bryan, R. F. (1971a). Tumor inhibitors. LXVIII. Liatrin, a novel antileukemic sesquiterpene lactone from *Liatris chapmanii*. *Journal of the American Chemical Society, 93*, 4916-4918.

Kupchan, S. M., Eakin, M. A., & Thomas, A. M. (1971b). Tumor inhibitors. 69. Structure-cytotoxicity relations among the sesquiterpene lactones. *Journal of Medicinal Chemistry, 14*, 1147-1152.

Kupchan, S. M., Fessler, D. C., Eakin, M. A., & Giacobbe, T. J. (1970). Reactions of alpha methylene lactone tumor inhibitors with model biological nucleophiles. *Science, 168*, 376-378.

Lane, H. A., & Nigg, E. A. (1996). Antibody microinjection reveals an essential role for human polo-like kinase 1 (Plk1) in the functional maturation of mitotic centrosomes. *The Journal of Cell Biology, 135*, 1701-1713.

Laurell, E., Beck, K., Krupina, K., Theerthagiri, G., Bodenmiller, B., Horvath, P., et al. (2011). Phosphorylation of Nup98 by multiple kinases is crucial for Npc disassembly during mitotic entry. *Cell, 144*, 539-550.

Law, M. E., Corsino, P. E., Narayan, S., & Law, B. K. (2015). Cyclin-dependent kinase inhibitors as anticancer therapeutics. *Molecular Pharmacology, 88*, 846-852.

Lee, C. W., Lee, S. H., Lee, M.-Y., Kang, H.-M., Han, D. C., Son, K.-H., et al. (2003). Anti-tumor activity of the farnesyl-protein transferase inhibitors arteminolides, isolated from *Artemisia*. *Bioorganic & Medicinal Chemistry, 11*, 4545-4549.

Lee, K. H., Huang, E. S., Piantadosi, C., Pagano, J. S., & Geissman, T. A. (1971). Cytotoxicity of sesquiterpene lactones. *Cancer Research, 31*, 1649-1649.

Lee, S.-H., Lee, U. C., Lee, H., Kang, H.-M., Song, H.-C., Son, K.-H., et al. (2000). Sesquiterpene lactones, inhibitors of farnesyl protein transferase, isolated from the flower of *Artemisia sylvatica*. *Tetrahedron, 56*, 4711-4715.

Lewis, C. W., Taylor, R. G., Kubara, P. M., Marshall, K., Meijer, L., & Golsteyn, R. M. (2013). A western blot assay to measure cyclin dependent kinase activity in cells or in vitro without the use of radioisotopes. *FEBS Letters, 587*, 3089-3095.

Lewis, R. A., Li, J. J., Allenby, N. E. E., Errington, J., Hayles, J., & Nurse, P. (2017). Screening and purification of natural products from actinomycetes that affect the cell shape of fission yeast. *Journal of Cell Science, 130*, 3173-3185.

Li, Y., & Benezra, R. (1996). Identification of a human mitotic checkpoint gene: Hsmad2. *Science, 274*, 246-248.

Li, Y., Yu, W., Liang, Y., & Zhu, X. L. (2007). Kinetochore dynein generates a poleward pulling force to facilitate congression and full chromosome alignment. *Cell Research, 17*, 701-712.

Lin, Y., Bai, L., Chen, W., & Xu, S. (2010). The NF-kappa B activation pathways, emerging molecular targets for cancer prevention and therapy. *Expert Opinion on Therapeutic Targets, 14*, 45-55.

Liu, C.-Y., Chang, H.-S., Chen, I.-S., Chen, C.-J., Hsu, M.-L., Fu, S.-L., et al. (2011a). Costunolide causes mitotic arrest and enhances radiosensitivity in human hepatocellular carcinoma cells. *Radiation Oncology, 6*, 56-56.

Liu, Y., Chen, X.-Q., Liang, H.-X., Zhang, F.-X., Zhang, B., Jin, J., et al. (2011b). Small compound 6-O-Angeloylplenolin induces mitotic arrest and exhibits therapeutic potentials in multiple myeloma. *Plos One, 6*, e21930.

Liu, Y. Q., Wang, X. L., Cheng, X., Lu, Y. Z., Wang, G. Z., Li, X. C., et al. (2015). Skp1 in lung cancer: clinical significance and therapeutic efficacy of its small molecule inhibitors. *Oncotarget, 6*, 34953-34967.

Lyss, G., Knorre, A., Schmidt, T. J., Pahl, H. L., & Merfort, I. (1998). The anti-inflammatory sesquiterpene lactone helenalin inhibits the transcription factor NF-kappa B by directly targeting p65. *Journal of Biological Chemistry, 273*, 33508-33516.

MacGregor, J. T. (1977). Mutagenic activity of hymenovin, a sesquiterpene lactone from western bitterweed. *Food and Cosmetics Toxicology, 15*, 225.

Macías, F. A., Torres, A., Molinllo, J. G., Varela, R. M., & Castellano, D. (1996). Potential allelopathic sesquiterpene lactones from Sunflower leaves. *Phytochemistry, 43*, 1205-1215.

Maguire, B. (1938). *A monograph of the genus Arnica. The subgenera Arctica and Austromontana.* (PhD thesis), Cornell University.

Maiato, H., Gomes, A., Sousa, F., & Barisic, M. (2017). Mechanisms of chromosome congression during mitosis. *Biology, 6*, 13.

Majak, W., Brooke, B. M., & Ogilvie, R. T. (2008). *Stock-poisoning plants of Western Canada*. Ottawa, Ontario: Research Branch Agriculture Canada.

Manners, G. D., Ivie, G. W., & MacGregor, J. T. (1978). Mutagenic activity of hymenovin in *Salmonella typhimurium*: association with the bishemiacetal functional group. *Toxicology and Applied Pharmacology, 45*, 629-633.

Marcel, A. T. M. v. V., Barbara, C. M. v. d. W., Vader, G., Janssen, H., Calafat, J., Klompmaker, R., et al. (2004). Polo-like kinase-1 is required for bipolar spindle formation but is dispensable for anaphase promoting complex/cdc20 activation and initiation of cytokinesis. *Journal of Biological Chemistry, 279*, 36841-36854.

Matsuura, H., Saxena, G., Farmer, S. W., Hancock, R. E. W., & Towers, G. H. N. (1996). An antibacterial thiophene from *Balsamorhiza sagittata*. *Planta Medica, 62*, 65-66.

Matthews, T. P., Jones, A. M., & Collins, I. (2013). Structure-based design, discovery and development of checkpoint kinase inhibitors as potential anticancer therapies. *Expert Opinion on Drug Discovery, 8*, 621-640.

McGrathHill, C. A., & Vicas, I. M. (1997). Case series of *Thermopsis* exposures. *Journal of Toxicology, 35*, 659-665.

McIntosh, J. R. (1991). Structural and mechanical control of mitotic progresison. *Cold Spring Harbor Symposia on Quantitative Biology, 56*, 613-619.

Merdes, A., Heald, R., Samejima, K., Earnshaw, W. C., & Cleveland, D. W. (2000). Formation of spindle poles by dynein/dynactin-dependent transport of Numa. *The Journal of Cell Biology, 149*, 851-861.

Merfort, I., & Wendisch, D. (1993). Sesquiterpene lactones of *Arnica cordifolia*, subgenus *Austromontana*. *Phytochemistry, 34*, 1436-1437.

Mialhe, A., Lafanechère, L., Treilleux, I., Peloux, N., Dumontet, C., Brémond, A., et al. (2001). Tubulin detyrosination is a frequent occurrence in breast cancers of poor prognosis. *Cancer Research, 61*, 5024.

Miller, J. S. (2011). The discovery of medicines from plants: a current biological perspective. *Economic Botany, 65*, 396-407.

Miller, Louis H., & Su, X. (2011). Artemisinin: discovery from the Chinese herbal garden. *Cell, 146*, 855-858.

Mitchison, T. (1988). Microtubule dynamics and kinetochore function in mitosis. *Annual Review of Cell and Developmental Biology, 4*, 527-549.

Mohamed, A., Ahmed, A. A., Wollenweber, E., Bohm, B., & Asakawa, Y. (2006). Highly oxygenated guaianolides and eudesman-12-oic acids from *Balsamorhiza sagittata* and *Balsamorhiza macrophylla*. *Chemical & Pharmaceutical Bulletin, 54*, 152-155.

Mori, M., Somogyi, K., Kondo, H., Monnier, N., Falk, Henning J., Machado, P., et al. (2014). An Arp2/3 nucleated F-actin shell fragments nuclear membranes at nuclear envelope breakdown in starfish oocytes. *Current Biology, 24*, 1421-1428.

Moss, E. H., & Packer, J. G. (1983). *Flora of Alberta: A manual of flowering plants, conifers, ferns and fern allies found growing without cultivation in the province of Alberta, Canada* (2nd ed.). Toronto: University of Toronto Press.

Moudgil, D. K., Westcott, N., Famulski, J. K., Patel, K., Macdonald, D., Hang, H., et al. (2015). A novel role of farnesylation in targeting a mitotic checkpoint protein, human Spindly, to kinetochores. *Journal of Cell Biology, 208*, 881-896.

Newman, D. J., & Cragg, G. M. (2016). Natural products as sources of new drugs from 1981 to 2014. *Journal of Natural Products, 79*, 629-661.

Newman, D. J., Cragg, G. M., & Snader, K. M. (2000). The influence of natural products upon drug discovery. *Natural Product Reports, 17*, 215-234.

Nigg, E. A. (2001). Mitotic kinases as regulators of cell division and its checkpoints. *Nature Reviews Molecular Cell Biology, 2*, 21-32.

Norman, J. O., Johnson, J. H., Mollenhauer, H. H., & Meola, S. M. (1976). Effects of sesquiterpene lactones on the growth of *Bacillus thuringiensis*. *Antimicrobial Agents and Chemotherapy, 9*, 535-539.

Nurse, P. (1990). Universal control mechanism regulating onset of M-phase. *Nature, 344*, 503-508.

O'Connell, M. J., Walworth, N. C., & Carr, A. M. (2000). The G2-phase DNA-damage checkpoint. *Trends in Cell Biology, 10*, 296-303.

Panero, J. L., & Funk, V. A. (2002). Toward a phylogenetic subfamilial classification for the Compositae (Asteraceae). *Proceedings of the Biological Society of Washington, 115*, 909-922.

Pavarini, D. P., Pavarini, S. P., Niehues, M., & Lopes, N. P. (2012). Exogenous influences on plant secondary metabolite levels. *Animal Feed Science and Technology, 176*, 5-16.

Peris, L., Thery, M., Fauré, J., Saoudi, Y., Lafanechère, L., Chilton, J. K., et al. (2006). Tubulin tyrosination is a major factor affecting the recruitment of CAP-Gly proteins at microtubule plus ends. *The Journal of Cell Biology, 174*, 839-849.

Peters, J. M. (2002). The anaphase-promoting complex: proteolysis in mitosis and beyond. *Molecular Cell, 9*, 931-943.

Petrova, M., Zayova, E., Vassilevska-Ivanova, R., & Vlahova, M. (2012). Biotechnological approaches for cultivation and enhancement of secondary metabolites in *Arnica montana* L. *Acta Physiologiae Plantarum, 34*, 1597-1606.

Pickart, C. M. (2001). Mechanisms underlying ubiquitination. *Annual Review of Biochemistry, 70*, 503-533.

Picman, A. K. (1986). Biological activities of sesquiterpene lactones. *Biochemical Systematics and Ecology*, *14*, 255-281.

Prasifka, J. R., Spring, O., Conrad, J., Cook, L. W., Palmquist, D. E., & Foley, M. E. (2015). Sesquiterpene lactone composition of wild and cultivated sunflowers and biological activity against an insect pest. *Journal of Agricultural and Food Chemistry, 63*, 4042-4049.

Prosser, S. L., & Pelletier, L. (2017). Mitotic spindle assembly in animal cells: a fine balancing act. *Nature Reviews Molecular Cell Biology, 18*, 187-201.

Putkey, F. R., Cramer, T., Morphew, M. K., Silk, A. D., Johnson, R. S., McIntosh, J. R., et al. (2002). Unstable kinetochore-microtubule capture and chromosomal instability following deletion of Cenp-E. *Developmental Cell, 3*, 351-365.

Quignon, F., Rozier, L., Lachages, A. M., Bieth, A., Simili, M., & Debatisse, M. (2007). Sustained mitotic block elicits DNA breaks: one-step alteration of ploidy and chromosome integrity in mammalian cells. *Oncogene, 26*, 165-172.

Rando, R. R. (1996). Chemical biology of protein isoprenylation/methylation. *Biochimica et Biophysica Acta, 1300*, 5-16.

Rieder, C. L., Davison, E. A., Lawrence, C. W. J., Cassimeris, L., & Salmon, E. D. (1986). Oscillatory movements of monooriented chromosomes and their position relative to the spindle pole result from the ejection properties of the aster and half-spindle. *The Journal of Cell Biology, 103*, 581-591.

Rieder, C. L., & Maiato, H. (2004). Stuck in division or passing through: what happens when cells cannot satisfy the spindle assembly checkpoint. *Developmental Cell, 7,* 637-651.

Rieder, C. L., Schultz, A., Cole, R., & Sluder, G. (1994). Anaphase onset in vertebrate somatic cells is controlled by a checkpoint that monitors sister kinetochore attachment to the spindle. *The Journal of Cell Biology, 127*, 1301-1310.

Rodriguez, E., Towers, G. H. N., & Mitchell, J. C. (1976). Biological activities of sesquiterpene lactones. *Phytochemistry, 15*, 1573-1580.

Rogakou, E. P., Pilch, D. R., Orr, A. H., Ivanova, V. S., & Bonner, W. M. (1998). DNA double-stranded breaks induce histone H2AX phosphorylation on serine 139. *Journal of Biological Chemistry, 273*, 5858-5868.

Rowinsky, E. K., & Donehower, R. C. (1995). Paclitaxel (taxol). *New England Journal of Medicine, 332*, 1004-1014.

Schafer-Hales, K., Iaconelli, J., Snyder, J. P., Prussia, A., Nettles, J. H., El-Naggar, A., et al. (2007). Farnesyl transferase inhibitors impair chromosomal maintenance in cell lines and human tumors by compromising Cenp-E and Cenp-F function. *Molecular Cancer Therapeutics, 6*, 1317-1328.

Schilling, E. E. (2006). *Helianthus*. In: Flora of North America Editorial Committee, eds. 1993 +. *Flora of North America North of Mexico* (Vol. 21, pp. 141-161). New York, NY: Oxford University Press.

Schmidt, M., & Bastians, H. (2007). Mitotic drug targets and the development of novel anti-mitotic anticancer drugs. *Drug Resistance Updates, 10*, 162-181.

Schmidt, T. (1999). Quantitative structure-cytotoxicity relationships within a series of helenanolide type sesquiterpene lactones. *Pharmaceutical and Pharmacological Letters, 9*, 9-13.

Schmidt, T. J., & Willuhn, G. (2000). Sesquiterpene lactone and flavonoid variability of the *Arnica angustifolia* aggregate (Asteraceae). *Biochemical Systematics and Ecology, 28*, 133-142.

Schmidt, T. J., Willuhn, G., Steigel, A., & Wendisch, D. (1995). Sesquiterpene lactones and inositol esters from *Arnica angustifolia*. *Planta Medica, 61*, 544.

Scotti, M. T., Fernandes, M. B., Ferreira, M. J. P., & Emerenciano, V. P. (2007). Quantitative structure–activity relationship of sesquiterpene lactones with cytotoxic activity. *Bioorganic & Medicinal Chemistry, 15*, 2927-2934.

Seaman, F. C. (1982). Sesquiterpene lactones as taxonomic characters in the Asteraceae. *Botanical Review, 48*, 121-595.

Siedle, B., Garcia-Pineres, A. J., Murillo, R., Schulte-Monting, J., Castro, V., Rungeler, P., et al. (2004). Quantitative structure - activity relationship of sesquiterpene lactones as inhibitors of the transcription factor NF-kappa B. *Journal of Medicinal Chemistry, 47*, 6042-6054.

Skoufias, D. A., & Wilson, L. (1992). Mechanism of inhibition of microtubule polymerization by colchicine - inhibitory potencies of unliganded colchicine and tubulin colchicine complexes. *Biochemistry, 31*, 738-746.

Solecki, R. S. (1975). Shanidar IV, a neanderthal flower burial in northern Iraq. *Science, 190*, 880-881.

Spring, O., Benz, T., & Ilg, M. (1989). Sesquiterpene lactones of the capitate glandular trichomes of *Helianthus annuus*. *Phytochemistry, 28*, 745-749.

Spring, O., & Schilling, E. E. (1991). The sesquiterpene lactone chemistry of *Helianthus* sect. *Atrorubentes* (Asteraceae: Heliantheae). *Biochemical Systematics and Ecology, 19*, 59-79.

Spring, O., Zitterell-Haid, B., Bierner, M. W., & Mabry, T. J. (1994). Chemistry of glandular trichomes in *Hymenoxys* and related genera. *Biochemical Systematics and Ecology, 22*, 171-195.

Strebhardt, K., & Ullrich, A. (2006). Opinion - targeting polo-like kinase 1 for cancer therapy. *Nature Reviews Cancer, 6*, 321-330.

Sturgeon, C. M., Craig, K., Brown, C., Rundle, N. T., Andersen, R. J., & Roberge, M. (2005). Modulation of the g2 cell cycle checkpoint by sesquiterpene lactones psilostachyins A and C isolated from the common ragweed *Ambrosia artemisiifolia*. *Planta medica, 71*, 938.

Sudakin, V., Gordon, K. T. C., & Yen, T. J. (2001). Checkpoint inhibition of the APC/C in Hela cells is mediated by a complex of Bubr1, Bub3, Cdc20, and Mad2. *The Journal of Cell Biology, 154*, 925-936.

Suh, Y. A., Kim, J. H., Sung, M. A., Boo, H. J., Yun, H. J., Lee, S. H., et al. (2013). A novel antitumor activity of deguelin targeting the insulin-like growth factor (IgF) receptor pathway via up-regulation of IgF-binding protein-3 expression in breast cancer. *Cancer Letters, 332*, 102-109.

Swift, L. H., & Golsteyn, R. M. (2016). Cytotoxic amounts of cisplatin induce either checkpoint adaptation or apoptosis in a concentration-dependent manner in cancer cells. *Biology of the Cell, 108*, 127-148.

Sylvia, V. L., Kim, H. L., Norman, J. O., & Busbee, D. L. (1987). The sesquiterpene lactone hymenoxon acts as a bifunctional alkylating agent. *Cell Biology and Toxicology, 3*, 39-49.

Tang, T.-K., Chiu, S.-C., Lin, C.-W., Su, M.-J., & Liao, M.-H. (2015). Induction of survivin inhibition, g_2 /m cell cycle arrest and autophagic on cell death in human malignant glioblastoma cells. *The Chinese Journal of Physiology, 58*, 95.

Taunton, J., Collins, J. L., & Schreiber, S. L. (1996). Synthesis of natural and modified trapoxins, useful reagents for exploring histone deacetylase function. *Journal of the American Chemical Society, 118*, 10412-10422.

The Plant List. Version 1.1. (2013). Retrieved 2018-03-14, from Royal Botanic Gardens Kew and Missouri Botanic Garden. http://www.theplantlist.org

Thornton, B. R., & Toczyski, D. P. (2003). Securin and B-cyclin/cdk are the only essential targets of the APC. *Nature Cell Biology, 5*, 1090-1094.

Tu, W.-Z., Li, B., Huang, B., Wang, Y., Liu, X.-D., Guan, H., et al. (2013). gamma-H2AX foci formation in the absence of DNA damage: Mitotic H2AX phosphorylation is mediated by the DNA-PKcs/Chk2 pathway. *FEBS Letters, 587*, 3437-3443.

Tu, Y. (2016). Artemisinin—a gift from traditional Chinese medicine to the world (nobel lecture). *Angewandte Chemie International Edition, 55*, 10210-10226.

Turner, N. J., Ignace, M. B., & Ignace, R. (2000). Traditional ecological knowledge and wisdom of aboriginal peoples in british columbia. *Ecological Applications, 10*, 1275-1287.

Uhlmann, F., Lottspeich, F., & Nasmyth, K. (1999). Sister-chromatid separation at anaphase onset is promoted by cleavage of the cohesin subunit Scc1. *Nature, 400*, 37-42.

Uprety, Y., Asselin, H., Dhakal, A., & Julien, N. (2012). Traditional use of medicinal plants in the boreal forest of Canada: review and perspectives. *Journal of Ethnobiology and Ethnomedicine, 8*, 7-7.

Vassilev, L. T., Tovar, C., Chen, S., Knezevic, D., Zhao, X., Sun, H., et al. (2006). Selective small-molecule inhibitor reveals critical mitotic functions of human Cdk1. *Proceedings of the National Academy of Sciences of the United States of America, 103*, 10660-10665.

Wang, Q. Z., Fan, S. J., Eastman, A., Worland, P. J., Sausville, E. A., & Oconnor, P. M. (1996). Ucn-01, a potent abrogator of G2 checkpoint function in cancer cells with disrupted p53. *Journal of the National Cancer Institute, 88*, 956-965.

Weaver, B. A., Bonday, Z. Q., Putkey, F. R., Kops, G. J., Silk, A. D., & Cleveland, D. W. (2003). Centromere-associated protein-E is essential for the mammalian mitotic checkpoint to prevent aneuploidy due to single chromosome loss. *The Journal of Cell Biology, 162*, 551-563.

Weber, W. A. (2006). *Balsamorhiza*. In: Flora of North America Editorial Committee, eds. 1993 +. *Flora of North America North of mexico* (Vol. 21, pp. 95). New York, NY: Oxford University Press.

Wei, Y., Yu, L., Bowen, J., Gorovsky, M. A., & Allis, C. D. (1999). Phosphorylation of histone H3 is required for proper chromosome condensation and segregation. *Cell, 97*, 99-109.

Whipple, R. A., Vitolo, M. I., Boggs, A. E., Charpentier, M. S., Thompson, K., & Martin, S. S. (2013). Parthenolide and costunolide reduce microtentacles and tumor cell attachment by selectively targeting detyrosinated tubulin independent from NF-κB inhibition. *Breast Cancer Research, 15*, R83.

Wink, M. (2003). Evolution of secondary metabolites from an ecological and molecular phylogenetic perspective. *Phytochemistry, 64*, 3-19.

Wolf, S. J. (2006). *Arnica*. In: Flora of North America Editorial Committee, eds. 1993 +. *Flora of North America North of Mexico* (Vol. 21, pp. 374). New York, NY: Oxford University Press.

Wolf, S. J., & Denford, K. E. (1983). Flavonoid variation in *Arnica cordifolia*: An apomictic polyploid complex. *Biochemical Systematics and Ecology, 11*, 111-114.

Wöll, S., Kim, S. H., Greten, H. J., & Efferth, T. (2013). Animal plant warfare and secondary metabolite evolution. *Natural Products and Bioprospecting, 3*, 1-7.

Wood, K. W., Lad, L., Luo, L., Qian, X., Knight, S. D., Nevins, N., et al. (2010). Antitumor activity of an allosteric inhibitor of centromere-associated protein-E. *Proceedings of the National Academy of Sciences of the United States of America, 107*, 5839-5844.

Wood, K. W., Sakowicz, R., Goldstein, L. S. B., & Cleveland, D. W. (1997). Cenp-E is a plus end–directed kinetochore motor required for metaphase chromosome alignment. *Cell, 91*, 357-366.

Yang, Z., Guo, J., Chen, Q., Ding, C., Du, J., & Zhu, X. (2005). Silencing mitosin induces misaligned chromosomes, premature chromosome decondensation before anaphase onset, and mitotic cell death. *Molecular and Cellular Biology, 25*, 4062-4074.

Yao, X., Abrieu, A., Zheng, Y., Sullivan, K. F., & Cleveland, D. W. (2000). Cenp-E forms a link between attachment of spindle microtubules to kinetochores and the mitotic checkpoint. *Nature Cell Biology, 2*, 484.

Yao, X., Anderson, K. L., & Cleveland, D. W. (1997). The microtubule-dependent motor centromere-associated protein E (Cenp-E) is an integral component of kinetochore corona fibers that link centromeres to spindle microtubules. *The Journal of Cell Biology, 139*, 435-447.

Yen, T. J., Li, G., Cleveland, D. W., Szilak, I., & Schaar, B. T. (1992). Cenp-E is a putative kinetochore motor that accumulates just before mitosis. *Nature, 359*, 536-539.

Zdero, C., & Bohlmann, F. (1990). Systematics and evolution within the Compositae, seen with the eyes of a chemist. *Plant Systematics and Evolution, 171*, 1-14.

Zeng, X., Sigoillot, F., Gaur, S., Choi, S., Pfaff, K. L., Oh, D.-C., et al. (2010). Pharmacologic inhibition of the anaphase-promoting complex induces a spindle checkpoint-dependent mitotic arrest in the absence of spindle damage. *Cancer Cell, 18*, 382-395.